Formal methods for evolutionary inference using ancient DNA

Liisa Loog
Linacre College
University of Oxford

A thesis submitted for the degree of
Doctor of Philosophy
Hilary Term 2018

Formal methods for evolutionary inference using ancient DNA

Liisa Loog
Linacre College, University of Oxford
A thesis submitted for the degree of *Doctor of Philosophy*
Hilary Term 2018

Abstract

Ancient DNA has revolutionised our ability to study past evolutionary processes by enabling direct observation of genetic variation in past populations. However, current formal methods for evolutionary inference are challenged by the sparse and heterogeneous distribution of data in space and in time, typical of ancient DNA datasets, as well as sample age uncertainty. In this thesis, I introduce analytical approaches that explicitly address these problems and show how inference from ancient DNA can greatly benefit from analysis that formally compares different evolutionary and demographic scenarios. I apply these approaches to three different cases that represent a range of demographic histories and evolutionary questions spanning different time-scales, species and types of data. The first approach combines space and time into a single matrix that can be used to estimate levels of past within population mobility. I apply this method to human ancient DNA data spanning the last 35 thousand years to recover changes in mobility over this time period. The second approach combines spatially and temporally explicit simulations with ancient mitochondrial genome data, spanning the Northern hemisphere and the last 50 thousand years to reconstruct large-scale population dynamics in Grey wolves over this time period. The third approach uses likelihood-based analysis to reconstruct episodes of past selection from time series of ancient DNA data. I apply this method to genotype data spanning two thousand years from two loci in domestic chicken to estimate a number of selection parameters including the starting time of the selection. These case studies all illustrate how formal hypothesis testing in spatially and temporally explicit frameworks make it possible to directly link evolutionary histories to the climatic and archaeological records as well as historical sources and show how identifying potential drivers of evolution allow building a more detailed and complete picture of the past.

Acknowledgements

I would like to thank all my co-authors for all the hard work they have put into our joint projects. I am especially grateful to Professor Mark G. Thomas and Dr. Andrea Manica and especially especially grateful to Dr. Anders Eriksson for sharing their insights and for valuable discussions leading to this thesis.

Index

List of figures and tables for Chapter 2

List of figures and tables for Chapter 3

List of figures and tables for Chapter 4

Introduction

Genetic data and population genetic modelling is a powerful combination for studying the evolutionary history of populations. It provides information complementary to archaeological and historical approaches and can therefore help us form a more informed picture of the past. Traditionally, genetic data has been generated solely from modern individuals. However, advances in laboratory, sequencing and computational techniques have made it possible to retrieve genetic information from fossil, archaeological, museum or otherwise degraded specimens, usually referred to as ancient DNA. The last decade has seen a surge in ancient DNA from wide range of organisms ranging from Pleistocene hominins to Medieval pathogens. The ability to study past genetic diversity directly brings major advantages to the evolutionary inference about the history of populations, and by doing so allows addressing long-standing questions in fields of paleoecology, archaeology and genetics. However, currently existing methods for inference using ancient DNA typically ignore the temporal or geographic information in the data. This renders the inferred evolutionary processes and past populations of interest abstract, and thereby limits the detail in which the results can be interpreted in the context of climatic, archaeological and historical information.

In this thesis I present three different population genetic approaches that are specifically tailored to quantitative hypotheses testing using ancient DNA. These examples cover a wide range of demographic histories and evolutionary questions spanning different time-scales, species and types of data, and as such provide a broadly representative sample of the analytical challenges in the field of ancient DNA research.

Chapter 1 gives an overview of ancient DNA data generation processes and critically reviews, in the light of the analytical challenges associated with ancient DNA, the current approaches used for evolutionary and demographic inference with genetic data.

In Chapter 2 I present a novel statistic where space and time are formally combined for estimating changes in the level of intra-population mobility from ancient DNA.

In Chapter 3 I present a spatially and temporally explicit simulation framework to formally test a range of different demographic scenarios of large-scale population dynamics, including local extinctions, population size changes and range expansions.

In Chapter 4 I present a novel analytical framework for inferring past genetic selection using sparse ancient DNA time series of genotypes or allele frequency data. This framework can account for uncertainty in sample ages as well as gene flow from external populations.

The approaches developed in this thesis are applicable to many current and future ancient DNA datasets and different evolutionary and archaeological questions. Furthermore, the approaches described in this thesis provide a way to unify analysis of genetic data and inference from archaeological and historical contexts by explicitly linking them through space and time.

Chapter 1 Ancient DNA Literature Review

Genetic sequences generated from ancient samples have been employed to address a number of long-standing questions in the fields of archaeology, anthropology and genetics. For example, ancient DNA can be used to tackle classical archaeological problems such as establishing the biological sex (Skoglund et al. 2013), providing species identification (e.g. Horsburgh 2008; Dalén et al. 2017), and to reconstruct past diets and environments (e.g. Willerslev et al. 2007). Additionally, ancient DNA can be been used to calibrate molecular clocks that measure the rates of evolution (e.g. Rieux et al. 2014; Skoglund et al. 2015; Palkopoulou et al. 2015). These can be used to date past demographic events such as population splits and admixture events, long-range migrations and fluctuations in population size (particularly in the recent past), as well as to generate date estimates for previously undated specimens. The ability to extract genetic data from archaeological specimens has also opened doors for previously inaccessible research areas. In some cases, meaningful information can be gained directly from the presence or absence of particular genetic markers: for example, ancient DNA has allowed researchers to directly estimate past phenotypes (e.g. Krause et al. 2007; Lalueza-Fox et al. 2007; Ludwig et al. 2009; Girdland Flink et al. 2014; Olalde et al. 2014). Ancient DNA can also provide exciting insights into past population dynamics such as migration events, changes in population size through time, population expansions and replacements, and intra- and inter-population relationships as well as other evolutionary processes such as adaptation and natural selection. However, these processes can rarely be directly observed and therefore need to be reconstructed using an inferential approach which, in the case of ancient DNA is not straightforward and comes with number of additional challenges. In this chapter, I will provide a brief overview of the difficulties associated with ancient DNA data generation and critically review the analytical challenges associated with use of ancient DNA data in evolutionary and demographic inferences. Several of the approaches discussed here have also been recently reviewed elsewhere (e.g. Malaspinas 2016; Slatkin 2016; Leonardi et al. 2017; Marciniak and Perry 2017; Yang and Fu 2018).

1.1 Ancient DNA data generation

1.1.1 Materials

DNA can be extracted from a wide range of archaeological or fossil material. Suitability of a specimen for DNA extraction depends on the quality and availability of the material

as well as on the research question. Ancient DNA is commonly extracted from bones, teeth or seeds of an organism of interest, as these are frequently preserved in the archaeological record. Retrieval of genetic material from hair (Gilbert et al. 2007; Rasmussen et al. 2010; Rasmussen et al. 2011), skins (Thomas et al. 1990), eggshells (Oskam et al. 2010), mollusc shells (Sarkissian et al. 2017), pollen (Parducci et al. 2005) or wood (Liepelt et al. 2006) can also be viable. While DNA from bones and teeth can be used to glean insights into past population dynamics, movements, interactions, and phenotypes, DNA from dental calculus (e.g. Adler et al. 2013) and mummified stomach contents (e.g. Rollo et al. 2002) or coprolites (e.g. Poinar et al. 2003) can be used to study past diets. DNA that was once in the cells of animals, plants, bacteria and fungi can even be retrieved from soil, sediments and ice cores and used to reconstruct past environments in the absence of macrofossils or archaeological remains (e.g. Willerslev et al. 2007, Haile et al. 2009).

1.1.2 Ancient DNA Preservation and Contamination

The retrieval of ancient DNA does not come without challenges. Following the death of an organism, DNA repair mechanisms cease and the DNA begins breaking down due to hydrolysis, the action of endogenous enzymes and microorganisms, as well as physical factors such UV light (Lindahl 1993; Collins et al. 2002; Dabney et al. 2013). These processes are amplified by heat, humidity, soil acidity, air and water flow, and fluctuations in temperature, resulting in additional damage to the DNA content (Collins et al. 2002; Smith et al. 2003; Bollongino and Vigne 2008; Allentoft et al. 2012). As a result, following the death of an organism, DNA degrades exponentially until there is no endogenous DNA molecules left to be extracted and sequenced (Lindahl 1993). Therefore, the age of a specimen is a strong predictor of the quantity and quality of recoverable DNA (Allentoft et al. 2012). However, it is well understood that the geographical, environmental and climatic conditions in which the specimen is preserved also play a large role in the process of DNA degradation and preservation (Collins et al. 2002; Smith et al. 2003).

The oldest and best preserved genetic data has been recovered from permafrost and (high altitude) caves, where conditions are dry, cool and stable, with small fluctuations around the annual mean (e.g. Reich et al. 2010; Meyer et al. 2016). The oldest DNA molecules currently isolated from skeletal material are from an approximately 700,000 year-old

equid preserved in Siberian permafrost (Orlando et al. 2013). However, temperate regions have yielded relatively good quality data from time periods as far back as the Upper Palaeolithic. With few exceptions (e.g. Llorente et al. 2015; Pinhasi et al. 2015; Skoglund et al. 2017), ancient DNA researchers have been less successful in recovering DNA from remains preserved in geographic areas where conditions are hot or humid such as Africa and the Middle-East.

Although the effects of sample age and geographic location on ancient DNA preservation are well described, DNA degradation in archaeological contexts remains a poorly understood process. Variation in aspects such as the season of the death, burial depth, local pH and water saturation levels and thickness and structure of the bones analysed can also cause large variations in DNA survival, resulting in a situation where variable results can be obtained within single sites, layers and even within individual specimens (Collins et al. 2002; Pinhasi et al. 2015).

1.1.3 Sequencing

The essence of biomolecular research is the ability to read genetic information. For the first couple of decades of ancient DNA research, data was generated using Sanger sequencing (first introduced in late 1970s). In traditional Sanger sequencing, a targeted DNA fragment is amplified using the polymerase chain reaction (PCR). The PCR cycles generate fragments of different lengths, all ending in radioactively or fluorescently labelled nucleotides (the building blocks of DNA), with different labels for different nucleotides. The fragments are then sorted and read in the order of their length. This allows for a straightforward determination of the order of DNA bases in the sequenced fragment. Although Sanger sequencing used to be the main technique for generating ancient DNA data for great majority of the history of ancient DNA research, High Throughput or Next Generation Sequencing (NGS) has revolutionised the field by enabling orders of magnitudes more data to be generated for a fraction of cost and manpower. The underlying principle of NGS is similar to Sanger sequencing: bases of DNA fragments are sequentially identified based on the signals they emit. A key difference between Sanger sequencing and NGS is that the latter technology allows billions of short DNA fragments to be sequenced in parallel. What is more, because NGS technology allows sequencing shorter fragments compared to Sanger sequencing, a higher proportion of endogenous DNA from ancient and archaeological specimens can

be sequenced (Knapp and Hofreiter 2010). As a result, entire genomes of archaeological or ancient individuals can be sequenced to high coverage, or the genomes of multiple individuals can be sequenced at lower coverage on a single run, provided there is sufficient endogenous DNA in the material.

Although whole genome sequences, especially those derived from ancient individuals or extinct species, are valuable in population genetics as they enable detection of previously uncharacterised variation, it is not always practical or achievable to generate whole genome sequences using the NGS approach. As the majority of DNA recovered from ancient samples is usually not endogenous to the organism of interest, but instead comes from microbes of the surrounding environment, a more cost efficient option for sequencing samples with low content of endogenous DNA might be targeted enrichment approach (Knapp and Hofreiter 2010; Carpenter et al. 2013; Pickrell and Reich 2014). In this approach, specially designed baits are used to capture small fragments of endogenous DNA so that the exogenous content can be excluded before sequencing. This approach enables researchers to focus on generating high quality information about specific loci. The design of the baits depends on the research question. In some cases researchers have targeted entire genomes, just the exome (the coding part of the genome), or regions that are known to be polymorphic in modern samples. Though attractive, this latter strategy possesses a potential ascertainment bias that could complicate the downstream analysis: If the targeted loci are selected based on a small number or closely related populations some variation may go undetected, resulting in a situation where differences between individuals can be artificially deflated or inflated depending what populations were included in the ascertainment of polymorphic loci (Nielsen 2004).

Whole genomes or regions of interest can then be reconstructed by mapping the resulting sequence fragments (known as reads) to reference genomes. Alternatively, genomes can be *de novo* reconstructed using overlapping ends of reads, allowing for determination of genetic sequence for species without an existing reference genome. However, this approach is only viable in cases where DNA in a given specimen is abundant and very well preserved in order to cover most of the genome in sufficient depth, making it not particularly viable application for ancient specimens.

The arrival of NGS technology has also reduced a major problem in ancient DNA research – contamination (Knapp and Hofreiter 2010): Due to the low concentration of

endogenous DNA in archaeological samples relative to DNA from the surrounding environments, ancient samples are highly prone to contamination from modern day sources. Living humans, soil microorganisms, and pathogens are the most common sources of DNA contamination as biological material from these organisms are ubiquitous in most excavation and laboratory environments, leading to a situation where contamination instead of endogenous DNA from archaeological material of interest is more likely to be sequenced.

That said, exogenous DNA can contain valuable information about the environment of past individuals as well as the pathogens they carried. For example, plague pathogen (*Yersenia pestis*) DNA has been recovered from ancient individuals and used to reconstruct the evolutionary history of the pathogen (Rasmussen et al. 2015; Andrades Valtueña et al. 2017).

NGS reduces the problem of contamination by providing means to detect it (Knapp and Hofreiter 2010). First, reads that do not map back to the organism of interest can be assumed to be exogenous DNA and, therefore, removed from the analyses. In this way, it may also be possible to identify the source(s) of the exogenous DNA (contamination). However, this approach only deals with contamination that comes from a species different from that of the target of the sequencing. Secondly, researchers can use the DNA damage patterns characteristic to ancient DNA (especially short fragment length and cytosine deamination near the ends of the reads) to differentiate between modern and degraded ancient DNA (Dabney et al. 2013; Jónsson et al. 2013; Skoglund, Northoff, et al. 2014). Contamination from conspecifics is substantially harder to detect and remove, especially if the contaminant also shows DNA damage (e.g. cross-contamination between museum samples). However, it may still be possible to quantify the level of contamination from the frequency of heterozygous sites called in haploid markers, such as mitochondrial DNA and, for male samples, the X chromosome.

1.1.4 Bioinformatics and dealing with low quality sequence data

The challenges associated with ancient DNA research do not end once the sequencing is complete. The billions of reads generated by high throughput sequencing also pose significant computational challenges. Ancient DNA data requires non-standard bioinformatics tools that can deal with damage and non-uniform read length and other features associated with ancient DNA (Pickrell and Reich 2014). Therefore, laboratories

specialising in ancient DNA data generation often have custom-made pipelines for processing raw sequence data, some of which have been packaged and published for wider use (e.g. Schubert et al. 2014; Peltzer et al. 2016).

Nevertheless, due to the factors outlined above, ancient DNA sequence data tends to have low coverage compared to modern sequence data. As a result, ancient DNA sequences contain significantly more missing data and are more likely to contain errors: calling genotypes from low coverage data is problematic because allelic dropout can result in false negatives for heterozygotes, and sequencing and damage errors can result in false positives for heterozygotes and homozygous alternative alleles (Nielsen et al. 2012). This makes inference challenging as missing data and sequence errors can bias downstream analyses. The sensitivity of downstream analysis to typical ancient DNA damage can be investigated using ancient DNA data simulators such as gargammel (Renaud et al. 2017) and several approaches exist in the field to mitigate these problems.

First, the problem of allelic dropout can be mitigated by randomly sampling an allele (or read) for each position, resulting in an artificial haploid genome (e.g. Skoglund et al. 2012; Allentoft et al. 2015; Haak et al. 2015; Mathieson et al. 2015; Fu et al. 2016; Lazaridis et al. 2016).

Secondly, data could be filtered to regions where high quality information is available for all samples in the analyses. This approach works well in cases where one or few low quality ancient DNA samples are analysed along side high quality (present-day) samples, but is less likely to be viable for multiple or large sets of low coverage ancient DNA data, as each low quality sample will result in loss of large proportion of the genome available for analyses.

An approach that attempts to avoid this problem is using large reference panels (Marchini and Howie 2010) of high quality genomes to impute the missing data (e.g. Gamba et al. 2014). The success of this approach depends largely on how well the reference panels capture the variation in the population as a whole and how representative the reference panel is of the source population of the ancient sample. Therefore, this approach works reasonably well for relatively recent samples but is increasingly problematic further back in time (Gamba et al. 2014).

Finally, tools such as ANGSD (Korneliussen et al. 2014) circumvent the problem of calling individual genotypes by estimating genome wide measures of genetic differentiation and diversity using a likelihood based approach that explicitly accounts for variable coverage and DNA damage as well as sequencing error rates.

1.1.5 Mitochondrial vs. genomic data

For the purpose of retrieval and analysis, ancient DNA from humans and other animals can be divided into genomic DNA, found in the cell nucleus, and mitochondrial DNA found in the cell mitochondria (organelles involved in the production of chemical energy within cells). Early ancient DNA studies focused exclusively on mitochondrial DNA and it remains a common target locus for ancient DNA studies. Mitochondrial DNA is more likely to survive in ancient remains, because each cell contains hundreds of mitochondria, each with an identical copy of the mitochondrial genome, whereas a cell usually contains only a single nucleus, home to just two homologous copies of each chromosome. Thus, the use of mitochondrial DNA can greatly benefit demographic inferences since it can provide information about samples with wider range of temporal and geographic contexts.

A key characteristic of mitochondrial DNA (as well as Y chromosome DNA) is that it does not recombine. Each individual inherits its mitochondria from their mother who has, in turn, inherited it from her mother. This simple inheritance mechanism makes the analyses of mitochondrial DNA deceptively straightforward. However, for reasons that will be further explained below, analyses of mitochondrial data often lack the statistical power to disentangle complex population histories (Rosenberg and Nordborg 2002; Ballard and Whitlock 2004; Nielsen and Beaumont 2009; Balloux 2010) .

In contrast, genetic variation in the nuclear genome gets shuffled in every generation between individual's chromosomes during recombination. In this case, each of the two homologous chromosomes possess a mix of the individual's maternal and paternal chromosomes, which, in turn, contains a mix of the individual's maternal and paternal grandparents' chromosomes, and so on. As a consequence, different parts of an individual's chromosomes come from different ancestors. Loci sufficiently far apart in the nuclear genome are statistically independent, and can be analysed as statistically independent stochastic outcomes (replicates) of an unknown population history. The resolution at which population history can be reconstructed increases with the number of

loci included in the analyses. Because the nuclear genome is typically orders of magnitude larger than the mitochondrial one (in humans, ca. 3 billion bases vs. 16 thousand bases), researchers can greatly benefit from including ancient nuclear DNA in the analyses when inferring population histories. However, in all but well-preserved fossils, the endogenous content of nuclear DNA is often very low, making isolating and sequencing enough DNA for analysis challenging and expensive. Furthermore, handling samples of variable quality and missing data complicates evolutionary and demographic inferences.

In summary, advances in sequencing, laboratory and bioinformatics techniques have resulted in a surge of genetic data generated from archaeological, historical and fossil material. However, the retrieval of ancient DNA data does not come without challenges. Availability of samples for DNA extraction and preservation of genetic material in samples depends on a number of climatic and taphonomic factors. As a result, ancient DNA samples are often sparsely distributed in space and time and the quality as well as the quantity of data from each sample is greatly reduced. As population genetic approaches for evolutionary and demographic inference are traditionally tailored for high quality data from large number of contemporary individuals, ancient DNA data poses a number of additional challenges to population genetic analyses.

1.2 Descriptive approaches for inferring population structure and spatial barriers to mobility and past movement of individuals

1.2.1 Phylogeography

Phylogeographic inference is an approach to reconstruct population histories that was especially popular in the early days of ancient DNA research (e.g. Oppenheimer 2012; Secher et al. 2014). Here, a phylogenetic tree is constructed based on the mutations in a non-recombining part of the genome (e.g. mitochondrial DNA or the Y chromosome). All sampled individuals are assigned to haplogroups and haplotypes, which are the branches and sub-branches, or lineages, on the phylogenetic tree. The root of the tree corresponds to the most recent common ancestor of all the samples (in the case of human mitochondrial DNA, often referred to as the "mitochondrial Eve"). When the mutation rate is known (or can be estimated), it is possible to estimate the dates of each branching point of the tree. Inferences about the past are based on the phylogenetic relationship between different haplotypes or haplogroups, their estimated splitting times, and their distribution in space and time.

The main problem with inferring the past from these constructed trees lies in that, on the level of individuals, demographic scenarios are highly stochastic, and therefore so are the phylogenetic trees of any single genetic locus such as mitochondrial DNA (or the Y chromosome). As a consequence, events in the phylogenetic trees do not generally correspond directly to population-level events but are simply stochastic outcomes of given population histories. Furthermore, different population history scenarios can give rise to similar gene trees and distribution of haplotypes. Although ancient DNA provides additional resolution by enabling the researchers to exclude less likely scenarios (e.g. Larson et al. 2007; Valdiosera et al. 2007; Thalmann et al. 2013), the conclusions can still be easily steered by the subjective biases of a particular researcher (Nielsen and Beaumont 2009). Furthermore, analyses of mitochondrial data often lack the statistical power to disentangle complex population histories (Rosenberg and Nordborg 2002; Ballard and Whitlock 2004; Nielsen and Beaumont 2009; Balloux 2010). However, as will be discussed below, these difficulties can be overcome by sufficient data and statistical modelling that accounts for the randomness of individual loci.

1.2.2 Descriptive methods for inferring population structure

Principal Component Analysis (PCA) is a commonly used technique for assessing the genetic similarity between individuals and the extent to which populations form distinct clusters. In PCA of genetic data, each locus is treated as an independent variable (dimension) and genetic variation among samples is reduced into main axis of variation - principal components (PCs), using the covariance matrix. PCA analysis of modern human populations has been shown to reflect geographic relationships between populations on different scales: on a global scale, populations from the same sub-continent tend to group together, and across Europe the genetic locations of samples in the PCA show striking similarity to their geographic locations (Novembre et al. 2008).

In the ancient DNA literature, modern populations are typically used to define the PCs and ancient individuals are projected onto them. Usually, only the first few axes of variation (PCs) are presented, representing a small proportion of total variation (typically only few percentages) present even in modern populations. However, the older the sample, the more likely it is that most of the variation ends up in an orthogonal axis to the ones used for inference. This problem is exacerbated by the projection method as individuals with more missing data are more likely to end up closer to the average of the

modern data points. In principle, it would be possible to overcome this problem by turning the analysis around: If sufficiently large amount of ancient genetic data were available, PCs could be defined using ancient samples, and modern samples could be projected onto them in order to investigate the genetic similarity between modern and ancient populations.

Nevertheless, the main problem with inferring population history from PCA is that it lacks an underlying population genetic model, and several different scenarios can result in similar distribution of samples on PCs. For example, a population can appear different in a PCA because it has been separate from other populations for a long time, or because a recent population bottleneck has caused extensive drift in allele frequencies within that population (Skoglund, Sjödin, et al. 2014). Therefore, it is not possible to directly relate the inferred distances between samples on PCs to demographic processes behind the observed variation.

Similar criticism applies to tools such as STRUCTURE (Pritchard et al. 2000), ADMIXTURE (Alexander et al. 2009), Finestructure, and Chromopainter (Lawson et al. 2012), all commonly used tools in demographic inference using modern and ancient DNA. These tools vary in their technical implementations but are all designed to identify major genetic clusters and express each sample as a mixture of these clusters. Frequently, the resulting statistical clusters are misleadingly referred to as “ancestral” or “source” populations. Similarly to inference using PCA, it is not inherently possible to identify which demographic scenarios have resulted in the observed patterns of variation because they lack formal underlying demographic model. In summary, although these tools can be very useful for summarising and visualizing complex population genetic data, they all lack a hypothesis testing component and a formal demographic model, which results in inference that is open to subjective interpretation of individual researchers.

1.2.3 Methods for inferring spatial barriers to mobility

From classical population genetics and ecology it is known that reduced mobility, for example caused by geographic barriers, can increase differences in allele frequencies between populations. For pairs of populations, this has traditionally been captured by F_{ST}, the ratio of the variance of allele frequencies between sub-populations to the variance in the whole population (Wright 1949). In an ideal setting, such as Wright's infinite island model (Wright 1931) where populations are located on an infinite square lattice, F_{ST} is

directly related to the number M of migrants per generation between neighbouring populations in the lattice [$F_{ST} = 1/(1+2M)$], such that no migrants yield $F_{ST} =1$ and "infinite" migration rate (i.e. a panmictic population) yields $F_{ST} =0$.

Several tools have been developed to extend this simple principle. CircuitScape (McRae and Beier 2007; McRae et al. 2008) is commonly used in landscape population genetics to test the effect of geographic features on population connectivity. It approximates the effect of gene flow as current through an electric circuit, where nodes are placed on a lattice (corresponding to geographic locations) and neighbouring nodes in the lattice are connected with wires with different conductivity. F_{ST} values between pairs of populations correspond to pairwise voltage measurements in the circuit. By solving the corresponding electrostatic equations, the program estimates gene flow along all paths. Recently, this tool was used to estimate different routes during the initial colonisation of Australia (Malaspinas et al. 2016).

Pagani et al. (2016) developed a simple analytical technique, based on Gaussian kernel interpolation, to directly quantify barriers to gene flow by quantifying spatial gradients in allele frequencies. They applied it to human whole genomes across Eurasia and found evidence for major mountain ranges and deserts as barriers to human gene flow. Petkova et al. (2016) introduced EEMS (Estimated Effective Migration Surfaces), a tool based on computational geometry designed to deal with spatially irregular patterns of data. Space is represented as a polygon that is automatically subdivided into triangles. Each of the triangles is associated with a local movement rate that is constant within the triangle. Finally, the method uses classical population genetics theory to find movement rates that corresponds to observed pairwise differences in allele frequencies among samples. Although these methods were originally applied to data from present-day populations (Pagani et al. 2016; Petkova et al. 2016), Mathieson et al. (2018) also applied the method to ancient DNA data by ignoring the heterogeneous ages of the ancient samples.

In summary, approaches commonly used to infer past levels of mobility and population structure rely on population differentiation for inference and explicitly or implicitly assume that the observed genetic differences between samples can be represented as a function of the geographical separation between them. However, in case of ancient DNA, genetic distances between sample-pairs depend not only sample proximity in space but also on their separation in time. Therefore, analyses that do not explicitly account for this,

set themselves up for being confounded by the underlying effects of time to the observed genetic distances and lose out on the valuable information contained in the temporal separation of samples.

In Chapter 2, I address this problem by developing an extension to the F_{ST} measure that unifies spatial and temporal distances into a single metric and show that this metric directly informs on past levels of mobility. I apply this method to genome-wide capture data from a large set of sparsely distributed ancient Europeans, temporally ranging from late Upper Palaeolithic to Iron Age.

1.3 Methods for inferring population histories

I argued above that methods such as PCA, Admixture or FineStructure are descriptive and narratives based purely on such results do not constitute a formal analysis of population history. In order to achieve robust demographic inference, alternative hypotheses need to be formulated as different demographic scenarios. The likelihood of different demographic scenarios can then be formally compared by calculating the probability of observing the data given each scenario.

In order to understand the properties of modern methods for inference of past population dynamics, and some of their weaknesses, it is useful to review the fundamental concept of population in population genetics: Conceptually, population genetic models treat populations as taxa (or lineages) within a taxonomic framework, in that they are distinct, homogenous entities, with a history that can be represented as a tree where branch points represent splits between ancient populations, and leaves of the tree are extant or archaeological populations for which samples are available.

Several methods of varying degree of complexity exist for constructing the phylogenetic tree representing the joint history of populations. Here, I will review the approaches most commonly used in the ancient DNA literature, as an exhaustive enumeration of all population genetic modelling methods would be beyond the scope of this thesis.

A class of methods are built on so-called *F*-statistics (Reich et al. 2009; reviewed in Patterson et al. 2012 in further detail), and have been used extensively in the ancient DNA literature to test hypotheses of the relationship between ancient and modern populations. These statistics rely on classical population genetics view of a population and use the assumption that genetic drift occurs independently in each population, i.e. on each branch

of the tree. The F_2 statistic measures the amount of drift along both lineages since the divergence from a shared ancestral population in the tree. The F_3 statistic measures the amount of shared drift between two pairs of samples relative to an out-group population. Subsequently, the F_3 statistic is often used to identify modern populations that are most similar to a given ancient sample. The F_4 statistic estimates the amount of shared drift between pairs of populations: If the shared drift is zero, the two pairs of populations must belong to different parts of the tree (i.e. separated by a more ancestral node in the tree). This principle can be used to test hypotheses of different ancestral tree topologies as explanations for the observed data.

Frameworks such as TreeMix (Pritchard et al. 2000), AdmixtureGraph (Patterson et al. 2012) and qpGraph (Castelo and Roverato 2012) build on this principle to construct taxonomic trees, using genome wide data and bootstrap analysis to assess the significance of population splits. However, although ancestral populations are internal to the tree, there is no systematic time scale: branch lengths reflect the amount of drift in a population, which depend on both time and population size (genetic drift is stronger in small populations than in large ones). Thus, in these graphs, only the leaves are real populations (or samples) for which geographic and temporal locations are known. The internal nodes of the tree, corresponding to ancestral populations with unknown geographic and temporal location, and are often referred to as "ghost populations" as they have no real-world correspondence, although DNA can provide some geographic information about these nodes and, therefore, add some resolution to the inference.

The F_4 statistic, and the related D statistic (the F_4 statistic divided by a positive scale factor that makes the D statistic have a range between -1 and 1), can also be used to detect gene flow between populations (Reich et al. 2009), or hybridisation between species (Green et al. 2010). In the frameworks that build on these statistics, such as TreeMix, AdmixtureGraph and qpGraph, gene flow between different branches are represented as instantaneous admixture events between pairs of populations (because of this, it is not possible to distinguish protracted gene flow from sudden admixture in these frameworks).

In summary, although the statistics allow quantification of the likelihood of different tree typologies and therefore evolutionary relationship between populations, it is often difficult to reconstruct past population histories with any detail because the inferred trees lack any geographical or temporal information. Furthermore, the statistics are influenced

by a large number of potentially confounding factors (such as geographic structure and population size changes through time). As a result, demographic inference based on these statistics is relatively qualitative and open to subjective interpretation of different researchers.

For single, isolated populations, coalescent theory provides a unique relationship between the size of a population through time and the distribution of time to the most recent common ancestor for pairs of sequences. As described earlier in this chapter, recombination means that individuals carry records of their population's past population size in their genomes. Li and Durbin (2011) developed PSMC (Pairwise Sequentially Markovian Coalescent) approach to implement this principle and reconstruct a detailed history of population size from a single genome sequence of sufficient depth to resolve heterozygote sites. However, in order to translate the analysis to real time and numbers of individuals, the mutation rates needs to be known.

This approach has been further refined and extended by Sheehan et al. (2013) and Schiffels and Durbin (2014) to additionally infer the history of gene flow between pairs of populations. However, the need for whole genome high-quality data means that this approach is often not available for analysis of ancient samples. A notable exception is Fu et al. (2014) who applied PSMC to a high-quality sample from Ust-Ishim to estimate mutation rate in the human genome by measuring how much, in units of genetic mutations, the population history of the ancient sample needs to be shifted to line up with the history of modern samples from the same region.

Several computationally intensive methods have been developed to estimate demographic parameters of past populations from sequence data (e.g. IMa (Hey and Nielsen 2007), fastsimcoal2 (Excoffier et al. 2013) and G-PhoCS (Gronau et al. 2011)) or allele frequency data (e.g. dadi (Gutenkunst et al. 2009)). These methods can estimate population sizes, gene flow between different branches in the population tree and, if the mutation rate is known, date of divergence between populations.

However, none of these methods have been explicitly tailored to ancient DNA analysis, and when ancient and modern genomes are combined in the same analysis, the branches leading to the ancient samples normally end up with artificially small effective population

size to reflect the shorter time available for drift to act (Slatkin 2016). This introduces a model bias that can affect testing of hypothesised demographic scenarios.

Explicit modelling of past samples offers a way around this problem. Rasmussen et al. (2014) introduced a maximum likelihood based test for whether an ancient sample can be considered directly ancestral to a given modern sample. This test is based on coalescent theory, and does not require modelling of population size changes. However, it does assume a model of a clean split between the ancient sample and the ancestral population of the modern sample, with no gene flow between the two populations following the separation. Posth et al. (2016) introduced a temporally explicit coalescent model of the history of late Pleistocene populations in Europe based on the mitochondrial tree of directly dated individuals. The combination of a powerful maximum likelihood framework and samples from both before and after the last glacial maximum allowed them to test the hypothesis of population turnover during this time period.

Even with temporally explicit modelling, a key obstacle for interpreting the genetic history of past populations is that the inferred ancestral populations, similar to the "ghost populations" discussed above, lack well-defined geographic locations. Thus, even though these populations can sometimes be placed in time, it is challenging to compare the inferred demographic history to the geographically explicit archaeological record. Overcoming this problem requires demographic models to be spatially as well as temporally explicit, with geographically well-defined subpopulations. Such simulation methods make assumptions explicit, and can accommodate very complex demographic scenarios. Crucially, they can also incorporate information from various sources (e.g. climatic and geographic information, and archaeological or linguistic data). However, the explicit nature of such models make them represent very specific demographic scenarios, therefore care must be taken that all plausible scenarios are represented in the analysis. Despite their flexibility and theoretical advantages, only relatively few studies have so far used spatially explicit models to reconstruct demographic history due to the fact that such simulation approaches can be complicated to set up and computationally demanding to perform. Early studies used linear steppingstone models to represent founder effects during the expansion of Anatomically Modern Humans out of Africa (Ramachandran et al. 2005; Liu et al. 2006) and the levels of shared genetic variation between humans and Neanderthals (Eriksson and Manica 2012). Warmuth et al. (2012) used a spatially explicit

model of Eurasia to infer the origin and timing of horse domestication. The SPLATCHE2 framework (Ray et al. 2010) uses a two-dimensional spatially explicit model, which has been used to study interbreeding between humans and Neanderthals (Currat and Excoffier 2011). Eriksson et al. (2012) used a global spatial model to link late Pleistocene human demography to climate, and this model was later used to test the hypothesis of whether Eskimo-Inuit populations in the Arctic derive from the same population as the original founders of Native American populations (Raghavan et al. 2015).

The complex relationships between populations in such models typically mean that formal likelihoods cannot be calculated analytically, but can be estimated by comparing descriptive statistics of simulated and observed data using the Approximate Bayesian Computation (ABC) (Rosenberg and Nordborg 2002; Sunnåker et al. 2013). Thus, unless parameters can be constrained using independent data (e.g. historical or archaeological information), it is usually necessary to consider a very large number of value combinations for each parameter in order to make reliable inferences about past, adding to the computational cost.

In summary, for robust demographic inference using ancient DNA, approaches need to be able to accommodate geographically and temporally sparse data, different demographic scenarios need to be explicitly tested and in order to take full advantage of time and geo-stamped genetic variation data, both geographical and temporal information should formally be included in the analyses (see Table 1.1 for a comparison of these properties for the different methods discussed in this section). In Chapter 3, I present a spatially and temporally explicit framework for reconstructing the demographic history of Grey Wolves (*Canis Lupus*) across the Northern Hemisphere during the Late Pleistocene and the Holocene using whole mitochondrial genomes from samples spanning the last 50,000 years. I use ABC to formally compare the goodness of fit of different demographic scenarios put forward in the literature in order to explain genetic relationships between extant Grey Wolf populations across the Northern hemisphere and changes to Grey Wolf morphology seen in the archaeological record over the studied time period.

Inference Technique	**A**	**B**	**C**	**D**	**E**
Inference based on phylogeographic trees	YES	YES	NO	YES	NO
Descriptive methods for inferring population structure					
Principal Component Analysis (PCA)	NO	NO	NO	NO	NO
STRUCTURE (Pritchard et al. 2000)	NO	NO	NO	YES	NO
ADMIXTURE (Alexander et al. 2009)	NO	NO	NO	YES	NO
Finestructure (Lawson et al. 2012)	NO	NO	NO	YES	NO
Chromopainter (Lawson et al. 2012)	NO	NO	NO	YES	NO
F_{ST}	NO	NO	NO	YES	NO
CircuitScape (McRae and Beier 2007; McRae et al. 2008)	NO	NO	YES	YES	NO
Pagani et al. (2016)	NO	NO	YES	YES	NO
EEMS (Petkova et al.(2016)	NO	NO	YES	YES	NO
Loog et al. (2017)	YES	YES	YES	YES	NO
Methods for inferring population histories					
F-statistics (F2, F3, F4 & D statistic) (Reich et al. 2009)	NO	NO	NO	YES	YES
TreeMix (Pritchard et al. 2000)	NO	NO	NO	YES	YES
AdmixtureGraph (Patterson et al. 2012)	NO	NO	NO	YES	YES
qpGraph (Castelo and Roverato 2012)	NO	NO	NO	YES	YES
PSMC (Li and Durbin 2011)	YES	YES	NO	YES	YES
Sheehan et al. (2013)	YES	YES	NO	YES	YES
MSMC (Schiffels and Durbin 2014)	YES	YES	NO	YES	YES
FastSimCoal2 (Excoffier et al. 2013)	YES	YES	YES*	YES	YES
G-PhoCS (Gronau et al. 2011))	YES	YES	NO	YES	YES
dadi (Gutenkunst et al. 2009)	YES	NO	NO	YES	YES
Rasmussen et al. (2014)	YES	NO	NO	YES	YES
Posth et al. (2016)	YES	YES	NO	YES	YES
SPLATCHE2 (Ray et al. 2010)	YES	NO	YES	YES	YES
Eriksson et al. (2012)	YES	NO	YES	YES	YES
Raghavan et al. (2015)	YES	YES	YES	YES	YES
Ramachandran et al.(2005)	YES	NO	YES	YES	YES
Eriksson and Manica (2012)	YES	YES	YES	YES	YES
Warmuth et al. (2012)	YES	NO	YES	YES	YES

Table 1.1: Comparison of approaches for demographic inference. Columns **A**-**E** are: **A** Allows temporally explicit inference. **B** Explicitly uses temporal distribution of samples. **C** Explicitly uses temporal distribution of sample and allows spatially explicit inference. **D** Allows formal hypothesis testing. **E** Allows population genetic model testing.

* Provided that space is explicitly used to set up relationships between populations

1.4 Methods for inferring genetic selection

Genetic selection encompasses a wide variety of processes that cause a genetic variant to be preferentially passed down the next generation as a consequence of the phenotypic effects of the variant (Sabeti et al. 2002) and how these affect survival and mate choice in a population. Positive selection is of great interest to researchers as it is the primary mechanism for adaptation and is therefore key to understanding the evolutionary history of past populations.

A number of tools have been developed to detect past selection from modern genomic data that exploit the characteristic signals left by selection at the target loci and genomic areas surrounding it. These tools typically rely on allele frequency spectra, haplotype structure or population differentiation for identifying signatures of past selective sweeps and use summary statistics to compare the observed patterns of variation to expectations under the null-hypothesis of neutrality (Vitti et al. 2013).

Genetic selection can operate at different time scales. At the longest time scale, of millions of years, selection can be detected by studying the accumulation of non-synonymous changes at protein coding sites relative to synonymous changes by comparing to closely related taxa (McDonald and Kreitman 1991). However, except in extremely rapidly evolving organisms, such as viruses and some fungi and bacteria, these methods normally lack the power to detect more recent selection as mutations happen at a rate too slow to generate detectable patterns at this scale.

A number of methods have been designed to specifically detect recent, strong selection, usually within populations of the same taxa (further reviewed in Vitti et al. 2013). These methods rely on the observation that selection on a novel advantageous allele appearing on a given chromosome copy shapes genetic variation around the selected locus in characteristic ways. As genetic variants at that locus are replaced by the advantageous mutation, a primary consequence of such selection is a loss of diversity in the vicinity of the selected locus. Consequently, the region becomes characterised by an excess of low-frequency (rare) genetic variants. This phenomenon is often quantified using the Tajima's *D* statistic (Tajima 1989). If selection is present only in some populations, the effect of selection will also generate genetic differences between populations. These can be

detected using statistics such as F_{ST} and the Population Branch Statistic (PBS, Yi et al. 2010), which measures the amount of drift on a branch in a population tree leading down to the focal population. Extensions to this principle, using multiple outgroups, allow estimating selection in interior branches in the population tree (e.g. LSD (Librado et al. 2018)).

A different approach for detecting past selection using present-day samples relies on the observation that a novel selected allele will be physically linked to genetic variants in close proximity on the same chromosome. As the selection causes the selected variant to rise in frequency, the linked genetic variants will spread with it though the population. This phenomenon is often referred to as genetic hitchhiking, which results in a pattern of unusually long haplotypes surrounding the selected locus shared between individuals on the population. Extended Haplotype Homozygosity (EHH) (Sabeti et al. 2002) and integrated Haplotype Score (iHS) (Voight et al. 2006) are commonly used methods that rely on this principle.

Genome-wide selection scans on large quantities of modern data have identified a number of loci under recent selection in human and other animal populations, many of which have been experimentally validated in functional studies on animal models or cell cultures. However, as a result of low mutation and recombination rate in the nuclear DNA, modern genetic data has poor temporal resolution when it comes to reconstructing the timing of very recent selective sweeps (i.e. within the last ten thousand years). This results in little power to estimate the strength of past selective sweeps and also makes it difficult to link past episodes of selection to its drivers.

Ancient DNA data allows researchers to measure and quantify changes in allele frequencies though time and, therefore, directly study selection as well as its timing and strength. Until recently, such time series data was only available for model and laboratory organisms with short generation times and whose environments could be artificially modified and monitored within an experiment. The advances in ancient DNA techniques have made such data available from a wide range of extant and extinct species, allowing for direct study of allele frequency change through time. Furthermore, novel archaeological and historical finds, as well as increasingly accurate climate reconstructions, have created an opportunity to study the potential drivers of past selection in greater detail than ever before. However, in order to link past events with

genetic selection, it is necessary to have precise reconstructions of changes in allele frequencies through time.

Although ancient DNA contains the information needed for more detailed and accurate reconstruction of these processes, inferences from ancient DNA typically suffer from challenges such as: 1) small sample sizes compared to modern DNA studies, 2) samples typically occur sparsely and unevenly through time, and may have uncertain dates, and 3) confounding effects of demography, especially gene flow from an external genetically differentiated source such as an ancestral wild species or a population from different geographic location. As a result, it is not possible to directly observe the true underlying allele frequencies, and there is a need for a statistical modelling in order to take the effect of background demography as well as sample sparseness and age uncertainty explicitly into account.

In the past decade, several approaches have been developed to infer genetic selection from ancient DNA. One straightforward way to utilize information from ancient DNA is to obtain a sufficiently large amount of data from a single time slice or compress data from different time points into a single approximate time slice. Subsequently, the probability of observing differences in allele frequencies between any two time slices (e.g. the ancient and the modern period) can be calculated by simulating hypothetical differences in allele frequency under neutrality (the null-model) and different selection coefficients. This approach, however, requires relatively large number of sufficiently contemporaneous samples, often not attainable in archaeological context, or sacrifice power to detect the strength and type of selection that occurred.

A large number of methods for inferring selection from ancient DNA data fit models of selection to time-series of allele frequency data by maximizing the likelihood of the data given the underlying allele frequency trajectory through time. The advantage of using time-series data over data from single time points (or slices) is that it allows determining the allele frequency trajectory more precisely. This allows not only for more accurate estimation of selection parameters but also estimating the mode of selection with greater precision. The methods differ in how they represent this trajectory, in what kind selection can be represented, and in what demographic factors are taken into account.

The simplest way to infer the action of natural selection is to treat it as a deterministic process. In this population genetics model, the allele frequency trajectory is modelled as an ordinary differential equation and can be calculated numerically by knowing the initial frequency and the strength of selection. However, this approach ignores the process of genetic drift, i.e. that in relatively small populations allele frequencies can fluctuate between generations due to stochasticity in the population dynamics (e.g. individual mate choice and survival) and, thus, it is possible that the observed allele frequencies change are purely a result of chance. Several approaches have focused on explicitly incorporating the stochastic component when modelling the allele frequency trajectory. These methods typically rely on diffusion approximations of the underlying Wright-Fisher model of selection and genetic drift (Wright 1931). Bollback et al. (2008) provided the first implementation of this using ancient DNA. They took advantage of a partial differential equation that approximates the Wright-Fisher model and described the evolution of the allele frequency distribution in the population. They calculate the probabilities of the observed sample allele frequencies by numerically solving this equation. This approach allows for estimation of strength of additive selection and effective population size while accounting for genetic drift. Later methods have extended and built upon this approach. The work by Malaspinas et al. (2012) added a recessive selection model and a method to estimate the age of the allele under selection, assuming that the strength of selection was constant since the beneficial mutation emerged. This selection model has further been generalized to arbitrary degrees of dominance (e.g. Steinrücken et al. 2014). In a recent paper, Schraiber et al. (2016) used a different approach. Rather than working with allele frequency distributions and the corresponding partial differential equation, they worked with the equivalent stochastic differential equation describing individual allele frequency trajectories, and presented a search algorithm for efficiently sampling the space of trajectories that best describe the data. In addition to a general diploid selection model and estimation of the age of the selected allele, they allowed population size to vary between different time periods.

Additionally, several methods have been developed that are specifically suited to study evolution at an experimental setting where selection is strong and drift is minimal (e.g. Feder et al. 2014; Lacerda and Seoighe 2014).

All of these methods, however, assume that selection is acting in a single panmictic (freely mixing) population. In reality, this limits their applicability as most natural populations are structured. In structured populations the allele frequencies can vary between subpopulations, and often differences in allele frequencies increase with increasing geographic distance between the sub-populations (a pattern of genetic differences often called "isolation-by-distance"). Therefore, gene flow between populations can lead to changes in allele frequencies within subpopulations that mimic the effect of natural selection in an isolated population. As a result, it may be vital to account for the effects of gene flow between subpopulations when inferring the effect of natural selection. Using the same inference framework as the above described approaches, (Mathieson and McVean 2013) developed a model to infer selection in metapopulations (a group of populations connected by gene flow), assuming steady population sizes and constant gene flow between subpopulations. This method was applied to human pigmentation and height data from Holocene Europe (Mathieson et al. 2015). Although this approach explicitly accounts for background gene flow and allows for different selection coefficients in different subpopulations, similarly to the other approaches discussed above it assumes the strength of selection is constant through time. Therefore, it is best suited to inference about closely related populations over short time periods where gene flow and selection can be assumed to be constant but not in situations where gene flow is known to have been episodic and where selection strength is likely to vary through time. In case of humans and many domestic animals (the key targets of many ancient DNA studies to date), this is likely to be the case as selection pressures can dramatically fluctuate even over short time scales in response to changes in cultural and behavioural practices. See Table 1.2 for a comparison of properties for the different methods for inferring past selection discussed in this section.

In Chapter 4, I present a Bayesian statistical framework for quantifying the timing and strength of selection using ancient DNA data. This framework explicitly addresses the issues of uneven sampling through time and uncertainties in sample dating as well as formally accounts for the confounding effects of episodic gene flow. I apply this method to ancient genotype data from two loci in European domestic chickens spanning the last 2500 years.

Methods for inferring genetic selection	A	B	C	D	E	F
Tajima's *D*	NO	NO[§]	NO	NO	NO	WITHIN
F^{ST}	NO	NO[§]	NO	NO	NO	BETWEEN
Population Branch Statistic (PBS) (Yi et al. 2010)	NO	NO[§]	NO	NO	NO	BETWEEN
LSD (Librado et al. 2018)	NO	NO[§]	NO	NO	NO	BETWEEN
EHH (Sabeti et al. 2002)	NO	NO[§]	NO	NO	NO	WITHIN
iHS (Voight et al. 2006)	NO	NO[§]	NO	NO	NO	WITHIN
XP-EHH (Sabeti et al. 2007)	NO	NO[§]	NO	NO	NO	BETWEEN
Bollback et al. (2008)	YES	YES	NO	YES	NO	WITHIN
Malaspinas et al. (2012)	YES	YES	NO	YES	YES*	WITHIN
Steinrücken et al. (2014)	YES	YES	NO	YES	YES*	WITHIN
Schraiber et al. (2016)	YES	YES	NO	YES	YES*	WITHIN
Feder et al. (2014)	YES	YES	NO	YES	NO	WITHIN
Mathieson and McVean (2013)	YES	YES	YES	YES	NO	WITHIN
Approach described in Loog et al. (2017)	YES	NO	YES	YES	YES	WITHIN

Table 1.2: Comparison of approaches for inferring genetic selection. Columns **A**-**F** are: **A** Explicitly uses temporal distribution of samples and allows temporally explicit inference. **B** Explicitly models genetic drift. **C** Incorporates population structure/gene flow. **D** Estimates strength of selection. **E** Estimates the starting time of selection. **F** Inference based within or between Populations

[§]The effect of drift is assumed to be reflected in the genome wide distribution of the statistic.

***** Starting time assumed to equal to age of the allele.

Chapter 2: Estimating Mobility Using Sparse Data: Application to Human Genetic Variation

This work was published in 2017 in the Proceedings of the National Academy of Sciences of the United States of America (PNAS) 114(46):12213-12218.

2.1 Annex to Chapter 2: Statement of my contribution

Original idea and design of research

I generated the idea behind the article and planned the research together with Professor M.G. Thomas.

Method development

I developed the code for the calculation of the statistic under the supervision of Prof M. G. Thomas. I participated in development of the simulation code, performed the simulations and analyses of the simulation output data.

Method application and statistical analysis

I designed the method application. I curated the ancient human dataset and performed the analysis on the data. I developed the code for calculating and performed uncertainty estimates.

Manuscript

I wrote the manuscript and generated all the tables and figures with input from Professor M. G. Thomas and A. Eriksson.

2.2 List of authors and affiliations

Liisa Loog[1,2,3,4*], Marta Mirazón Lahr[5], Mirna Kovacevic[1,6], Andrea Manica[3], Anders Eriksson[7], Mark G Thomas[1*]

[*]Corresponding authors: liisaloog@gmail.com (L.L.), m.thomas@ucl.ac.uk (M.G.T)

Affiliations

1. Research Department of Genetics, Evolution and Environment, University College London, Gower Street, London WC1E 6BT, UK.
2. Research Laboratory for Archaeology & the History of Art, University of Oxford, Dyson Perrins Building, South Parks Road, Oxford OX1 3QY, UK
3. Department of Zoology, University of Cambridge, Downing Street, Cambridge CB2 3EJ, UK.
4. Manchester Institute of Biotechnology, School of Earth and Environmental Sciences, University of Manchester, Manchester, M1 7DN, UK
5. Leverhulme Centre for Human Evolutionary Studies, Department of Archaeology & Anthropology, University of Cambridge, Cambridge CB2 1QH, UK
6. Centre for Mathematics and Physics in the Life Sciences and Experimental Biology, University College London, Physics Building, Gower Street, London WC1E 6BT, UK
7. Department of Medical & Molecular Genetics, King's College London, Guys Hospital, London SE1 9RT, UK.

2.3 Abstract

Mobility is one of the most important processes shaping spatio-temporal patterns of variation in genetic, morphological and cultural traits. However, current approaches for inferring past migration episodes in the fields of archaeology and population genetics lack either temporal resolution or formal quantification of the underlying mobility, are poorly suited to spatially and temporally sparsely sampled data, and permit only limited systematic comparison between different time periods or geographic regions. Here we present a new estimator of past mobility that addresses these issues by explicitly linking trait differentiation in space and time. We demonstrate the efficacy of this estimator using spatiotemporally explicit simulations and apply it to a large set of ancient genomic data from Western Eurasia. We identify a sequence of changes in human mobility from the Late Pleistocene to the Iron Age. We find that mobility among European Holocene farmers was significantly higher than among European hunter-gatherers both pre- and postdating the Last Glacial Maximum. We also infer that this Holocene rise in mobility occurred in at least three distinct stages: the first centering on the well-known population expansion at the beginning of the Neolithic, and the second and third centering on the beginning of the Bronze Age and the late Iron Age, respectively. These findings suggest a strong link between technological change and human mobility in Holocene Western Eurasia and demonstrate the utility of this framework for exploring changes in mobility through space and time.

2.4 Significance statement

Migratory activity is a critical factor in shaping processes of biological and cultural change through time. We introduce a new method to estimate changes in underlying migratory activity that can be applied to genetic, morphological or cultural data, and is well-suited to samples that are sparsely distributed in space and through time. By applying this method to ancient genome data we infer a number of changes in human mobility in Western Eurasia, including higher mobility in pre- than post-Last Glacial Maximum hunter-gatherers, and oscillations in Holocene mobility with peaks centering on the Neolithic transition, the beginnings of the Bronze Age and the Late Iron Age.

2.5 Introduction

One of the major goals of population history inference is to assess the role played by past mobility in shaping patterns of genetic, phenotypic and cultural variation. It is well recognized that the past movement of people shapes geographic patterns of genetic variation (Hanski and Gilpin 1991) and the subsequent ecological and evolutionary properties of populations (Lande 1988). This is due to the fact that gene flow changes allele frequencies, shapes genetic drift, and can affect (Itan et al. 2009) or even mimic (Klopfstein et al. 2006) natural selection processes. It is also recognized that migration activity can influence cultural evolutionary processes (Powell et al. 2009; Kline and Boyd 2010). However, despite the general agreement that mobility has played an important role in shaping past and present patterns of genetic, phenotypic and cultural variation among humans, relatively little is known about its temporal and geographic variation in the past (Cox and Hammer 2010).

Inferring past mobility is challenged by the sparseness and unevenness of sampling in time and space. As a result, studies of prehistorical mobility are typically limited to descriptive approaches, where major attested migration episodes or events are used as a proxy for general mobility. Data sources such as stable isotopes have enabled some quantification of mobility by allowing researchers to identify individuals within an archaeological community who have migrated into a region during their lifetime (e.g. (Gregoricka 2013). The underlying logic behind this approach is that differences between isotope ratios – particularly strontium – within organisms reflect the isotope ratios acquired from the local environment (as a result of variation in underlying geology) (Makarewicz and Sealy 2015). However, it is challenging to extrapolate within-community mobility rates to migration rates across larger geographic regions or over long time periods. Furthermore, isoscapes are still often poorly characterized, and isotope ratios can be relatively constant over large areas (Bowen 2010; Makarewicz and Sealy 2015), and so are not always informative.

Most standard population genetic tools used for quantifying population structure, such as ADMIXTURE analysis (Pickrell and Pritchard 2012), *f*-statistics (Patterson et al. 2012), and TREEMIX (Pickrell and Pritchard 2012) are poorly suited for estimating underlying mobility change through time. In classical population genetic analysis, estimators of migration rates between hypothesized sub-populations have been developed, including

statistics such as F_{ST} (Wright 1990). Some of these statistics have also been applied to large sets of quantitative trait data, such as variation in craniometric morphology (e.g (Relethford 1994; Betti et al. 2010). However, such statistics quantify differentiation among a set of contemporaneous samples, and only inform on migration rates under idealized demographic scenarios – such as gene flow between discrete sub-populations – and are also influenced by other factors, such as subpopulation split times and population size fluctuations. Furthermore, these estimators reflect past migration between hypothesized sub-populations over large periods of time, and therefore lack temporal resolution. Some researchers interpret the estimated ages and geographic distribution of clades on a phylogenetic tree of uniparental genetic systems (mtDNA or the Y chromosome) as proxies for the rate of spread of populations (e.g. (Underhill and Kivisild 2007). However, such approaches do not permit a formal quantification of mobility and have been criticized as a tool for demographic inference (Goldstein and Chikhi 2002; Nielsen and Beaumont 2009; Pinhasi et al. 2012).

Thus, existing methods allow us to identify migration episodes to some extent, but lack the temporal resolution and formal quantification of underlying mobility, are poorly suited to spatially and temporarily sparsely sampled data, and do not permit systematic comparison between different time periods or geographic regions. To overcome these problems, we present a new estimator of past mobility that is particularly suited to sparsely distributed morphological, cultural or genetic variation data, and provide a first application to a large set of genome-wide data from ancient individuals from across Western Eurasia. We define mobility as the average distance moved by entities in a given time period.

2.6 Estimating past migration rates

Under a general model of identity-by-descent with modification and isolation by distance (Wright 1943; Nei 1972), trait (genetic, morphological or cultural) differences between any two entities (individuals or populations) increase monotonically as a function of both the temporal and spatial distance between them. We therefore expect that trait differences between entities correlate with temporal as well as spatial distances. However, the extent to which spatial and temporal differences explain observed trait variation depends on the level of spatial population structure, and therefore on the level of mobility. If mobility was low (i.e. strong spatial structure) then we would expect differences between entities

to be more strongly correlated with space, relative to time, while if mobility was high we would expect time to explain a relatively larger proportion of differences between entities (because of the homogenizing effects of high mobility across space).

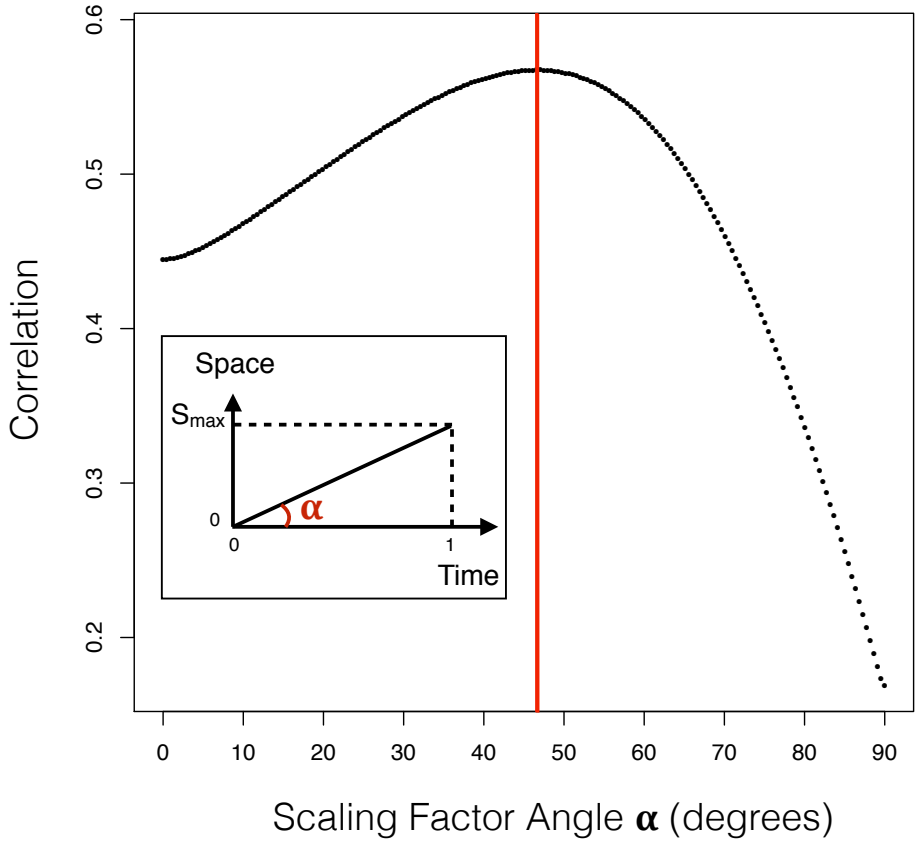

Fig. 2.1: Illustration of the principle of maximum time-space correlation. The black dots show a typical dependence of the correlation between genetic and time-space distances on the scaling factor angle α (in degrees). Here space alone (α =0) is a better predictor of genetic differences than time alone (α =90), but the best predictor (highest correlation) is found at an intermediate angle, indicated by the vertical red line. Inset: Geometrical interpretation of the Scaling Factor (S_{max}) as an angle (α).

Given that both spatial and temporal distances are expected to correlate with trait differences among entities, a matrix combining both spatial and temporal distance information should give a stronger correlation than either matrix alone (extra correlation, EC). However, since spatial and temporal distances are measured in different units (e.g. km and years), combining them requires a scaling factor (S). Here, we show that the scaling factor value (S_{max}) that maximizes the correlation between a trait difference matrix and a Euclidian distance matrix combining the spatial and temporal distance matrices provides an estimator of mobility over the period and region covered by the data (Fig. 2.1, see Materials and Methods). For convenience, we use a geometric interpretation of the scaling factor S_{max} as an angle, α, in the plane defined by the spatial and temporal distances ($\alpha = \text{atan}(S_{max})$, illustrated in the inset of Fig. 2.1; see Materials and Methods).

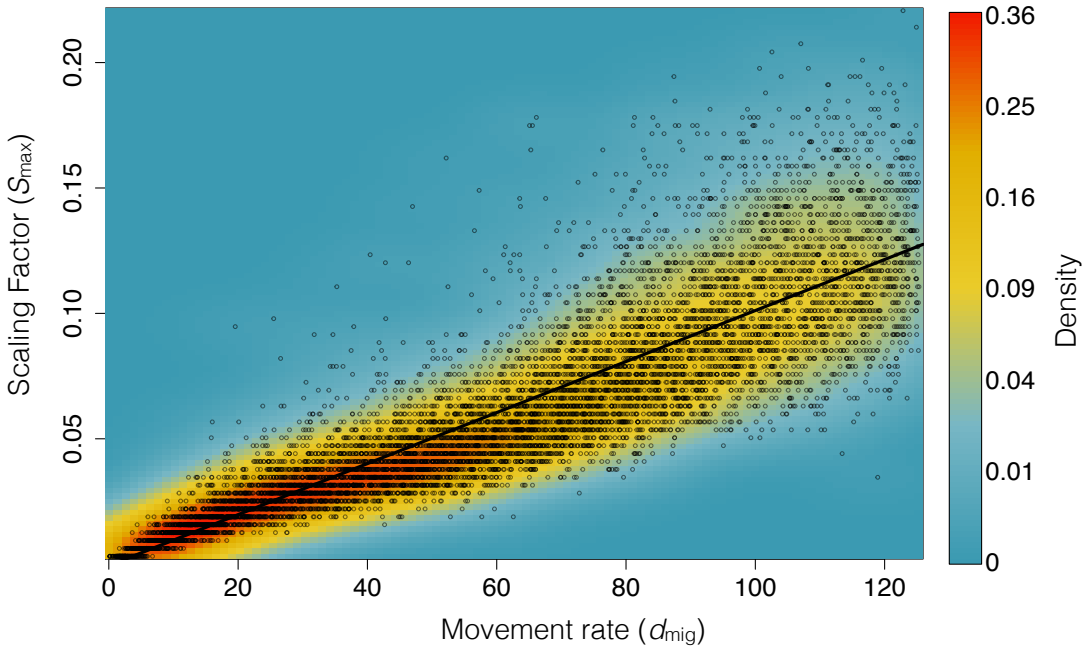

Fig. 2.2: Correlation between simulated movement rate (d_{mig}) and estimated scaling factor (S_{max}). Each black circle represents a single simulation. The colors correspond to the density of circles (see the color scale bar). The black line shows the best linear fit between d_{mig} and S_{max} ($R^2 = 0.8$), demonstrating that the scaling factor captures the underlying mobility in the simulated world.

To test the reliability and the robustness of S_{max} in recovering information about past mobility, we simulated data under a spatio-temporally explicit two-dimensional model, which includes simple population dynamics with population growth, density dependence and mobility (modeled as a Gaussian random walk) and generated variation data under different mobility parameter values (see Materials and Methods). We assessed the ability of S_{max} to infer simulated mobility values by correlation across simulations. We found a strong, positive linear relationship between the simulated average migration distance (i.e. mobility) and values of S_{max} (Fig. 2.2, $R^2 = 0.8$), thus demonstrating the utility of this statistic as an estimator for relative mobility. However, for this result to hold it is important that the trait differences are generated under an approximately constant mutation rate and vary neutrally within a population.

2.7 Migration rates among Pleistocene hunter-gathers and early farmers

Recent advances in sequencing technologies have allowed genomic data retrieval from a large sample of past individuals (e.g. (Allentoft et al. 2015; Haak et al. 2015; Mathieson et al. 2015; Fu et al. 2016; Lazaridis et al. 2016). Although these studies have not explicitly quantified underlying mobility in the past they have suggested several periods of large-scale population turnover in Western Eurasia.

Given that the S_{max} statistic is able to recover information on past mobility in simulated data, we applied the method to a sample (N = 329) of previously published genome-wide genotype data covering a time period from the beginning of the Upper Palaeolithic to the Iron Age to explore changes in past human mobility in Western Eurasia (see Materials and Methods). We also constructed non-parametric confidence intervals to account for date and sampling uncertainty, and estimated p-values for the S_{max} statistic by permutation under the null hypothesis of no isolation by distance in space and time, which allowed us to quantify the robustness of our estimates and identify time periods during which data are too sparse for the S_{max} statistic to be informative (see Material and Methods). First, we explored the extent to which mobility differed between pre- and post-Last Glacial Maximum (LGM) hunter-gatherers (Fig. 2.3). We found the average (median) mobility rates to be higher (α =18.1; 95% CI: 14.9–87.7; p = 0.08) among pre-LGM hunter-gatherers temporally ranging from 37,000 to 26,000 years ago compared to post-LGM hunter-gatherers (α =9.9; 95% CI: 9.5–10.9; p = 0.03), temporally ranging from 19,000 to 5,000 years ago. We also estimated mobility rates for Holocene farmers, temporally

ranging from 10,000 to 1,000 years ago and found even higher values (α =34.8; 95% CI: 33.9 – 35.3; $p < 0.0001$) than for both hunter-gatherer groups (see Table 2.S2 for full results).

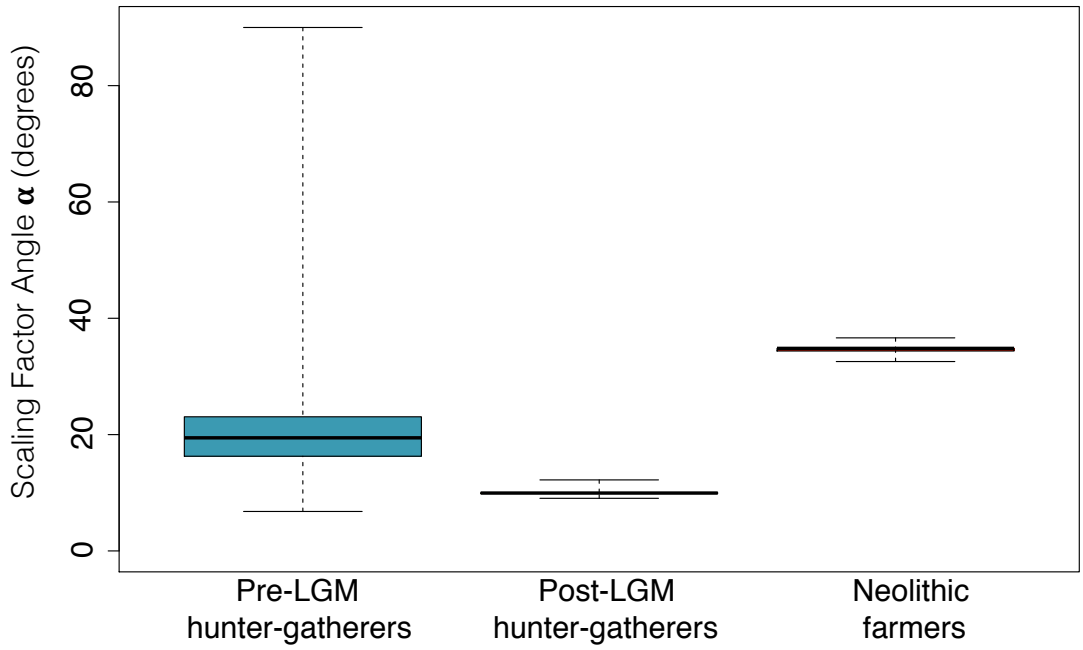

Fig. 2.3: Boxplot showing the mobility rate estimates (from jackknifing and date resampling) among pre-LGM hunter-gatherers temporally ranging from 37,000 to 26,000 years ago (N = 19), post LGM hunter-gatherers temporally ranging from 19,000 to 5,000 years ago (N = 47) and Holocene farmers temporally ranging from 10,000 to 1,000 years ago (N= 263). The black solid lines are the medians of the distributions. The boxes represent the interquartile ranges and the whiskers show the spans of the distributions.

Because Holocene western Eurasia is particularly well sampled for ancient genomic DNA, we performed a sliding window analysis to explore changes in mobility over the last 14,000 years in more detail (Fig. 2.4), using 4,000 year-wide windows to ensure sufficient temporal signal within each window. We inferred a reduction in mobility rate between 14,000 and 9,000 years ago, prior to the start of the Neolithic transition (Fig. 2.4a). However, throughout most of this period the p-values are not significant (see Fig. 2.4b). Because of the small sample size in the windows covering this time period (Fig. 2.4c) there is no significant correlation between genetic and temporal distances, and as a result we do not observe any extra correlation, and so lack power to estimate mobility (see Materials and Methods and Fig. 2.S3). We consequently treat the inferred decline in mobility in this time range with caution. Second, we infer a substantial increase in mobility centered on the beginning of the Neolithic, with a peak centered around 7,500 years ago (Fig. 2.4a). Notably, the inferred mobility rate does not remain at this level throughout the Holocene. Instead, we infer a Late Neolithic drop in mobility before a second increase centered on the beginning of the Bronze Age, around 5,000 years ago, then a decline in the Late Bronze Age and Early Iron Age, before a final increase centered on the Late Iron Age (Fig. 2.4a and Table 2.S3 for full results for each window).

To validate the efficacy of our method to identify changes in migration rate on the time scales found in the empirical dataset (Fig. 2.4), we modified our simulations to represent a population experiencing two changes in migration rate, resulting in three episodes of constant migration rate. We observe a good correspondence between changes in S_{max} and the simulated migration rate (Fig. 2.S4), supporting our interpretation of the empirical results in Fig. 2.4.

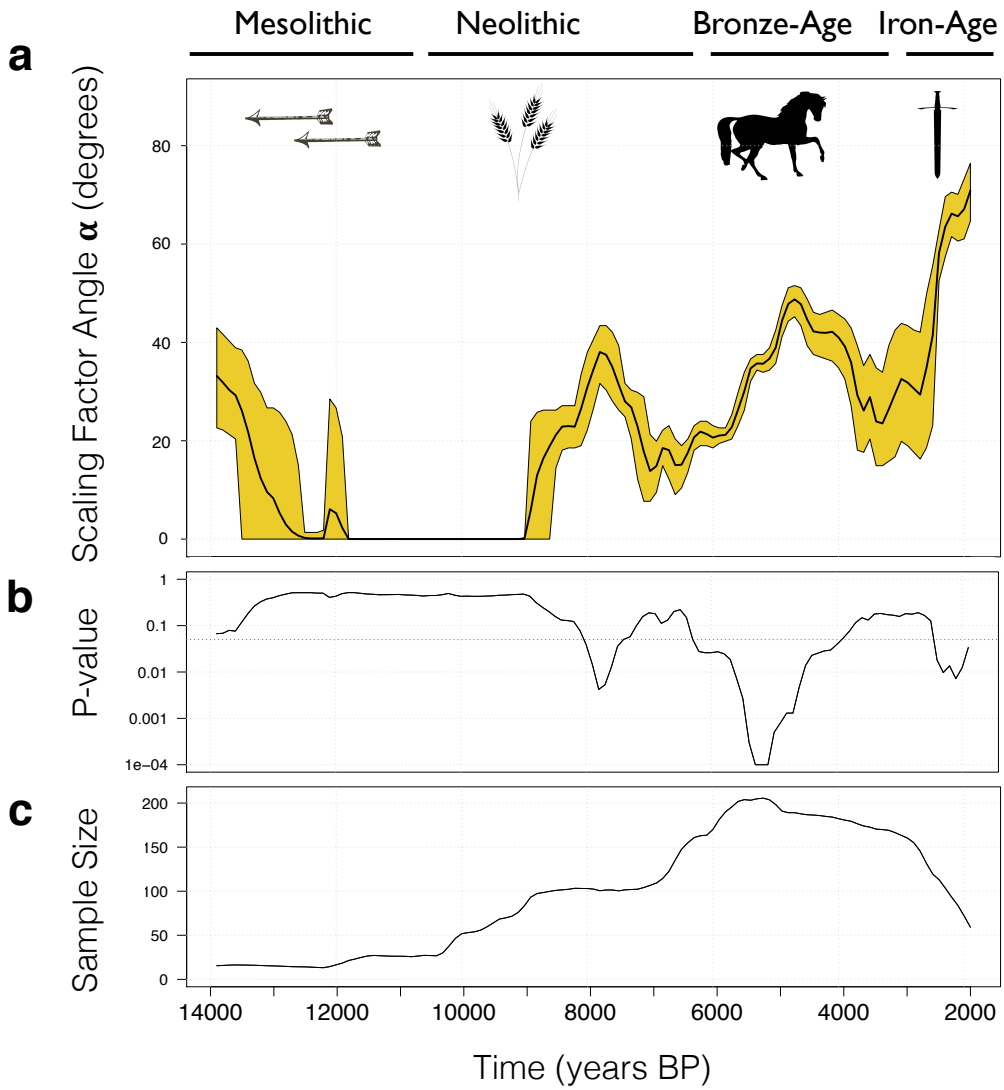

Fig. 2.4: Estimation of mobility through time from empirical data. (a) Relative mobility rate estimates in Western Eurasia over the last 14,000 years, using a 4,000 year sliding window (121 windows). The solid black line represents the mean α value from 10,000 date resampled iterations; The colored area represent the 95% confidence intervals of the jackknife distribution. (b) p-values for each 4,000 year window under the null-hypothesis of no Extra Correlation (EC), constructed by calculating the proportion of permuted datasets where the calculated EC value was as high or higher than the average EC value from the empirical dataset (see Material and Methods). The red dotted line represents the level above which 5% or more of the permuted datasets result in EC values as high or higher than the empirical dataset. (c) Sample size for each 4,000 year windows, averaged over 10,000 date resampled iterations.

Finally, we compare the performance of the S_{max} statistic to a simple Isolation By Distance (IBD) though time approach, where (the slope of) the linear relation between the genetic distances and geographic distances is used as an indicator of the level of past migratory activity: High levels of migration corresponds to shallow IBD patterns. We observe a trend of decreasing spatial structure, consistent with the cumulative effects of a series of high migratory activity episodes over this period. However, this approach fails to recover the timing of those changes in migratory activity in specific periods (Fig. 2.S5). Our method overcomes this lack of power to identify changes in migratory activity by explicitly considering the temporal dimension of the data.

2.8 Discussion

Through spatio-temporally explicit simulations, we have shown that the S_{max} statistic can be used as a reliable proxy for the underlying relative mobility of individuals within a given time period and geographic region. Because our statistic is based on correlations, it is well suited for analyzing data from archeological and palaeontological contexts, where preservation can vary significantly across different geographical areas and temporal ranges, and samples are commonly sparsely distributed across space and time. Nevertheless, in the extreme case of just a small number of sites from different geographic locations or temporal periods, spurious estimates of migratory activity may arise. The permutation procedure introduced in this study can be used to identify when the S_{max} estimator is uninformative. We choose only to consider relative changes in the value of the S_{max} estimator and do not attempt to interpret its values in absolute terms. This is because, whilst our intuition is that mutation rate and population size will not affect the relationship between absolute values of the S_{max} estimator and the true mobility rate, we admit the possibility that other factors may. Selection in response to ecological and environmental factors could also reduce the utility of the S_{max} statistic as a proxy for mobility because local selection can create confounding spatial or temporal population structure. However, this is a common problem for any analysis assuming neutral evolution, and can be dealt with by focusing on putatively neutrally varying traits or loci.

The S_{max} statistic offers a robust alternative to existing methods for the quantification of isolation by distance patterns in temporally heterogeneous datasets. In population genetics, correlations between trait differences and geographic distances are commonly used to infer past population structure and connectivity between populations (Manel et

al. 2003). In such approaches, temporal structure in data is usually either ignored or mathematically controlled for by using partial least squares (e.g. (Reyes-Centeno et al. 2014), but both of these practices have been criticized (Depaulis et al. 2009; Guillot and Rousset 2013; Skoglund, Sjödin, et al. 2014), and we show that while such approaches can inform on the cumulative effects of migration in terms of structure reduction, they are unable to recover temporal changes in migratory activity. Partial least squares analysis assumes that the effect of time on genetic differences can be decoupled from the effect of space, which is generally not the case. We avoid this problem by integrating space and time into a single distance measure. Finally, because the statistic contains information about both spatial and temporal structuring of the populations, it can be used as a potentially informative summary statistic in quantitative model fitting frameworks such as Approximate Bayesian Computation (Beaumont et al. 2002).

Using the S_{max} statistic on ancient genomic data, we identified a sequence of changes in human mobility from the late Pleistocene to the Iron Age in western Eurasia. We find some support for reduced mobility in west Eurasian post-LGM hunter-gatherers compared to pre-LGM populations. The reasons for this result are, as yet, unclear, although possible explanations include reduced resource availability in Pre-LGM Western Eurasia, requiring larger foraging ranges compared to Post-LGM conditions (Foley and Lahr 2001; Collard* and Foley 2002) and/or residual post-LGM population structure following recolonization of northern latitudes from LGM southern refugia (Miller 2012). Using a sliding window analysis, we find some suggestion of a decline in post-LGM hunter-gatherer mobility leading up to the Neolithic transition. However, we caution against over-interpretation of this result as the estimated p-values for the S_{max} statistic under the null hypothesis of no EC are mostly not significant. We find strong support for a rise in mobility during the Neolithic transition in western Eurasia, likely corresponding to a well-established demic expansion of farmers, originating in the Middle East and resulting in the spread of farming technologies throughout most of Western Eurasia (Menozzi et al. 1978; Skoglund et al. 2012; Hofmanová et al. 2016). This is followed by an inferred mobility decline towards the end of the Neolithic, possibly related to the terminal phase of the spread of farming across most of Western Eurasia, and increased sedentism (Bocquet-Appel et al. 2009; Isern and Fort 2012). We also find strong support for a rise in mobility centered on the onset of the Bronze Age. From

previous ancient DNA studies, this period has been associated with large-scale migration of Eurasian steppe populations, particularly those related to the Yamnaya culture, into Central and Northern Europe (Allentoft et al. 2015; Haak et al. 2015). However, the emergence of the first civilizations and the concomitant establishment of far reaching trade networks, as well as technological innovations such as horse-based transport (Warmuth et al. 2012), could also contribute to this increase in mobility (Warmuth et al. 2013). Finally, our sliding window analysis indicates a mobility reduction centered on the Late Bronze Age and Early Iron Age, starting around 3,000 years ago, before a final increase centered on the Late Iron Age in Western Eurasia (Fig. 2.4a). One possible explanation for this pattern is a significant increase in trade and warfare during that period (Sherratt and Sherratt 1993; Collis 2003; Beaujard 2010). Overall, our analysis suggests a strong link between technological change and human mobility in Holocene Western Eurasia. However, it should be noted that we have used wide windows (4,000 years), which necessarily reduces chronological resolution.

A major strength of our method is its applicability to any set of neutrally evolving heritable traits where differences between individuals can be quantified and increase monotonically with geographic distance and temporal difference. This means that, in principle, the S_{max} statistics could allow the quantification of migratory activity in temporal and environmental contexts where obtaining ancient genetic data is not feasible, by using phenotypic data such as variation in cranial morphology, which has been shown to fit the pattern of neutral evolution and closely follow the patterns observed in analyses of neutral genetic data in humans (Roseman and Weaver 2007; von Cramon-Taubadel and Weaver 2009). Another exciting possibility is the quantification of movement based on cultural variation data, provided that appropriate near-neutral traits are used (e.g. (Shennan 2000; Eerkens and Lipo 2007; Lycett and Norton 2010). Whilst it should not be assumed that the movement of artefacts always coincides with that of people, contrasting measures of movement based on genetics and cultural artefacts obtained under the same conceptual framework would allow quantification of demic vs cultural diffusion processes. This might permit identification periods and regions where genetic, phenotypic and cultural processes are coupled, or decoupled. Given its robustness and flexibility, we anticipate that the S_{max} estimator will be applicable to a wide range of

genetic, phenotypic, and cultural traits, allowing the quantification of mobility in a wide variety of scenarios in which this type of analysis has previously been challenging.

2.9 Materials and Methods

The proposed migration rate estimator, $S_{max,}$, is the value of a scaling factor combining spatial and temporal distance matrices into a single distance matrix that maximizes its correlation with a matrix of trait distances. In order to estimate that value, the geographical, temporal and trait distance matrices are calculated as described below.

2.9.1 Geographic, temporal and trait distances

The geographic distance between all sample pairs was calculated in kilometers using the Haversine Formula (Sinnott 1984) to account for the curvature of the Earth as follows:

$$G_{ij} = 2r \arcsin\left(\sqrt{\sin\left((\varphi_j - \varphi_i)/2\right)^2 + \cos(\varphi_i)\cos(\varphi_j)\sin\left((\lambda_i - \lambda_j)/2\right)^2}\right) \text{ (Eq. 2.1)}$$

Where G is the distance in kilometers between individuals i and j; φ_i and φ_j are the latitude coordinates of individuals i and j, respectively; λ_i and λ_j are the longitude coordinates of individuals i and j, respectively; and r is the radius of the earth in kilometres.

Temporal distances between samples were calculated as time in years between sample pairs. Previously reported date ranges based on stratigraphy or direct radiocarbon dating were used for all individuals (See Table 2.S1). In all analyses, sample dates were randomly drawn from a uniform distribution corresponding to the upper and lower bounds of a time period for a given specimen.

Genetic distances were calculated as pairwise proportion of alleles that are not identical by state (pairwise heterozygosity), using the function *ibs.dist* from the Bioconductor package *SNPstats* v.1.18.0 (Clayton 2014) in the R statistical analysis environment v3.2.2 (R Core Team 2015).

2.9.2 The S_{max} Estimator

In order to consider the full range of scaling factors on a finite interval, we choose to represent S as the tangent of an angle α between 0 and 90 degrees, where $\alpha = 0$ corresponds to $S = 0$ (geographic variation alone explains the observed trait distances between entities) and $\alpha = \pi/2$ corresponds to $S = \infty$ (temporal variation alone explains the

observed trait distances between entities). Formally, the time-space product matrix (D) was calculated as follows:

$$D_{ij} = \sqrt{G_{ij}^2 + \left(ST_{ij}\right)^2} \quad \text{(Eq. 2.2)}$$

where i and j are the specimens considered, D is the time-space product matrix, G is the geographical distance matrix, T the temporal distance matrix (given by the difference in age of the samples); and S is the scaling factor ($S = \tan(\alpha)$).

To find the scaling factor, S_{max}, that maximizes the correlation between the trait distance matrix and D, the time-space product matrix, we calculated the Pearson correlation coefficient between these matrices for 200 (500 for the simulated data) scaling factor values (see Fig. 2.1). The scaling factor value in the time-space product matrix that produced the strongest correlation with the trait distance matrix is recorded as S_{max}, the mobility estimator.

2.9.3 Simulation tests

The reliability and the robustness of the S_{max} statistic in recovering information about past mobility was explored using a spatiotemporally explicit simulation model. The simulation world consists of a grid of 8000 by 8000 demes. Each simulation starts with one entity placed in a randomly chosen deme, and lasts 20,000 generations. The model simulated exponential population growth to a carrying capacity of 10,000 entities, followed by a stochastic birth-death process (54), mobility and trait mutation. We generated spatiotemporal trait variation data under different mobility parameter values using the same S_{max} estimation protocols as described above for each data set. 10,000 independent replicates of the simulations and analyses were generated, and the utility of the S_{max} statistic in recovering information about mobility was assessed by correlation.

The migratory process was modeled as Gaussian random walks: In each generation each entity moves independently in the x and y directions by distances picked randomly from a normal distribution with mean = 0 and standard deviation = σ_{mig}. This corresponds to the average distance moved in a single step (d_{mig}) of $\sqrt{\pi/2}\ \sigma_{mig} = 1.2533\ \sigma_{mig}$. Thus, d_{mig} is the parameter of interest. We choose 1,000 random values of d_{mig} from a uniform distribution with range 1 to 100. We modelled drift as a Moran-type birth-death process (Moran 1958). At each generation each entity undergoes binary fission with probability

p = 0.1, creating a duplicate of itself at the same location. The two entities subsequently move and evolve independent of each other. When the number of entities reaches or exceeds the carrying capacity (10,000), excess entities are deleted at random among all entities present in that generation. Mutation was modelled as a one-dimensional Gaussian random walk for each trait (N_{traits} = 50). Each trait was assigned an initial value of 1000 and new (mutated) values picked from a random normal distribution with mean equal to the current value and standard deviation fixed at 0.05

Following a burn-in period of 10,000 generations, entities were sampled from simulations with a probability of 0.00001 at each generation. The x and y coordinates, time of sampling in generations and the values for the 50 traits were recorded for all sampled entities.

Pairwise trait distances between all sampled entities in each of the simulated datasets were calculated using the Euclidean distance formula as follows:

$$M_{ij} = \sqrt{\sum_{k=1}^{n} \left(d_{ik} - d_{jk}\right)^2} \qquad \text{(Eq. 2.3)}$$

Where, M_{ij} is the distance between the two entities i and j; d_{ik} and d_{jk} are the values of the trait k for individuals i and j respectively, and n is the number of recorded traits.

Out of 10,000 simulations 9866 (98.66%) resulted in extra correlation greater than zero. In order to match the simulated data with the empirical data we filtered the simulated data based on the measured EC values and removed all simulations that produced an EC value smaller than 0.001. This resulted in 9155 simulations being used in the correlation analysis.

In order to assess the reliability of the S_{max} statistic in recovering information about mobility, R^2 values were calculated for the correlation between the simulated d_{mig} values and their corresponding S_{max} values.

2.9.4 Human mobility in late Pleistocene and Holocene.

We considered genome-wide data comprising 354,199 SNPs typed in 329 West Eurasian (i.e. west of the Ural mountains) individuals (see supplementary Fig. 2.1) temporally ranging from approximately 39,000 to 1,000 years before present see supplementary Fig. 2.2). We merged the overlapping SNPs typed in archaeological samples published in

(Keller et al. 2012; Gamba et al. 2014; Lazaridis et al. 2014; Olalde et al. 2014; Seguin-Orlando et al. 2014; Skoglund, Malmström, et al. 2014; Allentoft et al. 2015; Haak et al. 2015; Jones et al. 2015; Mathieson et al. 2015; Fu et al. 2016; Lazaridis et al. 2016) (see supplementary Table S1 for list of samples and references) that met the geographic and temporal criteria described above. No additional bioinformatic processing of the data was carried out for this study.

The 329 individuals were assigned to one of following three groups based on their estimated age, and subsistence strategy based on their archaeological context: Pre-LGM hunter-gathers N = 19 (temporally ranging from 39,000 years BP to 26,000 years BP); post-LGM hunter-gathers N= 47, temporally ranging from 19,000 years BP to 5,000 years BP; and Holocene farmers N = 263, temporally ranging from 10,000 years BP to 500 years BP.

Sliding window analysis was performed on all individuals in the dataset postdating 16,000 years B.P. The $S_{\max}$ statistic was estimated for 121 overlapping 4,000 year windows, each differing by 100 years.

To take age uncertainty into account, we report the mean scaling factor angle from 10,000 replicates with sample dates randomly resampled from their age ranges. 95% confidence intervals were estimate through a jackknifing procedure in which a randomly chosen sample in each window was removed from analysis, and the 0.025 and 0.095 quantiles were calculated from the resulting distribution.

To estimate the Isolation By Distance (IBD) signal through time we fitted a linear model of genetic distances as a function of geographic distances in each time window (with sample jackknifing and age resampling as before, using the *lm* function from the R package *base* version 3.2.2. (R Core Team 2015)), and reported the slope of the line.

2.9.5 Confidence intervals and robustness of S_{max} estimator

We tested the assumption that there is an isolation by distance pattern by correlating the genetic (trait) distance matrices in all time-bins and in all windows with the respective geographic distance matrices and the date-resampled temporal distance matrices and calculated the p-values for these correlations. We find a positive and statistically significant isolation by distance pattern in space in all windows (Fig. 2.S3a and 2.S3b, respectively and Fig. 2.S6). The isolation by temporal distance pattern is positive and

significant for most windows, but some windows show negative correlations or are not significant. We find that these windows correspond to time periods where we observe low extra correlation (Fig. 2.S3c) and also low p-values for the extra correlation (Fig. 2.4b).

To account for the uncertainty in sample ages we calculated the scaling factor angle 10,000 times using dates resampled at random from a uniform distribution for each sample, as described above, and report the average of the scaling factor angle of the given distribution as a point estimate.

We also performed a leave-one-out analysis (10,000 replicates, combined with sample date resampling) to explore the combined effect of sampling and dating uncertainty, and constructed approximate equal-tailed 95% confidence intervals for all groups and windows.

To assess the statistical significance of S_{max} estimates we consider the extra correlation (EC); defined as the Pearson correlation coefficient between the trait difference matrix and the time-space product matrix when $S = S_{max}$, minus the Pearson correlation coefficient between the trait difference matrix and either the temporal or geographical distance matrix alone, whichever is higher.

To obtain a null-distribution of EC, we permuted trait data for individuals among the spatiotemporal sample locations 10,000 times and calculated EC for each permutation, as described above. Finally, we calculate the proportion of EC values from the permuted datasets that are equally high or higher than that obtained from the observed data. This permutation test permits assessment of how frequently the extra correlation (EC) for the observed data is produced by chance alone or, alternatively, as the result of method used for estimating the S_{max} statistic. The resultant p-value is the probability of observing an equally high or higher EC value in permuted, supposedly signal-less data, and provides an indication of the information content of each dataset.

2.9.6 Simulated scenario of changing migration rate

We modified our simulations to represent a population experiencing two changes in migration rate, resulting in three episodes of constant migration rate. We assumed a generation time of 25 years and chose the effective population size to be $2N_e = 10{,}000$, standard figures in population genetic models of European populations (Gronau et al.

2011). We next chose three levels of migration with relative magnitude on par with what was inferred from the empirical data: m_1=0.0002, m_2=0.01, m_3=0.05. To ensure equilibrium conditions during the start of the sampling period, we discarded the first 10,000 steps of the simulation (using migration rate m_1). We then simulated a time period of 20,000 years, divided into three episodes with constant migration rate: m_1 for 25,000-15,000 years ago, m_2 for 15,000-10,000 years ago and m_3 for the last 5,000 years of the simulation. This roughly corresponds to the time spans associated with Mesolithic hunter-gatherers, Neolithic farmers, and post-Neolithic cultures in our empirical data set. From a population genetic point of view, whole genome data as used in the empirical estimates correspond to a large number of approximately independent replicates. Because our model does not include recombination, we accounted for this effect by increasing the sample size to 10,000 individuals. Fig. 2.S4 shows the migration rate estimation using the S_{max} statistic using a 4,000 year wide sliding window.

R version 3.2.2 (R Core Team 2015) was used for analyses throughout this manuscript. The correlations between temporal, geographic and trait distance matrices were calculated using the *mantel* (method = "pearson") function in R package *Vegan* version 2.3.0 (Oksanen et al. 2015). The permutation and bootstrap tests were performed using the function *sample* in the R package *base* version 3.2.2. (R Core Team 2015).

The R code used for analyses is available from the GitHub repository (https://github.com/LiisaLoog/SpaceTime-Framework) and upon request from the corresponding authors.

2.10 Acknowledgements

The authors are very grateful to Robert Foley for valuable discussions during the formulation of the approach, to Mike Parker-Pearson for advice on Holocene migration processes, and to Tamsin O'Connell for advice on stable isotopes. L.L was supported by Natural Environment Research Council, UK (grant numbers NE/K005243/1, NE/K003259/1) and European Research Council grant (339941-ADAPT). M.G.T. was supported by Wellcome Trust Senior Investigator Award (grant number 100719/Z/12/Z) and Leverhulme Trust (grant number RP2011-R-045). A.M. & A.E. were supported by a European Research Council Consolidator grant (grant number 647787-LocalAdaptation). M.M.L. was supported by a European Research Council Advanced grant (grant number 295907, In-Africa). M.K. was funded by the Engineering and Physical Sciences Research

Council (EPSRC) through the Centre for Mathematics and Physics in the Life Sciences and Experimental Biology (CoMPLEX).

2.11 Bibliography

Allentoft ME, Sikora M, Sjögren K-G, Rasmussen S, Rasmussen M, Stenderup J, Damgaard PB, Schroeder H, Ahlström T, Vinner L, et al. 2015. Population genomics of Bronze Age Eurasia. Nature 522:167–172.

Beaujard P. 2010. From Three Possible Iron-Age World-Systems to a Single Afro-Eurasian World-System. J. World Hist. 21:1–43.

Beaumont MA, Zhang W, Balding DJ. 2002. Approximate Bayesian Computation in Population Genetics. Genetics 162:2025–2035.

Betti L, Balloux F, Hanihara T, Manica A. 2010. The relative role of drift and selection in shaping the human skull. Am. J. Phys. Anthropol. 141:76–82.

Bocquet-Appel J-P, Naji S, Linden MV, Kozlowski JK. 2009. Detection of diffusion and contact zones of early farming in Europe from the space-time distribution of 14C dates. J. Archaeol. Sci. 36:807–820.

Bowen GJ. 2010. Isoscapes: Spatial Pattern in Isotopic Biogeochemistry. Annu. Rev. Earth Planet. Sci. 38:161–187.

Clayton D. 2014. SnpStats: SnpMatrix and XSnpMatrix classes and methods. v. 1.18.0 Accessed 1/1/2017 Available from: https://www.bioconductor.org/packages/release/bioc/html/snpStats.html

Collard IF, Foley RA. 2002. Latitudinal patterns and environmental determinants of recent human cultural diversity: do humans follow biogeographical rules? Evol. Ecol. Res. 4:371–383.

Collis J. 2003. The Celts: origins, myths & inventions. Tempus

Cox MP, Hammer MF. 2010. A question of scale: Human migrations writ large and small. BMC Biol. 8:98.

von Cramon-Taubadel N, Weaver TD. 2009. Insights from a quantitative genetic approach to human morphological evolution. Evol. Anthropol. Issues News Rev. 18:237–240.

Depaulis F, Orlando L, Hänni C. 2009. Using Classical Population Genetics Tools with Heterochroneous Data: Time Matters! PLoS ONE 4:e5541.

Eerkens JW, Lipo CP. 2007. Cultural Transmission Theory and the Archaeological Record: Providing Context to Understanding Variation and Temporal Changes in Material Culture. J. Archaeol. Res. 15:239–274.

Foley RA, Lahr MM. 2001. The anthropological, demographic and ecological context of human evolutionary genetics. In: Genes, Fossils, and Behaviour: An Integrated Approach to Human Evolution. p. 258.

Fu Q, Posth C, Hajdinjak M, Petr M, Mallick S, Fernandes D, Furtwängler A, Haak W, Meyer M, Mittnik A, et al. 2016. The genetic history of Ice Age Europe. Nature 534:200–205.

Gamba C, Jones ER, Teasdale MD, McLaughlin RL, Gonzalez-Fortes G, Mattiangeli V, Domboróczki L, Kővári I, Pap I, Anders A, et al. 2014. Genome flux and stasis in a five millennium transect of European prehistory. Nat. Commun. 5:5257.

Goldstein DB, Chikhi and L. 2002. HUMAN MIGRATIONS AND POPULATION STRUCTURE: What We Know and Why it Matters. Annu. Rev. Genomics Hum. Genet. 3:129–152.

Gregoricka LA. 2013. Residential mobility and social identity in the periphery: strontium isotope analysis of archaeological tooth enamel from southeastern Arabia. J. Archaeol. Sci. 40:452–464.

Gronau I, Hubisz MJ, Gulko B, Danko CG, Siepel A. 2011. Bayesian inference of ancient human demography from individual genome sequences. Nat. Genet. 43:1031–1034.

Guillot G, Rousset F. 2013. Dismantling the Mantel tests. Methods Ecol. Evol. 4:336–344.

Haak W, Lazaridis I, Patterson N, Rohland N, Mallick S, Llamas B, Brandt G, Nordenfelt S, Harney E, Stewardson K, et al. 2015. Massive migration from the steppe was a source for Indo-European languages in Europe. Nature 522:207–211.

Hanski I, Gilpin M. 1991. Metapopulation dynamics: brief history and conceptual domain. Biol. J. Linn. Soc. 42:3–16.

Hofmanová Z, Kreutzer S, Hellenthal G, Sell C, Diekmann Y, Díez-del-Molino D, Dorp L van, López S, Kousathanas A, Link V, et al. 2016. Early farmers from across Europe directly descended from Neolithic Aegeans. Proc. Natl. Acad. Sci. 113:6886–6891.

Isern N, Fort J. 2012. Modelling the effect of Mesolithic populations on the slowdown of the Neolithic transition. J. Archaeol. Sci. 39:3671–3676.

Itan Y, Powell A, Beaumont MA, Burger J, Thomas MG. 2009. The Origins of Lactase Persistence in Europe. PLoS Comput Biol 5:e1000491.

Jones ER, Gonzalez-Fortes G, Connell S, Siska V, Eriksson A, Martiniano R, McLaughlin RL, Llorente MG, Cassidy LM, Gamba C, et al. 2015. Upper Palaeolithic genomes reveal deep roots of modern Eurasians. Nat. Commun. 6:8912.

Keller A, Graefen A, Ball M, Matzas M, Boisguerin V, Maixner F, Leidinger P, Backes C, Khairat R, Forster M, et al. 2012. New insights into the Tyrolean Iceman's origin and phenotype as inferred by whole-genome sequencing. Nat. Commun. 3:698.

Kline MA, Boyd R. 2010. Population size predicts technological complexity in Oceania. Proc. R. Soc. Lond. B Biol. Sci. 277:2559–2564.

Klopfstein S, Currat M, Excoffier L. 2006. The Fate of Mutations Surfing on the Wave of a Range Expansion. Mol. Biol. Evol. 23:482–490.

Lande R. 1988. Genetics and demography in biological conservation. Science 241:1455–1460.

Lazaridis I, Nadel D, Rollefson G, Merrett DC, Rohland N, Mallick S, Fernandes D, Novak M, Gamarra B, Sirak K, et al. 2016. Genomic insights into the origin of farming in the ancient Near East. Nature 536:419–424.

Lazaridis I, Patterson N, Mittnik A, Renaud G, Mallick S, Kirsanow K, Sudmant PH, Schraiber JG, Castellano S, Lipson M, et al. 2014. Ancient human genomes suggest three ancestral populations for present-day Europeans. Nature 513:409–413.

Lycett SJ, Norton CJ. 2010. A demographic model for Palaeolithic technological evolution: The case of East Asia and the Movius Line. Quat. Int. 211:55–65.

Makarewicz CA, Sealy J. 2015. Dietary reconstruction, mobility, and the analysis of ancient skeletal tissues: Expanding the prospects of stable isotope research in archaeology. J. Archaeol. Sci. 56:146–158.

Manel S, Schwartz MK, Luikart G, Taberlet P. 2003. Landscape genetics: combining landscape ecology and population genetics. Trends Ecol. Evol. 18:189–197.

Mathieson I, Lazaridis I, Rohland N, Mallick S, Patterson N, Roodenberg SA, Harney E, Stewardson K, Fernandes D, Novak M, et al. 2015. Genome-wide patterns of selection in 230 ancient Eurasians. Nature 528:499–503.

Menozzi P, Piazza A, Cavalli-Sforza L. 1978. Synthetic maps of human gene frequencies in Europeans. Science 201:786–792.

Miller R. 2012. Mapping the expansion of the Northwest Magdalenian. Quat. Int. 272–273:209–230.

Moran P a. P. 1958. Random processes in genetics. Math. Proc. Camb. Philos. Soc. 54:60–71.

Nei M. 1972. Genetic Distance between Populations. Am. Nat. 106:283–292.

Nielsen R, Beaumont MA. 2009. Statistical inferences in phylogeography. Mol. Ecol. 18:1034–1047.

Oksanen J, Blanchet FG, Kindt R, Legendre P, Minchin PR, O'Hara RB, Simpson GL, Solymos P, Stevens MHH, Wagner H. 2015. vegan: Community Ecology Package. Available from: http://CRAN.R-project.org/package=vegan

Olalde I, Allentoft ME, Sánchez-Quinto F, Santpere G, Chiang CWK, DeGiorgio M, Prado-Martinez J, Rodríguez JA, Rasmussen S, Quilez J, et al. 2014. Derived immune and ancestral pigmentation alleles in a 7,000-year-old Mesolithic European. Nature 507:225–228.

Patterson N, Moorjani P, Luo Y, Mallick S, Rohland N, Zhan Y, Genschoreck T, Webster T, Reich D. 2012. Ancient Admixture in Human History. Genetics 192:1065–1093.

Pickrell JK, Pritchard JK. 2012. Inference of Population Splits and Mixtures from Genome-Wide Allele Frequency Data. PLoS Genet. [Internet] 8. Available from: http://www.ncbi.nlm.nih.gov/pmc/articles/PMC3499260/

Pinhasi R, Thomas MG, Hofreiter M, Currat M, Burger J. 2012. The genetic history of Europeans. Trends Genet. 28:496–505.

Powell A, Shennan S, Thomas MG. 2009. Late Pleistocene Demography and the Appearance of Modern Human Behavior. Science 324:1298–1301.

R Core Team. 2015. R: A language and environment for statistical computing. R Foundation for Statistical Computing, Vienna, Austria. v. 3.2.2. Accessed 1/1/2017. Available from: https://www.R-project.org/

Relethford JH. 1994. Craniometric variation among modern human populations. Am. J. Phys. Anthropol. 95:53–62.

Reyes-Centeno H, Ghirotto S, Détroit F, Grimaud-Hervé D, Barbujani G, Harvati K. 2014. Genomic and cranial phenotype data support multiple modern human

dispersals from Africa and a southern route into Asia. Proc. Natl. Acad. Sci. 111:7248–7253.

Roseman CC, Weaver TD. 2007. Molecules versus morphology? Not for the human cranium. BioEssays News Rev. Mol. Cell. Dev. Biol. 29:1185–1188.

Seguin-Orlando A, Korneliussen TS, Sikora M, Malaspinas A-S, Manica A, Moltke I, Albrechtsen A, Ko A, Margaryan A, Moiseyev V, et al. 2014. Genomic structure in Europeans dating back at least 36,200 years. Science 346:1113–1118.

Shennan S. 2000. Population, Culture History, and the Dynamics of Culture Change. Curr. Anthropol. 41:811–835.

Sherratt S, Sherratt A. 1993. The growth of the Mediterranean economy in the early first millennium BC. World Archaeol. 24:361–378.

Sinnott R. 1984. Virtues of the Haversine. Sky Telesc. 68:159.

Skoglund P, Malmström H, Omrak A, Raghavan M, Valdiosera C, Günther T, Hall P, Tambets K, Parik J, Sjögren K-G, et al. 2014. Genomic Diversity and Admixture Differs for Stone-Age Scandinavian Foragers and Farmers. Science 344:747–750.

Skoglund P, Malmström H, Raghavan M, Storå J, Hall P, Willerslev E, Gilbert MTP, Götherström A, Jakobsson M. 2012. Origins and Genetic Legacy of Neolithic Farmers and Hunter-Gatherers in Europe. Science 336:466–469.

Skoglund P, Sjödin P, Skoglund T, Lascoux M, Jakobsson M. 2014. Investigating Population History Using Temporal Genetic Differentiation. Mol. Biol. Evol. 31:2516–2527.

Underhill PA, Kivisild T. 2007. Use of Y Chromosome and Mitochondrial DNA Population Structure in Tracing Human Migrations. Annu. Rev. Genet. 41:539–564.

Warmuth V, Eriksson A, Bower MA, Barker G, Barrett E, Hanks BK, Li S, Lomitashvili D, Ochir-Goryaeva M, Sizonov GV, et al. 2012. Reconstructing the origin and spread of horse domestication in the Eurasian steppe. Proc. Natl. Acad. Sci. 109:8202–8206.

Warmuth VM, Campana MG, Eriksson A, Bower M, Barker G, Manica A. 2013. Ancient trade routes shaped the genetic structure of horses in eastern Eurasia. Mol. Ecol. 22:5340–5351.

Wright S. 1943. Isolation by Distance. Genetics 28:114–138.

Wright S. 1990. Evolution in mendelian populations. Bull. Math. Biol. 52:241–295.

2.12 Permission from all co-authors to use our joint work as a contribution towards this thesis

I hereby give permission to Liisa Loog to use our joint work *"Estimating mobility using sparse data: Application to human genetic variation. Proceedings of the National Academy of Sciences (2017), 114(46), pp.12213-12218."* as contribution towards her D.Phil. thesis to be submitted for examination at Oxford University.

I confirm that to the best of my knowledge, the author contribution statement below is accurate and Liisa Loog's contribution towards the work is greater than that of any other co-author.

Article author contribution statement: M.G.T. devised the approach in discussion with M.M.L.; L.L. & M.G.T. developed the method with input from A.E.; M.K., A.E. & M.G.T. developed the simulation code with input from L.L.; L.L. performed the analyses with input from A.E. & M.G.T.; L.L., A.E. & M.G.T. wrote the paper with input from M.M.L, M.K. & A.M.

Date: 11.2.2018

Name(s): Marta Mirazón Lahr

Signature(s):

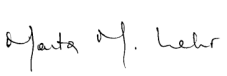

Date: 14.02.2018

Name(s): Mirna Kovacevic

Signature(s):

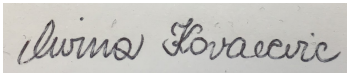

Date: 11/2/18

Name(s): Mark G Thomas (M.G.T.)

Signature(s):

Date: 12/2/18

Name(s): Andrea Manica

Signature(s):

Date: 11/2/2018

Name(s): Anders Eriksson

Signature(s):

2.S1 Supplementary figures

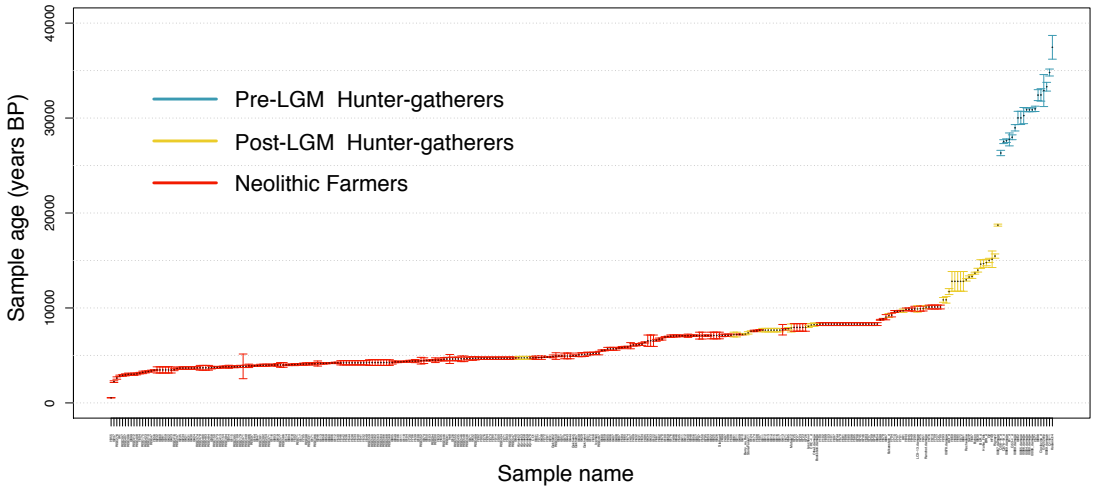

Fig. 2.S1: Sample distribution though time. Colored vertical lines represent age ranges; black dots represent mean ages for all samples; colors represent sample groups used in the analysis.

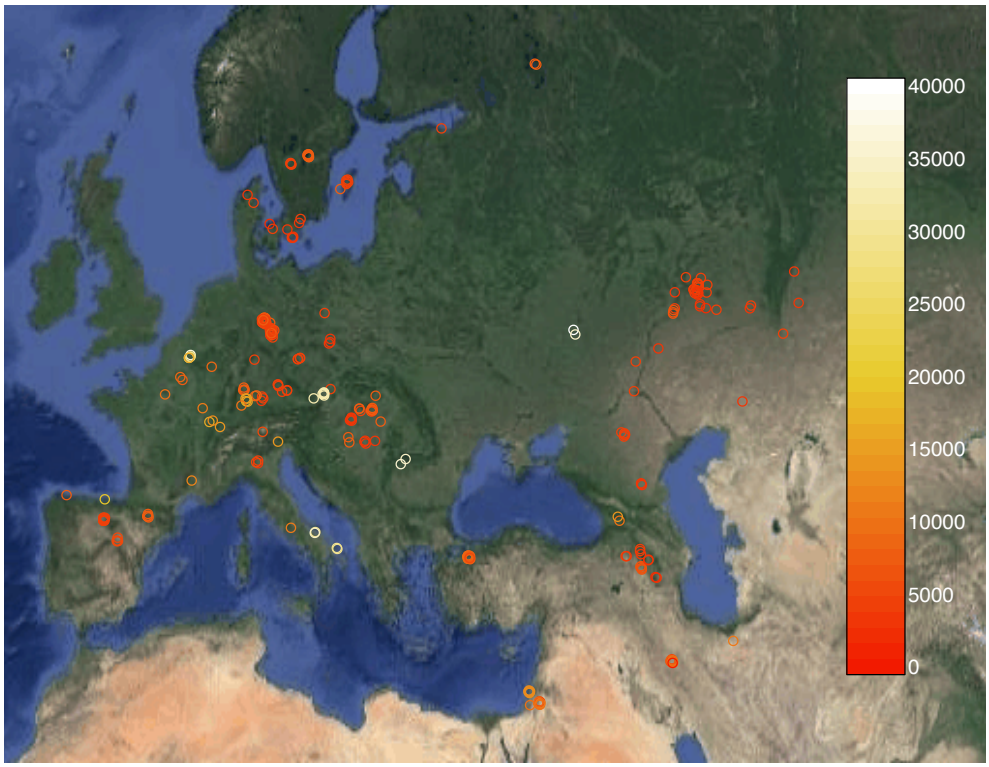

Fig. 2.S2: Sample distribution in space. The circles represent locations of samples used in the analyses. Each circle is colored by its sample age (in years cal BP), see color scale on the right.

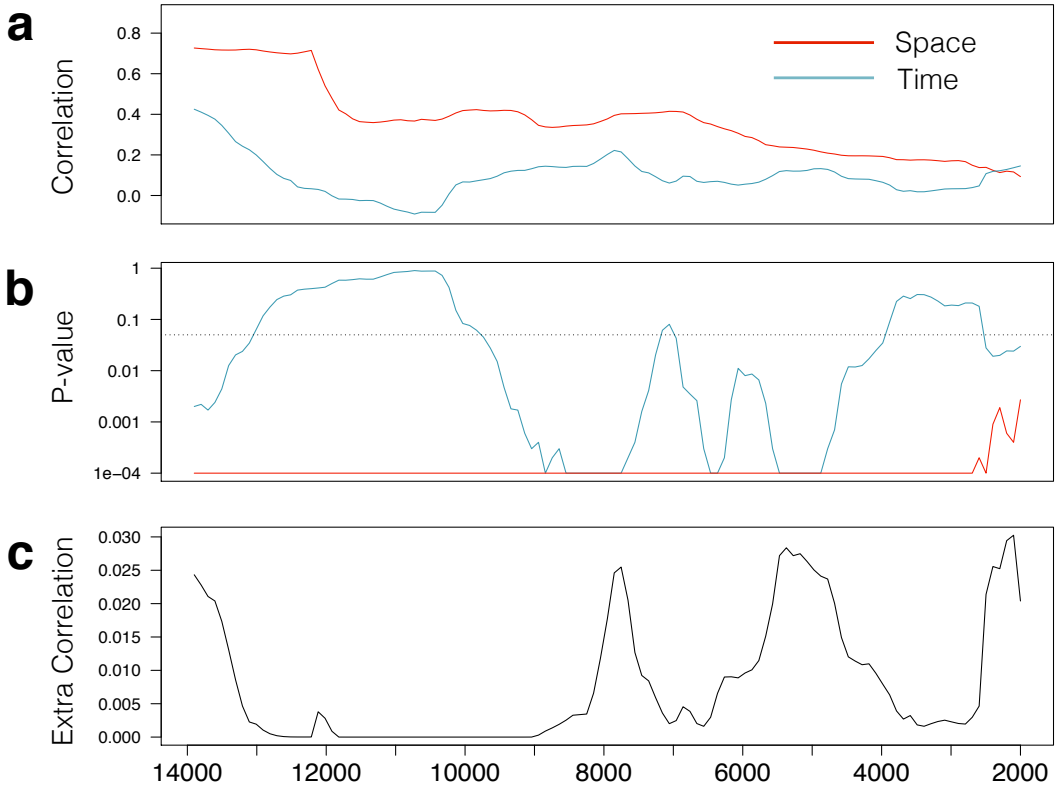

Fig. 2.S3: (a) Pearson correlation between geographic and genetic (trait) distance matrices for all windows (red line), and between temporal and genetic distance matrices (blue line). (b) The p-values for the spatial and temporal correlations in all windows. The dotted black line shows the p-value of 0.05. (c) The resulting extra correlation when spatial and temporal information is considered together.

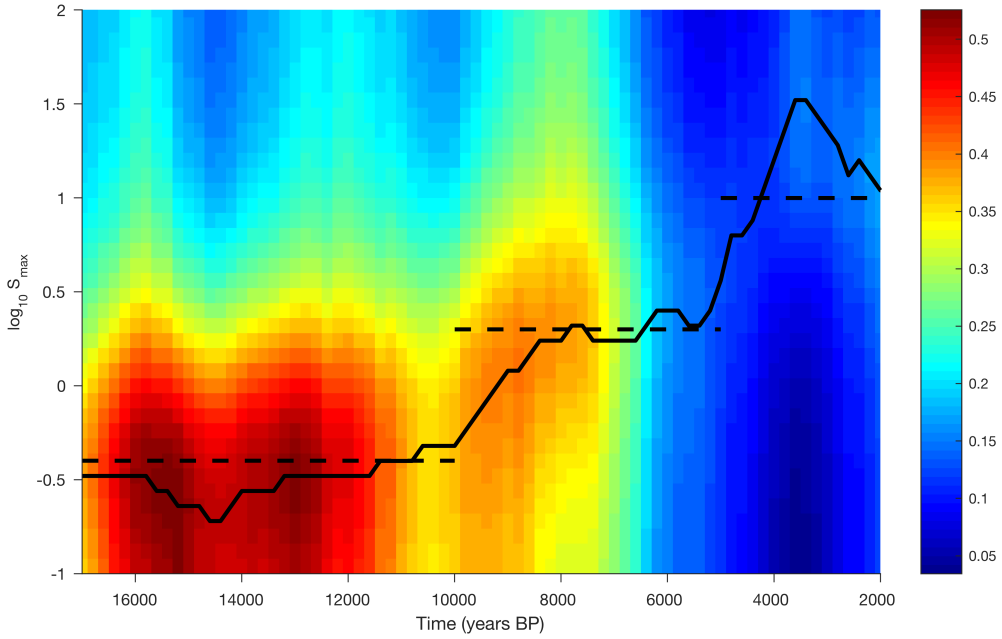

Fig. 2.S4: Sliding window analysis of simulated data (4,000 year wide windows). Colours represent the correlation between genetic and space-time distances for a given value of S_{max} (vertical axis) and time before present (BP, mid-point of window, horizontal axis). The solid line shows the estimator of S_{max} (maximum correlation), and the dashed lines shows the relative levels of migration rate used in the simulations (for clarity, the absolute level of the dashed lines were adjusted to be in line with the S_{max} in the oldest time period).

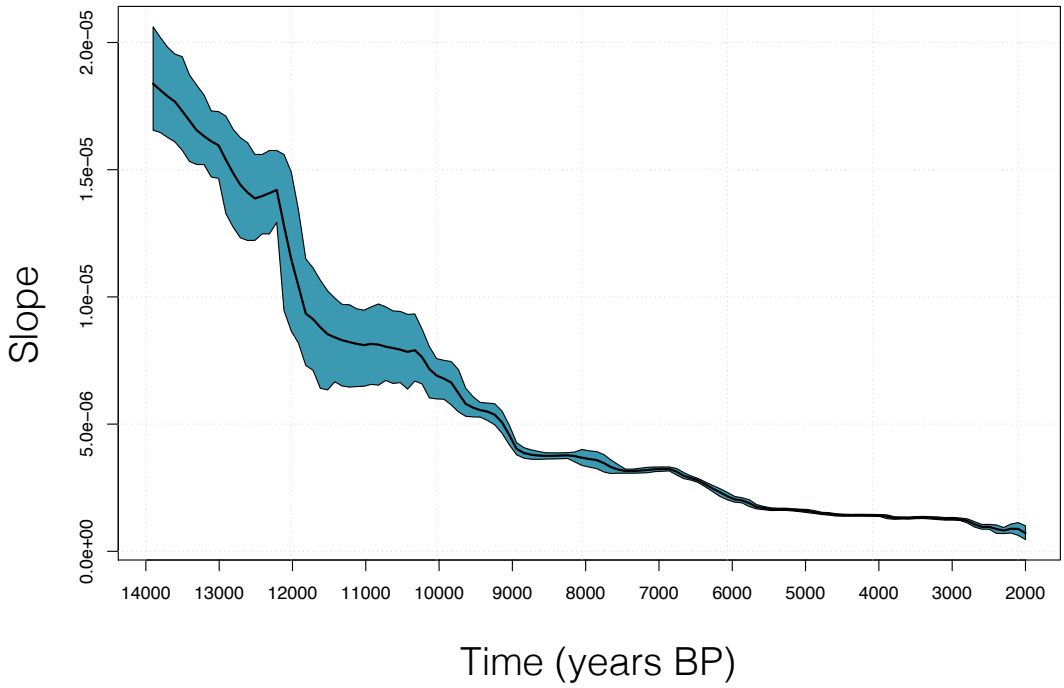

Fig. 2.S5: Isolation By Distance (IBD) pattern (slope of the linear relation between the genetic distances and geographic distances) through time in Western Eurasia over the last 14,000 years, using a 4,000-year sliding window (121 windows). The solid black line represents the mean slope from 10,000 date-resampled iterations; the blue area represents the 95% confidence intervals of the date-resampled distribution.

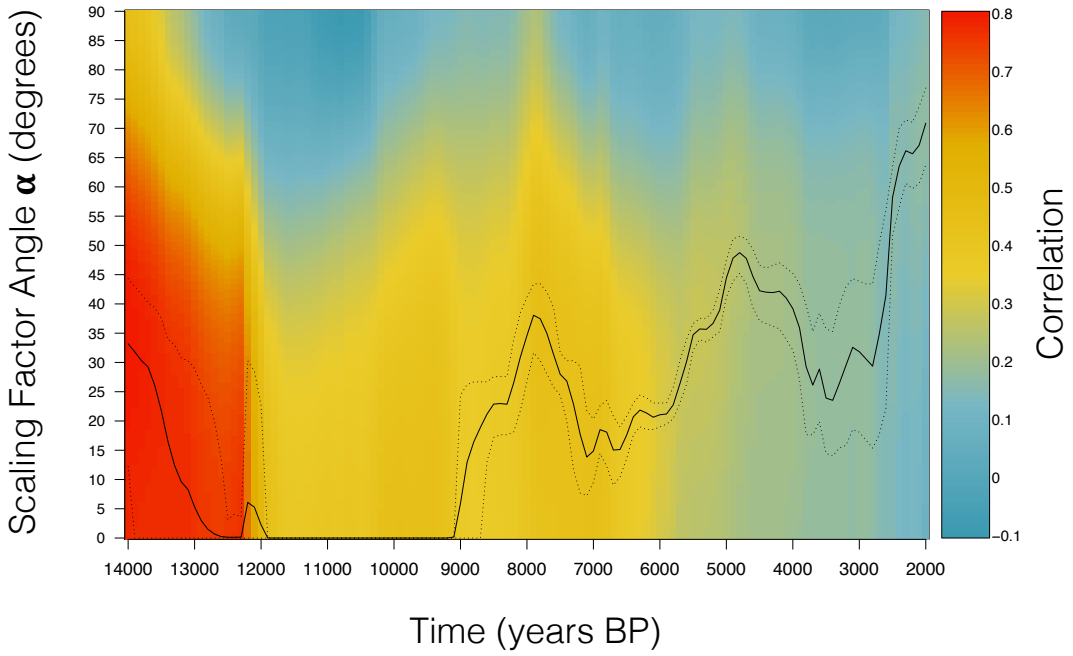

Fig. 2.S6: Relative mobility rate estimates in Western Eurasia over the last 14,000 years, using a 4,000-year sliding window (121 windows). Colors represent the correlation between genetic distance matrix and combined time-space distance matrix (see the color bar on the right). Values of α=0 and α=90 correspond to maximum correlation with only spatial and with only temporal distances, respectively, while at intermediate α values the combined space and time distance matrix gave the maximum correlation. The solid black line represents the mean α value from 10,000 date-resampled iterations; dotted lines represent the 95% confidence intervals of the jackknife distribution.

ID	Country	Lat.	Long.	Date from	Date to	Dating	Sub	Ref
CO1	Hungary	47.79	19.68	4853	4649	C14	F	2
IR1	Hungary	47.80	20.79	2928	2784	C14	F	2
Stora Forvar11	Sweden	57.28	17.97	7500	7250	NA	HG	3
Ajvide52	Sweden	57.5	18.55	4900	4600	NA	HG	3
Ajvide53	Sweden	57.5	18.55	4900	4600	NA	HG	3
Ajvide58	Sweden	57.5	18.55	4900	4600	NA	HG	3
Ajvide59	Sweden	57.5	18.55	4900	4600	NA	HG	3
Ajvide70	Sweden	57.5	18.55	4900	4600	NA	HG	3
Gokhem2	Sweden	58.17	13.40	5050	4750	NA	F	3
Gokhem4	Sweden	58.17	13.40	5280	4890	NA	F	3
Gokhem5	Sweden	58.17	13.40	5050	4890	NA	F	3
Gokhem7	Sweden	58.17	13.40	5050	4890	NA	F	3
Ire8	Sweden	57.5	18.55	5100	4150	NA	F	3
Iceman	Italy	46.75	10.92	5350	5100	NA	F	1
I0011	Sweden	58.53	15.04	7848	7481	C14	HG	7
I0012	Sweden	58.53	15.04	7848	7481	C14	HG	7
I0013	Sweden	58.53	15.04	7848	7481	C14	HG	7
I0014	Sweden	58.53	15.04	7848	7481	C14	HG	7
I0015	Sweden	58.53	15.04	7848	7481	C14	HG	7
I0016	Sweden	58.53	15.04	7848	7481	C14	HG	7
I0017	Sweden	58.53	15.04	7848	7481	C14	HG	7
I0022	Germany	48.78	9.18	7450	6750	NA	F	7
I0025	Germany	48.78	9.18	7450	6750	NA	F	7
I0026	Germany	48.78	9.18	7450	6750	NA	F	7
I0046	Germany	51.89	11.04	7156	6954	C14	F	7
I0047	Germany	51.89	11.04	3972	3887	C14	F	7
I0048	Germany	51.89	11.04	7156	7002	C14	F	7
I0049	Germany	51.41	11.67	4404	4241	C14	F	7
I0054	Germany	51.66	11.53	7159	7020	C14	F	7
I0056	Germany	51.89	11.04	7156	7002	C14	F	7
I0057	Germany	51.89	11.04	7157	7017	C14	F	7
I0058	Germany	51.82	10.91	4233	4096	C14	F	7
I0059	Germany	51.82	10.91	4236	4103	C14	F	7
I0060	Germany	51.45	11.54	4244	4156	C14	F	7
I0061	Russia	61.65	35.65	7450	6950	NA	HG	7
I0099	Germany	51.89	11.04	3063	2971	C14	F	7
I0100	Germany	51.89	11.04	6982	6896	C14	F	7
I0103	Germany	51.41	11.67	4516	4427	C14	F	7
I0104	Germany	51.41	11.67	4423	4298	C14	F	7

I0106	Germany	51.41	11.67	4404	4241	C14	F	7
I0108	Germany	51.45	11.54	4447	4386	C14	F	7
I0111	Germany	51.45	11.54	4364	4283	C14	F	7
I0112	Germany	51.78	11.14	4290	4140	C14	F	7
I0113	Germany	51.78	11.14	4240	4080	C14	F	7
I0114	Germany	51.27	11.65	4081	3929	C14	F	7
I0115	Germany	51.27	11.65	3881	3730	C14	F	7
I0116	Germany	51.27	11.65	4068	3911	C14	F	7
I0117	Germany	51.27	11.65	4149	4014	C14	F	7
I0118	Germany	51.45	11.63	4409	4295	C14	F	7
I0124	Russia	53.4	50.4	7600	7505	C14	HG	7
I0164	Germany	51.78	11.14	3962	3869	C14	F	7
I0171	Germany	51.82	10.91	4154	4086	C14	F	7
I0172	Germany	51.41	11.67	5310	5036	C14	F	7
I0174	Hungary	46.2	18.7	7660	7500	C14	F	7
I0176	Hungary	46.4	18.74	7160	6890	C14	F	7
I0231	Russia	52.42	48.24	4860	4825	C14	F	7
I0357	Russia	53.38	50.39	5040	4860	C14	F	7
I0370	Russia	51.27	58.18	5250	4650	NA	F	7
I0405	Spain	41.25	-2.32	5850	5550	NA	F	7
I0406	Spain	41.25	-2.32	5850	5550	NA	F	7
I0407	Spain	41.25	-2.32	5850	5550	NA	F	7
I0408	Spain	41.25	-2.32	5850	5550	NA	F	7
I0409	Spain	42.5	0.5	7261	7168	C14	F	7
I0410	Spain	42.5	0.5	7261	7168	C14	F	7
I0411	Spain	42.5	0.5	7128	7016	C14	F	7
I0412	Spain	42.5	0.5	7127	7018	C14	F	7
I0413	Spain	42.5	0.5	8260	7156	C14	F	7
I0429	Russia	53.38	50.39	5289	4867	C14	F	7
I0438	Russia	53.38	50.38	4971	4585	C14	F	7
I0439	Russia	53.38	50.39	5255	4875	C14	F	7
I0441	Russia	52.3	52.05	4960	4572	C14	F	7
I0443	Russia	53.38	50.39	5250	4650	NA	F	7
I0444	Russia	53.1	51.13	5250	4650	NA	F	7
I0550	Germany	51.27	11.65	4514	4425	C14	F	7
I0559	Germany	51.78	11.14	5595	5487	C14	F	7
I0560	Germany	51.78	11.14	5590	5460	C14	F	7
I0659	Germany	51.89	11.04	7029	6947	C14	F	7
I0795	Germany	51.27	11.65	7157	7020	C14	F	7
I0803	Germany	51.16	11.84	4065	3916	C14	F	7
I0804	Germany	51.17	11.85	4081	3932	C14	F	7
I0806	Germany	51.78	11.14	4246	4156	C14	F	7
I0807	Germany	51.41	11.67	5837	5747	C14	F	7
Loschbour	Luxemb.	49.79	6.28	8170	7940	C14	HG	4
Stuttgart	Germany	48.78	9.18	7450	6750	C14	F	4

Kostenki 14	Russia	51.39	39.04	38700	36200	C14	HG	5
I0235	Russia	53.14	50.01	3800	3550	NA	F	9
I0234	Russia	53.14	50.01	3800	3550	NA	F	9
I0421	Russia	53.08	50.36	3800	3550	NA	F	9
I0431	Russia	53.08	50.36	3800	3550	NA	F	9
I0430	Russia	53.08	50.36	3800	3550	NA	F	9
I0424	Russia	53.12	48.37	3800	3550	NA	F	9
I0354	Russia	53.03	50.39	3966	3642	C14	F	9
I0371	Russia	53.34	50.34	4825	4530	C14	F	9
I0126	Russia	53.31	51.15	4817	4434	C14	F	9
I0440	Russia	53.74	49.38	4835	4615	C14	F	9
I0432	Russia	53.66	50.67	4875	4486	C14	F	9
I0418	Russia	53.12	50.07	4075	3994	C14	F	9
I0419	Russia	53.12	50.07	4150	3850	NA	F	9
I0246	Russia	53.12	50.07	4419	3878	C14	F	9
I0434	Russia	52.22	48.1	7150	5950	NA	F	9
I0433	Russia	52.22	48.1	7150	5950	NA	F	9
I0122	Russia	52.22	48.1	7150	5950	NA	F	9
I0232	Russia	48.1	54.44	3800	3150	NA	F	9
I0360	Russia	53.03	50.39	3800	3150	NA	F	9
I0358	Russia	53.03	50.39	3863	3579	C14	F	9
I0361	Russia	53.03	50.39	3800	3150	NA	F	9
I0359	Russia	53.03	50.39	3800	3150	NA	F	9
I1282	Spain	42.33	-3.5	4830	4580	NA	F	9
I1302	Spain	42.33	-3.5	4830	4580	NA	F	9
I1276	Spain	42.33	-3.5	4830	4580	NA	F	9
I1284	Spain	42.33	-3.5	4830	4580	NA	F	9
I1274	Spain	42.33	-3.5	4830	4580	NA	F	9
I1280	Spain	42.33	-3.5	4830	4580	NA	F	9
I1314	Spain	42.33	-3.5	4830	4580	NA	F	9
I1277	Spain	42.33	-3.5	4780	4770	C14	F	9
I1272	Spain	42.33	-3.5	4830	4780	C14	F	9
I1281	Spain	42.33	-3.5	4845	4805	C14	F	9
I1300	Spain	42.33	-3.5	4830	4580	NA	F	9
I0585	Spain	43.47	-6.85	7940	7690	C14	HG	6
I1546	Germany	51.82	10.91	4450	4000	NA	F	9
I0805	Germany	51.79	11.15	4417	4092	C14	F	9
I1530	Germany	51.45	11.54	4295	4148	C14	F	9
I1542	Germany	51.42	11.68	4450	4000	NA	F	9
I1536	Germany	51.42	11.68	4450	4000	NA	F	9
I1544	Germany	51.42	11.68	4450	4000	NA	F	9
I1538	Germany	51.42	11.68	4450	4000	NA	F	9
I1539	Germany	51.42	11.68	4575	4241	C14	F	9
I1534	Germany	51.42	11.68	4450	4000	NA	F	9

I1540	Germany	51.42	11.68	4450	4000	NA	F	9
I1541	Germany	51.42	11.68	4450	4000	NA	F	9
I1532	Germany	51.42	11.68	4450	4000	NA	F	9
I0211	Russia	61.65	35.65	7450	6950	NA	HG	9
I0797	Germany	51.28	11.65	7450	6725	NA	F	9
I0551	Germany	51.52	11.85	5350	4975	NA	F	9
I1508	Hungary	47.20	21.53	7663	7516	C14	F	2
I1500	Hungary	47.80	20.79	7245	6900	C14	F	2
I1100	Turkey	40.3	29.57	8450	8150	NA	F	9
I1102	Turkey	40.3	29.57	8450	8150	NA	F	9
I1099	Turkey	40.3	29.57	8450	8150	NA	F	9
I1103	Turkey	40.3	29.57	8450	8150	NA	F	9
I1101	Turkey	40.3	29.57	8450	8150	NA	F	9
I1097	Turkey	40.3	29.57	8450	8150	NA	F	9
I0744	Turkey	40.3	29.57	8450	8150	NA	F	9
I1579	Turkey	40.3	29.57	8450	8150	NA	F	9
I1581	Turkey	40.3	29.57	8450	8150	NA	F	9
I1096	Turkey	40.3	29.57	8450	8150	NA	F	9
I1580	Turkey	40.3	29.57	8450	8150	NA	F	9
I1098	Turkey	40.3	29.57	8450	8150	NA	F	9
I1585	Turkey	40.3	29.57	8450	8150	NA	F	9
I0708	Turkey	40.3	29.57	8450	8150	NA	F	9
I0745	Turkey	40.3	29.57	8450	8150	NA	F	9
I0746	Turkey	40.3	29.57	8450	8150	NA	F	9
I1583	Turkey	40.3	29.57	8450	8150	NA	F	9
I0707	Turkey	40.3	29.57	8450	8150	NA	F	9
I0709	Turkey	40.3	29.57	8450	8150	NA	F	9
I0725	Turkey	40.26	29.65	8350	7550	NA	F	9
I0727	Turkey	40.26	29.65	8350	7550	NA	F	9
I0724	Turkey	40.26	29.65	8350	7550	NA	F	9
I0736	Turkey	40.3	29.57	8450	8150	NA	F	9
I1499	Hungary	48.41	21.17	7231	6976	C14	F	2
I1502	Hungary	47.80	20.79	4144	3927	C14	F	2
I1497	Hungary	47.80	20.79	7239	7004	C14	F	2
I1495	Hungary	47.79	19.68	6441	6307	C14	F	2
I1498	Hungary	47.80	20.79	7241	7006	C14	F	2
I1507	Hungary	47.80	20.79	7731	7596	C14	F	2
I1504	Hungary	47.80	20.79	3216	3061	C14	F	2
I1506	Hungary	47.80	20.79	7256	7021	C14	F	2
I1496	Hungary	47.79	19.68	7161	6942	C14	F	2
I1505	Hungary	47.80	20.79	7161	6961	C14	F	2
RISE00	Estonia	59.40	27.02	4750	4250	culture	F	8
RISE47	Denmark	56.97	9.55	3449	3274	C14	F	8
RISE61	Denmark	55.70	11.85	4801	4442	C14	F	8
RISE71	Denmark	56.67	10.03	4146	3973	C14	F	8

RISE94	Sweden	56.02	14.23	4571	4422	C14	F	8
RISE97	Sweden	55.55	13.05	3975	3835	C14	F	8
RISE98	Sweden	55.38	13.44	4225	3982	C14	F	8
RISE109	Poland	50.98	17.06	3904	3722	C14	F	8
RISE150	Poland	50.91	16.95	3835	3643	C14	F	8
RISE154	Poland	50.94	16.94	3875	3715	C14	F	8
RISE175	Sweden	55.39	13.6	3345	3082	C14	F	8
RISE179	Sweden	55.39	13.6	3960	3726	C14	F	8
RISE210	Sweden	55.99	14.10	3382	3242	C14	F	8
RISE240	Russia	46.58	43.67	4830	4582	C14	F	8
RISE247	Hungary	47.32	18.89	3696	3561	C14	F	8
RISE254	Hungary	47.32	18.89	4078	3859	C14	F	8
RISE276	Denmark	55.91	11.56	2744	2497	C14	F	8
RISE349	Hungary	46.35	20.98	3984	3734	C14	F	8
RISE371	Hungary	46.22	20.19	4086	3891	C14	F	8
RISE373	Hungary	46.22	20.19	3836	3646	C14	F	8
RISE374	Hungary	46.22	20.19	3816	3569	C14	F	8
RISE386	Russia	52.45	55.16	4248	3995	C14	F	8
RISE391	Kazakhstan	50.59	46.83	4070	3837	C14	F	8
RISE392	Russia	53.87	59.07	4076	3846	C14	F	8
RISE394	Russia	52.45	55.16	3899	3704	C14	F	8
RISE395	Russia	52.63	59.53	3910	3706	C14	F	8
RISE431	Poland	52.14	16.53	4236	3998	C14	F	8
RISE434	Germany	48.93	12.25	4830	4580	C14	F	8
RISE435	Germany	48.93	12.25	4813	4448	C14	F	8
RISE436	Germany	48.93	12.25	4818	4530	C14	F	8
RISE446	Germany	50.00	10.18	4779	4415	C14	F	8
RISE471	Germany	48.17	10.81	5150	2550	NA	F	8
RISE479	Hungary	47.34	18.89	3950	3450	culture	F	8
RISE480	Hungary	47.34	18.89	3950	3450	culture	F	8
RISE483	Hungary	47.34	18.89	3950	3450	culture	F	8
RISE484	Hungary	47.34	18.89	3950	3450	culture	F	8
RISE486	Italy	45.26	10.37	4084	3723	C14	F	8
RISE487	Italy	45.26	10.37	5433	5057	C14	F	8
RISE489	Italy	45.26	10.37	4858	4528	C14	F	8
RISE546	Russia	46.53	43.69	4950	4350	culture	F	8
RISE547	Russia	46.53	43.69	4837	4584	C14	F	8
RISE548	Russia	46.53	43.69	4950	4350	culture	F	8
RISE550	Russia	46.55	43.67	5284	4585	C14	F	8
RISE552	Russia	46.61	43.33	4799	4093	C14	F	8
RISE555	Russia	48.71	44.5	4807	4447	C14	F	8
RISE559	Germany	48.33	10.89	4550	3950	culture	F	8
RISE560	Germany	48.33	10.89	4550	3950	culture	F	8
RISE562	Germany	48.66	12.70	4550	3950	culture	F	8
RISE563	Germany	48.69	13.01	4550	3950	culture	F	8

RISE564	Germany	48.69	13.01	4550	3950	culture	F	8
RISE566	Czech Rep.	50.11	14.25	4550	3950	culture	F	8
RISE568	Czech Rep.	50.19	14.15	4550	3950	culture	F	8
RISE569	Czech Rep.	50.19	14.15	4550	3950	culture	F	8
RISE577	Czech Rep.	50.16	14.31	4250	3750	culture	F	8
RISE586	Czech Rep.	48.79	17.02	4250	3750	culture	F	8
I0581	Spain	42.33	-3.5	4960	4925	C14	F	9
I0422	Russia	52.54	50.5	3800	3150	NA	F	9
I0854	Turkey	40.3	29.57	8450	8150	NA	F	9
I1271	Spain	42.33	-3.5	4830	4580	NA	F	9
I1303	Spain	42.33	-3.5	4830	4580	NA	F	9
I1549	Germany	51.82	10.91	4450	4000	NA	F	9
I1550	Germany	51.89	11.04	7450	6725	NA	F	9
I0247	Russia	52.43	51.16	2330	2150	C14	F	9
I0374	Russia	49.97	44.67	4750	4150	NA	F	9
I0423	Russia	52.54	50.5	3800	3150	NA	F	9
I0723	Turkey	40.26	29.65	8350	7550	NA	F	9
I0726	Turkey	40.26	29.65	8350	7550	NA	F	9
Bichon	Switzerland	47.01	6.96	13770	13560	C14	HG	10
KK1	Georgia	42.27	43.29	9895	9529	C14	HG	10
SATP	Georgia	42.40	43.14	13380	13132	C14	HG	10
Motala12	Sweden	58.53	15.03	8311	7466	C14	HG	12
I9030	Italy	46.15	12.21	14180	13780	Dir.UF	HG	11
I0898	Russia	51.23	39.3	32990	31840	Layer	HG	11
I0062	Czech Rep.	48.53	16.39	30710	29319	Layer	HG	11
I0066.damage	Czech Rep.	48.53	16.39	31110	29410	Layer	HG	11
I0909.damage	Romania	45.11	23.46	33760	32840	Direct. UF	HG	11
I0004.damage	Czech Rep.	48.53	16.39	31070	30670	Layer	HG	11
I0080.damage	Czech Rep.	48.53	16.39	31070	30670	Layer	HG	11
I0065.damage	Czech Rep.	48.53	16.39	30710	29319	Layer	HG	11
I0889.damage	Italy	40.73	17.57	29310	28640	Direct. UF	HG	11
I0869.damage	Italy	40.73	17.57	27810	27430	Direct. UF	HG	11
I0878.damage	Italy	41.96	13.54	11200	10510	Layer	HG	11
I0006_damage	Czech Rep.	48.53	16.39	31070	30670	Layer	HG	11
I0907.damage	Spain	43.26	-3.45	18830	18616	Direct. UF	HG	11

Ranchot.damage	France	47.91	5.43	10240	9930	Direct. Not.UF	HG	11
Bockstein.damage	Germany	48.33	10.09	8370	8160	Layer	HG	11
Ofnet.damage	Germany	48.49	10.27	8430	8060	Layer	HG	11
LCX-13.damage	France	48.52	2.11	10240	9560	Direct. Not.UF	HG	11
Berry_au_Bac	France	49.24	3.54	7320	7170	Direct. Not.UF	HG	11
Q116-1	Belgium	50.26	4.28	35160	34430	Direct. Not.UF	HG	11
Cioclovina_d	Romania	45.35	23.84	33090	31780	Direct. UF	HG	11
B1_d	Italy	41.65	15.61	28430	27070	Layer	HG	11
Q53-1_d	Belgium	50.26	4.28	28230	27720	Direct. Not.UF	HG	11
Q376-19_d	Belgium	50.26	4.28	27720	27310	Direct. Not.UF	HG	11
Q56-16_d	Belgium	50.26	4.28	26600	26040	Direct. Not.UF	HG	11
GA252snp	Italy	41.65	15.61	34580	31210	Layer	HG	11
Hohle_Fels	Germany	48.22	9.45	15070	14270	Direct. UF	HG	11
HF49	Germany	48.22	9.45	16000	14260	Layer	HG	11
Rigney2	France	47.23	6.1	15690	15240	Direct. Not.UF	HG	11
Q2	Belgium	50.26	4.28	15230	14780	Direct. Not.UF	HG	11
BRI_d	Germany	48.24	9.46	15120	14440	Direct. UF	HG	11
BUR_d	Germany	48.32	9.35	15080	14150	Direct. Not.UF	HG	11
Rochedane	France	47.21	6.45	13090	12830	Direct. Not.UF	HG	11
ADI_d	France	44.29	4.46	12040	11410	Direct. Not.UF	HG	11
Falkenstein_d	Germany	48.06	9.04	9410	8990	Direct. Not.UF	HG	11
CRC-1_d	France	49.24	3.46	8360	8050	Direct. Not.UF	HG	11
I1577	Austria	48.41	15.59	31250	30690	Layer	HG	11
I1634	Armenia	39.73	45.2	6330	6060	C14	F	12
I1632	Armenia	39.73	45.2	6230	6000	C14	F	12
I1631	Armenia	39.73	45.2	6250	6050	C14	F	12

I1635	Armenia	40.65	45.1	4619	4465	C14	F	12
I1633	Armenia	40.65	45.11	4619	4410	C14	F	12
I1658	Armenia	40.38	43.87	5347	5092	C14	F	12
I1656	Armenia	40.37	43.93	3501	3402	C14	F	12
I1409	Armenia	39.73	45.2	6229	5985	C14	F	12
I1407	Armenia	39.73	45.2	6350	5700	NA	F	12
I1290	Iran	34.45	48.11	10179	9613	C14	F	12
I1069	Israel	32.65	35.06	13840	11760	NA	HG	12
I1687	Israel	32.65	35.06	13520	13110	C14	HG	12
I1690	Israel	32.65	35.06	13840	11760	NA	HG	12
I1685	Israel	32.65	35.06	13840	11760	NA	HG	12
I1072	Israel	32.65	35.06	13840	11760	NA	HG	12
I1705	Jordan	31.98	35.97	4198	3966	C14	F	12
I1706	Jordan	31.98	35.97	4490	4300	NA	F	12
I1679	Jordan	31.98	35.97	8900	8800	NA	F	12
I1416	Jordan	31.98	35.97	10300	9900	NA	F	12
I1415	Jordan	31.98	35.97	10197	9653	C14	F	12
I1414	Jordan	31.98	35.97	10300	9900	NA	F	12
I1701	Jordan	31.98	35.97	9750	9569	C14	F	12
I1709	Jordan	31.98	35.97	10300	9900	NA	F	12
I1727	Jordan	31.98	35.97	10300	9900	NA	F	12
I1710	Jordan	31.98	35.97	9733	9526	C14	F	12
I1707	Jordan	31.98	35.97	9722	9541	C14	F	12
I1704	Jordan	31.98	35.97	9446	9058	C14	F	12
I1730	Jordan	31.98	35.97	4489	4299	C14	F	12
I1700	Jordan	31.98	35.97	10300	9900	NA	F	12
I1699	Jordan	31.98	35.97	8800	8700	NA	F	12
I1670	Iran	34.5	47.96	6839	6617	C14	F	12
I1662	Iran	34.5	47.96	6831	6612	C14	F	12
I1674	Iran	34.5	47.96	5972	5800	C14	F	12
I1665	Iran	34.5	47.96	5956	5796	C14	F	12
I1661	Iran	34.5	47.96	6696	6491	C14	F	12
I1671	Iran	34.5	47.96	7837	7659	C14	F	12
RISE396	Armenia	39.2	46.6	3142	2887	C14	F	8
RISE397	Armenia	39.2	46.6	2998	2805	C14	F	8
RISE407	Armenia	40.15	45.86	3065	2845	C14	F	8
RISE408	Armenia	40.15	45.86	3159	2959	C14	F	8
RISE412	Armenia	40.38	45.18	3143	2895	C14	F	8
RISE413	Armenia	44.14	45.26	3856	3648	C14	F	8
RISE416	Armenia	44.14	45.26	3593	3395	C14	F	8
RISE423	Armenia	44.14	45.26	3352	3161	C14	F	8
I0867	Israel	31.79	35.16	9300	8750	NA	F	12
I0861	Israel	32.65	35.06	13840	11760	NA	HG	12
I1944	Iran	34.45	48.11	10000	9700	NA	F	12
I1945	Iran	34.45	48.11	10000	9700	NA	F	12

I1949	Iran	34.45	48.11	10000	9700	NA	F	12
I1951	Iran	34.45	48.11	10202	9681	C14	F	12
I1955	Iran	34.45	48.11	570	515	C14	F	12
I1584	Turkey	40.3	29.56	5943	5708	C14	F	12
I1293	Iran	35.59	53.5	11100	10600	NA	HG	12

Table 2.S1: Samples used in the analyses (col1: ID), their country of origin (col2: Country), longitude (col3: Longitude), latitude, (col4: Latitude), age range (col5 & col6: Date.from & Date.to; calibrated years before present), dating method (col:7 dating method), proposed subsistence strategy based on archaeological context (col8: Sub) and reference to the publication where the data was first published (col:8. Ref).

Publication list referred to in Table 2.S1

1. Keller A, et al. (2012) New insights into the Tyrolean Iceman's origin and phenotype as inferred by whole-genome sequencing. Nat Commun 3:698.
2. Gamba C, et al. (2014) Genome flux and stasis in a five millennium transect of European prehistory. Nat Commun 5:5257.
3. Skoglund P, et al. (2014) Genomic Diversity and Admixture Differs for Stone-Age Scandinavian Foragers and Farmers. Science 344(6185):747–750.
4. Lazaridis I, et al. (2014) Ancient human genomes suggest three ancestral populations for present-day Europeans. Nature 513(7518):409–413.
5. Seguin-Orlando A, et al. (2014) Genomic structure in Europeans dating back at least 36,200 years. Science 346(6213):1113–1118.
6. Olalde I, et al. (2014) Derived immune and ancestral pigmentation alleles in a 7,000-year-old Mesolithic European. Nature 507(7491):225–228.
7. Haak W, et al. (2015) Massive migration from the steppe was a source for Indo-European languages in Europe. Nature 522(7555):207–211.
8. Allentoft ME, et al. (2015) Population genomics of Bronze Age Eurasia. Nature 522(7555):167–172.
9. Mathieson I, et al. (2015) Genome-wide patterns of selection in 230 ancient Eurasians. Nature 528(7583):499–503.
10. Jones ER, et al. (2015) Upper Palaeolithic genomes reveal deep roots of modern Eurasians. Nat Commun 6:8912.

11. Fu Q, et al. (2016) The genetic history of Ice Age Europe. Nature 534(7606):200–205.
12. Lazaridis I, et al. (2016) Genomic insights into the origin of farming in the ancient Near East. Nature 536(7617):419–424.

Group	Time from	Time to	N	Scaling factor angle (alpha)	p.value	CI: lower 95	CI: upper 95
Neolithic farmers	37000	26000	19	34.824	<0.0001	35.27	33.91
PostLGM hunter-gatherers	19000	5000	47	9.949	0.0348	10.85	9.49
PreLGM hunter-gatherers	10000	1000	263	18.090	0.0841	87.73	9.49

Table 2.S2: Results for analyses exploring changes in human mobility in three sample groups. Each row in the table represents a group for which the scaling factor and confidence intervals were estimated for. N is the sample size.

Window	Time from	Time to	Mean time	Mean Sample size	Scaling factor angle (alpha)	p-value	CI: lower 95	CI: upper 95
1	16000	12000	14000	15.48	33.18	0.0560	12.21	44.32
2	15900	11900	13900	15.82	31.81	0.0604	0.00	42.96
3	15800	11800	13800	16.17	30.31	0.0699	0.00	41.61
4	15700	11700	13700	16.36	29.23	0.0640	0.00	40.25
5	15600	11600	13600	16.26	26.08	0.0823	0.00	39.35
6	15500	11500	13500	16.14	21.73	0.1052	0.00	37.54
7	15400	11400	13400	16.00	16.44	0.1467	0.00	33.92
8	15300	11300	13300	15.72	12.35	0.2066	0.00	33.02
9	15200	11200	13200	15.47	9.59	0.2741	0.00	30.75
10	15100	11100	13100	15.31	8.30	0.2857	0.00	30.30
11	15000	11000	13000	15.05	5.31	0.3369	0.00	28.94
12	14900	10900	12900	14.75	2.97	0.3950	0.00	26.23
13	14800	10800	12800	14.42	1.50	0.4328	0.00	23.97
14	14700	10700	12700	14.29	0.68	0.4847	0.00	19.90
15	14600	10600	12600	14.19	0.25	0.4997	0.00	13.58
16	14500	10500	12500	13.88	0.14	0.5110	0.00	3.17
17	14400	10400	12400	13.51	0.14	0.5153	0.00	4.07
18	14300	10300	12300	13.21	0.15	0.5036	0.00	3.62
19	14200	10200	12200	14.50	6.08	0.2490	0.00	30.30
20	14100	10100	12100	16.46	5.27	0.2584	0.00	28.49
21	14000	10000	12000	18.47	2.25	0.3430	0.00	22.61
22	13900	9900	11900	21.42	0.02	0.5164	0.00	0.00
23	13800	9800	11800	23.02	0.00	0.5225	0.00	0.00
24	13700	9700	11700	24.94	0.00	0.5123	0.00	0.00
25	13600	9600	11600	26.49	0.00	0.4857	0.00	0.00
26	13500	9500	11500	27.13	0.00	0.4859	0.00	0.00
27	13400	9400	11400	26.78	0.00	0.4840	0.00	0.00
28	13300	9300	11300	26.49	0.00	0.4831	0.00	0.00
29	13200	9200	11200	26.28	0.00	0.4809	0.00	0.00
30	13100	9100	11100	26.22	0.00	0.4771	0.00	0.00
31	13000	9000	11000	26.16	0.00	1.0000	0.00	0.00
32	12900	8900	10900	25.74	0.00	1.0000	0.00	0.00
33	12800	8800	10800	26.41	0.00	1.0000	0.00	0.00
34	12700	8700	10700	27.26	0.00	1.0000	0.00	0.00
35	12600	8600	10600	27.02	0.00	1.0000	0.00	0.00
36	12500	8500	10500	26.78	0.00	1.0000	0.00	0.00
37	12400	8400	10400	30.12	0.00	1.0000	0.00	0.00
38	12300	8300	10300	38.00	0.00	1.0000	0.00	0.00
39	12200	8200	10200	46.62	0.00	1.0000	0.00	0.00
40	12100	8100	10100	51.82	0.00	1.0000	0.00	0.00
41	12000	8000	10000	53.07	0.00	1.0000	0.00	0.00
42	11900	7900	9900	53.93	0.00	1.0000	0.00	0.00
43	11800	7800	9800	55.89	0.00	1.0000	0.00	0.00
44	11700	7700	9700	59.55	0.00	1.0000	0.00	0.00

45	11600	7600	9600	63.95	0.00	1.0000	0.00	0.00
46	11500	7500	9500	68.42	0.00	1.0000	0.00	0.00
47	11400	7400	9400	69.79	0.00	1.0000	0.00	0.00
48	11300	7300	9300	71.68	0.00	1.0000	0.00	0.00
49	11200	7200	9200	76.03	0.00	0.4817	0.00	0.00
50	11100	7100	9100	83.69	0.18	0.4786	0.00	0.00
51	11000	7000	9000	93.36	5.92	0.3100	0.00	24.42
52	10900	6900	8900	97.36	12.99	0.2251	0.00	26.23
53	10800	6800	8800	98.53	16.43	0.1908	0.00	26.68
54	10700	6700	8700	99.82	18.90	0.1672	0.00	26.68
55	10600	6600	8600	100.98	21.19	0.1450	13.12	26.68
56	10500	6500	8500	101.59	22.88	0.1246	17.19	27.59
57	10400	6400	8400	102.18	22.98	0.1222	17.64	27.59
58	10300	6300	8300	103.31	22.86	0.1210	17.64	27.59
59	10200	6200	8200	103.13	26.50	0.0635	18.09	33.92
60	10100	6100	8100	103.04	30.89	0.0249	21.71	38.44
61	10000	6000	8000	102.41	34.59	0.0065	26.68	41.16
62	9900	5900	7900	100.52	38.06	0.0016	31.66	43.42
63	9800	5800	7800	101.43	37.47	0.0013	30.30	43.42
64	9700	5700	7700	101.40	34.96	0.0056	28.04	42.06
65	9600	5600	7600	100.46	31.38	0.0306	25.78	39.35
66	9500	5500	7500	101.57	27.99	0.0501	24.42	31.66
67	9400	5400	7400	101.95	26.80	0.0607	19.90	30.30
68	9300	5300	7300	102.27	22.88	0.0890	11.76	30.30
69	9200	5200	7200	104.21	17.75	0.1366	7.69	29.40
70	9100	5100	7100	106.65	13.84	0.1781	7.24	21.71
71	9000	5000	7000	109.32	14.86	0.1669	9.50	20.35
72	8900	4900	6900	114.36	18.52	0.1134	14.47	22.61
73	8800	4800	6800	122.58	18.09	0.1285	12.21	23.52
74	8700	4700	6700	135.39	15.04	0.1873	9.05	20.80
75	8600	4600	6600	147.59	15.12	0.2101	10.40	18.99
76	8500	4500	6500	154.88	17.59	0.1467	13.57	20.80
77	8400	4400	6400	160.86	20.71	0.0493	17.64	23.07
78	8300	4300	6300	162.91	21.86	0.0255	18.99	24.42
79	8200	4200	6200	163.45	21.36	0.0261	18.54	23.97
80	8100	4100	6100	170.09	20.64	0.0277	18.54	23.07
81	8000	4000	6000	181.29	21.06	0.0249	18.99	23.07
82	7900	3900	5900	189.98	21.20	0.0259	19.45	23.07
83	7800	3800	5800	195.67	22.74	0.0185	20.35	25.78
84	7700	3700	5700	201.84	26.32	0.0070	23.07	30.30
85	7600	3600	5600	203.95	30.08	0.0016	26.23	33.92
86	7500	3500	5500	203.23	34.73	0.0003	32.11	36.63
87	7400	3400	5400	204.85	35.72	0.0001	33.92	37.54
88	7300	3300	5300	205.57	35.66	0.0001	33.47	37.54
89	7200	3200	5200	203.71	36.69	0.0002	34.37	38.89
90	7100	3100	5100	198.27	38.94	0.0002	35.28	42.51
91	7000	3000	5000	190.89	44.42	0.0007	41.16	47.49
92	6900	2900	4900	189.04	47.83	0.0008	43.87	51.11

93	6800	2800	4800	189.08	48.76	0.0003	45.23	51.56
94	6700	2700	4700	187.77	47.78	0.0022	43.42	51.11
95	6600	2600	4600	186.71	44.67	0.0096	39.35	49.30
96	6500	2500	4500	186.40	42.24	0.0207	37.09	46.58
97	6400	2400	4400	185.82	42.00	0.0248	36.63	46.13
98	6300	2300	4300	184.86	41.94	0.0289	36.18	46.58
99	6200	2200	4200	184.14	42.17	0.0225	35.73	47.04
100	6100	2100	4100	182.29	41.01	0.0387	33.92	46.13
101	6000	2000	4000	180.65	39.20	0.0524	32.11	45.23
102	5900	1900	3900	179.36	35.94	0.0692	27.12	43.42
103	5800	1800	3800	176.49	29.26	0.1145	17.64	39.80
104	5700	1700	3700	174.00	26.14	0.1387	17.64	35.28
105	5600	1600	3600	172.66	28.88	0.1239	19.90	38.44
106	5500	1500	3500	170.43	23.91	0.1711	14.47	35.73
107	5400	1400	3400	169.91	23.53	0.1845	14.02	35.28
108	5300	1300	3300	169.09	26.42	0.1700	15.38	39.80
109	5200	1200	3200	166.47	29.52	0.1611	15.83	42.96
110	5100	1100	3100	163.36	32.57	0.1479	18.54	44.32
111	5000	1000	3000	160.16	31.84	0.1617	18.09	43.87
112	4900	900	2900	154.91	30.61	0.1725	16.73	43.42
113	4800	800	2800	145.51	29.37	0.1774	15.38	43.42
114	4700	700	2700	131.61	34.80	0.1489	17.64	50.20
115	4600	600	2600	119.41	41.44	0.1270	22.16	56.08
116	4500	500	2500	113.12	58.19	0.0137	51.56	63.32
117	4400	400	2400	103.56	63.54	0.0071	56.53	70.10
118	4300	300	2300	93.39	66.17	0.0079	60.60	71.46
119	4200	200	2200	83.99	65.66	0.0042	59.70	71.01
120	4100	100	2100	71.92	67.09	0.0040	60.60	73.72
121	4000	0	2000	59.16	70.88	0.0186	63.77	76.88

Table 2.S3: Results for analyses exploring changes in human mobility in Late-Pleistocene & Holocene using 4000 year wide sliding window. Each row in the table represents a window for which the scaling factor and confidence intervals were estimated for.

Chapter 3: Modern wolves trace their origin to a late Pleistocene expansion from Beringia

This work is currently under review in the journal Molecular Biology and Evolution.

3.1 Annex to Chapter 3: Statement of my contribution

Original idea and design of research

I generated the idea behind the article and planned the research together with Dr A. Eriksson and Dr A. Manica.

Data

I curated the previously published and novel data (generated by my co-authors from 3 different laboratories) and sample background information (provided by my co-authors). I coordinated the bioinformatics treatment of NGS data between the laboratories involved and performed quality checks and filtering of the data.

Analysis

I designed the phylogenetic analysis of genetic data under the supervision of Dr A. Eriksson and Dr A. Manica. I performed phylogenetic analysis of the data. I performed mutation rate calculations, calibration of all radiocarbon-dated samples, molecular dating of the samples and validation of the molecular dating method. I designed the population genetic spatial framework with Dr A. Eriksson and Dr A. Manica. I performed the spatial population genetic analysis with input from Dr A. Eriksson. I interpreted the results within the archaeological context with input from several co-authors.

Manuscript

I wrote the manuscript with Dr A. Eriksson and Dr O. Thalmann. I generated all the tables and figures. I curated and edited the information presented in supplementary information section one and section two and wrote the supplementary information section three.

3.2 List of authors and affiliations

Liisa Loog[1,2,3]*, Olaf Thalmann[4†], Mikkel-Holger S. Sinding[5,6,7†], Verena J. Schuenemann[8,9†], Angela Perri[10], Mietje Germonpré[11], Herve Bocherens[9,12], Kelsey E. Witt[13], Jose A. Samaniego Castruita[5], Marcela S. Velasco[5], Inge. K. C. Lundstrøm[5], Nathan Wales[5], Gontran Sonet[15], Laurent Frantz[2], Hannes Schroeder[5,15], Jane Budd[16], Elodie-Laure Jimenez [11], Sergey Fedorov[17], Boris Gasparyan[18], Andrew W. Kandel[19], Martina Lázničková-Galetová[20,21,22], Hannes Napierala[23], Hans-Peter Uerpmann[8], Pavel A. Nikolskiy[24,25], Elena Y. Pavlova[26,25], Vladimir V. Pitulko[25], Karl-Heinz Herzig[4,27], Ripan S. Malhi[26], Eske Willerslev[2,5,29], Anders J. Hansen[5,7], Keith Dobney[30,31,32], M. Thomas P. Gilbert[5,33], Johannes Krause[8,34], Greger Larson[1]*, Anders Eriksson[35,2]*, Andrea Manica[2]*

*Corresponding Authors: L.L. (liisaloog@gmail.com), G.L. (greger.larson@arch.ox.ac.uk), A.E. (anders.eriksson@kcl.ac.uk), A.M. (am315@cam.ac.uk)

[†]These authors contributed equally to this work

Affiliations

1. Palaeogenomics & Bio-Archaeology Research Network Research Laboratory for Archaeology and History of Art, University of Oxford, Dyson Perrins Building, South Parks Road, Oxford OX1 3QY, UK
2. Department of Zoology, University of Cambridge, Downing Street, Cambridge CB2 3EJ, UK
3. Manchester Institute of Biotechnology, School of Earth and Environmental Sciences, University of Manchester, Manchester, M1 7DN, UK
4. Department of Pediatric Gastroenterology and Metabolic Diseases, Poznan University of Medical Sciences, Szpitalna 27/33, 60-572 Poznan, Poland
5. Centre for GeoGenetics, Natural History Museum of Denmark, University of Copenhagen, Øster Voldgade 5-7, DK-1350 Copenhagen, Denmark
6. Natural History Museum, University of Oslo, P.O. Box 1172 Blindern, NO-0318 Oslo, Norway
7. The Qimmeq project, University of Greenland, Manutooq 1, PO Box 1061, 3905 Nuussuaq, Greenland

8. Institute for Archaeological Sciences, University of Tübingen, Rümelinstr. 23, 72070 Tübingen, Germany
9. Senckenberg Centre for Human Evolution and Palaeoenvironment, University of Tübingen, 72070 Tübingen, Germany
10. Department of Human Evolution, Max Planck Institute for Evolutionary Anthropology, Deutscher Platz 6, 04103 Leipzig, Germany
11. OD Earth and History of Life, Royal Belgian Institute of Natural Sciences, Vautierstraat 29, 1000 Brussels, Belgium
12. Department of Geosciences, Palaeobiology, University of Tübingen, Tübingen, Germany
13. School of Integrative Biology, University of Illinois at Urbana-Champaign, 109A Davenport Hall, 607 S. Mathews Avenue, Urbana IL 61801, USA
14. OD Taxonomy and Phylogeny, Royal Belgian Institute of Natural Sciences, Vautierstraat 29, 1000 Brussels, Belgium
15. Faculty of Archaeology, Leiden University, Postbus 9514, 2300 RA Leiden, The Netherlands
16. Breeding Centre for Endangered Arabian Wildlife, PO Box 29922 Sharjah, United Arab Emirates
17. Mammoth Museum, Institute of Applied Ecology of the North of the North-Eastern Federal University, ul. Kulakovskogo 48, 677980 Yakutsk, Russia
18. National Academy of Sciences, Institute of Archaeology and Ethnography, Charents St. 15, Yerevan 0025, Armenia
19. Heidelberg Academy of Sciences and Humanities: The Role of Culture in Early Expansions of Humans, Rümelinstr. 23, 72070 Tübingen, Germany
20. Departement of Anthropology, University of West Bohemia, Sedláčkova 15, 306 14 Pilzen, Czech republic
21. Moravian museum, Zelný trh 6, 659 37 Brno, Czech republic
22. Hrdlička Museum of Man, Faculty of Science, Charles University, Viničná 1594/7,128 00 Praha, Czech republic
23. Institute of Palaeoanatomy, Domestication Research and History of Veterinary Medicine, Ludwig-Maximilians-University Munich, Kaulbachstraße 37 III/313, D-80539 Munich, Germany

24. Geological Institute, Russian Academy of Sciences, 7 Pyzhevsky per., 119017 Moscow, Russia
25. Institute for Material Culture History, Russian Academy of Sciences, 18 Dvortsovaya nab., St Petersburg 191186, Russia
26. Arctic and Antarctic Research Institute, 38 Bering St., St Petersburg 199397, Russia
27. Insitute of Biomedicine and Biocenter of Oulu, Medical Research Center and University Hospital, University of Oulu, Aapistie 5, 90220 Oulu University, Finland
28. Carl R. Woese Institute for Genomic Biology, University of Illinois at Urbana-Champaign, 1206 W Gregory Dr., Urbana, Illinois 61820, USA
29. Wellcome Trust Sanger Institute, Hinxton, Cambridge CB10 1SA, UK
30. Department of Archaeology, Classics and Egyptology, University of Liverpool, 12-14 Abercromby Square, Liverpool L69 7WZ, UK
31. Department of Archaeology, University of Aberdeen, St Mary's, Elphinstone Road, Aberdeen AB24 3UF, UK
32. Department of Archaeology, Simon Fraser University, Burnaby, B.C. V5A 1S6, 778-782-419, Canada
33. Norwegian University of Science and Technology, University Museum, N-7491 Trondheim, Norway
34. Max Planck Institute for the Science of Human History, Khalaische Straße 10, 07745 Jena, Germany
35. Department of Medical & Molecular Genetics, King's College London, Guys Hospital, London SE1 9RT, UK

3.3 Abstract

Grey wolves (*Canis lupus*) are one of the few large terrestrial carnivores that maintained a wide geographic distribution across the Northern Hemisphere throughout the Pleistocene and Holocene. Recent genetic studies have suggested that, despite this continuous presence, major demographic changes occurred in wolf populations between the late Pleistocene and early Holocene, and that extant wolves trace their ancestry to a single late Pleistocene population. Both the geographic origin of this ancestral population and how it became widespread remain a mystery. Here we analysed a large dataset of novel modern and ancient mitochondrial wolf genomes, spanning the last 50,000 years, using a spatially and temporally explicit modelling framework to show that contemporary wolf populations across the globe trace their ancestry to an expansion from Beringia at the end of the Last Glacial Maximum - a process most likely driven by the significant ecological changes that occurred across the Northern Hemisphere during this period. This study provides direct ancient genetic evidence that long-range migration has played an important role in the population history of a large carnivore and provides an insight into how wolves survived the wave of megafaunal extinctions at the end of the last glaciation. Moreover, because late Pleistocene grey wolves were the likely source from which all modern dogs trace their origins, the demographic history described in this study has fundamental implications for understanding the geographical origin of the dog.

3.4 Introduction

The Pleistocene epoch harboured a large diversity of top predators though most became extinct during or soon after the Last Glacial Maximum (LGM) ~24 thousand years ago. The grey wolf (*Canis lupus*) was one of the few large carnivores that survived and maintained a wide geographical range throughout the period (Puzachenko and Markova 2016), and both the palaeontological and archaeological records attest to the continuous presence of grey wolves across the Northern Hemisphere for at least the last 300,000 years (Sotnikova and Rook 2010) (reviewed in Supplementary Information 1). This geographical and temporal continuity across the Northern Hemisphere contrasts with analyses of complete modern genomes which have suggested that all contemporary wolves and dogs descend from a common ancestral population that existed as recently as ~20,000 years ago (Freedman et al. 2014; Skoglund et al. 2015; Fan et al. 2016). These analyses point to a bottleneck followed by a rapid radiation from an ancestral population

around or just after the LGM, but the geographic origin and dynamics of this radiation remain unknown. Resolving these demographic changes is necessary for understanding the ecological circumstances that allowed wolves to survive the late Pleistocene megafaunal extinctions. Furthermore, because dogs were domesticated from late Pleistocene grey wolves (Larson et al. 2012), a detailed insight into wolf demography during this time period would provide an essential context for reconstructing the history of dog domestication.

Reconstructing past demographic events solely from modern genomes is challenging since multiple demographic histories can lead to similar genetic patterns in present-day samples (Groucutt et al. 2015). Analyses that incorporate ancient DNA sequences can eliminate some of these alternative histories by quantifying changes in population genetic differences through time. While nuclear markers provide greater power relative to mitochondrial DNA (mtDNA), the latter is more easily retrievable and better preserved in ancient samples due to its higher copy number compared to the nuclear DNA, thus allowing for the generation of datasets with greater geographical and temporal coverage. Furthermore, the nuclear mutation rate in canids is poorly understood, leading to wide date ranges for past demographic events reconstructed from panels of modern whole genomes (e.g. Freedman et al. 2014; Fan et al. 2016). Having samples from a broad time period can reduce mutation rate uncertainty by calibrating the evolutionary rate with directly dated samples (Rambaut 2000; Drummond et al. 2002; Rieux et al. 2014).

Although mtDNA can be retrieved from a wider range of ancient samples, the sparseness of samples across space and time, compounded by the stochasticity of a single non-recombining genetic marker, can lead to patterns that are difficult to interpret intuitively (Groucutt et al. 2015). Population genetic models that explicitly capture the expected temporal (e.g. Posth et al. 2016) and spatial (e.g. Warmuth et al. 2012; Raghavan et al. 2015) differences between samples can be used to overcome this problem.

In order to reconstruct the demographic history of wolves, we assembled a substantial dataset (Fig. 3.1, Table 3.S1) consisting of 90 modern and 45 ancient wolf whole mitochondrial genomes (55 of which are newly sequenced), spanning the last 50,000 years and the geographic breadth of the Northern Hemisphere. We first used the ancient mitogenomes to estimate a wolf mutation rate using BEAST. We then designed a spatially and temporally explicit population genetic (coalescent) model that accounts for the

stochasticity of the mitochondrial phylogenetic tree, as well as the uneven spatial and temporal distribution of the samples. We used our spatial model to investigate the origin and population dynamics of the expansion of grey wolves during the LGM.

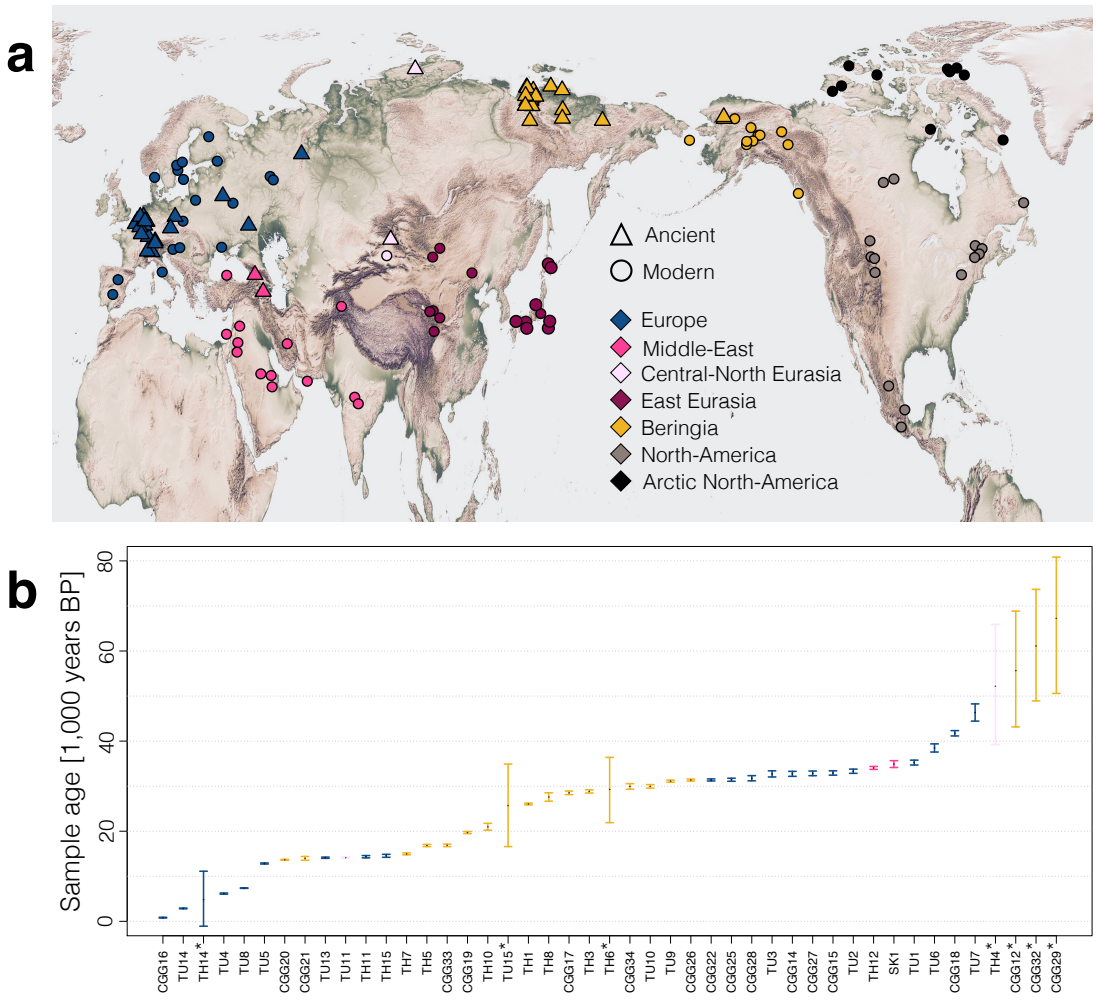

Fig. 3.1: Geographic distribution of modern (circles) and ancient (triangles) samples, grouped into seven geographic regions (demes, colour coded) (a) and temporal distribution of ancient samples (b) used in the analyses. * Samples dated by molecular dating.

3.5 Results

3.5.1 Phylogenetic Analyses

All sequences included in the study were subjected to stringent quality criteria with respect to coverage and damage patterns. We used the 38 ancient samples for which we had direct radiocarbon dates to estimate mitochondrial mutation rates using BEAST (Drummond et al. 2012), and molecularly dated the remaining seven ancient samples (Supplementary Information 3.S3.1).

Our Bayesian phylogenetic analysis suggests that the most recent common ancestor of all North Eurasian and American wolf samples dates to ca. 90,000 (95% CIs: 82.000 – 99.000) years ago (Fig. 3.2, see Figs. 3.S11 and 3.S12 for node support values and credibility intervals). At the root of this tree, we find a divergent clade consisting exclusively of ancient samples from Europe and the Middle East that has not contributed to present day mitochondrial diversity in our data (see also Thalmann et al. 2013). The rest of the tree consists of a monophyletic clade made up of ancient and modern samples from across the Northern Hemisphere and shows a pattern of rapid bifurcations of genetic lineages centred on 25,000 years ago. A Bayesian skyline analysis (Fig. 3.S13, see Supplementary Information 3.S3.1 for details) also shows a recent reduction in effective population size. This pattern is compatible with a scenario of rapid radiation that has also been suggested by whole genome studies (e.g. Freedman et al. 2014; Fan et al. 2016). At the root of this clade we find predominantly samples from Beringia, pointing to a possible expansion out Northeast Eurasia or the Americas. However, given the uneven temporal and geographic distribution of our samples and the stochasticity of a single genetic marker (Nielsen and Beaumont 2009), it is important to explicitly test the extent to which this pattern can occur by chance under other plausible demographic scenarios, taking the geographic and temporal distribution of our samples into account.

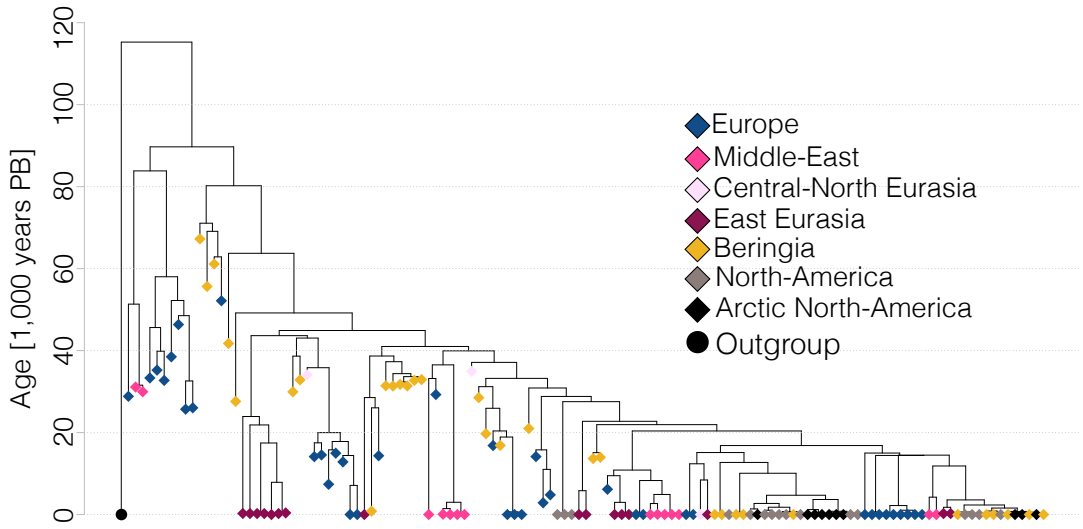

Fig. 3.2: Tip calibrated BEAST tree of all samples used in the spatial analyses (diamonds), coloured by geographic region. The circle represents an outgroup (modern Indian wolf, not used in the analyses).

3.5.2 A spatially explicit model of the expansion

Motivated by the population structure observed in whole genome studies of modern wolves (Fan et al. 2016), we tested the degree of spatial genetic structure among the modern wolf samples in our dataset, and found a strong pattern of genetic isolation by distance across Eurasia (ρ=0.3, p<0.0001; see Fig. 3.S8). To take this structure into account in our spatial framework, we represented the wolf distribution in the Northern Hemisphere as seven demes (Fig. 3.1), each of which is defined by major geographic barriers including mountain ranges, seas, oceans and deserts (see Materials and Methods). We then used coalescent simulations (see Materials and Methods) to test a range of different explicit demographic scenarios (illustrated in Fig. 3.3a), with sampling matching the empirical spatial and temporal distribution of our samples.

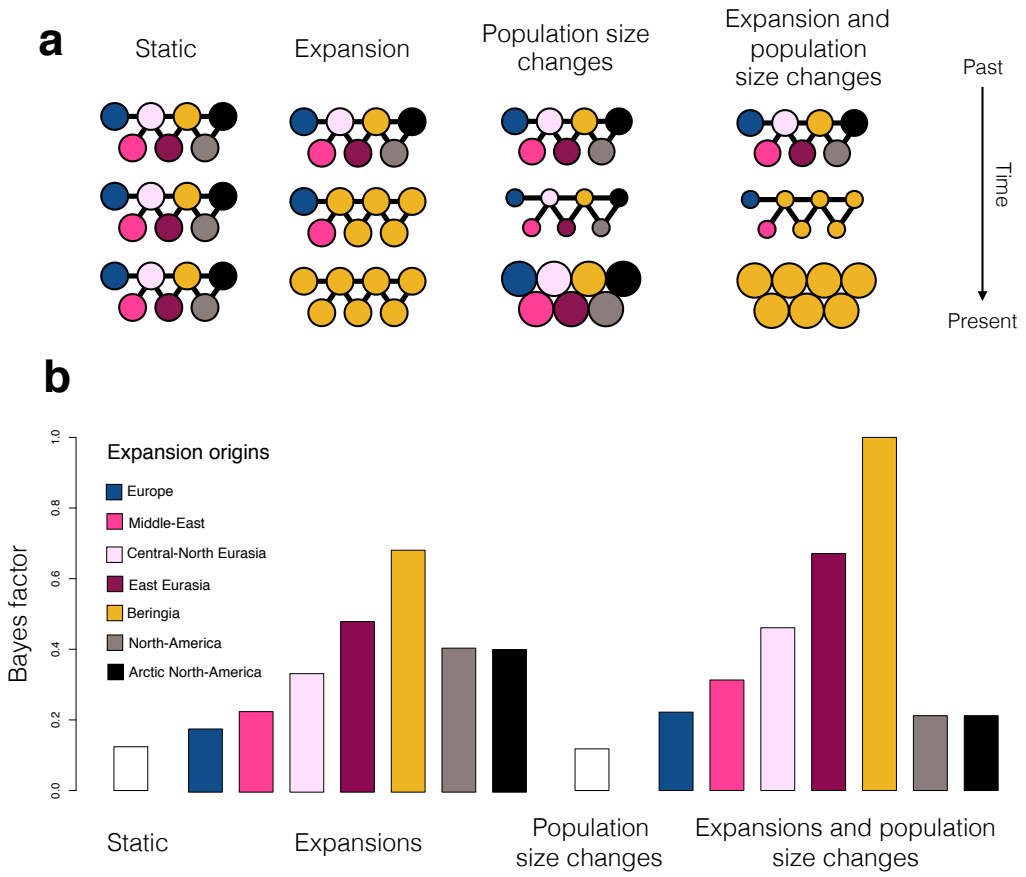

Fig. 3.3: Spatially and temporally explicit analysis. (a) Illustration of the different scenarios, with circles representing one deme each for the seven different geographic regions (see panel b for colour legend and text for full description of the scenarios). Solid lines represent population connectivity. The *static* scenario (far left) shows stable populations through time. The *expansion* scenarios (middle left) shows how one deme (here yellow, corresponding to Beringia) expands and sequentially replaces the populations in all other demes (from top to bottom). The *population size change scenario* (middle right) illustrates how population size in the demes can change through time (large or small population size shown as large or small circles, respectively. We also show a combined scenario (far right) of both expansion and population size change. (b) Likelihood of each demographic scenario relative to the most likely scenario, shown as Bayes factors, estimated using Approximate Bayesian Computation analyses (see text for details). For expansion scenarios (including the combined expansion and population size changes), we colour code each bar according to the origin of the expansion (see colour legend).

The first scenario consisted of a constant population size and uniform movement between neighbouring demes. This allowed us to test the null hypothesis that drift within a structured population alone can explain all the patterns observed in the mitochondrial tree. We then considered two additional demographic processes that could explain the observed patterns: 1) a temporal sequence of two population size changes that affected all demes simultaneously (thus allowing for a bottleneck); and 2) an expansion out of one of the demes, which had a continuous population through time and sequentially replaced the populations in the other demes (repeated for all seven possible expansion origins). We considered each demographic event in isolation as well as their combined effect (resulting in a total of 16 scenarios) and used Approximate Bayesian Computation (ABC) to calculate the likelihood of each scenario and estimate parameter values.

Both the null scenario and the scenario of only population size change in all demes were strongly rejected (Bayes Factor (BF) $\leq$ 0.1, Fig. 3.3b and Table 3.S6), illustrating the power of combining a large dataset of ancient samples with statistical modelling. Scenarios that combined an expansion with a change in population size (bottleneck) were better supported than the corresponding scenarios (i.e. with the same origin) with constant population size (Fig. 3.3b). The best-supported scenario (BF 1, Fig. 3.4) was characterized by the combination of a rapid expansion of wolves out of the Beringian deme ~25,000 years ago (95% CI: 33,000-14,000 years ago) with a population bottleneck between 15,000 and 40,000 years ago, and limited gene flow between neighbouring demes (see Table 3.S7 and Fig. 3.S15 for posterior distributions of all model parameters). We also found relatively strong support for a scenario that describes a wolf expansion out of the East Eurasian deme (BF 0.7) with nearly identical parameters to the best-supported scenario (Table 3.S8 & Fig. 3.S16). This can be explained by geographic proximity of East Eurasia to Beringia and the genetic similarity of wolves from these areas.

3.6 Discussion

Recent whole-genome studies (Freedman et al. 2014; Skoglund et al. 2015; Fan et al. 2016) found that modern grey wolves (*Canis lupus*) across Eurasia are descended from a single source population. The results of our analyses using both ancient and modern grey wolf samples (Fig. 3.1) within a spatially and temporally explicit modelling framework (Fig. 3.3), suggest that this process began ~24,000 (95% CI:13,000-33,000) years ago when a population of wolves from Beringia (or a Northeast Asian region in close

geographic proximity) expanded outwards and replaced indigenous Pleistocene wolf populations across Eurasia (Fig. 3.4). The star-like topology of modern wolves observed in these whole genome studies is also consistent with our inferred scenario (Fig. 3.4) in which the wave of expansion is divided by geographic barriers, leading to divergence of subpopulations within the Northern Hemisphere due to subsequent limited gene flow.

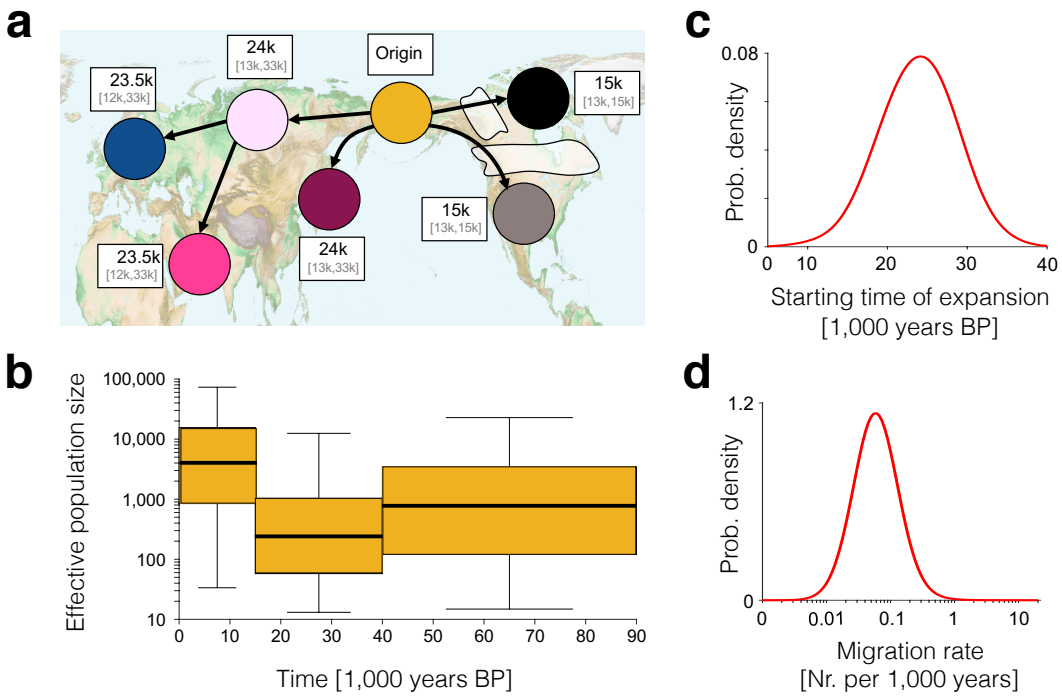

Fig. 3.4: The inferred scenario of wolf demography from the Bayesian analysis using our spatially and temporally explicit model (see Fig. 3.3 and the main text). (a) Geographic representation of the expansion scenario (out of Beringia) with median and 95% CI for the date of the population replacement in each deme given in white boxes next to each deme. (b) Effective population size (thick line, boxes and whiskers show the median, interquartal range and 95% CI, respectively, for each time period). (c) Posterior distribution of migration rate and (d) starting time of expansion.

In the Americas, the Beringian expansion was delayed due to the presence of ice sheets extending from Greenland to the northern Pacific Ocean (Fig. 3.4) (Raghavan et al. 2015). A recent study by Koblmüller et al. (2016) suggested that wolf populations that were extant south of these ice sheets were replaced by Eurasian wolves crossing the Beringian land bridge. Our analyses support the replacement of North American wolves (following the retreat of the ice sheets), and our more extensive ancient DNA sampling combined with a spatially explicit model has allowed us to narrow down the geographic origin of this expansion.

Were the wolves before and after this replacement ecologically equivalent? Analyses of wolf specimens have noted morphological differences between Late-Pleistocene and Holocene wolves: late Pleistocene specimens have been described as cranio-dentally more robust than the present-day grey wolves, as well as having specialized adaptations for carcass and bone processing (Kuzmina and Sablin 1993; Leonard et al. 2007; Baryshnikov et al. 2009) associated with megafaunal hunting and scavenging (Fox-Dobbs et al. 2008; Germonpré et al. 2017). In contrast, the early Holocene archaeological record has only yielded a single sample with the Pleistocene wolf morphotype (in Alaska) (Leonard et al. 2007), suggesting that this ecomorph had largely disappeared from the Northern Hemisphere by the Pleistocene-Holocene transition. This change in wolf morphology coincides with a shift in wolf isotope composition (Bocherens 2015) and the disappearance of many megafaunal herbivores as well as other large predators, such as cave hyenas and cave lions, suggesting a possible change in the ecological niche of wolves.

It has been unclear whether the morphological change was the result of population replacement (genetic turnover), a plastic response to a dietary shift, or both. Our results suggest that the Pleistocene-Holocene transition was accompanied by a genetic turnover in most of the Northern Hemisphere wolf populations since most indigenous wolf populations experienced a large-scale replacement resulting in the loss of all native Pleistocene genetic lineages (Fig. 3.4). Similar population dynamics of discontinuity and replacement by conspecifics have been observed in several other large Pleistocene mammals in Europe including cave bears, woolly mammoths (Stuart et al. 2004; Palkopoulou et al. 2013), giant deer (Stuart et al. 2004) and even humans (Fu et al. 2016; Posth et al. 2016).

The geographic exception to this pattern of widespread replacement is Beringia, where we infer demographic continuity between late Pleistocene and Holocene wolf populations (Fig. 3.4). This finding is consistent with a recent study using the mtDNA control region by Ersmark *et al.* (2016) that failed to reject continuity in this region, but at odds with a previous suggestion of genetic turnover in Beringia (Leonard et al. 2007). This contradiction is likely the result of both the amount of data available and the analytical methodology: Leonard et al. (2007) used a short segment (427 bases long) of the mitochondrial control region and employed a descriptive phylogeographic approach, whereas our conclusions are based on an expanded dataset both in terms of sequence length, sample number, and geographic and temporal range (Fig. 3.1) and a formal hypothesis testing within a Bayesian framework (Figs. 3.3 and 3.4). As a consequence, the morphological and dietary shift observed in Beringian wolves between the late Pleistocene and Holocene (Leonard et al. 2007) cannot be explained by a population turnover, but instead requires an alternative explanation such as adaptation or plastic responses to the substantial environmental and ecological changes that took place during this period. Indeed, grey wolves are a highly adaptable species. Studies of modern grey wolves have found that differences in habitat - specifically precipitation, temperature, vegetation, and prey specialization, can strongly affect their cranio-dental morphology (Geffen et al. 2004; Pilot et al. 2006; O'Keefe et al. 2013; Flower and Schreve 2014; Leonard 2015).

The specific causal factors for the replacement of indigenous Eurasian wolves during the LGM by their Beringian conspecifics (and American wolves following the disappearance of the Cordilleran and Laurentide ice sheets) are beyond the scope of this study. However, one possible explanation may be related to the relatively stable climate of Beringia compared to the substantial climatic fluctuations that impacted the rest of Eurasia and Northern America during the late Pleistocene (Clark et al. 2012). These fluctuations have been associated with dramatic changes in food webs, leading to the loss of most of the large Pleistocene predators in the region (Lister and Stuart 2008; Hofreiter and Stewart 2009; Lorenzen et al. 2011; Bocherens 2015). In addition, the hunting of large Pleistocene predators by Upper Palaeolithic people (e.g. Münzel and Conard 2004; Germonpré and Hämäläinen 2007; Cueto et al. 2016) may have also negatively impacted large carnivore populations (Fan et al. 2016). An interdisciplinary approach involving morphological,

isotopic as well as genetic data is necessary to better understand the relationship between wolf population dynamics and dietary adaptations in the late Pleistocene and early Holocene period.

In summary, we have found that that, despite a continuous fossil record through the late Pleistocene, wolves experienced a complex demographic history involving population bottlenecks and replacements (Fig. 3.4). Our analysis suggests that long-range migration played an important role in the survival of wolves through the wave of megafaunal extinctions at the end of the last glaciation. These results will enable future studies to examine specific local climatic and ecological factors that enabled the Beringian wolf population to survive and expand across the Northern Hemisphere.

Lastly, the complex demographic history of Eurasian grey wolves reported here (Fig. 3.4) also has significant implications for identifying the geographic origin(s) of wolf domestication and the subsequent spread of dogs. For example, the limited understanding of the underlying wolf population structure may explain why previous studies have produced conflicting geographic and temporal scenarios. Numerous previous studies have focused on the patterns of genetic variation in modern domestic dogs, but have failed to consider potential genetic variation present in late Pleistocene wolf population, thereby implicitly assuming a homogenous wolf population source. As a result, both the domestication and the subsequent human-mediated movements of dogs were the only processes considered to have affected the observed genetic patterns in dog populations. However, both domestication from and admixture with a structured wolf population will have consequences for patterns of genetic variation within dogs.

In light of the complex demographic history of wolves (and the resulting population genetic structure) reconstructed by our analysis, several of the geographic patterns of haplotype distribution observed in previous studies, including differences in levels of diversity found within local dog populations (Wang et al. 2016), and the deep phylogenetic split between Eastern and Western Eurasian dogs (Frantz et al. 2016), could have resulted from known admixture between domestic dogs and grey wolves (Verardi et al. 2006; Godinho et al. 2011; Freedman et al. 2014; Fan et al. 2016). Future analyses should therefore explicitly include the demographic history of wolves and demonstrate that the patterns of variation observed within dogs fall outside expectations that take admixture with geographically structured wolf populations into account.

3.7 Materials and methods

3.7.1 Data preparation

We sequenced whole mitochondrial genomes of 40 ancient and 22 modern wolf samples. Sample information, including geographic locations, estimated ages and archaeological context information for the ancient samples, is provided in the Table 3.S1 and Supplementary Information 3.S1.2. Of the 40 ancient samples, 24 were directly radiocarbon dated for this study and calibrated using the IntCal13 calibration curve (see Table 3.S1 for radiocarbon dates, calibrated age ranges and AMS laboratory reference numbers). DNA extraction, sequencing and quality filtering, and mapping protocols used are described in 3.S2.

We included 16 previously published ancient mitochondrial wolf genomes (Table 3.S1 and 3.S2). In order to achieve a uniform dataset, we re-processed the raw reads from previously published samples using the same bioinformatics pipeline as for the newly generated sequences.

We subjected the aligned ancient sequences to strict quality criteria in terms of damage patterns and missing data (Figs. 3.S3 – 3.S5). First, we excluded all whole mitochondrial sequences that had more than 1/3 of the whole mitochondrial genome missing (excluding the mitochondrial control region – see below) at minimum three-fold coverage. Secondly, we excluded all ancient whole mitochondrial sequences that contained more than 0.1% of singletons showing signs of deamination damage typical for ancient DNA (C to T or A to G singletons). After quality filtering, we were left with 32 newly sequenced and 13 published ancient whole mitochondrial sequences (Table 3.S1).

We also excluded sequences from archaeological specimens that postdate the end of Pleistocene and that have been identified as dogs (Table 3.S1), since any significant population structure resulting from a lack of gene flow between dogs and wolves could violate the assumption of a single, randomly mating canid population. Some of the Pleistocene specimens used in the demographic analyses (TH5, TH12, TH14) have been argued to show features commonly found in modern dogs and have therefore been suggested to represent Paleolithic dogs (e.g. Sablin and Khlopachev 2002; Germonpré et al. 2009; Germonpré et al. 2012; Druzhkova et al. 2013; Germonpré et al. 2015; Germonpré et al. 2017). Here, we disregard such status calls because of the controversy that surrounds them (Crockford and Kuzmin 2012; Morey 2014; Drake et al. 2015; Perri

2016), and because early dogs would have been genetically similar to the local wolf populations form which they derived. This reasoning is supported by the close proximity of these samples to other wolf specimens confidently described as wolves in the phylogenetic tree (see Fig. 3.S10).

Finally, we added 66 modern published wolf sequences from NCBI and two sequences from Freedman et al. (2014) (Table 3.S1) resulting in a final dataset of 135 complete wolf mitochondrial genome sequences, of which 45 were ancient and 90 were modern. We used ClustalW alignment tool (version 2.1) (Larkin et al. 2007) to generate a joint alignment of all genomes. In order to avoid the potentially confounding effect of recurrent mutations in the mitochondrial control region (Excoffier and Yang 1999) in pairwise difference calculations, we removed this region from all subsequent analyses. This resulted in an alignment of sequences 15,466bp in length, of which 1301 sites (8.4%) were variable. The aligned dataset is located in Supplementary File S1 (this dataset is too large to include in the printed thesis, but is available upon request from L. Loog).

3.7.2 Phylogenetic analysis

We calculated the number of pairwise differences between all samples (Fig. 3.S6) and generated a neighbour-joining tree based on pairwise differences (Fig. 3.S7). This tree shows a clade consisting of samples exclusively from the Tibetan region and the Indian sub-continent that are deeply diverged from all ancient and other modern wolf samples (see also Sharma et al. (2004) and Aggarwal et al. (2007)). A recent study of whole gnome data showed a complex history of South Eurasian wolves (Fan et al. 2016) that is beyond the scope of our study. While their neighbour-joining phylogeny grouped South Eurasian wolves with East and North East Asian wolves (Fig. 3 in Fan et al. (2016)), they cluster outside of all other grey wolves in a Principal Component Analysis (Fig. 4 in Fan et al. (2016)), and also show a separate demographic history within a PSMC analysis (Fig. 5 in Fan et al. (2016)). Because our study did not possess sufficient samples from the Himalayas and the Indian subcontinent to unravel their complex demography, we excluded samples from these regions and focused on the history of North Eurasian and North American wolves, for which we have good coverage through time and space.

We used PartitionFinder (Lanfear et al. 2012) and BEAST (v.1.8.0) (Drummond et al. 2012) to build a tip calibrated wolf mitochondrial tree (with a strict global clock, see section 3.S3.2 for full details) from modern and directly dated ancient samples, and to

estimate mutation rates for four different partitions of the wolf mitochondrial genome (see Tables 3.S3 and 3.S4 for results).

We used BEAST to molecularly date seven sequences from samples that were not directly radiocarbon dated (TH4, TH6, TH14, TU15) or that had been dated to a period beyond the limit of reliable radiocarbon dating (>48,000 years ago) (CGG12, CGG29, CGG32). We estimated the ages of the samples by performing a BEAST run where the mutation rate was fixed to the mean estimates from the previous BEAST analysis and all other parameter settings were set as described in the 3.S3.2. We cross-validated this approach through a leave-one-out analysis where we sequentially removed a directly dated sample and estimated its date as described above. We find a close fit (R^2=0.86) between radiocarbon and molecular dates (Fig. 3.S9). We combined the seven undated samples with the 110 ancient and modern samples from the previous run and used a uniform prior ranging from 0 to 100,000 years to estimate the ages of the seven undated samples (see Table 3.S5 for results).

Finally, in order to estimate the mitochondrial divergence time between the South Eurasian (Tibetan and Indian) and the rest of our wolf samples, we performed an additional BEAST run in which we included all modern and ancient grey wolves (*N* = 129) as well as five Tibetan and one Indian wolf, and used parameters identical to the ones described above. The age of the ancient samples was set as the mean of the calibrated radiocarbon date distribution (for radiocarbon dated samples) or as the mean of the age distribution from the BEAST analyses (for molecularly dated samples).

3.7.3 Isolation by distance analysis

We performed isolation by distance (IBD) analyses to see the extent to which wolf mitochondrial genetic variation shows population structure. To this end, we regressed the pairwise geographic distances between 84 modern wolf samples (Table 3.S1) against their pairwise genetic (mitochondrial) distances. The geographic distance between all sample pairs was calculated in kilometres as the great circle distance from geographic coordinates, using the Haversine Formula (Sinnott 1984) to account for the curvature of the Earth as follows:

$$G_{ij} = 2r \arcsin\left(\sqrt{\sin\left((\varphi_j - \varphi_i)/2\right)^2 + \cos(\varphi_i)\cos\left(\varphi_j\right)\sin\left((\lambda_i - \lambda_j)/2\right)^2}\right)$$

Where G is the distance in kilometres between individuals i and j; ϕ_i and ϕ_j are the latitude coordinates of individuals i and j, respectively; λi and λj are the longitude coordinates of individuals i and j, respectively; and r is the radius of the earth in kilometres. The pairwise genetic distances were calculated as the proportion of sites that differ between each pair of sequences (excluding the missing bases), using *dist.dna* function in the R package APE (Paradis et al. 2004).

3.7.4 Geographical deme definitions

We represented the wolf geographic range as seven demes, defined by major geographic barriers through time.

1. The *European* deme is bordered by open water from the North and the West (the Arctic and the Atlantic oceans, respectively); the Ural Mountains from the East; and the Mediterranean, the Black and the Caspian Sea and the Caucasus mountains from the South.
2. The *Middle-Eastern* deme consists of the Arabian Peninsula, Anatolia and Mesopotamia and is bordered by the Black Sea, the Caspian Sea and the Aral Sea in the North; the Indian Ocean in the South; the Tien Shen mountain range, the Tibetan Plateau and the Himalayas from the East; and the Mediterranean Sea in the West.
3. The *Central North Eurasian* deme consist of the Siberian Plateau and is bordered by the Arctic Ocean from the North; the Ural Mountains from the West; the Lena River and mountain ranges of North Eastern Siberia (Chersky and Verkhoyansk ranges) from the East; and the Tien Shen mountain range, the Tibetan Plateau and the Gobi Desert from South-East.
4. The *East Eurasian deme* is bordered by the Tien Shen mountain range, the Tibetan Plateau and Gobi desert from the West; the Pacific Ocean from the East; and the Lena river and the mountain ranges of North Eastern Siberia (Chersky and Verkhoyansk ranges) from the North.
5. The *Beringia* deme spans the Bering Strait, which was a land bridge during large parts of the Late Pleistocene and the Early Holocene. It is bordered to the West by the Lena River and mountain ranges of North Eastern Siberia (Chersky and Verkhoyansk ranges), and to the South and East by the extent of the Cordillerian and Laurentide ice sheets during the Last Glacial Maximum.

6. The *Arctic North America* deme consists of an area of the North American continent east of the Rocky Mountains and west of Greenland, that was covered by ice during the last Glaciation and is at present known as the Canadian Arctic Archipelago.
7. The *North America* deme consists of an area in the Northern American sub-continent that was south of the Cordillerian and Laurentide ice sheets during the last glaciation (Raghavan et al. 2015).

3.7.5 Demographic scenarios

We tested a total of 16 demographic scenario combinations, from four different kinds of demographic scenarios (illustrated in Fig. 3.3a in the main text):

1. Static model (the null hypothesis) – neighbouring demes exchange migrants, no demographic changes.
2. Bottleneck scenarios – demes exchange migrants as in the static model but populations have different size in different time periods. We consider three time periods: 0-15k years ago, 15k-40k years ago, and >40k years ago.
3. Expansion scenarios - demes exchange migrants like in the static model but a single deme experiences an expansion starting between 5k and 40k years ago (at a minimum rate of 1,000 years per deme, so the whole world could be colonized within 3,000 years or faster).
4. Combinations of scenarios 2 & 3.

3.7.6 Population genetic coalescent framework

We implemented coalescent population genetic models for the different demographic scenarios to sample gene genealogies.

In the static scenario, we simulated local coalescent processes (Kingman 1982) within each deme (scaled to rate $1/K$ per pair of lineages, where K is the mean time to most recent common ancestor in a deme and is thus proportional to the effective population size). In addition, we moved lineages between demes according to a Poisson process with rate m per lineage. To match the geographic and temporal distribution of the data, we represented each sample with a lineage from the corresponding deme and date.

The bottleneck scenario was implemented as the static one but with piecewise constant values for K as a function of time. We considered three time periods, each with its own

value of K (K_1, K_2 and K_3), motivated by the archaeological and genetic evidence of wolf population changes described in the main text. The first time period was from present to early Holocene, 0-15k years ago. The second time period extended from early Holocene to late Pleistocene and covered the last glacial maximum, 15-40k years ago. Finally, the third time period covered the late Pleistocene and beyond, i.e. 40k years ago and older.

The population expansion scenarios were based on the static model but with an added population expansion model with founder effects and replacement of local populations (we refer to populations not yet replaced by the expansion as "indigenous"). Starting at time T, the population expanded from the initial deme and replaced its neighbouring populations. After the start of the expansion, the expansion proceeded in fixed steps of ΔT (in time). At each step, colonised populations replaced neighbouring indigenous populations (if an indigenous deme bordered to more than one colonised deme, these demes contributed equally to the colonisation of the indigenous deme). In the coalescent framework (that simulates gene genealogies backwards in time) the colonisation events corresponds to forced migrations from the indigenous deme to the source deme. If there were more than one source deme, the source of each lineage was chosen randomly with equal probability. Finally, founder effects during the colonisation of an indigenous deme were implemented as a local, instantaneous population bottleneck in the deme (after the expansion), with a severity scaled to give a fixed probability x of a coalescent event for each pair of lineages in the deme during the bottleneck (Eriksson and Mehlig 2004). (x=1 correspond to a complete loss of genetic diversity in the bottleneck, and x=0 corresponds to no reduction in genetic diversity.)

Finally, the combined scenario of population expansion and bottlenecks was implemented by making the population size parameter K in the population expansion model time dependent as in the population bottleneck model.

3.7.7 Approximate Bayesian Computation analysis

We used Approximate Bayesian Computation (ABC) analysis (Beaumont et al. 2002) with ABCtoolbox (Wegmann et al. 2010) to formally test the fit of our different demographic models. This approach allows formal hypothesis testing using likelihood ratios in the cases where the demographic scenarios are too complex for a direct calculation of the likelihoods given the models. We used the most likely tree from BEAST

(see section 3.S3.2 for details) as data, and simulated trees using the coalescent simulations described above.

To match the assumption of random mixing within each deme in the population genetic model, we removed closely related sequences if they came from the same geographic location and time period, by randomly retaining one of the closely related sequences to be included in the analysis (Table 3.S1, column "Samples used in Simulation Analysis").

To robustly measure differences between simulated and observed trees we use the matrix of time to most recent common ancestor (TMRCA) for all pairs of samples. This matrix also captures other allele frequency based quantities frequently used as summary statistics with ABC, such as F_{ST}, as they can be calculated from the components of this matrix.

In principle the full matrix could be used, but in practice it is necessary to use a small number of summary statistics for ABC to work properly (Wegmann et al. 2010). To this end, we grouped our seven demes into four super demes (Fig. 3.S14), based on geographic proximity and genetic similarity in the dataset, and used mean TMRCA within each super deme and mean TMRCAs between all super demes as summary statistics in the ABC analysis. The four super demes are 1) Europe; 2) Middle East; 3) North East Eurasia, Beringia and East Eurasia combined; and 4) Artic and Continental North America combined. This resulted in 10 summery statistics in total.

An initial round of fitting the model showed that all scenarios underestimate the within-super deme TMRCA for the Middle East, while the rest of the summary statistics were well captured by the best fitting demographic scenarios. This could be explained by a scenario where the Middle East was less affected by the reduction in population size during the last glacial maximum. However, we currently lack sufficient number of samples from this area to explicitly test a more complex scenario such as this hypothesis. To avoid outliers biasing the likelihood calculations in ABC (Wegmann et al. 2010) we removed this summary statistic, resulting in nine summary statistics in total.

For each of the 16 scenarios we performed 1 billion simulations with randomly chosen parameter combinations, chosen from the following parameter intervals for the different scenarios:

1. The static scenario: m in [0.001,20] and K in [0.01,100].

2. The bottleneck scenarios: m in [0.001,20] and K_1, K_2, K_3 in [0.01,100].
3. The expansion scenarios: m in [0.001,20], K in [0.01,100], x in [0,1], T in [5,40] and ΔT in [0.001,1]. For expansion out of the North American scenario and the expansion out of the Arctic North American scenario, the glaciation and during the LGM in North American and sea level rise during the de-glaciation mean that T must be in the range [9,16]
4. The combined bottleneck and expansion scenarios: m in [0.001,20], K_1,K_2,K_3 in [0.01,100], x in [0,1], T in [5,40] and ΔT in [0.001,1].

The parameter m is measured in units of 1/1,000 years, and T, ΔT, K, K_1, K_2 and K_3 are measured in units of 1,000 years. The parameters x, T and ΔT were sampled according to a uniform distribution over the interval, while all other parameters were sampled from a uniform distribution of their log-transformed values. To identify good parameter combinations for ABC, we first calculated the Euclidian square distances between predicted and observed statistics and restricted analysis to parameter combinations within 10% of the variation of summary statistics. We then ran the ABCtoolbox (Wegmann et al. 2010) on the accepted parameter combinations to estimate posterior distributions of the model parameters, and to calculate the likelihood of each scenario as described in the ABCtoolbox manual.

See Table 3.S6 for ABC likelihoods and Bayes factors for all demographic scenarios tested.

See Tables 3.S7 and 3.S8 for posterior probability estimates and Figs. 3.S15 and 3.S16 for posterior density distributions for estimated parameters (ΔT, T, $\log_{10} K_1$, $\log_{10} K_2$, $\log_{10} K_3$, $\log_{10} m$, x) in the two most likely models (An expansion out of Beringia with a population size change and an expansion out of East Eurasia with a population size change).

3.7.8 Data availability

New sequences are available to download from GenBank database (accession numbers XX-XX). The raw sequence reads are available from ENA database (accession numbers XX-XX). The scripts used in the analyses are available up on request from L.L. and A.E.

3.8 References

Aggarwal RK, Kivisild T, Ramadevi J, Singh L. 2007. Mitochondrial DNA coding region sequences support the phylogenetic distinction of two Indian wolf species. J. Zool. Syst. Evol. Res. 45:163–172.

Baryshnikov GF, Mol D, Tikhonov AN. 2009. Finding of the Late Pleistocene carnivores in Taimyr Peninsula (Russia, Siberia) with paleoecological context. Russ. J. Theriol. 8:107–113.

Beaumont MA, Zhang W, Balding DJ. 2002. Approximate Bayesian Computation in Population Genetics. Genetics 162:2025–2035.

Bocherens H. 2015. Isotopic tracking of large carnivore palaeoecology in the mammoth steppe. Quat. Sci. Rev. 117:42–71.

Clark PU, Shakun JD, Baker PA, Bartlein PJ, Brewer S, Brook E, Carlson AE, Cheng H, Kaufman DS, Liu Z, et al. 2012. Global climate evolution during the last deglaciation. Proc. Natl. Acad. Sci. 109:E1134–E1142.

Crockford SJ, Kuzmin YV. 2012. Comments on Germonpré et al., Journal of Archaeological Science 36, 2009 "Fossil dogs and wolves from Palaeolithic sites in Belgium, the Ukraine and Russia: osteometry, ancient DNA and stable isotopes", and Germonpré, Lázkičková-Galetová, and Sablin, Journal of Archaeological Science 39, 2012 "Palaeolithic dog skulls at the Gravettian Předmostí site, the Czech Republic." J. Archaeol. Sci. 39:2797–2801.

Cueto M, Camarós E, Castaños P, Ontañón R, Arias P. 2016. Under the Skin of a Lion: Unique Evidence of Upper Paleolithic Exploitation and Use of Cave Lion (Panthera spelaea) from the Lower Gallery of La Garma (Spain). PLOS ONE 11:e0163591.

Drake AG, Coquerelle M, Colombeau G. 2015. 3D morphometric analysis of fossil canid skulls contradicts the suggested domestication of dogs during the late Paleolithic. Sci. Rep. 5:8299.

Drummond AJ, Nicholls GK, Rodrigo AG, Solomon W. 2002. Estimating Mutation Parameters, Population History and Genealogy Simultaneously From Temporally Spaced Sequence Data. Genetics 161:1307–1320.

Drummond AJ, Suchard MA, Xie D, Rambaut A. 2012. Bayesian Phylogenetics with BEAUti and the BEAST 1.7. Mol. Biol. Evol. 29:1969–1973.

Druzhkova AS, Thalmann O, Trifonov VA, Leonard JA, Vorobieva NV, Ovodov ND, Graphodatsky AS, Wayne RK. 2013. Ancient DNA Analysis Affirms the Canid from Altai as a Primitive Dog. PLOS ONE 8:e57754.

Eriksson A, Mehlig B. 2004. Gene-history correlation and population structure. Phys. Biol. 1:220.

Ersmark E, Klütsch CFC, Chan YL, Sinding M-HS, Fain SR, Illarionova NA, Oskarsson M, Uhlén M, Zhang Y, Dalén L, et al. 2016. From the Past to the Present: Wolf Phylogeography and Demographic History Based on the Mitochondrial Control Region. Front. Ecol. Evol. [Internet] 4. Available from: http://journal.frontiersin.org/article/10.3389/fevo.2016.00134/abstract

Excoffier L, Yang Z. 1999. Substitution rate variation among sites in mitochondrial hypervariable region I of humans and chimpanzees. Mol. Biol. Evol. 16:1357–1368.

Fan Z, Silva P, Gronau I, Wang S, Armero AS, Schweizer RM, Ramirez O, Pollinger J, Galaverni M, Del-Vecchyo DO, et al. 2016. Worldwide patterns of genomic variation and admixture in gray wolves. Genome Res. 26:163–173.

Flower LOH, Schreve DC. 2014. An investigation of palaeodietary variability in European Pleistocene canids. Quat. Sci. Rev. 96:188–203.

Fox-Dobbs K, Leonard JA, Koch PL. 2008. Pleistocene megafauna from eastern Beringia: Paleoecological and paleoenvironmental interpretations of stable carbon and nitrogen isotope and radiocarbon records. Palaeogeogr. Palaeoclimatol. Palaeoecol. 261:30–46.

Frantz LAF, Mullin VE, Pionnier-Capitan M, Lebrasseur O, Ollivier M, Perri A, Linderholm A, Mattiangeli V, Teasdale MD, Dimopoulos EA, et al. 2016. Genomic and archaeological evidence suggest a dual origin of domestic dogs. Science 352:1228.

Freedman AH, Gronau I, Schweizer RM, Vecchyo DO-D, Han E, Silva PM, Galaverni M, Fan Z, Marx P, Lorente-Galdos B, et al. 2014. Genome Sequencing Highlights the Dynamic Early History of Dogs. PLOS Genet 10:e1004016.

Fu Q, Posth C, Hajdinjak M, Petr M, Mallick S, Fernandes D, Furtwängler A, Haak W, Meyer M, Mittnik A, et al. 2016. The genetic history of Ice Age Europe. Nature 534:200–205.

Geffen E, Anderson MJ, Wayne RK. 2004. Climate and habitat barriers to dispersal in the highly mobile grey wolf. Mol. Ecol. 13:2481–2490.

Germonpré M, Fedorov S, Danilov P, Galeta P, Jimenez E-L, Sablin M, Losey RJ. 2017. Palaeolithic and prehistoric dogs and Pleistocene wolves from Yakutia: Identification of isolated skulls. J. Archaeol. Sci. 78:1–19.

Germonpré M, Hämäläinen R. 2007. Fossil Bear Bones in the Belgian Upper Paleolithic: The Possibility of a Proto Bear-Ceremonialism. Arct. Anthropol. 44:1–30.

Germonpré M, Lázničková-Galetová M, Losey RJ, Räikkönen J, Sablin MV. 2015. Large canids at the Gravettian Předmostí site, the Czech Republic: The mandible. Quat. Int. 359–360:261–279.

Germonpré M, Lázničková-Galetová M, Sablin MV. 2012. Palaeolithic dog skulls at the Gravettian Předmostí site, the Czech Republic. J. Archaeol. Sci. 39:184–202.

Germonpré M, Sablin MV, Stevens RE, Hedges REM, Hofreiter M, Stiller M, Després VR. 2009. Fossil dogs and wolves from Palaeolithic sites in Belgium, the Ukraine and Russia: osteometry, ancient DNA and stable isotopes. J. Archaeol. Sci. 36:473–490.

Godinho R, Llaneza L, Blanco JC, Lopes S, Álvares F, García EJ, Palacios V, Cortés Y, Talegón J, Ferrand N. 2011. Genetic evidence for multiple events of hybridization between wolves and domestic dogs in the Iberian Peninsula. Mol. Ecol. 20:5154–5166.

Groucutt HS, Petraglia MD, Bailey G, Scerri EML, Parton A, Clark-Balzan L, Jennings RP, Lewis L, Blinkhorn J, Drake NA, et al. 2015. Rethinking the dispersal of Homo sapiens out of Africa. Evol. Anthropol. Issues News Rev. 24:149–164.

Hofreiter M, Stewart J. 2009. Ecological Change, Range Fluctuations and Population Dynamics during the Pleistocene. Curr. Biol. 19:R584–R594.

Kingman JFC. 1982. The coalescent. Stoch. Process. Their Appl. 13:235–248.

Koblmüller S, Vilà C, Lorente-Galdos B, Dabad M, Ramirez O, Marques-Bonet T, Wayne RK, Leonard JA. 2016. Whole mitochondrial genomes illuminate ancient intercontinental dispersals of grey wolves (Canis lupus). J. Biogeogr. 43:1728–1738.

Kuzmina I., Sablin MV. 1993. Pozdnepleistotsenovyi pesets verhnei Desny. In: Materiali po mezozoickoi i kainozoickoi istorii nazemnykh pozvonochnykh. Trudy 17 Zoologicheskogo Instituta RAN 249. p. 93–104.

Lanfear R, Calcott B, Ho SYW, Guindon S. 2012. PartitionFinder: Combined Selection of Partitioning Schemes and Substitution Models for Phylogenetic Analyses. Mol. Biol. Evol. 29:1695–1701.

Larkin MA, Blackshields G, Brown NP, Chenna R, McGettigan PA, McWilliam H, Valentin F, Wallace IM, Wilm A, Lopez R, et al. 2007. Clustal W and Clustal X version 2.0. Bioinformatics 23:2947–2948.

Larson G, Karlsson EK, Perri A, Webster MT, Ho SYW, Peters J, Stahl PW, Piper PJ, Lingaas F, Fredholm M, et al. 2012. Rethinking dog domestication by integrating genetics, archeology, and biogeography. Proc. Natl. Acad. Sci. 109:8878–8883.

Leonard JA. 2015. Ecology drives evolution in grey wolves. Evol. Ecol. Res. 16:461–473.

Leonard JA, Vilà C, Fox-Dobbs K, Koch PL, Wayne RK, Van Valkenburgh B. 2007. Megafaunal Extinctions and the Disappearance of a Specialized Wolf Ecomorph. Curr. Biol. 17:1146–1150.

Lister AM, Stuart AJ. 2008. The impact of climate change on large mammal distribution and extinction: Evidence from the last glacial/interglacial transition. Comptes Rendus Geosci. 340:615–620.

Lorenzen ED, Nogués-Bravo D, Orlando L, Weinstock J, Binladen J, Marske KA, Ugan A, Borregaard MK, Gilbert MTP, Nielsen R, et al. 2011. Species-specific responses of Late Quaternary megafauna to climate and humans. Nature 479:359–364.

Morey DF. 2014. In search of Paleolithic dogs: a quest with mixed results. J. Archaeol. Sci. 52:300–307.

Münzel SC, Conard NJ. 2004. Change and continuity in subsistence during the Middle and Upper Palaeolithic in the Ach Valley of Swabia (south-west Germany). Int. J. Osteoarchaeol. 14:225–243.

Nielsen R, Beaumont MA. 2009. Statistical inferences in phylogeography. Mol. Ecol. 18:1034–1047.

O'Keefe FR, Meachen J, Fet EV, Brannick A. 2013. Ecological determinants of clinal morphological variation in the cranium of the North American gray wolf. J. Mammal. 94:1223–1236.

Palkopoulou E, Dalén L, Lister AM, Vartanyan S, Sablin M, Sher A, Edmark VN, Brandström MD, Germonpré M, Barnes I, et al. 2013. Holarctic genetic structure and range dynamics in the woolly mammoth. Proc R Soc B 280:20131910.

Paradis E, Claude J, Strimmer K. 2004. APE: Analyses of Phylogenetics and Evolution in R language. Bioinformatics 20:289–290.

Perri A. 2016. A wolf in dog's clothing: Initial dog domestication and Pleistocene wolf variation. J. Archaeol. Sci. 68:1–4.

Pilot M, Jedrzejewski W, Branicki W, Sidorovich VE, Jedrzejewska B, Stachura K, Funk SM. 2006. Ecological factors influence population genetic structure of European grey wolves. Mol. Ecol. 15:4533–4553.

Posth C, Renaud G, Mittnik A, Drucker DG, Rougier H, Cupillard C, Valentin F, Thevenet C, Furtwängler A, Wißing C, et al. 2016. Pleistocene Mitochondrial Genomes Suggest a Single Major Dispersal of Non-Africans and a Late Glacial Population Turnover in Europe. Curr. Biol. 26:827–833.

Puzachenko AY, Markova AK. 2016. Diversity dynamics of large- and medium-sized mammals in the Late Pleistocene and the Holocene on the East European Plain: Systems approach. Quat. Int. [Internet]. Available from: http://www.sciencedirect.com/science/article/pii/S1040618215007077

Raghavan M, Steinrücken M, Harris K, Schiffels S, Rasmussen S, DeGiorgio M, Albrechtsen A, Valdiosera C, Ávila-Arcos MC, Malaspinas A-S, et al. 2015. Genomic evidence for the Pleistocene and recent population history of Native Americans. Science:aab3884.

Rambaut A. 2000. Estimating the rate of molecular evolution: incorporating non-contemporaneous sequences into maximum likelihood phylogenies. Bioinformatics 16:395–399.

Rieux A, Eriksson A, Li M, Sobkowiak B, Weinert LA, Warmuth V, Ruiz-Linares A, Manica A, Balloux F. 2014. Improved calibration of the human mitochondrial clock using ancient genomes. Mol. Biol. Evol.:msu222.

Sablin M, Khlopachev G. 2002. The Earliest Ice Age Dogs: Evidence from Eliseevichi 1. Curr. Anthropol. 43:795–799.

Sharma DK, Maldonado JE, Jhala YV, Fleischer RC. 2004. Ancient wolf lineages in India. Proc. R. Soc. Lond. B Biol. Sci. 271:S1–S4.

Sinnott R. 1984. Virtues of the Haversine. Sky Telesc. 68:159.

Skoglund P, Ersmark E, Palkopoulou E, Dalén L. 2015. Ancient Wolf Genome Reveals an Early Divergence of Domestic Dog Ancestors and Admixture into High-Latitude Breeds. Curr. Biol. 25:1515–1519.

Sotnikova M, Rook L. 2010. Dispersal of the Canini (Mammalia, Canidae: Caninae) across Eurasia during the Late Miocene to Early Pleistocene. Quat. Int. 212:86–97.

Stuart AJ, Kosintsev PA, Higham TFG, Lister AM. 2004. Pleistocene to Holocene extinction dynamics in giant deer and woolly mammoth. Nature 431:684–689.

Thalmann O, Shapiro B, Cui P, Schuenemann VJ, Sawyer SK, Greenfield DL, Germonpré MB, Sablin MV, López-Giráldez F, Domingo-Roura X, et al. 2013. Complete Mitochondrial Genomes of Ancient Canids Suggest a European Origin of Domestic Dogs. Science 342:871–874.

Verardi A, Lucchini V, Randi E. 2006. Detecting introgressive hybridization between free-ranging domestic dogs and wild wolves (Canis lupus) by admixture linkage disequilibrium analysis. Mol. Ecol. 15:2845–2855.

Wang G-D, Zhai W, Yang H-C, Wang L, Zhong L, Liu Y-H, Fan R-X, Yin T-T, Zhu C-L, Poyarkov AD, et al. 2016. Out of southern East Asia: the natural history of domestic dogs across the world. Cell Res. 26:21–33.

Warmuth V, Eriksson A, Bower MA, Barker G, Barrett E, Hanks BK, Li S, Lomitashvili D, Ochir-Goryaeva M, Sizonov GV, et al. 2012. Reconstructing the origin and spread of horse domestication in the Eurasian steppe. Proc. Natl. Acad. Sci. 109:8202–8206.

Wegmann D, Leuenberger C, Neuenschwander S, Excoffier L. 2010. ABCtoolbox: a versatile toolkit for approximate Bayesian computations. BMC Bioinformatics 11:116.

3.9 Acknowledgements

The authors are grateful to Daniel Klingberg Johansson & Kristian Murphy Gregersen from the Natural History Museum of Denmark; Gabriella Hürlimann from the Zurich Zoo; Jane Hopper from the Howlett's & the Port Lympne Wild Animal Parks; Cyrintha Barwise-Joubert & Paul Vercammen from the Breeding Centre for Endangered Arabian Wildlife; Link Olson from the University of Alaska Museum of the North; Joseph Cook & Mariel Campbell from the Museum of Southwestern Biology; Lindsey Carmichael & David Coltman from the University of Alberta; North American Fur Auctions; Department of Environment Nunavut and Environment and Natural Resources Northwest Territories for DNA samples from the modern wolves.

The authors are also grateful to the staff at the Danish National High-Throughput Sequencing Centre for technical assistance in the data generation; the Qimmeq project, funded by The Velux Foundations and Aage og Johanne Louis-Hansens Fond, for providing financial support for sequencing ancient Siberian wolf samples; the Rock Foundation (New York, USA) for supporting radiocarbon dating of ancient samples from the Yana site; to Stephan Nylinder from the Swedish Museum of Natural History for advice on phylogenetic analyses and Terry Brown from the University of Manchester for comments on this manuscript.

L.L., K.D. & G.L. were supported by Natural Environment Research Council, UK (grant numbers NE/K005243/1, NE/K003259/1); LL. was also supported by the European Research Council grant (339941-ADAPT); A.M. & A.E. were supported by the European Research Council Consolidator grant (grant number 647787-LocalAdaptation); L.F. & G.L. were supported by the European Research Council grant (ERC-2013-StG 337574-UNDEAD); T.G was supported by European Research Council Consolidator grant (681396-Extinction Genomics) & Lundbeck Foundation grant (R52-5062); O.T. was supported by the National Science Center, Poland (2015/19/P/NZ7/03971) with funding from EU's Horizon 2020 program under the Marie Skłodowska-Curie grant agreement (665778) and Synthesys Project (BETAF 3062); V.P., E.P. & P.N. were supported by the Russian Science Foundation grant (N16-18-10265 RNF); A.P. was supported by the Max Planck Society; M.L-G. was supported by Czech Science Foundation grant (GAČR15-06446S).

3.10 Permission from all co-authors to use our joint work as a contribution towards this thesis

I hereby give permission to Liisa Loog to use our joint work *"Modern wolves trace their origin to a late Pleistocene expansion from Beringia"* as contribution towards her D. Phil. thesis to be submitted for examination at Oxford University.

I confirm that to the best of my knowledge, the author contribution statement below is accurate and Liisa Loog's contribution towards the work is greater than that of any other co-author.

Article author contribution statement: L.L., O.T., M.T.P.G., J.K., G.L., A.E. and A.M. designed the research; O.T., M-H.S.S., V.J.S., K.E.W., M.S.V., I.K.C.L., N.W. and G.S. performed ancient DNA laboratory work with input from J.K., M.T.P.G., H.S., K-H.H., R.S.M. and K-H.H.; M-H.S.S. performed modern DNA laboratory work with input from M.T.P.G; O.T., J.A.S.C. and L.L. performed bioinformatic analyses; L.L., A.E. and A.M. designed the population genetic analyses; L.L. Performed phylogenetic analyses; A.E. implemented the spatial analyses framework; L.L and A.E. performed spatial analyses; M.G., J.B., V.V.P., E.Y.P., P.A.N., S.E.F., J.E-L., A.W.K., B.G., H.N., H-P.U. and M.L-G. provided samples; V.V.P., M.G., M. L-G., H.B., H.N., A.W.K., E.Y.P. and P.A.N. provided context for archaeological samples; A.P., M.G., H.B. and K.D. Helped setting the results of genetic analyses into an archaeological context; A.M., M.T.P.G., A.J.H., G.L., J.K., E.W. and K.D. secured funding for the project; L.L., O.T. and A.E. wrote the initial draft of the manuscript with input from A.M.; L.L., O.T. and A.E wrote the manuscript and the supplementary information with input from A.P., M.G., H.B., M-H.S.S., M.T.P.G., K.E.W., A.M., G.L and K.D.; V.J.S., L.F., A.W.K., K-H.H., A.J.H., R.S.M., H.S., G.S., V.V.P., E.Y.P., P.A.N. and J.E-L. provided comments to the manuscript and/or to the supplementary information.

Date:
Feb 12, 2018

Name(s):
Andrew Kandel

Signature(s):

Date: 14.2.2018

Name(s): MARTINA GALETOVÁ

Signature(s):

Date: 13.2.18

Name(s): Hans-Peter Uerpmann

Signature(s): H.P. Uerpmann

Date: 11.02.2018

Name(s): Pavel A Nikolskiy

Signature(s):

Date: February 14, 2018

Name(s):

Pavlova, Elena Y.
Pitulko, Vladimir V.

Signature(s):

Date: 2/11/18

Name(s): Ripan S. Malhi

Signature(s):

Date: 17.feb. 2018

Name(s): Hannes Napierala

Signature(s):

Date: 12 February, 2018

Name: Prof. Eske Willerslev, University of Copenhagen, University of Cambridge

Signature(s):

Date: 12/2-2018

Name(s): Anders J Hansen

Signature(s):

Date: 11/02/18

Name(s): Prof Keith Dobney

Signature(s): Keith Dobney

Date: 11 Feb 18

Name(s): M T P Gilbert

Signature(s):

Date: 11th of Feb 2018

Name(s): Johannes Krause

Signature(s):

Date: 11/02/2018

Name(s): Gregor Larson

Signature(s):

Date: 11/2/2018

Name(s): Anders Eriksson

Signature(s):

Date: 12/2/2018

Name(s): Andrea Manica

Signature(s):

UNIVERSITY OF OULU
FACULTY OF MEDICINE
Institute of Biomedicine and Biocenter of Oulu
Karl-Heinz Herzig, MD, PhD;
Professor of Physiology and Internal Medicine

February 12th, 2018

School of Archaeology
University of Oxford
1 South Parks Road
Oxford
OX1 3TG
United Kingdom

Regarding: Elongation of residence permit for finalizing the PhD thesis and continuation of postdoctoral fellowship I hereby give permission to Liisa Loog to use our joint work *"Modern wolves trace their origin to a late Pleistocene expansion from Beringia"* as contribution towards her D. Phil. thesis to be submitted for examination at Oxford University.

Dear Madame or Sir,

I confirm that to the best of my knowledge, the author contribution statement below is accurate and Liisa Loog's contribution towards the work is greater than that of any other co-author.

Article author contribution statement:

L.L., O.T., M.T.P.G., J.K., G.L., A.E. and A.M. designed the research; O.T., M-H.S.S., V.J.S., K.E.W., M.S.V., I.K.C.L., N.W. and G.S. performed ancient DNA laboratory work with input from J.K., M.T.P.G., H.S., K-H.H., R.S.M. and K-H.H.; M-H.S.S. performed modern DNA laboratory work with input from M.T.P.G; O.T., J.A.S.C. and L.L. performed bioinformatic analyses; L.L., A.E. and A.M. designed the population genetic analyses; L.L. Performed phylogenetic analyses; A.E. implemented the spatial analyses framework; L.L and A.E. performed spatial analyses; M.G., J.B., V.V.P., E.Y.P., P.A.N., S.E.F., J.E-L., A.W.K., B.G., H.N., H-P.U. and M.L-G. provided samples; V.V.P., M.G., M. L-G., H.B., H.N., A.W.K., E.Y.P. and P.A.N. provided context for archaeological samples; A.P., M.G., H.B. and K.D. Helped setting the results of genetic analyses into an archaeological context; A.M., M.T.P.G., A.J.H., G.L., J.K., E.W. and K.D. secured funding for the project; L.L., O.T. and A.E. wrote the initial draft of the manuscript with input from A.M.; L.L., O.T. and A.E wrote the manuscript and the supplementary information with input from A.P., M.G., H.B., M-H.S.S., M.T.P.G., K.E.W., A.M., G.L and K.D.; V.J.S., L.F., A.W.K., K-H.H., A.J.H., R.S.M., H.S., G.S., V.V.P., E.Y.P., P.A.N. and J.E-L. provided comments to the manuscript and/or to the supplementary information.

Sincerely,

Karl-Heinz Herzig; MD, PhD
Professor of Physiology and Internal Medicine

Web side: http://cc.oulu.fi/~fysiowww/KHHmpr.html
Institute of Biomedicine and Biocenter of Oulu
P.O.Box 5000 (street address: Aapistie 5)
90014 Oulu University, Finland

Tel. + 358 8 537 5280
Mobile + 358-503753124
Email: karl-heinz.herzig@oulu.fi

3.S1 – Archaeological Background and Sample Information

3.S1.1 Paleontological history of grey wolves

Grey wolves (*Canis lupus*) are a highly adaptable species, able to live in a range of environments and with a wide natural distribution. Studies of modern grey wolves have found distinct subpopulations living in close proximity (Musani et al., 2007; Schweizer et al., 2016). This variation is closely linked to differences in habitat - specifically precipitation, temperature, vegetation, and prey specialization, which particularly affect cranio-dental plasticity (Geffen et al., 2004; Pilot et al., 2006; Flower and Schreve, 2014; Leonard, 2015).

The earliest evidence for *Canis lupus* comes from the sites of Cripple Creek Sump (Alaska, United States) and Old Crow (Yukon, Canada; Tedford et al. 2009), indicating Eastern Beringia as the likely center of origin. The age of this material may be up to 1.0 Ma, though the geological attribution and dating is controversial (Repenning 1992, Tedford et al. 2009, Westgate et al. 2013). In Eurasia, *Canis lupus* appears nearly simultaneously during the late Middle Pleistocene, including in Siberia (500-300 ka BP; Sotnikova and Rook 2010), France (400-350 ka BP; Bonifay, 1971, Brugal and Boudadi-Maligne, 2011), and Italy (340-320 ka BP; Anzidei et al. 2012), probably representing the origin of true modern grey wolves (Sardella et al. 2014). By the end of the Middle Pleistocene, grey wolves are found across all of Eurasia (e.g. Kahlke, 1994; Boeskorov and Baryshnikov, 2013).

Late Pleistocene seems to harbor considerable morphological diversity among wolves. However, the Pleistocene wolf morphotypes have been described as cranio-dentally more robust than the present day grey wolves and as having specialized adaptations (e.g., shortened rostrum, pronounced development of the temporalis muscle, robust premolars) for carcass and bone processing (Kuzmina and Sablin 1995, Leonard et al. 2007, Baryshnikov et al. 2009) associated with megafaunal hunting and scavenging.

First described by Olsen (1985) as “short-faced wolves”, a Late Pleistocene hypercarnivorous grey wolf morph with a, broad snout, robust mandible, and large carnassials used for targeting Pleistocene megafauna and scavenging carcasses has been more recently referred to as the Beringian wolf (Leonard et al., 2007; Baryshnikov et al., 2009; Boeskorov and Baryshnikov, 2013; Meachen et al., 2016, Germonpré et al., 2017). The ecomorph is known from just two sites – the eastern Beringian type site in Fairbanks,

Alaska (specimens dated to before 50-12.5 ka; Olsen 1985, Leonard 2007) and Natural Trap Cave, Wyoming in the northern continental United States (specimens dated to 25.8-14.3 ka; Kohn and McKay 2012, Meachen et al., 2016). However, similar robust ecomorphs have been found from western Beringia. Baryshnikov et al. (2009) described a small, but robust wolf also specialized for megafaunal hunting and scavenging from Lake Taimyr, Siberia (dated to c. 19.3 ka; MacPhee et al., 2002). They associated this Lake Taimyr wolf with a similar morphological wolf subspecies from Late Pleistocene Europe, the cave (or "Ice Age") wolf (*Canis lupus spelaeus/Canis lupus brevis*), also a specialized Pleistocene ecomorph. Like the Beringian and Lake Taimyr wolves, the cave wolf was smaller-bodied, but robust cranio-dentally for megafaunal hunting and scavenging (Stiner 2004, Baryshnikov et al., 2009, Diedrich 2013). Though there are clear affinities between these Late Pleistocene morphs, there is very little associated data and more work is needed to better understand any relationships between them. Though a single Pleistocene "Beringian" wolf morphotype has been documented from early Holocene Alaska, most specimens date to the Late Pleistocene, suggesting this Late Pleistocene ecomorph had disappeared by the Pleistocene-Holocene transition, coinciding with the disappearance of many megafaunal herbivores.

The east Beringian environment during the Late Pleistocene was a cold glacial steppe populated by megafauna that included mammoth, bison, horse and muskox. Stable isotope analysis of Beringian wolves confirms that they had a diet consisting of a mix of megafaunal prey species (Leonard et al., 2007), though mammoth may have been rare in their diets (Fox-Dobbs et al., 2008). In fact, the diet of Beringian wolves may have differed depending on the temporal and climatic conditions in which they lived. In the pre-glacial period (up to c. 22 ka), some specialized in forest herbivores (woodland muskox and deer), while others were generalists. During the Last Glacial Maximum (LGM: c. 21-17 ka; Tamm et al., 2007; Pilot et al., 2010) some wolves appear to have been mammoth specialists – though it is unclear if they were hunters or scavengers of this prey – and only the early Holocene wolf had a diet of forest cervids (Fox-Dobbs et al., 2008). It has been found that Pre-LGM European wolves have also had a diet constant with high proportion of mammoth (Bocherens et al., 2015). The diet of the western Beringian Lake Taimyr wolf has yet to be analysed.

Bibliography for 3.S1.1

AnzideI, A.P., Bulgarelli, G.M., Catalano, P., Cerilli, E., Gallotti, R., Lemorini, C., Milli, S., Palombo, M.R., Pantano, W. and Santucci, E., 2012. Ongoing research at the late Middle Pleistocene site of La Polledrara di Cecanibbio (central Italy), with emphasis on human–elephant relationships. Quaternary International, 255, pp.171-187.

Baryshnikov, G.F., Mol, D., Tikhonov, A.N., 2009. Finding of the Late Pleistocene carnivores in Taimyr peninsula (Russia, Siberia), with paleoecological context. Russian Journal of Theriology 8, 107-113.

Bocherens, H., Drucker, D.G., Germonpré, M., Lázničková-Galetová, M., Naito, Y.I., Wissing, C., Brůžek, J., Oliva, M., 2015. Reconstruction of the Gravettian food-web at Předmostí I using multi-isotopic tracking (13C, 15N, 34S) of bone collagen. Quaternary International 359-360, 211-228.

Boeskorov, G.G.,Baryshnikov, G.F., 2013. Late Quaternary Carnivora of Yakutia. Saint-Petersburg: Nauka. 199 p. [in Russian]

Bonifay, M.-F., 1971. Carnivores quaternaires du sud-est de la France. Mémoires du Muséum National d'Histoire Naturelle, Série C, 21, 49-377.

Boeskorov, G.G., Baryshnikov, G.F., 2013. Late Quaternary Carnivora of Yakutia.Nauka, Saint-Petersburg.

Brugal, J.-P., Boudadi-Maligne, M., 2011.Quaternary small to large canids in Europe: Taxonomic statusand biochronological contribution. Quaternary International 243, 171-182.

Diedrich, C.G., 2013. Extinctions of Late Ice Age cave bears as a result of climate/habitat change and large carnivore lion/hyena/wolf predation stress in Europe. ISRN Zoology, 2013, pp. 1-25.

Flower, L.O., Schreve, D.C., 2014. An investigation of palaeodietary variability in European Pleistocene canids. Quat. Sci. Rev. 96, 188-203.

Fox-Dobbs, K., Leonard, J.A., Koch, P.L., 2008. Pleistocene megafauna from eastern Beringia: Paleoecological and paleoenvironmental interpretations of stable carbon and nitrogen isotope and radiocarbon records. Palaeogeography, Palaeoclimatology, Palaeoecology 261, 30-46.

Geffen, E.L.I., Anderson, M.J., Wayne, R.K., 2004. Climate and habitat barriers to dispersal in the highly mobile grey wolf. Mol. Eco. 13 (8), 2481e2490.

Germonpré, M., Fedorov, S., Danilov, P., Galeta, P., Jimenez, E.-L., Sablin, M., Losey, R.J., 2017. Palaeolithic and prehistoric dogs and Pleistocene wolves from Yakutia: Identification of isolated skulls. J. Archaeol. Sc 78, 1-19.

Kahlke, R.D., 1994. Die Entstehungs-, Entwicklungs- und Verbreitungsgeschichte des oberpleistozänen Mammuthus-Coelodonta-Faunenkomplexes in Eurasien (Grosssäuger). Abhandlungen der Senckenbergischen Naturforschenden Gesellschaft 546, 1-164.

Kohn, M.J., McKay, M.P., 2012. Paleoecology of late Pleistocene–Holocene faunas of eastern and central Wyoming, USA, with implications for LGM climate models. Palaeogeography, Palaeoclimatology, Palaeoecology 326, 42-53.

Kuzmina, I.E., Sablin, M.V., 1993. Pozdnepleistotsenovyi pesets verhnei Desny. In: Baryshnikov, G.F., Kuzmina, I.E. (Eds.), Materiali po mezozoickoi i kainozoickoi istorii nazemnykh pozvonochnykh. Trudy Zoologicheskogo Instituta RAN 249, pp. 93–104 [in Russian with English summary].

Leonard, J.A., Vilà, C., Fox-Dobbs, K., Koch, P.L., Wayne, R.K., Van Valkenburgh, B., 2007. Megafaunal extinctions and the disappearance of a specialized wolf ecomorph. Current Biology 17, 1146-1150.

Leonard, J.A., 2015. Ecology drives evolution in grey wolves. Evolutionary Ecology Research, 16(6), pp.461-473.

MacPhee, R.D., Tikhonov, A.N., Mol, D., De Marliave, C., Van Der Plicht, H., Greenwood, A.D., Flemming, C. Agenbroad, L., 2002. Radiocarbon chronologies and extinction dynamics of the Late Quaternary mammalian megafauna of the Taimyr Peninsula, Russian Federation. Journal of Archaeological Science, 29(9), pp.1017-1042.

Meachen, J.A., Brannick, A.L., Fry, T.J., 2016. Extinct Beringian wolf morphotype found in the continental U.S. has implications for wolf migration and evolution. Ecology and Evolution 6, 3430-3438.

Musiani, M., Leonard, J.A., Cluff, H., Gates, C.C., Mariani, S., Paquet, P.C., Vilà, C.,

Wayne, R.K., 2007. Differentiation of tundra/taiga and boreal coniferous forest wolves: genetics, coat colour and association with migratory caribou. Mol. Ecol. 16 (19), 4149-4170.

Olsen, S.J., 1985. Origins of the Domestic Dog: The Fossil Record. University of Arizona Press, Tucson.

Pilot, M., Branicki, W., Je˛drzejewski, W., Goszczy_nski, J., Je˛drzejewska, B., Dykyy, I., Shkvyrya, M., Tsingarska, E., 2010. Phylogeographic history of grey wolves in Europe. BMC Evol. Biol. 10, 104.

Repenning, C.A., 1992. Allophaiomys and the age of the Olyor Suite, Krestovka sections, Yakutia. U.S. Geological Survey Bulletin 2037: 1–98.

Sardella, R., Bertè, D., Iurino, D.A., Cherin, M. and Tagliacozzo, A., 2014. The wolf from Grotta Romanelli (Apulia, Italy) and its implications in the evolutionary history of Canis lupus in the Late Pleistocene of Southern Italy. Quaternary International, 328, pp.179-195.

Schweizer, R.M., vonHoldt, B.M., Harrigan, R., Knowles, J.C., Musiani, M., Coltman, D., Novembre, J., Wayne, R.K., 2016. Genetic subdivision and candidate genes under selection in North American gray wolves. Molecular Ecology 25, 380-402.

Sotnikova, M., Rook, L., 2010. Dispersal of the Canini (Mammalia, Canidae: Caninae) across Eurasia during the Late Miocene to Early Pleistocene. Quaternary International, 212 (2). 86-97.

Stiner, M.C., 2004. Comparative ecology and taphonomy of spotted hyenas, humans, and wolves in Pleistocene Italy. Revue de Paléobiologie, 23(2), pp.771-785.

Tamm, E., Kivisild, T., Reidla, M., Metspalu, M., Smith, D.G., Mulligan, C.J., Bravi, C.M., Rickards, O., Martinez-Labarga, C., Khusnutdinova, E.K., Fedorova, S.A., Golubenko, M.V., Stepanov, V.A., Gubina, M.A., Zhadanov, S.I., Ossipova, L.P., Damba, L., Voevoda, M.I., Dipierri, J.E., Villems, R., Malhi, R.S., 2007. Beringian standstill and spread of Native American founders. PLoS One 9, 8291–8296.

Tedford, R.H., Wang, X., Taylor, B.E., 2009. Phylogenetic systematic of the North American fossil Caninae (Carnivora, Canidae). Bulletin of the American Museum of Natural History, 325.

Westgate, J.A., Pearce, G.W., Preece, S. J., Schweger, C.E., Morlan, R.E., Pearce, N.J.G., Perkins, T.W., 2013. Tephrochronology, magnetostratigraphy and mammalian faunas of Middle and Early Pleistocene sediments at two sites on the Old Crow River, northern Yukon Territory, Canada. Quaternary Research 79 (1), 75-85

3.S1.2 Archaeological site descriptions

Armenia

Aghitu (TU9, TU10)

Aghitu-3 is a shallow cave at the base of a 126-111 ka basalt flow, located in a paleomeander of the Vorotan River, a tributary of the Araxes River, which flows into the Caspian Sea. Between 2009 and 2015, A.W. Kandel and B. Gasparyan excavated this 5 m-thick, Upper Paleolithic sequence dated between 40-24,000 y cal BP. Faunal assemblages from five cultural horizons (AH VII-III) contain mainly wild goat, wild sheep and horse, with other species being less frequent (Kandel et al., 2014). Two mitochondrial genomes were newly sequenced and analyzed in this study. The first sample is from a well-preserved, complete cranium including both mandibles (TU10) of a large canid dated to 30,000 y cal BP found at the interface of layers AH Ve and VI; the specimen has cut marks, likely made by stone tools, as well as bite marks, likely made by a canid-sized carnivore. The second sample is from a well-preserved proximal left radius (TU9) of a large canid dated to 31,100 y cal BP found near the top of layer AH VI.

Belgium

Goyet, the third cave (TH2, TH3, TU6)

The third cave of Goyet is located in the Belgian Mosan basin. This cave was first excavated in 1868 by the geologist Edouard Dupont (1872). He described five successive bone horizons. The material from the Dupont excavations is housed at the Royal Belgian Institute of Natural Sciences (RBINS) and consists of at least 30,000 bone fragments (Rougier et al., 2016b). Mitochondrial genomes from two canid elements from the Goyet third cave were analyzed in this study: a mandible (TH3) and an upper carnassial (P4) (TU6), which was newly sequenced and analyzed in this study. According to Dupont's unpublished notes, the lower jaw, with an age of 28,800 y cal BP, was found in Bone Horizon 4 in a side gallery adjacent to the entrance of the cave, together with remains from mammoth, lynx, red deer and large canids. The upper carnassial was excavated from Bone Horizon 2.

Pont-à-Lesse, Trou Magrite (TU1, TU2, TU3)

This large cave lies about 3 km upstream of the confluence of the Lesse River with the Meuse River. Although E. Dupont (1867), who started the excavations in 1867, distinguished four bone-bearing layers, the exact provenance of the bones has not been

noted, and their stratigraphic position is unfortunately not available. At the RBINS, the Dupont collection of the mammal remains from the Trou Magrite cave amounts to about 50,000 specimens (Jimenez et al, 2016, Smolderen, 2016). The mammal assemblages are primarily composed of remains of horse, reindeer and woolly rhinoceros, some of which show evidence of gnawing by cave hyenas (Jimenez, 2016). The wolves form the most frequent carnivore group, although, few cave bear, cave hyena and cave lion bones have been discovered (Jimenez, 2016). According to Dupont (unpublished notes), the remains of wolves were found together with the consumption refuse and the wolves were likely eaten by the prehistoric people. However, no clear anthropogenic traces could be discerned on the wolf bones that are all broken. Mitochondrial genomes from three large canid specimens have been newly sequenced and analyzed in this study: two maxilla fragments (TU1 and TU2) with ages of resp. 35,200 y cal BP and 33,300 y cal BP, and a distal tibia fragment (TU3) with an age of 32,700 y cal BP.

Walzin, Trou de l'Ours (TU5)

Trou de l'Ours, a long and small cave that is a part of the Walzin cave complex, is located on the left bank of the Lesse River, a tributary of the Meuse River. E. Dupont started the excavations here in 1866. He noted that the cave was used by badgers. The assemblages from the three bone-bearing layers contain cave bear, elk, wild boar and horse, among other species (Dupont, 1867; Dupont, unpublished notes; Ehrenberg, 1966). A mitochondrial genome from an upper carnassial (TU5) from a large canid, dated to 12,800 y cal BP has been newly sequenced and analyzed in this study.

Furfooz, Trou des Nutons (TH1)

The Trou des Nutons cave is situated in a limestone cliff on the right bank of the Lesse River. This site was also excavated by E. Dupont in the 1860s. The main bone horizon yielded Magdalenian artefacts and the Pleistocene mammal assemblage includes horse and reindeer. However, this horizon also contains younger material, such as remains from sheep, goat, pig, badger, as well as older Pleistocene bones (Charles, 1998). A partly associated skeleton of a large canid excavated by E. Dupont was identified as wolf (Dupont unpublished notes, Germonpré et al., 2009). Interestingly, the right humerus displays cut marks. The skull has an age of 26,000 y cal BP. Previously published mitochondrial genome from this specimen (TH1) is analyzed in this study.

Furfooz, Trou du Frontal (TU4)

This small cave is located on the right bank of the Lesse River near the Trou des Nutons cave. Excavations by E. Dupont started here in 1864. The mammal assemblage contains a mixture of remains dating from the Late Glacial and the Postglacial. A cut-marked horse bone has an age of 15,300 y cal BP (Charles, 1998). A mitochondrial genome from a radius of a large canid (TU4) dated to 6,200 y cal BP was newly sequenced and analyzed in this study.

Furfooz, Trou de Praules (TU8)

This small cave is located on the left bank of the Lesse River 30 m above the river bed and was excavated by E. Dupont in 1866. The mammal assemblage includes remains from reindeer, red deer, horse and brown bear (Dupont, unpublished notes). Lithic artefacts were also discovered (Dupont, 1866). A mitochondrial genome from a canid mandible (TU8) dated to 7,400 y cal BP was newly sequenced and analyzed in this study.

Hastière, Caverne Marie-Jeanne (TU7)

The Caverne Marie-Jeanne in the Belgian Mosan basin is a cave site located on the right bank of the Féron, a small tributary of the Meuse River near Hastière-Lavaux. Excavations at this site were initiated by M. Glibert of the RBINS in 1943. The cave deposits are composed of clay, silt, and sand that had been washed into the cave along joints. Several bone-bearing layers were described (de Heinzelin, 1980). AMS dates of level 2 suggests a mixture of material dating from the Late Glacial (14,400 y cal BP) and the LGM (25,000 y cal BP), AMS dates from layers 4, 5 and 6 are at least resp. 46,800 y cal BP, 44,500 y cal BP and > 43,000 y cal BP years old (Brace et al., 2012). The mammal assemblages from layers 3 and 4 are dominated by remains from cave hyena, foxes, horse, woolly rhinoceros and large bovids (Jimenez, 2016). The microfauna includes lemmings, voles and mice (Gautier, 1980). A mitochondrial genome from a canid mandible (TU7) from this cave was newly sequenced and analyzed in this study. No information on its stratigraphic position is available but the specimen has been dated to 46,300 y cal BP.

Czech Republic

Předmostí (TU14, TU15, TU16, TU17)

Předmostí is an open air site located in the Moravian Corridor, Czech Republic. The first organized excavations started in the 1880s (Absolon and Klíma, 1977; Oliva, 1997, Svoboda 2008). The mammal assemblage is dominated by mammoths that most likely

were hunted and eaten by the Gravettian inhabitants of the site (Oliva, 1997; Bocherens et al., 2015). Large canids are the second most abundant group, with a minimum number of individuals of 120 individuals based on the mandibles (Germonpré et al., 2015). Two morphotypes have been described among the large canid material: Palaeolithic dogs and Pleistocene wolves (Germonpré et al., 2012; Germonpré et al., 2015). Mitochondrial genomes from four canid jaw bones were newly sequenced and analyzed in this study. TU14 is directly dated to 2900 y cal BP, the other three specimens date back to Pleistocene based on dated context. The three Pleistocene specimens (TU15, TU16, TU17) have also been analyzed for the $\delta^{13}C$ and $\delta^{15}N$ values of their bone collagen (Bocherens et al., 2015).

Switzerland

Kesserloch (TU11, TU12, TU13 & TH7, TH11, TH15)

Kesserloch is a cave site located near Thayngen in the Swiss canton of Schaffhausen, in the northernmost part of Switzerland. It was excavated between 1874 and 1903 in several campaigns by three different excavators (published in Merk 1875, Nüesch 1904, Heierli 1907). It lies within the maximum extension of the late glacial alpine ice sheet. Among the rich faunal assemblage that was reviewed in 2007, reindeer, horse and snow hare are the most frequent species both by number and by bone weight (Napierala 2008). Among the carnivores, the canids are the most numerous, dated from around 17,500 to 14,300 y cal BP (Merck, 1876; Höneisen, 1986; Napierala, 2008; Napierala and Uerpmann, 2012). Isotopic investigations of the trophic structure of this fauna revealed that the large canids were predators of large ungulates from the site (Bocherens et al., 2011; Bocherens, 2015). Mitochondrial genomes from three canid specimens have been newly sequenced and analyzed for this study: a maxilla (TU11) (described in Napierala & Uerpmann 2010), another maxilla (TU12) very similar in preservation to TU11, a right mandibular fragment from a large canid (TU13), all directly dated to c. 14,100 y cal BP. Three additional previously published canid sequences (Thalmann et al., 2013) from Kesserloch cave have been analyzed in this study (TH7, TH11, TH15).

Russia

Badyarikha River site (CGG34)

The Badyarikha River site in northeastern Arctic Siberia is located on the left bank of the Badyarikha River (67°54'49"N, 146°30'56"E"), a tributary of the Indighirka River

(Germonpré et al., 2017). The total height of the permafrost cliff is about 20 m. A mitochondrial genome from an isolated canid skull (CGG34), collected 6 m above the waterline and dated to c. 29,900 y cal BP has been newly sequenced for this study. There is no archaeological context associated with this find.

Tirekhtyakh River site (CGG32)

The Tirekhtyakh River site is situated 5 km from the junction of the Tirekhtyakh tributary with the Indighirka River (68°53'39"N, 147°12'45"E) in northeastern Arctic Siberia (Germonpré et al., 2017). The river terrace here is 8 m high. An isolated canid skull was discovered 2 m below the surface. A mitochondrial genome from this specimen (CGG32) has been newly sequenced and analyzed in this study. Direct radiocarbon dating suggests that this specimen is more than 50,000 years old. There is no archaeological context associated with this find.

Ulakhan Sular site (CGG33)

The Ulakhan Sular site in northeastern Arctic Siberia (67°41'40"N, 135°44'24"E) is a 65 m high and 1.2 km long bluff located on the right bank of the Adycha River, a tributary of the Yana River (Germonpré et al., 2017). According to Lee et al. (2015), four main stratigraphic units are present. The lowest unit (layer 1) consists of gravel and pebbles in a sandy matrix. The fauna includes remains from *Archidiskodon* sp., *Equus verae* and *Praealces* sp. and dates from the Early Pleistocene. The faunal assemblage of the next unit (layer 2) consists of bones from *Panthera* sp., *E.nordostensis, Cervalces latifrons* (Lazarev, 2002) and *Canis* cf. *variabilis* (Lee et al., 2015). The third stratigraphic unit (layer 3) is a loamy sand deposit and its fauna includes *Bison priscus crassicornis* remains. The sequence is topped by layer 4 that consists of silty sands with a peat layer. Here, the faunal assemblage contains typical mammoth species such as woolly mammoth, woolly rhinoceros, horse, red deer, reindeer, bison, muskox, bear, lion and wolf (Lazarev, 2002). A mitochondrial genome from a canid skull, with unknown stratigraphic position (CGG33), dated to 16,900 y cal BP has been newly sequenced and analyzed in this study. There is no archaeological context associated with this find.

Malyi Lyakhovsky Island (CGG31)

Malyi Lyakhovsky Island is one the New Siberian Islands that separate Laptev and East Siberian Sea in The Siberian Arctic. A canid skull was collected on the south coast of this island near a river mouth at the base of a 20 m high permafrost cliff (Germonpré et al.,

2017). A mitochondrial genome from this specimen (CGG31), dated to 800 y cal BP has been newly sequenced for this study. There is no archaeological context associated with this find.

Duvannyi Yar, Kolyma River downstream (CGG12, CGG13)

Duvanny Yar is situated on the right bank of the lower Kolyma River in northeastern Arctic Siberia at 68°37'N; 159°06'E (Kaplina et al., 1978; Sher et al., 1979). This 12-km-long outcrop of polifacial permafrost sediments reaches up to 53 m height. Giterman et al. (1982) have distinguished four stratigraphic units within the sequence. Unit One which is lacustrine silts filling in the ice-wedge casts, is exposed at the water level. It is suggested to be last interglacial. Sediments rich with woody plant and peaty organics of the Unit Two are middle Late Pleistocene, while Unit Three is described as loess-like ice and organic-rich permafrost deposits. These compose the most of the sequence. Numerous remains of mammals and plant remains have been found from this site (Yashina et al., 2012). Vasil'chuk et al. (2001) as well as Zanina et al. (2011) suggested that the Unit Three deposits accumulated between >45,000 and 13,500 ^{14}C BP. The uppermost Unit Four is the Holocene cover on the top of the sequence. *Canis lupus* remains from this site, are associated with the lowermost portion of the Unit Three. The age of these fossils is c. 45,000 ^{14}C BP or older. A mitochondrial genome from two canid mandibls from this site (GGG12 and CGG13), both radiocarbon dated to be older than 45,000 y cal BP (Lee et al., 2015) have been newly sequenced and analyzed in this study. This sample was collected by Pavel Nikolskiy in 2005 (GIN RAS accessing number 1131-1). There is no archaeological context associated with these finds.

Yana site

Yana RHS is a complex of geoarchaeological objects that is located in the lower part of the Yana River in northeastern Arctic Siberia. Systematic interdiciplinary investigation of the Yana site complex is led by Pitulko since 2001. The site structure includes several separate localities (at least seven of them) discovered within the body of a river terrace (Pitulko et al., 2004; Pitulko et al., 2013; Pitulko and Pavlova, 2016). Different localities represent separate but roughly contemporaneous archaeological sites. Samples analyzed in this study come from four different localities (YMAM, Yana/SP, and Yana/UP, Yana/Northern Point). Yana RHS bone collections are being studied by Pavel Nikolskiy.

Yana site - Northern Point Locality (CGG22-CGG28)

Northern Point Locality is the main excavation area studied in 2003 through 2016. Excavations at this site have yielded a large number of bone fragments and artifacts both lithic and organic including a number of mammoth ivory tools, personal ornaments and decorations (Pitulko et al., 2013; Pitulko and Pavlova, 2016). Although not numerous, Pleistocene canid remains (mostly cranial bones, postcranial bones are less frequent) have been found in situ from the occupation level and mapped with exact provenience. All bones have been collected by Pitulko and Pavlova from in situ during the archaeological excavations and directly dated to be c. 32,000 y cal BP. Mitochondrial genomes from seven canid specimens from this site (CGG22-CGG28), have been newly sequenced and analyzed in this study. Three samples (CGG22, CGG25, and CGG28) come from three complete skulls. Three samples (CGG23, CGG24 CGG27) come from partial mandibles (two left and one right). One sample (CGG26) comes from a facial fragment of a canid skull. All samples come from the same layer of the site, but from different units.

Yana site - YMAM locality (CGG14,CGG15, CGG17)

Yana mass accumulation of mammoth, or YMAM is a structural part of the Yana site complex (Pitulko et al., 2013; Pitulko and Pavlova, 2016). *Canis lupus* remains have been collected from the bone-bearing permafrost deposits of the YMAM (Basilyan et al., 2011) by Pitulko and Pavlova in 2008-2012 and dated to c. 30,000 y cal BP, in agreement with multiple radiocarbon dates obtained from the site (see, e.g., Basilyan et al., 2011; Pitulko et al., 2013). Mitochondrial genomes from three canid specimens from this site (CGG14, CGG15 and CGG17), have been newly sequenced and analyzed in this study.

Yana site - SP locality (GGG16)

SP locality is in close proximity to the river bank exposure of YMAM area. The geological sequence is crowned by thick organic-rich Holocene permafrost deposit. A partial canid mandible from this site was collected by V. Pitulko in 2003 (Basilyan et al., 2011). A mitochondrial genome from this specimen (GGG16), radiocarbon dated to be 800 y cal BP has been newly sequenced and analyzed in this study.

Yana site area, Upstream Point locality (CGG18)

Upstream Point is probably the oldest of the localities composing the Yana site complex (Pitulko et al., 2013). Although, numerous lithic artifacts have been collected on the river bank in different years, in situ cultural deposits have never been located at this site.

Numerous bone fragments of different Pleistocene species (examined by Pavel Nikolskiy) have been found eroded from the permafrost deposits that compose the geological sequence of the river bank, including a partial canid mandible (left side) collected by Elena Pavlova and Vladimir Pitulko in 2013. A mitochondrial genome from this canid specimen (CGG18), dated to 41,700 y cal BP, has been newly sequenced and analyzed in this study.

Mus-Khaya exposure (CGG19)

Mus-Khaya exposure is located on the left bank of the Yana River in northeastern Arctic Siberia, 5km downstream from the Yana site complex (Pitulko et al., 2011). This exposure is a fragment of high geomorphological surface whose height reaches roughly 50m above the water level (30m in its downstream portion). The Mus-Khaya locality has been known since the late 19th century and actively investigated in the 1960s and 1970s (Katasonov, 2009). It is formed of the Ice Complex deposits of polygenetic origin and as a result, units of different age are recognized in the upper part of its stratigraphic sequence (22,000-18,000; 18,000-14,000; 14,000-10,000 years and Holocene cover). A fragment of Pleistocene wolf mandible (right by body side) was collected by Pitulko and Pavlova in 2012 in the middle part of the exposure on the river bank. A mitochondrial genome from this canid specimen (CGG19), dated to 19,700 y cal BP, has been newly sequenced and analyzed in this study. There is no archaeological context associated with this find.

Bunge-Toll-1885 site (CGG29)

The Bunge-Toll 1885 site locates on the Yana River at N 68° 55', E 134° 28' in northeastern Arctic Siberia (Pitulko et al., 2014b). The site is named after the Russian Arctic explorers Alexander von Bunge and Eduard von Toll who conducted the expedition dispatched by the Russian Academy of Science and the Russian Geographic Society in 1884-86. The Pleistocene faunal assemblage of this site includes numerous remains of wooly rhinoceros and bison, less frequently reindeer and red deer. Mammoth remains have also been found but are rare. The faunal remains come from the upper part of the permafrost sediments, which fills the bedrock depressions around 50m above the river level. Radiocarbon dating indicates that water-washing by local residents looking for mammoth ivory likely exposed the upper portions of the Yana River's third terrace sediments. Radiocarbon dating of mammoth, rhinoceros, and bison remains suggests an age of at least 40,000 years (uncalibrated). There is no known archaeological context

related to these finds, however, Pitulko et al. (2016b) report a hunting lesion on a canid humerus suggesting human contact. A mitochondrial genome from the canid humerus (CGG29), at least 45,000 years old (based on direct radiocarbon dating) (Pitulko et al., 2014b; Pitulko et al., 2016b), has been newly sequenced and analyzed in this study. This sample was collected by Aleksei Tikhonov of Zoological Institute (Russian Academy of Sciences) in 2012.

Nikita Lake site, Muksunuokha River (GGG20)

Nikita Lake site (NKL) is a recently found mass accumulation of mammoth bones that contains the evidence for human involvement in its formation. It is located in the northern part of the Yana-Indighirka coastal lowland on the right bank of the Maksunuokha River under 71°34′56.5″ N and 141°37′03.5″ E in 400 m northwest of the northern shore of Nikita Lake in northeastern Arctic Siberia (Pitulko et al., 2016a). It is known since late 1990s. In 2013, it was investigated by Pitulko and Pavlova. It was found that the location is significantly damaged by the ivory mining activities: It has been almost entirely destroyed by the washing out of sediments, performed by local residents mainly in 2011 – 2013. Near the washouts in both, the northern and the southern part, bones of mammoths and other animals are common on the surface. Based on the radiocarbon dating of the faunal remains associated with human activity, people inhabited the site c. 12,000 to 11,800 years ago (uncalibrated). Paleogeographic event sequence reconstruction, based on the available geological data, indicates that during that period humans lived on the shores of the paleo-lake. The evidence of human habitation of this site (faunal remains of mammoth, wolf, wolverine, reindeer, and others, as well as the few stone artifacts) was subsequently picked up by the river and re-deposited into the alluvial sediments and some of these objects were incorporated into erosion channels due to active thermoerosion (Pitulko et al., 2016a). Pleistocene wolf humerus identified by morphology produced one of the youngest radiocarbon ages for this locality – 13,700 y cal BP (Pitulko et al., 2016a). A mitochondrial genome from this specimen (GGG20) has been newly sequenced and analyzed in this study.

Berelekh geoarchaeological complex, Berelekh River (CGG21)

Berelekh is a well-known geoarchaeological complex with a long history of investigation (Pitulko et al, 2011) that starts in 1947 when it was first scientifically described by Grigoriev (Grigoriev, 1957). The site is located on the Berelekh River, a lover left

tributary of Indighirka River in northeastern Arctic Siberia, in the middle part of the river valley (70˚ 30' N and 144˚ 02' E), in so-called Ugamyt Tract locality, where two terrace levels can be found. The lower terrace (7m high) formed in the Holocene while the formation of the higher one (12 to 14 m high) is believed to have happened within the Late Pleistocene. The Berelekh geoarchaeological complex belongs to this geomorphic level and includes both mass accumulation of mammoth remains (the 'graveyard') and the 'archaeological site'. Radiocarbon dating of mammoth remains at Berelekh suggests that they were accumulated rapidly during the Bølling warming. Human involvement is unlikely since there is no overlap between radiocarbon dates associated with past human activity, and that of mammoth bone bed. However, lithic artifacts, ivory and bone fragments have been found in sediments exposed on the river bank, next to the bone bed suggesting that humans may have used the mammoth remains after the bone bed was deposited (Pitulko et al., 2014a). Postcranial skeletal elements from canid species have also been found from this exposure. A mitochondrial genome from a canid femur (CGG21) has been newly sequenced and analyzed in this study. The sample has been dated to 14,000 y cal BP (Pitulko et al., 2014a)

Gorky settlement, Ob River (CGG30)

Gorki settlement is located in low Ob River, Western Siberia, Russia (65° 03' N, 65° 17' E), on the right river bank. Concentration of Pleistocene faunal remains was found during the low water stand in the late fall of 2014 by local residents. The bone-bearing level is overlaid by thick sand deposits that make the river terrace, around 15m high. No geological description is available for this place. The assemblage is composed of remains from mammoth, bison, woolly rhinoceros, and a single wolf humerus). The remains were collected by local the local people and handed over to the museum in Salekhard. A mitochondrial genome from the canid humerus (CGG30), radiocarbon dated to be older than 45,000 y cal BP (Pitulko, 2016) has been newly sequenced in this study.

Bibliography for 3.S1.2

Absolon, K., Klíma, B., 1977. Předmostí Ein Mammutjägerplatz in Mähren. Fontes Archeologiae Moraviae 8.

Basilyan, A.E., M.A. Anisimov, P.A. Nikolskiy, and V.V. Pitulko. 2011. Wooly mammoth mass accumulation next to the Paleolithic Yana RHS site, Arctic Siberia:

its geology, age, and relation to past human activity. Journal of Archaeological Science 38, 2461-2474. DOI: 10.1016/j.jas.2011.05.017.

Bocherens, H., Drucker, D.G., Germonpré, M., Lázničková-Galetová, M., Naito, Y.I., Wissing, C., Brůžek, J., Oliva, M., 2015. Reconstruction of the Gravettian food-web at Předmostí I using multi-isotopic tracking (^{13}C, ^{15}N, ^{34}S) of bone collagen. Quaternary International 359-360, 211-228.

Bocherens, H., Drucker, D.G., Bonjean, D., Bridault, A., Conard, N.J., Cupillard, C., Germonpré, M., Höneisen, M., Münzel, S.C., Napierala, H., Patou-Mathis, M., Stephan, E., Uerpmann, H.-P., Ziegler, R. 2011. Isotopic evidence for dietary ecology of cave lion (*Panthera spelaea)* in North-western Europe: prey choice, competition and implications for extinction. Quaternary International 245: 249-261

Bocherens, H., 2015. Isotopic tracking of large carnivore palaeoecology in the mammoth steppe. Quaternary Science Reviews 117: 42-71.

Brace, S., Palkopoulou, E., Dalén, L., Lister, A.M., Miller, R., Otte, M., Germonpré, M., Blockley, S.P.E., Stewart, J.R., Barnes, I., 2012. Serial population extinctions in a small mammal indicate Late Pleistocene ecosystem instability. Proceedings of the National Academy of Sciences 109, 20532-20536.

Charles, R., 1998. Late Magdalenian Chronology and faunal exploitation in the North-Western Ardennes. BAR International Series 737.

De Heinzelin, J., 1980. Archéologie, In A. Gautier and J. de Heinzelin (Eds), La caverne Marie-Jeanne (Hastière-Lavaux, Belgique), Mémoire Institut royal des Sciences Naturelles de Belgique 177, 25-42.

Dupont, E., 1866. Etude sur les fouilles scientifiques exécutées pendant l'hiver de 1865-1866 dans les cavernes des bords de la Lesse. Bulletin de l'Académie royale des Sciences, des Lettres et des Beaux-Arts de Belgique, 2me Série, 22, 31-68.

Dupont, E., 1867. Etude sur cinq cavernes explorées dans la vallée de la Lesse et le ravin de Falmignoul pendant l'été de 1866. Bulletin de l'Académie royale des Sciences, des Lettres et des Beaux-Arts de Belgique, 2me Série, 23, 244-265.

Dupont, E., 1872. L'Homme pendant les âges de la pierre dans les environs de Dinant-sur-Meuse. Bruxelles, Mucquardt.

Ehrenberg, K.,1966. Die Plistozänen Bären Belgiens. III. Teil: Cavernes de Montaigle (Schluss), Cavernes de Walzin, Caverne de Freyr, Cavernes de Pont-à-Lesse. Mémoires Institut royal des Sciences Naturelles de Belgique 155, 1-74.

Gautier, A., 1980. Notes sur les mammifères. In A. Gautier and J. de Heinzelin (Eds), La caverne Marie-Jeanne (Hastière-Lavaux, Belgique), Mémoires Institut royal des Sciences Naturelles de Belgique 177, 25-42.

Germonpré, M., Lázničková-Galetová, M., Sablin, M. 2012. Palaeolithic dog skulls at the Gravettian Předmostí site, the Czech Republic. J. Archaeol. Sc. 39, 184-202.

Germonpré, M., Lázničková-Galetová, M., Losey, R.J., Räikkönen, J., Sablin, M.V., 2015. Large canids at the Gravettian Předmostí site, the Czech Republic: the mandible. Quaternary International 359-360, 261-279

Germonpré, M., Fedorov, S., Danilov, P., Galeta, P., Jimenez, E.-L., Sablin, M., Losey, R.J., 2017. Palaeolithic and prehistoric dogs and Pleistocene wolves from Yakutia: Identification of isolated skulls. J. Archaeol. Sc 78, 1-19.

Giterman, R.E., A.V. Sher, and J.V. Matthews. 1982. Comparison of the development of tundra-steppe environments in west and east Beringia: Pollen and macrofossil evidence from key sections. In: Hopkins D.M, J.V. Matthews, C.E. Schweger, and S.B. Young (eds.). Paleoecology of Beringia. Academic Press: San Diego, CA. pp. 43-73.

Grigoriev, N.F. 1957. Finds of mammoths: Overview of the materials received by the editorial board. Priroda 5, 104–106 (in Russian).

Heierli J. 1907 (ed.). Das Kesslerloch bei Thaingen. Neue Denkschriften der Schweizerischen Naturforschenden Gesellschaft XLIII. Zürcher & Furrer: Zürich.

Höneisen, M., 1986. Kesslerloch und Schweizersbild: Zwei Rentierjäger-Stationen in der Nordschweiz. Archäologie der Schweiz, 9: 28-33.

Jimenez, E.-L., 2016. Palaeoecology and Subsistence Strategies in Belgium and Northwestern Europe during the MIS 3 through the Reassessment of Forgotten Collections: A Methodological Approach. Papers from the Institute of Archaeology, 25, 1-8, DOI: http://dx.doi.org/10.5334/pia-486.

Jimenez, E.-L., Smolderen A., Jadin I., Germonprpre, M., 2016 Exhumation de la collection faunique d'Édouard Dupont provenant du Trou Magrite (Pont-à-Lesse). Quelles données et quelles perspectives pour une collection du XIX^{e} siècle ? *Notae Praehistoricae*, 36/2016 : 167-190

Kandel, A.W., Gasparyan, B., Nahepetyan, S., Taller, A., Weissbrod, L., 2014. The Upper Paleolithic Settlement of the Armenian Highlands. In: M. Otte & F. Le Brun-Ricalens (Eds.) Modes de contacts et de déplacements au Paléolithique

eurasiatique, Actes du colloque international de la commission 8 (Paléolithique supérieur) de l'UISPP, Université de Liège, 28-31 mai 2012. ERAUL 140:39-60.

Kaplina, T.N., R.E. Giterman, O.V. Lakhtina, B.A. Abrashov, S.V. Kiselyov, A.V. Sher. 1978. Duvannyy Yar - A key section of Upper Pleistocene deposits of the Kolyma lowland, Bulletin of Quaternary Committe 48, 49–65 (in Russian).

Katasonov, E.M. 2009. Lithology of Frozen Quaternary Deposits (Cryolithology) of the Yana Coastal Lowland. Moscow: PNIIS.

Lee, E.J., D.A. Merriwether, A.K. Kasparov, P.A. Nikolskiy, M.V. Sotnikova, E.Y. Pavlova, and V.V. Pitulko. 2015. Ancient DNA Analysis of the Oldest Canid Species from the Siberian Arctic and Genetic Contribution to the Domestic Dog. PLoS ONE 10(5), e0125759. DOI:10.1371/journal.pone.0125759

Merk, C., 1876. Excavations at the Kesslerloch near Thaygen, Switzerland Longmans, Green and Co. London 65p.

Merk K. 1875. Der Höhlenfund im Kesslerloch bei Thayngen / Originalbericht des Entdeckers. Mittheilungen der Antiquarischen Gesellschaft in Zürich 19: 1–44.

Napierala H. 2008. Die Tierknochen aus dem Kesslerloch - Neubearbeitung der paläolithischen Fauna. Beiträge zur Schaffhauser Archäologie 2. Kantonsarchäologie Schaffhausen: Beiträge zur Schaffhauser Archäologie, pp. 1-128.

Napierala H. & H.-P. Uerpmann, 2010. A „New“ Palaeolithic Dog from Central Europe. Int. J. Osteoarchaeol. 2010. doi 10.1002/oa.1182.

Nüesch J. 1904. Das Kesslerloch, eine Höhle aus paläolithischer Zeit / Neue Grabungen und Funde, Neue Denkschriften der allgemeinen Schweizerischen Gesellschaft für die gesammten Naturwissenschaften XXXIX. Zürcher & Furrer, Zürich; 1-72.

Oliva, M., 1997. Les sites pavloviens près de Předmostí. A propos de la chasse au mammouth au Paléolithique supérieur. Acta Mus. Moraviae, Sci. Soc. 82, 3-64.

Pitulko, V.V., P.A. Nikolsky, E.Y. Girya, A.E. Basilyan, V.E. Tumskoy, S.A. Koulakov, S.N. Astakhov, E.Y. Pavlova, M.A. Anisimov. 2004. The Yana RHS Site: Humans in the Arctic before the Last Glaciation. Science 303, 52-56.

Pitulko, V.V. 2011. The Berelekh Quest: A Review of Forty Years of Research in the Mammoth Graveyard in Northeast Siberia. Geoarchaeology 26, 5-32. DOI:10.1002/gea.20342

Pitulko V.V., E.Y. Pavlova, A.E. Basilyan, M. A. Anisimov, P.A. Nikolsky. 2011. Geoarchaeological objects of the low river terraces in the area of the Yana Paleolithic site (Low Yana River, Arctic Siberia), their age and relation to geomorphology and matrix sediments. In: Shurygin, B.N., N.K. Lebedeva, A.A. Goryacheva (eds). Mesosoic and Cenozoic Paleontology, Stratigraphy, and Paleogeography of Boreal Regions. Vol. 2. Novosibirsk: Trofimuk Institute for Oil & Gas Geology. Pp. 133-136.

Pitulko, V., P. Nikolskiy, A. Basilyan, E. Pavlova. 2013. Chapter 2. Human habitation in the Arctic Western Beringia prior the LGM. In K.E. Graf, C.V. Ketron, M.R. Waters (eds). Paleoamerican Odyssey. CSFA, Dept. of Anthropology, Texas A&M University. Pp.13 – 44.

Pitulko, V.V., A. E. Basilyan, E. Y. Pavlova. 2014a. The Berelekh Mammoth Graveyard: New Chronological and Stratigraphical Data from the 2009 field season. Geoarchaeology 29, 277–299.

Pitulko, V.V., A.N. Tikhonov, K.E. Kuper, R.N. Polozov. 2014b. Human-inflicted lesion on a 45,000-year-old Pleistocene wolf humerus from the Yana River, Arctic Siberia. VIth International Conference on Mammoths and their Relatives, Thessaloniki, Greece, May 5th – May 12th, 2014. Abstracts. Scientific Annals of the School of Geology, Aristotle University of Thessaloniki, Greece 102, 156-157.

Pitulko, V.V., and Pavlova, E.Y. 2016. Geoarchaeology and Radiocarbon Chronology of Stone Age Northeast Asia. Center for the Study of the First Americans: Texas A&M University Press, College Station.

Pitulko, V.V. 2016. Evidence for the early human habitation across Arctic Eurasia: new findings and research perspectives. In: Tupakhin, D.S. and N.V. Fedorova (eds). Arctic Archaeology. Vol. 3. Kaliningrad: ID ROS-DOAFK. P. 91-116.

Pitulko, V.V., E.Y. Pavlova, and A.E. Basilyan. 2016a. Mass accumulations of mammoth (mammoth 'graveyards') with indications of past human activity in the northern Yana-Indighirka lowland, Arctic Siberia. Quaternary International 406, 202-217. doi 10.1016/j.quaint.2015.12.039

Pitulko, V.V., A.N. Tikhonov, E.Y. Pavlova, P.A. Nikolskiy, K.E. Kuper, and R.N. Polozov. 2016b. Early human presence in the Arctic: evidence from 45,000-year-old mammoth remains. Science 351, 260-263.

Rougier, H., Crevecoeur, I., Beauval, C., Posth, C., Flas, D., Wißing, C., Furtwängler, A., Germonpré, M., Gómez-Olivencia, A., Semal, P., van der Plicht, J., Bocherens, H., Krause, J., 2016b. Neandertal cannibalism and Neandertal bones used as tools in Northern Europe. Scientific Reports 6, 29005, DOI:10.1038/srep29005

Sher, A.V., T.N. Kaplina, R.E. Giterman, A.V. Lozhkin, A.A. Arkhangelov, S.V. Kiselyov, Y.V. Kouznetsov, E.I. Virina, V.S. Zazhigin. 1979. Late Cenozoic of the Kolyma Lowland. XIV Pacific Science Congress, Tour Guide XI, Khabarovsk August 1979. Moscow, Academy of Sciences of the USSR: XIV Pacific Science Congress, 1-116.

Smolderen, A., 2016. Cinquante nuances de noir. Problèmes de diagnostic en archéologie du feu : études de cas du bassin mosan belge au MIS3. Thèse du grade académique de Docteur en Histoire de l'Art et Archéologie, ULB, Faculté de Philosophie et Sciences sociales.

Svoboda, J. (2008). "The Upper Paleolithic burial area at Předmostí: Ritual and taphonomy." Journal of Human Evolution 54: 15-33.

Vasilchuk, Y.K., A.C. Vasil'chuk, D. Rank, W. Kutschera, J.G. Kim. 2001. Radiocarbon dating of δ18O-δD plots in late Pleistocene ice-wedges of the DuvannyYar (lower Kolyma River, northern Yakutia). Radiocarbon 43, 541-553.

Yashina, S., S. Gubin, S. Maksimovich, A. Yashina, E. Gakhova, D. Gilichinsky. 2012. Regeneration of whole fertile plants from 30,000-y-old fruit tissue buried in Siberian permafrost. PNAS 109, 4008-4013.

Zanina, O.G., S.V. Gubin, S.A. Kuzmina, S.V. Maximovich, D.A. Lopatina. 2011. Late-Pleistocene (MIS 3–2) palaeoenvironments as recorded by sediments, palaeosols, and ground-squirrel nests at Duvanny Yar, Kolyma lowland, northeast Siberia. Quaternary Science Reviews 30, 2107–2123.

3.S2 – DNA Extraction, Sequencing and Bioinformatics.

Here we outline the laboratory and bioinformatics procedures used to generate all new sequences published in this study. In order to achieve a uniform dataset we reprocessed raw reads from previously published samples (from Thalmann et al., 2013 and Skoglund et al., 2015) using the same bioinformatics pipeline as for the newly generated sequences.

3.S2.1 DNA Extractions

We used six different methods to extract endogenous DNA from ancient and modern canids, described below. The method used for each sample is also listed in the supplementary table 1 (column *Extraction*).

1. Eight samples (TU1-TU8) originating from various European excavation sites and dating to the Pleisto- and Holocene were extracted in four batches in clean room facilities of the Royal Belgian Institute for Natural Sciences (RBINS) in Brussels, Belgium. The laboratories are physically separated from any lab in which contemporary material is treated and also from any storage facility of the institute. The ancient DNA laboratories of the RBINS are pressurized reducing air-influx and equipped with UV-radiation to minimize exogenous DNA contamination. The samples were extracted following the procedure described in Rohland and Hofreiter (2007) and each extraction batch was complemented with a mock sample that contained water instead of actual sample material. In brief, bone or teeth samples were ground with mortar and pestle yielding approx. 50 mg powdered material that was subjected to an overnight lysis. Silica based binding and subsequent washing steps resulted in a final 50 µl eluate that was stored at -20°C until further use.
2. DNA extractions for a total of nine samples (TU9-TU17) were conducted in clean room facilities dedicated to ancient DNA work at the University of Tübingen from 50 mg bone powder per sample. A silica purification protocol was applied as described in Dabney et al. (2013) with the following modifications: the Zymo-Spin V columns (Zymo Research) were UV irradiated for 60 minutes and the total elution volume was raised to 100 µl.
3. A piece of tanned hide from a museum specimen (Ms1) of the Natural History Museum of Denmark was pre-digested for minimally three hours and subsequently fully digested in 1ml buffer as described in Gilbert et al 2007. The

supernatant was mixed with 1ml phenol, rotated for 5 min and centrifuged at 3.000 G for 5 min, the aqueous product was mixed with 1 ml chloroform, rotated for 5 min and centrifuged at 3.000 G for 5 min yielding a final aqueous product. The final supernatant was mixed 1:10 with a binding buffer optimized for ancient DNA as detailed in Allentoft et al. (2015) and spun through a MinElute purification column (Qiagen) attached to an Zymo-Spin extension reservoir (Zymo Research) in a 50 ml falcon tube (Fisher Scientific) as detailed in Dabney et al. 2013, and centrifuge for 30 min at 200 G. The purification column was flowingly washed in 700 µl PE buffer and spun at 8.000 G for 1 min and dry spun at 12.000 G for 2 min. DNA bound to the columns was eluted in two times 25 µl EB buffer after incubation at 37 C for 10 min. All extraction and purification tubes were DNA-lobind (Eppendorf).

4. For 19 samples (CGG13, CGG19-CGG34, Ms6, Ms25), 50-300 mg of crushed bone or tooth was pre-digested in 1 ml buffer as outlined in Ersmark et al 2015. The following steps were identical to procedure 3).
5. 19 (Ms2, Ms4, Ms5, Ms7–Ms22) samples were extracted using the DNeasy Blood & Tissue Kit (Qiagen) following manufacturer's guidelines.
6. Six samples (CGG12, CGG14-CGG18) were digested, extracted and purified using a silica extraction method as described in Allentoft et al. (2015).

3.S2.2 Library preparation

We used three different methods to generate the sequencing libraries. The three methods, described below, vary in the details but are highly comparable as they all build upon an individual barcoding approach. The method used for each sample is also listed in the supplementary table 1 (column *Library_build*).

1. A total of 17 (TU1-TU17) samples were treated the following way. Aliquots of 20 µl extract were converted into double-stranded Illumina libraries using a well-established protocol (Meyer and Kircher, 2010; Kircher et al., 2012). The libraries were quantified before and after the addition of the individual barcodes to monitor the efficiency of the indexing reaction with a quantification assay using the primerset IS7/IS8 and IS5/IS5 (Meyer and Kircher, 2010), the DyNAmo Flash SYBR Green qPCR Kit (Biozym) and the Lightcycler 96 (Roche). The libraries were then amplified using 100 µl reactions for each library containing 5µl library

template, 4 units AccuPrime Taq DNA Polymerase High Fidelity (Invitrogen), 1 unit 10X AccuPrime buffer (containing dNTPs) and 0.3 µM IS5 and IS6 primers (Meyer and Kircher, 2010) and the following performed thermal profile: 2-min initial denaturation at 94°C, followed by 4 to 17 cycles consisting of 30-sec denaturation at 94°C, a 30-sec annealing at 60°C and a 2-min elongation at 68°C and a 5-min final elongation at 68°C. After amplification the libraries were purified with the MinElute PCR purification kit (Qiagen, Hilden, Germany) and quantified using Agilent 2100 Bioanalyzer DNA 1000 chips.

2. For each of 39 samples (CGG13, CGG19-CGG34, Ms1, Ms2, Ms4-Ms22, Ms25), 42,5 µl extract was incorporated into a DNA library using NEBNext DNA Sample Prep Master Mix Set 2 (E6070S - New England Biolabs Inc., Beverly, MA, USA) and Illumina-specific adapters (Meyer and Kircher, 2010). Library build followed producer's guidelines with the following modifications, no initial nebulization step, binding buffer detailed in Allentoft et al. (2015) in the End-repair step, End-repair, adapter ligation and fill-in was performed as in Schroeder et al. (2015) but with 42,5 µl extract as input. Libraries of ancient and historical material were amplified and indexed in reactions of 5 µl library, 32 µl H2O, 1X PCR buffer, 2 µl BSA (20 mg/mL), 1 µl dNTPs (25 mM), 1,5 µl of each of Illumina's Multiplexing PCR primer (1,5 µM of inPE1.0 5'-AATGATACGGCGACCACCGAGATCTACACTCTTTCCCTACACGACGC TCTTCCGATCT and a custom-designed index primer with a six nucleotide index 5'-CAAGCAGAAGACGGCATACGAGATNNNNNNGTGACTGGAGTTC), and 2 µl PfuTurbo Cx Hotstart DNA Polymerase (Agilent Technologies).
3. Libraries on modern material was amplified and indexed in reactions of 5 µl library, 29,5 µl H2O, 1X PCR buffer, 1 µl dNTPs (25 mM), 2 µM of each of Illumina's Multiplexing PCR primer (same as detailed above), and 0,5 µl Q5 High-Fidelity DNA Polymerase (New England Biolabs Inc). Libraries were purified subsequently over a MinElute (Qiagen) column, following manufacturer's guidelines, eluted in 35 µl EB buffer. DNA concentration in purified amplified libraries was measured using an Agilent 2100 bioanalyzer and pooled in equimolar amounts
4. For six samples (CGG12, CGG14-CGG18) DNA Libraries were built using the NEBNext DNA Sample Prep Master Mix Set 2, following the protocol with

modifications. The DNA extract was mixed with 10 µl End Repair buffer and 5 µl End Repair Enzyme Mix and water up to a volume of 100 µl. The mix was incubated for 20 minutes at 12°C and 15 minutes at 37°C, and purified using a Qiagen MinElute PCR Purification Kit. The protocol was followed as directed except that only 30 µl of EB Buffer was used and the column was incubated for 15 minutes at 37°C prior to elution. The eluted DNA was combined with 10 µl NEBNext 5x Quick Ligation Buffer, 5 µl T4 Ligase, and 5 µl P5/P7 Adaptors, diluted to a concentration of 20 uM. This mix was incubated for 20 minutes at 20°C, then purified using a MinElute PCR Purification Kit as described above. 42 µl DNA was eluted and incubated with 5 µl NEBNext Adaptor Fill-In Buffer and 3 µl *Bst* DNA Polymerase for 20 minutes at 65°C and 20 minutes at 80°C. The finished libraries were amplified using Taq Gold in a mix that included 10 µl Taq Gold Buffer, 10 µl MgCl2, 4 µl BSA, 49.2 µl H2O, 0.8 µl dNTPs, 2 µl of each of Illumina's Multiplexing PCR primer (1.5 µM of inPE1.0 5'-AATGATACGGCGACCACCGAGATCTACACTCTTTCCCTACACGACGC TCTTCCGATCT and a custom-designed index primer with a six nucleotide index 5'- CAAGCAGAAGACGGCATACGAGATNNNNNNGTGACTGGAGTTC), and 2 µl Taq Gold. The PCR conditions were according to manufacturer's directions (10-14 cycles). The PCR reaction was purified using the QIAQuick PCR Purification Kit, with elution of 30 µl EB Buffer and an incubation for 10 minutes prior to the elution step. DNA concentration was assayed using a Qubit 3.0 Fluorimeter, following manufacturer's instructions. If the DNA concentration was less than 20 ng/µl, a second PCR amplification was performed using Phusion. The mix included 20 µl template DNA, 2 µl each of primers IS5 and IS6, 50 µl Phusion Master Mix, and 26 µl H2O. The PCR program followed manufacturer's instructions but for 6-10 cycles, and was purified with a QIAQuick PCR Purification Kit as described above. The DNA concentration of the libraries was assessed using an Agilent 2100 Bioanalyzer.

3.S2.3 Sequence generation

We used three different methods to generate full mitochondrial genome sequences. The method used for each sample is also listed in the supplementary table 1 (column *Sequence generation*).

1. Seventeen samples (TU1-TU17) were enriched for the dog mitochondrial genome using the amplified libraries, pooled in equimolar amounts, and bead capture enrichment as detailed elsewhere (Maricic et al., 2010; Thalmann et al., 2013). After enrichment the libraries were amplified in 100 µl reactions with 15 µl template, 2 units Phusion High Fidelity DNA polymerase, 1 unit 5x HF buffer, 0.25 mM dNTPs and 0.3 µM IS5 and IS6 primers, and the following thermal profile: 5-min initial denaturation at 95°C, followed by 16 to 23 cycles consisting of 30-sec denaturation at 95°C, a 30-sec annealing at 60°C and a 45-sec elongation at 72°C and a 5-min final elongation at 72°C. Finally, the libraries were purified using MinElute columns (Qiagen, Hilden, Germany), quantified with Agilent 2100 Bioanalyzer DNA 1000 chips and diluted to 10 nM for sequencing. Sequencing was conducted with a paired-end dual index run on an Illumina Hiseq 2500 platform with 2*100+7+7 cycles and the manufacturer's protocols for multiplex sequencing (TruSeq PE Cluster Kit v3-cBot-HS).
2. 'Shot-gun' sequences were generated for a total of 39 samples (CGG13, CGG19-CGG34, Ms1, Ms2, Ms4-Ms22, Ms25) on an Illumina HiSeq 2500 platform, using 100 bp single read chemistry for ancient and historical material and 200 bp paired end read chemistry for modern samples.
3. Six libraries (CGG12, CGG14-CGG18) were captured using a Mycroarray MYBaits kit, which included custom RNA probes that corresponded to 4x tiling of the dog mitogenome. The capture was performed according to manual version 2.3.1, with a hybridization time of 18 hours and a temperature of 65°C. Following capture, the DNA was amplified using KAPA HI-Fi HotStart DNA Polymerase, using a mix of 15 µl captured DNA, 25 µl KAPA Hi-Fi HotStart Master Mix, 0.75 µl primers IS5 and IS6 at a concentration of 10 µM, and 8.5 µl H2O. The thermocycler program corresponded to manufacturer's instructions, and the samples were amplified for 14 cycles and then purified with a QIAQuick PCR Purification Kit as previously described. The DNA concentration of the captures was assessed using an Agilent 2100 Bioanalyzer, then they were pooled in equimolar amounts and sequenced on a HiSeq 2500 with 100 bp single read chemistry.

3.S2.4 Raw Sequence Data Processing

Raw sequencing reads of all newly generated samples were de-tagged from their individual barcodes and cleaned of all adapters needed for sequencing. A merging procedure was applied to sequences generated with paired-end technology (sample codes beginning with "TU") as detailed in Thalmann et al. (2013). In brief, all forward and reverse reads of each sequenced individual were merged into a single read based on overlap identity and all other, un-merged reads were excluded. Sequences generated with single-end technology (CGG) were processed individually.

Two assembly protocols were adapted and the resulting consensus sequences compared for conformity.

1. All merged reads and single-end reads were implemented into a reference guided, iterative assembly employing the program MIA (Green et al., 2008). The following command was used: "mia –r NC_002008.fas –f SAMPLE.fq –c –C –U –F –k 12 –s ANCIENT_SUBMAT.txt –m SAMPLE_OUT.maln." As reference (-r) served the dog mt-genome (NC_002008, Kim et al., 1998). SAMPLE.fq (-f) indicates all merged reads for each individual in .fastq format and a scoring matrix (-s) for aligning sequencing reads generated from ancient materials (ANCIENT_SUBMAT.txt) was also applied. Other parameters used here can be found in the MIA documentation. A consensus sequence was called for each individual with default parameters but only positions with a min of 3-fold coverage were retained in the final consensus sequence. This is a difference to the approach in Thalmann et al. (2013) and sequences generated in there were newly filtered for 3x coverage in order to further eliminate ambiguous positions. Moreover, we omitted a comprehensive screen for nuclear-mitochondrial inserts (Ishiguro et al., 2002, Thalmann et al., 2013) since previous analyses have shown that only a negligible small number of reads generated from similar materials mapping preferentially to the nuclear genome of the dog.
2. A second mapping approach using the methods outlined below did not reveal significant differences in the generated consensus sequences. Paleomix (Schubert et al., 2014) was used to align the reads of 19 samples against the dog reference mitochondria genome (NC_002008). Illumina reads were trimmed using default settings in AdapterRemoval2 (Schubert et al., 2016), except using a minimal read

length of 25bp. Cleaned reads were inspected for quality control using FastQC (http://www.bioinformatics.babraham.ac.uk/projects/fastqc) and aligned using BWA (Li & Durbin 2009), disabling the seed (Schubert et al., 2012). Mapped reads to multiple positions and with mapping quality scores inferior to 30 were removed using SAMtools (Li et al., 2009). Sequence duplicates were removed using MarkDuplicates from Picard (http://www.broadinstitute.github.io/picard). The final alignment was realigned and SNPs were called using GATK (McKenna et al., 2010) and filtered using Vcftools (Danecek et al., 2011). Consensus sequences were made in two ways using GATK. One way was using SNPs that passed the majority count threshold and the other adding IUPAC bases where GATK called as "heterozygous" site (McKenna et al., 2010). Mapping and coverage statistics were computed using Paleomix (Schubert et al., 2014) internal scripts. This previous methodology was also applied to the 1 million reads subset in order to compare them with other samples.

3.S2.5. Molecular characteristics of newly generated, ancient sequences

In order to assess the quality and molecular characteristics of the newly generated ancient sequences we performed additional analyses. We remapped all reads generated in capture experiments against the complete dog genome (canFam3) following the method outlined in 3.SI2.4. We extracted all quality filtered reads, removed PCR duplicates and investigated the fraction of filtered reads that mapped exclusively against the mitochondrial genome. We only retained read pairs generated with paired-end sequencing technology that were collapsed into a single read (merged). Table 3.S2 provides a summary of this analysis. Samples generated using a shot-gun approach (CGG) generally deliver a higher fraction of reads successfully mapped, however, the target specificity towards the small mitochondrial genome is low. This can be increased by using DNA capture procedures (Gnirke et al. 2009). While in the shot-gun approach the fraction of reads mapping exclusively to the dog mitochondrial genome ranges between 0.005%-0.549% of all filtered reads mapping successfully to the complete dog genome, this ratio is increased to almost 100% (see Table 3.S2) for captured mitochondrial DNA fragments. On average, capture approaches gave a 500-fold increase in the fraction of reads mapping exclusively to the dog mitochondrial genome. Interestingly, the efficiency of different capture methods varies as evidenced by the higher percentage of filtered reads mapping

against the dog mitochondrial genome for the re-captured CGG samples (CGG12-CGG18 all above 85%, values in brackets in Table 3.S2, see 3.SI2.3.3) compared to those generated from samples TU (2.4%-98.66%, lower panel in Table 3.S2, see 3.SI2.3.1).

There is no apparent correlation between sample age and fragment size (Fig. 3.S1) or deamination patterns (Fig. 3.S2). Some of the longest fragments were retrieved from samples approximately 30,000 to 46,000 years old (CGG18, TU1, TU2, TU3, TU7) while shorter fragments were observed in younger samples (CGG20, TU14, TU4). Intriguingly, TU1, TU2, TU3, TU7 and the younger TU8 originated from caves in Belgium (Table 3.S1). Furthermore, previous findings suggested that the frequency of C to T misincorporations at the 5' end (or G to A misincorporations at the 3' end) of ancient molecules increases with age of the sample (Sawyer et al. 2012). However, the ancient DNA fragments newly generated for this study do not show this pattern (Fig. 3.S2) but instead show a (slight) decreasing trend with increasing age of the samples (R^2=0.015). Taken together this points towards factors other than sample age shaping the characteristics of ancient molecules.

Table 3.S1, part 1.

ID	Latitude	Longitude	Age	Age_Class	Dating Method	GenBank_ID	IBD	Partition Finder	BEAST mut.rate	Simulation included	DEME
TH1	50.380237	4.798605	26036.5	ANCIENT	AMS	KF661078	0	0	1	1	Europe
TH3	50.446314	5.009754	28834.5	ANCIENT	AMS	KF661080	0	0	1	1	Europe
TH4	62.05	58.166667	52153.715	ANCIENT	BEAST	KF661081	0	0	0	1	Europe
TH5	53.167696	33.656024	16830	ANCIENT	AMS	KF661082	0	0	1	1	Europe
TH6	51.4	39.033333	29272.436	ANCIENT	BEAST	KF661085	0	0	0	1	Europe
TH7	47.745282	8.693176	14968	ANCIENT	AMS	KF661087	0	0	1	1	Europe
TH8	68.488441	-161.05478	27599.5	ANCIENT	AMS	KF661088	0	0	1	1	Beringia
TH10	68.488441	-161.05478	20988.5	ANCIENT	AMS	KF661090	0	0	1	1	Beringia
TH11	47.745282	8.693176	14341.5	ANCIENT	AMS	KF661091	0	0	1	1	Europe
TH12	49	89	34048	ANCIENT	AMS	KF661092	0	0	1	1	CN_Eurasia
TH14	50.544755	6.658935	4802.368	ANCIENT	BEAST	KF661094	0	0	0	1	Europe
TH15	47.745282	8.693176	14542.5	ANCIENT	AMS	KF661095	0	0	1	1	Europe
CGG12	68.630556	159.135278	55643.388	ANCIENT	BEAST	-	0	0	0	1	Beringia
CGG14	70.72375	135.414667	32734	ANCIENT	AMS	-	0	0	1	0	Beringia
CGG15	70.72375	135.414667	32925.5	ANCIENT	AMS	-	0	0	1	1	Beringia
CGG16	70.72375	135.414667	818.5	ANCIENT	AMS	-	0	0	1	1	Beringia
CGG17	70.72375	135.414667	28519.5	ANCIENT	AMS	-	0	0	1	1	Beringia
CGG18	70.713694	135.372583	41738.5	ANCIENT	AMS	-	0	0	1	1	Beringia
CGG19	70.722	135.536833	19710	ANCIENT	AMS	-	0	0	1	1	Beringia
CGG20	71.581194	141.618583	13660	ANCIENT	AMS	-	0	0	1	0	Beringia
CGG21	70.500194	144.038944	13974.5	ANCIENT	AMS	-	0	0	1	1	Beringia
CGG22	70.723306	135.425222	31377	ANCIENT	AMS	-	0	0	1	0	Beringia
CGG25	70.723306	135.425222	31423.5	ANCIENT	AMS	-	0	0	1	1	Beringia
CGG26	70.723306	135.425222	31351	ANCIENT	AMS	-	0	0	1	1	Beringia
CGG27	70.723306	135.425222	32844	ANCIENT	AMS	-	0	0	1	1	Beringia
CGG28	70.723306	135.425222	31758	ANCIENT	AMS	-	0	0	1	1	Beringia
CGG29	68.918111	134.4795	67239.038	ANCIENT	BEAST	-	0	0	0	1	Beringia
TU1	50.219527	4.92335	35235.5	ANCIENT	AMS	-	0	0	1	1	Europe
TU2	50.219527	4.92335	33318	ANCIENT	AMS	-	0	0	1	1	Europe
TU3	50.219527	4.92335	32723	ANCIENT	AMS	-	0	0	1	1	Europe
TU4	51.715	4.667778	6160	ANCIENT	AMS	-	0	0	1	1	Europe
TU5	50.85	4.35	12837	ANCIENT	AMS	-	0	0	1	1	Europe
TU6	50.444489	5.012985	38481.5	ANCIENT	AMS	-	0	0	1	1	Europe
TU7	50.217	4.817	46348.5	ANCIENT	AMS	-	0	0	1	1	Europe
TU8	50.351565	4.846722	7375.5	ANCIENT	AMS	-	0	0	1	1	Europe
TU9	39.51375	46.082081	31109.5	ANCIENT	AMS	-	0	0	1	1	Middle_East
TU10	39.51375	46.082081	29957	ANCIENT	AMS	-	0	0	1	0	Middle_East
TU11	47.745282	8.693176	14130.5	ANCIENT	AMS	-	0	0	1	1	Europe
TU13	47.745282	8.693176	14120	ANCIENT	AMS	-	0	0	1	1	Europe
TU14	50.040718	14.661924	2861.5	ANCIENT	AMS	-	0	0	1	1	Europe
TU15	50.040718	14.661924	25694.856	ANCIENT	BEAST	-	0	0	0	1	Europe
SK1	74	98	34900.5	ANCIENT	AMS	-	0	0	1	1	CN_Eurasia
CGG32	68.894167	147.2125	61110.94	ANCIENT	BEAST	-	0	0	0	1	Beringia
CGG33	67.694444	135.74	16863.5	ANCIENT	AMS	-	0	0	1	1	Beringia
CGG34	67.913611	146.515556	29935	ANCIENT	AMS	-	0	0	1	1	Beringia
Ma1	33.566667	133.533333	264.5	MODERN	NA	AB499818	1	0	1	1	SE_Asia
Ma2	35.447508	139.642344	242.5	MODERN	NA	AB499821	1	0	1	1	SE_Asia
Ma3	35.447508	139.642344	242.5	MODERN	NA	AB499822	1	0	1	1	SE_Asia
Ma4	32.783333	130.733333	398	MODERN	NA	AB499823	1	0	1	1	SE_Asia
Ma5	34.385278	132.455278	242.5	MODERN	NA	AB499823	1	0	1	0	SE_Asia
Ma6	36.633333	138.183333	242.5	MODERN	NA	AB499822	1	0	1	0	SE_Asia
Ma7	43	142	242.5	MODERN	NA	AB499819	1	0	1	1	SE_Asia
Ma8	43	142	242.5	MODERN	NA	AB499820	1	0	1	1	SE_Asia
Ma9	35.683333	139.766667	0	MODERN	NA	AB499824	1	1	1	1	SE_Asia
Bj1	59.375478	47.980469	0	MODERN	NA	DQ480503	1	1	1	0	Europe
Bj2	59.329444	18.068611	0	MODERN	NA	DQ480504	1	1	1	1	Europe
Bj3	40.413862	-3.694231	0	MODERN	NA	DQ480505	1	1	1	0	Europe
Bj4	24.70648	46.738758	0	MODERN	NA	DQ480506	1	1	1	1	Middle_East
Bj5	24.70648	46.738758	0	MODERN	NA	DQ480507	1	1	1	0	Middle_East
Bj6	45.420833	-75.69	0	MODERN	NA	DQ480508	1	1	1	1	N_America
Zh3	43.965693	117.161283	0	MODERN	NA	GQ374438	1	1	1	1	SE_Asia
Zh4	46.956904	88.512984	0	MODERN	NA	KC461238	1	1	1	1	CN_Eurasia
Zh5	46.108046	104.241362	0	MODERN	NA	KC896375	1	1	1	1	SE_Asia
Pa1	35.019971	101.048385	0	MODERN	NA	EU789787	1	1	1	1	SE_Asia
Pa2	35.019971	101.048385	0	MODERN	NA	EU789788	1	1	1	1	SE_Asia
Tha1	65.008988	25.463556	0	MODERN	NA	KF661038	1	1	1	1	Europe
Tha2	58.59574	49.65067	0	MODERN	NA	KF661039	1	1	1	0	Europe
Tha3	59.35	18.066667	0	MODERN	NA	KF661040	1	1	1	1	Europe
Tha4	35	103	0	MODERN	NA	KF661041	1	1	1	0	SE_Asia
Tha5	33.00451	35.78071	0	MODERN	NA	KF661042	1	1	1	1	Middle_East
Tha6	21	78	0	MODERN	NA	KF661043	1	1	1	1	Middle_East
Tha7	59.952189	30.421875	0	MODERN	NA	KF661044	1	1	1	1	Europe
Tha8	52.216667	21.033333	0	MODERN	NA	KF661045	1	1	1	1	Europe
Tha9	53.27038	34.351425	0	MODERN	NA	KF661046	1	1	1	1	Europe

Table 3.S1, part 1 (continued).

Tha10	46.652636	32.600708	0	MODERN	NA	KF661047	1	1	1	1	Europe
Tha11	41.9	12.483333	0	MODERN	NA	KF661048	1	1	1	1	Europe
Tha12	50.219165	19.030882	0	MODERN	NA	KF661049	1	1	1	1	Europe
Tha13	23.6	58.55	0	MODERN	NA	KF661050	1	1	1	1	Middle_East
Tha14	32	53	0	MODERN	NA	KF661051	1	1	1	1	Middle_East
Tha15	59.35	18.066667	0	MODERN	NA	KF661052	1	1	1	0	Europe
Tha16	35	103	0	MODERN	NA	KF661053	1	1	1	1	SE_Asia
Tha17	45.8	16	0	MODERN	NA	KF661054	1	1	1	1	Europe
Tha18	31	35	0	MODERN	NA	KF661055	1	1	1	1	Middle_East
Tha19	59.244895	-104.4375	0	MODERN	NA	KF661056	1	1	1	1	N_America
Tha20	73.44	-121.925	0	MODERN	NA	KF661057	1	1	1	1	AN_America
Tha21	64	-150	0	MODERN	NA	KF661058	1	1	1	0	Beringia
Tha22	64.586978	-138.37796	0	MODERN	NA	KF661059	1	1	1	1	Beringia
Tha23	24.92394	-105.28005	0	MODERN	NA	KF661060	1	1	1	0	North_Ameri
Tha24	75.13613	-84.926685	0	MODERN	NA	KF661061	1	1	1	1	AN_America
Tha25	73.128783	-120.36235	0	MODERN	NA	KF661062	1	1	1	0	AN_America
Tha26	65.12	-140.52	0	MODERN	NA	KF661063	1	1	1	0	Beringia
Tha27	47.798597	-113.20885	0	MODERN	NA	KF661064	1	1	1	0	N_America
Tha28	19	-99	0	MODERN	NA	KF661065	1	1	1	0	N_America
Tha29	64	-150	0	MODERN	NA	KF661066	1	1	1	1	Beringia
Tha30	64	-150	0	MODERN	NA	KF661067	1	1	1	1	Beringia
Tha31	44.428055	-110.58674	0	MODERN	NA	KF661068	1	1	1	0	N_America
Tha32	44.428055	-110.58674	0	MODERN	NA	KF661069	1	1	1	1	N_America
Tha33	44.428055	-110.58674	0	MODERN	NA	KF661070	1	1	1	1	N_America
Tha34	63.114198	-151.19089	0	MODERN	NA	KF661071	1	1	1	1	Beringia
Tha35	63.114198	-151.19089	0	MODERN	NA	KF661072	1	1	1	1	Beringia
Tha36	63.114198	-151.19089	0	MODERN	NA	KF661073	1	1	1	1	Beringia
Tha37	45.4	-75.666667	0	MODERN	NA	KF661074	1	1	1	1	N_America
Tha38	45.4	-75.666667	0	MODERN	NA	KF661075	1	1	1	0	N_America
Tha39	45.4	-75.666667	0	MODERN	NA	KF661076	1	1	1	0	N_America
Tha40	45.4	-75.666667	0	MODERN	NA	KF661077	1	1	1	0	N_America
Ar1	59.35	18.066667	0	MODERN	NA	AM711902	1	1	1	1	Europe
Fr1	31	35	0	MODERN	NA	-	1	1	1	0	Middle_East
Fr2	45.8	16	0	MODERN	NA	-	1	1	1	0	Europe
Ms1	36.532784	70.374934	52	MODERN	NA	-	1	1	1	1	Middle_East
Ms2	56	10	0	MODERN	NA	-	1	1	1	0	Europe
Ms25	21	78	0	INDIAN	NA	-	0	1	1	0	S_Asia
Ms4	46	105	0	MODERN	NA	-	1	1	1	1	S_Asia
Ms5	24.65	46.766667	0	MODERN	NA	-	1	1	1	1	Middle_East
Ms6	40.943056	32.530556	70	MODERN	NA	-	1	1	1	1	Middle_East
Ms7	56.75	-133.5	0	MODERN	NA	-	1	1	0	0	Beringia
Ms8	63.7797222	-171.74111	0	MODERN	NA	-	1	1	0	1	Beringia
Ms9	67	-158	0	MODERN	NA	-	1	1	0	1	Beringia
Ms10	54.9	-59.78	0	MODERN	NA	-	1	1	0	1	N_America
Ms11	72.7	-77.98	0	MODERN	NA	-	1	1	0	1	AN_America
Ms12	65.17	-65.5	0	MODERN	NA	-	1	1	0	1	AN_America
Ms13	74.13	-119.75	0	MODERN	NA	-	1	1	0	1	AN_America
Ms14	77.22	-85.42	0	MODERN	NA	-	1	1	0	1	AN_America
Ms15	76.42	-82.88	0	MODERN	NA	-	1	0	0	0	AN_America
Ms16	64.43	-93.1	0	MODERN	NA	-	1	1	0	1	AN_America
Ms17	55.1	-105.28	0	MODERN	NA	-	1	1	0	1	N_America
Ms18	43.72	-79.55	0	MODERN	NA	-	1	0	0	1	N_America
Ms19	72.77	-111.02	0	MODERN	NA	-	1	0	0	0	AN_America
Ms20	33.5	36.3	0	MODERN	NA	-	1	1	1	1	Middle_East
Ms21	19.433333	-99.133333	0	MODERN	NA	-	1	0	1	1	N_America
Ms22	40.433333	-3.7	0	MODERN	NA	-	1	1	1	1	Europe
Zh1	43.965693	117.161283	0	MODERN	NA	EU442884	0	0	0	0	S_Asia
Zh2	35.653849	95.446682	0	MODERN	NA	FJ032363	0	0	0	0	S_Asia
Zh6	30.058537	91.090393	0	MODERN	NA	KF573616	0	0	0	0	S_Asia
Zh7	43.965693	117.161283	0	MODERN	NA	NC_010340	0	0	0	0	S_Asia
Zh8	35.019971	101.048385	0	MODERN	NA	NC_011218	0	0	0	0	S_Asia
SAMPLES EXCLUDED FROM ANALYSES											
TH2	50.446314	5.009754	35769	ANCIENT	AMS	KF661079	0	0	0	0	NA
TH9	68.488441	-161.05478	21316	ANCIENT	AMS	KF661089	0	0	0	0	NA
TH13	50.713889	7.166667	13917.5	ANCIENT	Context_date	KF661093	0	0	0	0	NA
CGG13	68.630556	159.135278	48500	ANCIENT	AMS	-	0	0	0	0	NA
CGG23	70.723306	135.425222	33019.5	ANCIENT	AMS	-	0	0	0	0	NA
CGG24	70.723306	135.425222	32479.5	ANCIENT	AMS	-	0	0	0	0	NA
CGG30	65.05	65.283333	48892.5	ANCIENT	AMS	-	0	0	0	0	NA
CGG31	73.96	140.795	826.5	ANCIENT	AMS	-	0	0	0	0	NA
TU12	47.745282	8.693176	14425	ANCIENT	AMS	-	0	0	0	0	NA
TU16	50.040718	14.661924	30424.5	ANCIENT	Context_date	-	0	0	0	0	NA
TU17	50.040718	14.661924	30424.5	ANCIENT	Context_date	-	0	0	0	0	NA

Table 3.S1, part 2.

ID	AMS Reference	AMS Lab Code	AMS Date	AMS Error	From calBP	To calBP	Mean calBP	Mean BEAST Date	Stdev BEAST Date	BEAST Date From	BEAST Date To
TH1	Germonpré e	KIA-25298	21810	90	26229	25844	26036.5	NA	NA	NA	NA
TH3	Germonpré e	KIA-25297	24780	140	29184	28485	28834.5	NA	NA	NA	NA
TH4	NA	NA		NA	19000	17000	NA	52153.715	6813.0532	65899.259	39259.1785
TH5	Sablin & Khlc	NA	13905	55	17075	16585	16830	NA	NA	NA	NA
TH6	NA	NA		NA	23000	21000	NA	29272.436	3743.0213	36390.9274	21900.1268
TH7	This Study	MAMS-2387	12620	40	15179	14757	14968	NA	NA	NA	NA
TH8	Leonard et al	NA	23380	470	28536	26663	27599.5	NA	NA	NA	NA
TH10	Leonard et al	NA	17330	290	21751	20226	20988.5	NA	NA	NA	NA
TH11	This Study	MAMS-2387	12320	40	14599	14084	14341.5	NA	NA	NA	NA
TH12	Ovodov et al.	NA	29950	170	34376	33720	34048	NA	NA	NA	NA
TH14	NA	NA	10107.5	70	12019	11360	11689.5	4802.368	3179.748	11121.1716	-1077.3547
TH15	This Study	MAMS-2387	12430	40	14872	14213	14542.5	NA	NA	NA	NA
CGG12	Lee et al. 20	Beta-231445	>47000	NA	50000	47000	48500	55643.388	6611.2515	68838.1615	43151.1409
CGG14	This study	MAMS-2424	28660	130	33285	32183	32734	NA	NA	NA	NA
CGG15	This study	MAMS-2424	28760	130	33405	32446	32925.5	NA	NA	NA	NA
CGG16	This study	AAR-21020	884	25	905	732	818.5	NA	NA	NA	NA
CGG17	This study	AAR-21019	24510	170	28912	28127	28519.5	NA	NA	NA	NA
CGG18	This study	Beta 362937	37260	380	42328	41149	41738.5	NA	NA	NA	NA
CGG19	This study	AAR-21021	16300	75	19940	19480	19710	NA	NA	NA	NA
CGG20	Pitulko et al.,	Beta-362943	11840	50	13765	13555	13660	NA	NA	NA	NA
CGG21	Pitulko et al.,	LE-8936	12060	140	14394	13555	13974.5	NA	NA	NA	NA
CGG22	This study	MAMS-2483	27620	120	31604	31150	31377	NA	NA	NA	NA
CGG25	Pitulko et al.,	Beta-243114	27610	190	31757	31090	31423.5	NA	NA	NA	NA
CGG26	This study	MAMS-2483	27580	120	31568	31134	31351	NA	NA	NA	NA
CGG27	This study	MAMS-2424	28710	130	33359	32329	32844	NA	NA	NA	NA
CGG28	Pitulko et al.,	NA	27840	220	32333	31183	31758	NA	NA	NA	NA
CGG29	Pitulko et al.	GrA-57022	44650	825	50000	46419	48209.5	67239.038	7616.3877	80836.7417	50579.1862
TU1	This Study	ETH-61246	31316	252	35776	34695	35235.5	NA	NA	NA	NA
TU2	This Study	ETH-61247	29137	200	33786	32850	33318	NA	NA	NA	NA
TU3	This Study	ETH-61248	28678	181	33403	32043	32723	NA	NA	NA	NA
TU4	This Study	ETH-61243	5398	30	6287	6033	6160	NA	NA	NA	NA
TU5	This Study	ETH-61245	10963	41	12957	12717	12837	NA	NA	NA	NA
TU6	This Study	ETH-61241	34024	326	39387	37576	38481.5	NA	NA	NA	NA
TU7	This Study	ETH-61244	42662	921	48258	44439	46348.5	NA	NA	NA	NA
TU8	This Study	ETH-61242	6471	32	7435	7316	7375.5	NA	NA	NA	NA
TU9	Kandel et al.	KIA-39642	27120	170	31340	30879	31109.5	NA	NA	NA	NA
TU10	This Study	MAMS-2330	25760	90	30351	29563	29957	NA	NA	NA	NA
TU11	Napierala &	NA	12225	45	14286	13975	14130.5	NA	NA	NA	NA
TU13	This Study	MAMS-2387	12220	40	14256	13984	14120	NA	NA	NA	NA
TU14	Germonpré e	ETH-52774	2759	37	2947	2776	2861.5	NA	NA	NA	NA
TU15	NA	NA	25503.25	303.25	30974	29875	30424.5	25694.856	4647.6916	34901.8937	16597.0261
SK1	Skoglund et a	NA	30920	380	35659	34142	34900.5	NA	NA	NA	NA
CGG32	Germonpré e	OxA-31945	> 50300	NA	50000	55000	52500	61110.94	6353.722	73682.795	48920.877
CGG33	Germonpré e	OxA-31946	13925	70	17142	16585	16863.5	NA	NA	NA	NA
CGG34	Germonpré e	OxA-31944	25690	220	30551	29319	29935	NA	NA	NA	NA
Ma1	NA			NA	0	100	NA	NA	NA	NA	NA
Ma2	NA			NA	0	100	NA	NA	NA	NA	NA
Ma3	NA			NA	0	100	NA	NA	NA	NA	NA
Ma4	NA			NA	0	100	NA	NA	NA	NA	NA
Ma5	NA			NA	0	100	NA	NA	NA	NA	NA
Ma6	NA			NA	0	100	NA	NA	NA	NA	NA
Ma7	NA			NA	0	100	NA	NA	NA	NA	NA
Ma8	NA			NA	0	100	NA	NA	NA	NA	NA
Ma9	NA			NA	0	100	NA	NA	NA	NA	NA
Bj1	NA			NA	0	100	NA	NA	NA	NA	NA
Bj2	NA			NA	0	100	NA	NA	NA	NA	NA
Bj3	NA			NA	0	100	NA	NA	NA	NA	NA
Bj4	NA			NA	0	100	NA	NA	NA	NA	NA
Bj5	NA			NA	0	100	NA	NA	NA	NA	NA
Bj6	NA			NA	0	100	NA	NA	NA	NA	NA
Zh3	NA			NA	0	100	NA	NA	NA	NA	NA
Zh4	NA			NA	0	100	NA	NA	NA	NA	NA
Zh5	NA			NA	0	100	NA	NA	NA	NA	NA
Pa1	NA			NA	0	100	NA	NA	NA	NA	NA
Pa2	NA			NA	0	100	NA	NA	NA	NA	NA
Tha1	NA			NA	0	100	NA	NA	NA	NA	NA
Tha2	NA			NA	0	100	NA	NA	NA	NA	NA
Tha3	NA			NA	0	100	NA	NA	NA	NA	NA
Tha4	NA			NA	0	100	NA	NA	NA	NA	NA
Tha5	NA			NA	0	100	NA	NA	NA	NA	NA
Tha6	NA			NA	0	100	NA	NA	NA	NA	NA
Tha7	NA			NA	0	100	NA	NA	NA	NA	NA

Table 3.S1, part 2 (continued).

Tha8	NA		NA	0	100	NA	NA	NA	NA	NA
Tha9	NA		NA	0	100	NA	NA	NA	NA	NA
Tha10	NA		NA	0	100	NA	NA	NA	NA	NA
Tha11	NA		NA	0	100	NA	NA	NA	NA	NA
Tha12	NA		NA	0	100	NA	NA	NA	NA	NA
Tha13	NA		NA	0	100	NA	NA	NA	NA	NA
Tha14	NA		NA	0	100	NA	NA	NA	NA	NA
Tha15	NA		NA	0	100	NA	NA	NA	NA	NA
Tha16	NA		NA	0	100	NA	NA	NA	NA	NA
Tha17	NA		NA	0	100	NA	NA	NA	NA	NA
Tha18	NA		NA	0	100	NA	NA	NA	NA	NA
Tha19	NA		NA	0	100	NA	NA	NA	NA	NA
Tha20	NA		NA	0	100	NA	NA	NA	NA	NA
Tha21	NA		NA	0	100	NA	NA	NA	NA	NA
Tha22	NA		NA	0	100	NA	NA	NA	NA	NA
Tha23	NA		NA	0	100	NA	NA	NA	NA	NA
Tha24	NA		NA	0	100	NA	NA	NA	NA	NA
Tha25	NA		NA	0	100	NA	NA	NA	NA	NA
Tha26	NA		NA	0	100	NA	NA	NA	NA	NA
Tha27	NA		NA	0	100	NA	NA	NA	NA	NA
Tha28	NA		NA	0	100	NA	NA	NA	NA	NA
Tha29	NA		NA	0	100	NA	NA	NA	NA	NA
Tha30	NA		NA	0	100	NA	NA	NA	NA	NA
Tha31	NA		NA	0	100	NA	NA	NA	NA	NA
Tha32	NA		NA	0	100	NA	NA	NA	NA	NA
Tha33	NA		NA	0	100	NA	NA	NA	NA	NA
Tha34	NA		NA	0	100	NA	NA	NA	NA	NA
Tha35	NA		NA	0	100	NA	NA	NA	NA	NA
Tha36	NA		NA	0	100	NA	NA	NA	NA	NA
Tha37	NA		NA	0	100	NA	NA	NA	NA	NA
Tha38	NA		NA	0	100	NA	NA	NA	NA	NA
Tha39	NA		NA	0	100	NA	NA	NA	NA	NA
Tha40	NA		NA	0	100	NA	NA	NA	NA	NA
Ar1	NA		NA	0	100	NA	NA	NA	NA	NA
Fr1	NA		NA	0	100	NA	NA	NA	NA	NA
Fr2	NA		NA	0	100	NA	NA	NA	NA	NA
Ms1	NA		NA	0	100	NA	NA	NA	NA	NA
Ms2	NA		NA	0	100	NA	NA	NA	NA	NA
Ms25	NA		NA	0	100	NA	NA	NA	NA	NA
Ms4	NA		NA	0	100	NA	NA	NA	NA	NA
Ms5	NA		NA	0	100	NA	NA	NA	NA	NA
Ms6	NA		NA	0	100	NA	NA	NA	NA	NA
Ms7	NA		NA	0	100	NA	NA	NA	NA	NA
Ms8	NA		NA	0	100	NA	NA	NA	NA	NA
Ms9	NA		NA	0	100	NA	NA	NA	NA	NA
Ms10	NA		NA	0	100	NA	NA	NA	NA	NA
Ms11	NA		NA	0	100	NA	NA	NA	NA	NA
Ms12	NA		NA	0	100	NA	NA	NA	NA	NA
Ms13	NA		NA	0	100	NA	NA	NA	NA	NA
Ms14	NA		NA	0	100	NA	NA	NA	NA	NA
Ms15	NA		NA	0	100	NA	NA	NA	NA	NA
Ms16	NA		NA	0	100	NA	NA	NA	NA	NA
Ms17	NA		NA	0	100	NA	NA	NA	NA	NA
Ms18	NA		NA	0	100	NA	NA	NA	NA	NA
Ms19	NA		NA	0	100	NA	NA	NA	NA	NA
Ms20	NA		NA	0	100	NA	NA	NA	NA	NA
Ms21	NA		NA	0	100	NA	NA	NA	NA	NA
Ms22	NA		NA	0	100	NA	NA	NA	NA	NA
Zh1	NA		NA	0	500	NA	NA	NA	NA	NA
Zh2	NA		NA	0	500	NA	NA	NA	NA	NA
Zh6	NA		NA	0	500	NA	NA	NA	NA	NA
Zh7	NA		NA	0	500	NA	NA	NA	NA	NA
Zh8	NA		NA	0	500	NA	NA	NA	NA	NA
SAMPLES EXCLUDED FROM ANALYSES										
TH2	Germonpré e	Beta-239920	31890	230	36287	35251	35769	NA	NA	NA	NA
TH9	Leonard et al	NA	17640	240	21947	20685	21316	NA	NA	NA	NA
TH13	NA	NA	12052.5	66.25	14083	13752	13917.5	NA	NA	NA	NA
CGG13	Lee et al. 20	NA	>47000		50000	47000	48500	NA	NA	NA	NA
CGG23	This Study	MAMS-2424	28830	130	33465	32574	33019.5	NA	NA	NA	NA
CGG24	Pitulko et al.,	NA	28520	240	33271	31688	32479.5	NA	NA	NA	NA
CGG30	Pitulko, 2016	AAR-21023	>45000		50000	47785	48892.5	NA	NA	NA	NA
CGG31	Germonpré e	OxA-31985	901	25	911	742	826.5	NA	NA	NA	NA
TU12	This Study	MAMS-2387	12370	40	14709	14141	14425	NA	NA	NA	NA
TU16	NA		25503.25	303.25	30974	29875	30424.5	NA	NA	NA	NA
TU17	NA		25503.25	303.25	30974	29875	30424.5	NA	NA	NA	NA

Table 3.S1, part 3.

ID	Newly sequenced	Extraction	Library build	Sequence generation	Coverage
TH1	0	NA	NA	NA	8.3
TH3	0	NA	NA	NA	20.4
TH4	0	NA	NA	NA	137.7
TH5	0	NA	NA	NA	6
TH6	0	NA	NA	NA	21.5
TH7	0	NA	NA	NA	14.7
TH8	0	NA	NA	NA	90.1
TH10	0	NA	NA	NA	625.7
TH11	0	NA	NA	NA	4.2
TH12	0	NA	NA	NA	100.8
TH14	0	NA	NA	NA	8.6
TH15	0	NA	NA	NA	9.2
CGG12	1	6	3	3	159
CGG14	1	6	3	3	101.7
CGG15	1	6	3	3	55.5
CGG16	1	6	3	3	189.4
CGG17	1	6	3	3	180.1
CGG18	1	6	3	3	215.1
CGG19	1	4	2	2	9.6
CGG20	1	4	2	2	7.7
CGG21	1	4	2	2	12.4
CGG22	1	4	2	2	10
CGG25	1	4	2	2	11.8
CGG26	1	4	2	2	7.7
CGG27	1	4	2	2	20.3
CGG28	1	4	2	2	6.8
CGG29	1	4	2	2	23.6
TU1	1	1	1	1	3.95
TU2	1	1	1	1	4
TU3	1	1	1	1	4
TU4	1	1	1	1	20.1
TU5	1	1	1	1	9.5
TU6	1	1	1	1	115.3
TU7	1	1	1	1	75.6
TU8	1	1	1	1	206
TU9	1	2	1	1	14.5
TU10	1	2	1	1	63.7
TU11	1	2	1	1	166.7
TU13	1	2	1	1	2.4
TU14	1	2	1	1	NA
TU15	1	2	1	1	3.8
SK1	0	NA	NA	NA	NA
CGG32	1	4	2	2	9.6
CGG33	1	4	2	2	9.4
CGG34	1	4	2	2	21.7
Ma1	0	NA	NA	NA	NA
Ma2	0	NA	NA	NA	NA
Ma3	0	NA	NA	NA	NA
Ma4	0	NA	NA	NA	NA
Ma5	0	NA	NA	NA	NA
Ma6	0	NA	NA	NA	NA
Ma7	0	NA	NA	NA	NA
Ma8	0	NA	NA	NA	NA
Ma9	0	NA	NA	NA	NA
Bj1	0	NA	NA	NA	NA
Bj2	0	NA	NA	NA	NA
Bj3	0	NA	NA	NA	NA
Bj4	0	NA	NA	NA	NA
Bj5	0	NA	NA	NA	NA
Bj6	0	NA	NA	NA	NA
Zh3	0	NA	NA	NA	NA
Zh4	0	NA	NA	NA	NA
Zh5	0	NA	NA	NA	NA
Pa1	0	NA	NA	NA	NA
Pa2	0	NA	NA	NA	NA
Tha1	0	NA	NA	NA	NA
Tha2	0	NA	NA	NA	NA
Tha3	0	NA	NA	NA	NA
Tha4	0	NA	NA	NA	NA
Tha5	0	NA	NA	NA	NA
Tha6	0	NA	NA	NA	NA
Tha7	0	NA	NA	NA	NA
Tha8	0	NA	NA	NA	NA
Tha9	0	NA	NA	NA	NA
Tha10	0	NA	NA	NA	NA
Tha11	0	NA	NA	NA	NA
Tha12	0	NA	NA	NA	NA
Tha13	0	NA	NA	NA	NA
Tha14	0	NA	NA	NA	NA
Tha15	0	NA	NA	NA	NA
Tha16	0	NA	NA	NA	NA
Tha17	0	NA	NA	NA	NA
Tha18	0	NA	NA	NA	NA
Tha19	0	NA	NA	NA	NA
Tha20	0	NA	NA	NA	NA
Tha21	0	NA	NA	NA	NA
Tha22	0	NA	NA	NA	NA
Tha23	0	NA	NA	NA	NA
Tha24	0	NA	NA	NA	NA
Tha25	0	NA	NA	NA	NA
Tha26	0	NA	NA	NA	NA
Tha27	0	NA	NA	NA	NA
Tha28	0	NA	NA	NA	NA
Tha29	0	NA	NA	NA	NA
Tha30	0	NA	NA	NA	NA
Tha31	0	NA	NA	NA	NA
Tha32	0	NA	NA	NA	NA
Tha33	0	NA	NA	NA	NA
Tha34	0	NA	NA	NA	NA
Tha35	0	NA	NA	NA	NA
Tha36	0	NA	NA	NA	NA
Tha37	0	NA	NA	NA	NA
Tha38	0	NA	NA	NA	NA
Tha39	0	NA	NA	NA	NA
Tha40	0	NA	NA	NA	NA
Ar1	0	NA	NA	NA	NA
Fr1	0	NA	NA	NA	NA
Fr2	0	NA	NA	NA	NA
Ms1	1	3	2	2	NA
Ms2	1	5	2	2	NA
Ms25	1	4	2	2	NA
Ms4	1	5	2	2	NA
Ms5	1	5	2	2	NA
Ms6	1	4	2	2	NA
Ms7	1	5	2	2	NA
Ms8	1	5	2	2	NA
Ms9	1	5	2	2	NA
Ms10	1	5	2	2	NA
Ms11	1	5	2	2	NA
Ms12	1	5	2	2	NA
Ms13	1	5	2	2	NA
Ms14	1	5	2	2	NA
Ms15	1	5	2	2	NA
Ms16	1	5	2	2	NA
Ms17	1	5	2	2	NA
Ms18	1	5	2	2	NA
Ms19	1	5	2	2	NA
Ms20	1	5	2	2	NA
Ms21	1	5	2	2	NA
Ms22	1	5	2	2	NA
Zh1	0	NA	NA	NA	NA
Zh2	0	NA	NA	NA	NA
Zh6	0	NA	NA	NA	NA
Zh7	0	NA	NA	NA	NA
Zh8	0	NA	NA	NA	NA
SAMPLES EXCLUDED FROM ANALYSES					
TH2	0	NA	NA	NA	4.1
TH9	0	NA	NA	NA	2.1
TH13	0	NA	NA	NA	1.9
CGG13	1	4	2	2	657.4
CGG23	1	4	2	2	2.8
CGG24	1	4	2	2	0.9
CGG30	1	4	2	2	1.4
CGG31	1	4	2	2	1.4
TU12	1	2	1	1	2.8
TU16	1	2	1	1	2.7
TU17	1	2	1	1	2.4

Table 3.S1: Sample information (presented in three parts for esthetical reasons) listing sample locations, archaeological contexts and dating information, and DNA sequencing and quality information.

Literature cited in Table 3.S1

Arnason, Ulfur, Anette Gullberg, Axel Janke, and Morgan Kullberg 2007 Mitogenomic Analyses of Caniform Relationships. Molecular Phylogenetics and Evolution 45(3): 863–874.

Björnerfeldt, Susanne, Matthew T. Webster, and Carles Vilà 2006 Relaxation of Selective Constraint on Dog Mitochondrial DNA Following Domestication. Genome Research 16(8): 990–994.

Freedman, Adam H., Ilan Gronau, Rena M. Schweizer, et al. 2014 Genome Sequencing Highlights the Dynamic Early History of Dogs. PLOS Genet 10(1): e1004016.

Germonpré, Mietje, Sergey Fedorov, Petr Danilov, et al. 2017 Palaeolithic and Prehistoric Dogs and Pleistocene Wolves from Yakutia: Identification of Isolated Skulls. Journal of Archaeological Science 78: 1–19.

Germonpré, Mietje, Martina Lázničková-Galetová, Robert J. Losey, Jannikke Räikkönen, and Mikhail V. Sablin 2015 Large Canids at the Gravettian Předmostí Site, the Czech Republic: The Mandible. Quaternary International 359–360. World of Gravettian Hunters: 261–279.

Germonpré, Mietje, Mikhail V. Sablin, Rhiannon E. Stevens, et al. 2009 Fossil Dogs and Wolves from Palaeolithic Sites in Belgium, the Ukraine and Russia: Osteometry, Ancient DNA and Stable Isotopes. Journal of Archaeological Science 36(2): 473–490.

Kandel, Andrew W., Boris Gasparyan, Angela A. Bruch, Lior Weissbrod, and Diana Zardaryan 2011 Introducing Aghitu-3, the First Upper Paleolithic Cave Site in Armenia. ARAMAZD: Armenian Journal of Near Eastern Studies 6(2): 7–23.

Kandel, Andrew W., Boris Gasparyan, Samvel Nahepetyan, Andreas Taller, and Lior Weissbrod 2014 The Upper Paleolithic Settlement of the Armenian Highlands. In M. Otte & F. Le Brun-Ricalens (Eds.) Modes de Contacts et de Déplacements Au Paléolithique Eurasiatique, Actes Du Colloque International de La Commission 8 (Paléolithique Supérieur) de l'UISPP Pp. 39–60.

Lee, Esther J., D. Andrew Merriwether, Alexei K. Kasparov, et al. 2015 Ancient DNA Analysis of the Oldest Canid Species from the Siberian Arctic and Genetic Contribution to the Domestic Dog. PLoS ONE 10(5) e0125759

Leonard, Jennifer A., Carles Vilà, Kena Fox-Dobbs, et al. 2007 Megafaunal Extinctions and the Disappearance of a Specialized Wolf Ecomorph. Current Biology 17(13): 1146–1150.

Matsumura, Shuichi, Yasuo Inoshima, and Naotaka Ishiguro 2014 Reconstructing the Colonization History of Lost Wolf Lineages by the Analysis of the Mitochondrial Genome. Molecular Phylogenetics and Evolution 80: 105–112.

Meng, Chao, Honghai Zhang, and Qingcheng Meng 2009 Mitochondrial Genome of the Tibetan Wolf. Mitochondrial DNA 20(2–3): 61–63.

Napierala, Hannes, and Hans-Peter Uerpmann 2012 A "new" Palaeolithic Dog from Central Europe. International Journal of Osteoarchaeology 22(2): 127–137.

Ovodov, Nikolai D., Susan J. Crockford, Yaroslav V. Kuzmin, et al. 2011 A 33,000-Year-Old Incipient Dog from the Altai Mountains of Siberia: Evidence of the Earliest Domestication Disrupted by the Last Glacial Maximum. PloS One 6(7): e22821.

Pang, Jun-Feng, Cornelya Kluetsch, Xiao-Ju Zou, et al. 2009 mtDNA Data Indicate a Single Origin for Dogs South of Yangtze River, Less Than 16,300 Years Ago, from Numerous Wolves. Molecular Biology and Evolution 26(12): 2849–2864.

Pitulko, V., P Nikolskiy, A. Basilyan, and E. Pavlova 2013 Human Habitation in the Arctic Western Beringia Prior the LGM. In Paleoamerican Odyssey Pp. 13 – 44. CSFA, Dept. of Anthropology, Texas A&M University.

Pitulko, V., A. Tikhonov, K Kuper, and R Polozov 2014 Human Inficted Lesion on a 45,000-Year-Old Pleistocene Wolf Humerus from the Yana River, Arctic Siberia. In Abstract Book of the VIth International Conference on Mammoths and Their Relatives. S.A.S.G. Pp. 156–157.

Pitulko, V. V., E. Y. Pavlova, and A. E. Basilyan 2016 Mass Accumulations of Mammoth (Mammoth "graveyards") with Indications of Past Human Activity in the Northern Yana-Indighirka Lowland, Arctic Siberia. Quaternary International 406, Part B. VIth International Conference on Mammoths and Their Relatives, Part 2: 202–217.

Pitulko, Vladimir V., Aleksandr E. Basilyan, and Elena Y. Pavlova 2014 The Berelekh Mammoth "Graveyard": New Chronological and Stratigraphical Data from the 2009 Field Season. Geoarchaeology 29(4): 277–299.

Sablin, MikhailV., and GennadyA. Khlopachev 2002 The Earliest Ice Age Dogs: Evidence from Eliseevichi 1. Current Anthropology 43(5): 795–799.

Skoglund, Pontus, Jan Storå, Anders Götherström, and Mattias Jakobsson 2013 Accurate Sex Identification of Ancient Human Remains Using DNA Shotgun Sequencing. Journal of Archaeological Science 40(12): 4477–4482.

Thalmann, O., B. Shapiro, P. Cui, et al. 2013 Complete Mitochondrial Genomes of Ancient Canids Suggest a European Origin of Domestic Dogs. Science 342(6160): 871–874.

Zhang, Honghai, Jin Zhang, Lei Chen, and Guangshuai Liu 2014 The Complete Mitochondrial Genome of Chinese Shinjang Wolf. Mitochondrial DNA 25(2): 106–108.

Zhang, Honghai, Jin Zhang, Chao Zhao, et al. 2015 Complete Mitochondrial Genome of Canis Lupus Campestris. Mitochondrial DNA 26(2): 255–256.

	Sequencing	Mapping		
Sample	# reads total	# filtered reads mapping the complete dog genome	# filtered reads mapping exclusively the dog mt-genome	% filtered reads mapping the dog mt-genome
CGG12	20,502,189 (8,795,253)	1,461,472 (22,120)	581 (21,779)	0.040 (98.46)
CGG13*	10,454,317 (9,837,169)	2,921,726 (35,942)	157 (30,711)	0.005 (85.45)
CGG14	29,231,546 (16,073,166)	304,327 (18,194)	1,394 (18,142)	0.458 (99.71)
CGG15	17,563,376 (5,028,725)	526,430 9,776)	419 (9,726)	0.080 (99.49)
CGG16	8,426,724 (6,982,988)	188,881 (24,367)	53 (23,740)	0.028 (97.43)
CGG17	27,612,032 (15,525,823)	3,406,363 (25,846)	1,224 (25,350)	0.036 (98.08)
CGG18	5,342,504 (8,845,755)	530,495 (23,048)	92 (22,421)	0.017 (97.28)
CGG19	44,387,927	2,747,206	2,227	0.081
CGG20	30,039,526	2,806,030	1,852	0.066
CGG21	31,161,726	6,880,522	3,014	0.044
CGG22	14,125,908	467,594	2,568	0.549
CGG23*	20,899,573	14,788,539	767	0.005
CGG24*	17,223,554	75,513	248	0.328
CGG25	13,204,816	7,208,601	2,883	0.040
CGG26	28,498,152	2,828,408	1,856	0.066
CGG27	28,947,324	22,295,797	4,696	0.021
CGG28	16,918,816	4,376,379	1,945	0.044
CGG29	40,530,428	23,217,595	5,728	0.025
CGG30*	89,127,852	246,756	310	0.126

CGG31*	10,524,144	895,714	1,948	0.217
CGG32	26,685,260	14,231,440	2,196	0.015
CGG33	24,737,165	18,241,333	5,500	0.030
CGG34	14,776,135	6,668,532	1,153	0.017
TU1	1,071,820	4,943	539	10.90
TU2	940,066	6,676	610	9.14
TU3	1,424,226	19,367	539	2.78
TU4	6,963,257	78,775	1,892	2.40
TU5	1,437,297	46,883	1,251	2.67
TU6	2,383,565	50,063	15,448	30.86
TU7	5,193,206	218,867	9,050	4.13
TU8	3,378,610	329,599	28,182	8.55
TU9	264,033	3,493	3,248	92.99
TU10	439,293	12,748	12,577	98.66
TU11	4,393,084	46,075	30,095	65.32
TU12*	856,459	1,135	502	44.23
TU13	4,607,297	4,974	1,697	34.12
TU14	852,538	7,933	3,017	38.03
TU15	1,063,036	1,943	1,213	62.43
TU16*	4,957,011	4,594	801	17.44
TU17*	2,330,648	1,262	767	60.78

Table 3.S2: Proportion of sequencing reads mapped against the dog nuclear genome and mitochondrial genomes. The upper panel shows data generated with single-end sequencing technology and the lower panel (TU) of those produced with paired-end technology. Numbers in brackets represent data generated using mt-genome capture technique (described in 3.SI2.3). Samples marked with an asterisk (*) were not included in the demographic analyses (Table 3.S1).

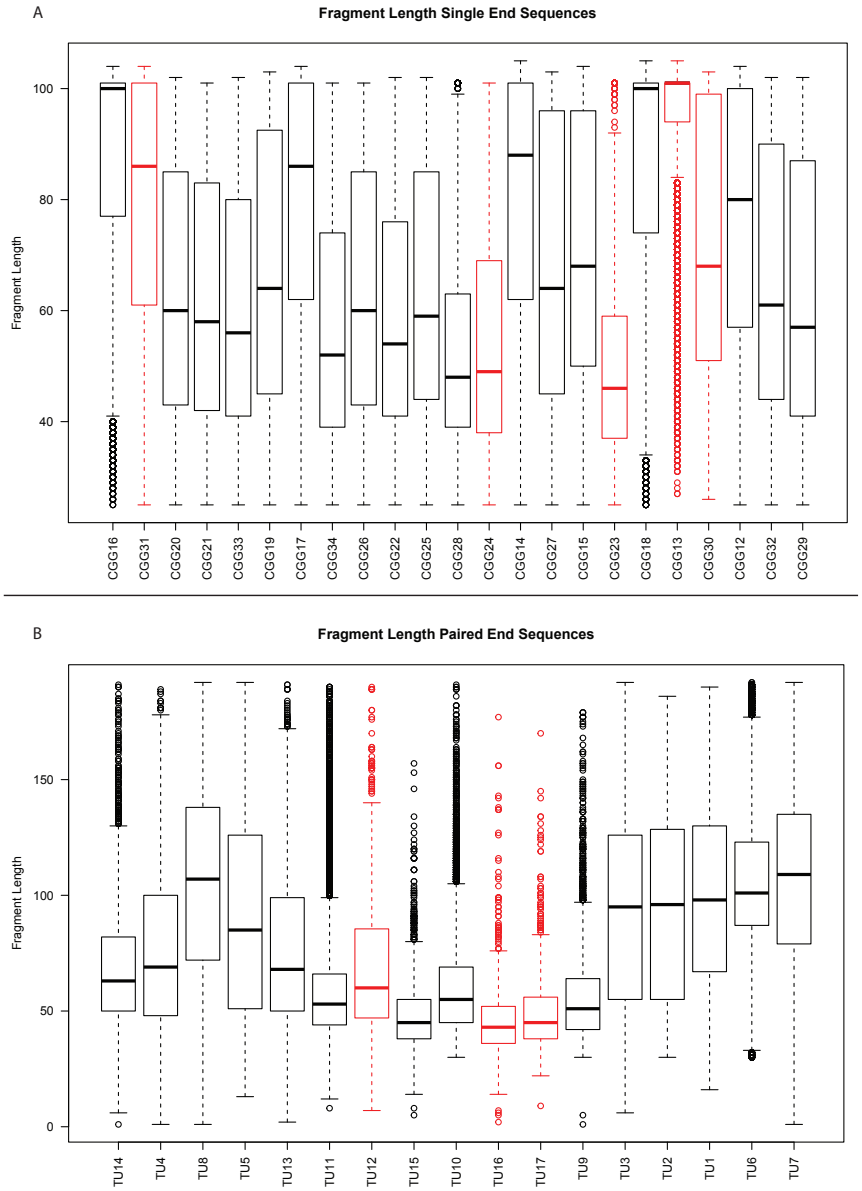

Fig. 3.S1: Fragment length distribution for all newly generated, ancient sequences. (A) Length of the fragments generated with single-end sequencing technology. (B) Length of the fragments generated with paired-end sequencing technology. Samples excluded from demographic analyses are highlighted in red. Samples are ordered by age with the youngest on the left.

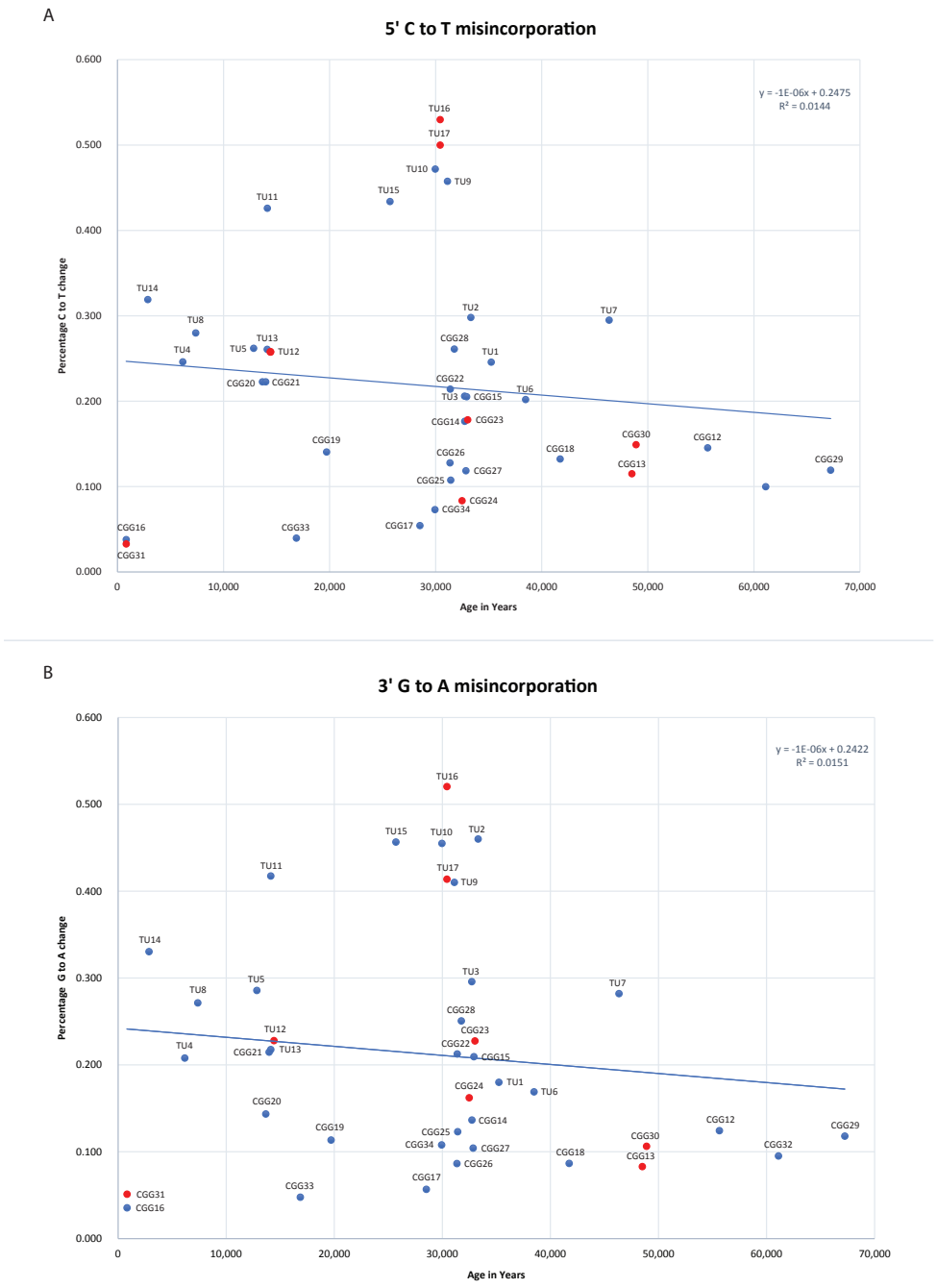

Fig. 3.S2: Deamination patterns at the respective start bases of the newly generated, ancient fragments as a function of sample age. (A) C to T misincorporation frequency at the first base of the 5' end of the fragments. (B) G to A misincorporation frequency at the first base of the 3' end of the fragments. The blue lines represent the best linear fit. Samples excluded from demographic analyses are highlighted in red.

3.S2.6 Bibliography

Allentoft, M. E. et al. 2015. Population genomics of Bronze Age Eurasia. *Nature* 522, 167-172.

Andrews, S., 2010. FastQC: a quality control tool for high throughput sequence data. (available at http://www.bioinformatics.babraham.ac.uk/projects/fastqc).

Broad Institute, Picard. A set of command line tools (in Java) for manipulating high-throughput sequencing (HTS) data and formats such as SAM/BAM/CRAM and VCF, (available at http://broadinstitute.github.io/picard/).

Dabney, J. et al. 2013. Complete mitochondrial genome sequence of a Middle Pleistocene cave bear reconstructed from ultrashort DNA fragments. *Proceedings of the National Academy of Sciences USA* 110, 15758-15763.

Danecek, P. et al. 2011. The variant call format and VCFtools. *Bioinformatics*. 27, 2156–8.

Ersmark, E. et al. 2015. Population demography and genetic diversity in the Pleistocene cave lion. *Open Quaternary*, 1, DOI: http://doi.org/10.5334/oq.aa.

Gilbert, M. T. P. et al. 2007. Whole-genome shotgun sequencing of mitochondria from ancient hair shafts. *Science* 317, 1927-1930.

Gnirke, A., et al. 2009. Solution hybrid selection with ultra-long oligonucleotides for massively parallel targeted sequencing. *Nature biotechnology* 27.2, 182-189.

Green, R. E. et al. 2008. Complete Neandertal mitochondrial genome sequence determined by high-throughput sequencing. *Cell* 134, 416–426.

Ishiguro, N., Nakajima, A., Horiuchi, M. & Shinagawa, M., 2002. Multiple nuclear pseudogenes of mitochondrial DNA exist in the canine genome. *Mammalian Genome* 13, 365–372.

Kim, K. S., Lee, S. E., Jeong, H. W. & Ha, J. H., 1998. The complete nucleotide sequence of the domestic dog (Canis familiaris) mitochondrial genome. *Molecular Phylogenetics and Evolution* 10, 210-220.

Kircher, M., Sawyer, S. & Meyer, M., 2012. Double indexing overcomes inaccuracies in multiplex sequencing on the Illumina platform. *Nucleic Acids Research* 40, e3

Kircher, M., 2012. in Ancient DNA (eds. Shapiro, B. & Hofreiter, M.) 840, 197–228 (Humana Press)

Li, H. & Durbin, R., 2009. Fast and accurate short read alignment with Burrows-Wheeler transform. *Bioinformatics* 25, 1754–60.

Li, H. et al. 2009. The Sequence Alignment/Map format and SAMtools. *Bioinformatics* 25, 2078–9.

Meyer, M. & Kircher, M., 2010. Illumina sequencing library preparation for highly multiplexed target capture and sequencing. *Cold Spring Harbor Protocols*, pdb.prot5448.

Maricic, T., Whitten, M. & Pääbo, S., 2010. Multiplexed DNA sequence capture of mitochondrial genomes using PCR products. *PLoS ONE* 5, e14004.

McKenna, A. et al. 2010. The Genome Analysis Toolkit: a MapReduce framework for analyzing next-generation DNA sequencing data. *Genome Research* 20, 1297–303.

Sawyer, S. et al. 2012. Temporal patterns of nucleotide misincorporations and DNA fragmentation in ancient DNA. *PLoS ONE* 7, e34131.

Schroeder, H. et al. 2015. Genome-wide ancestry of 17th-century enslaved Africans from the Caribbean. *Proceedings of the National Academy of Sciences USA* 112, 3669-3673.

Schubert, M. et al. 2012. Improving ancient DNA read mapping against modern reference genomes. *BMC Genomics*. 13, 178.

Schubert, M. et al. 2014. Characterization of ancient and modern genomes by SNP detection and phylogenomic and metagenomic analysis using PALEOMIX. *Nature Protocols* 9, 1056–1082.

Schubert, M., Lindgreen, S. & Orlando, L., 2016. AdapterRemoval v2: rapid adapter trimming, identification, and read merging. *BMC Research Notes* 9, 1–7.

Skoglund, P., Ersmark, E., Palkopoulou, E. & Dalén, L., 2015. Ancient Wolf Genome Reveals an Early Divergence of Domestic Dog Ancestors and Admixture into High-Latitude Breeds. *Current Biology*, 1515–1519.

Rohland, N. & Hofreiter, M., 2007. Ancient DNA extraction from bones and teeth. *Nature Protocols* 2, 1756–1762.

Thalmann, O. et al. 2013. Complete Mitochondrial Genomes of Ancient Canids Suggest a European Origin of Domestic Dogs. *Science* 342, 871-874.

3.S3 – Data Analyses & Results

3.S3.1 BEAST analyses & results

We used the BEAST tool (v.1.8.0) (Drummond et al., 2012) to build a tip calibrated wolf mitochondrial tree and to estimate mutation rates for the four different partitions of the wolf mitochondrial genome.

Partition finder

We used the PartitionFinder tool (Lanfear et al., 2012) and a subset of the gray wolf mitochondrial genome alignment containing 73 modern wolf samples (see supplementary table 1) to fit a substitution model to the partitions of the mitochondrial genome. The 6 partitions were based on the biological properties of the mammalian mitochondrial genome and defined as the 3 codons of the protein coding sequence (PCS1, PCS2 and PCS3), rRNA, tRNA and the D-Loop. The positions of the partitions in the sequence were established using an annotated dog mitochondrial sequence as a reference (Genbank accession nr NC_002008 (Kim et al., 1998)).

1. The "branch lengths" parameter was set as "linked"
2. The "model of evolution" parameter was set as "all"
3. The "model selection" parameter was set as "BIC"
4. The "search schemes" parameter was set as "greedy"
5. The best fitting mutation scheme suggested four partitions with independent mutation models listed in the Table 3.S3

Partition	Model
PCDS1, rRNA, tRNA	HKY+I
PCDS2	TrN+I
PCDS3	TrN+G
D-loop	TrN+I+G

Table 3.S3 :The best fitting mutation scheme from Partition Finder.

Mutation rate calculation

In order to estimate the grey wolf mitochondrial mutation rate, we combined modern grey wolf mitochondrial genome sequences (N = 78) with mitochondrial genome sequences from 38 ancient, directly radio carbon dated samples. All the sequences were subjected to strict quality criteria (see above). The ages (in years before present) of ancient samples in the BEAST analyses were set as a mean of calibrated radiocarbon age (years before present) distribution. See supplementary table 1 for list of samples and their radiocarbon ages included in the mutation mitochondrial rate estimation.

Input file settings

All input files for the BEAST analyses were created using the BEAUti (v.1.8.0) tool (Drummond et al., 2012) with default parameter settings, unless specified otherwise.

Based on the estimated best fitting partitioning scheme by PartitionFinder (see above), the mitochondrial genome was represented in the BEAST input file as four independent partitions: 1) tRNA & rRNA; 2) PCDS1; 3) PCDS2, 4) PCDS3 (defined as above)

To represent the fact that the mitochondrion is a single non-recombining locus, the tree models for all four partitions were linked while the site and the clock models for the four partitions were set as unlinked between the four partitions. The substitution model parameters for the four partitions were fixed to the ones estimated by Partition finder (see above).Our samples span 60 thousand years – a short time in an evolutionary scale - and come from a single species. As a result we used a strict (global) clock, which assumes no rate variation among different linages of the tree. However, relaxing the clock rate parameter had no measurable effect on the estimates. To allow for changes in population size through time, the Coalescent Bayesian Skyline (Drummond et al., 2005) was used as the tree prior, with a group size parameter set as 20.

Due to the fact that ancient samples are known to carry excess transition, we performed two independent BEAST runs: 1) where we did not use any sequence error model and 2) where we accounted for the potential the sequence error by using age-dependent (transition only) model. However, there was no noticeable difference between the estimates of the two runs, probably reflecting the strict quality criteria we subjected our sequences to. As a result, we did not include any sequence error model in subsequent runs.

Priors

1. A lognormal distribution with an offset of 0.0, a (log) mean of 1.0 and a (log) standard deviation of 1.25 was used as the *kappa* prior for all four partitions.
2. A uniform distribution with a lower bound of 0.0 and upper bound on 1.0 was used as *frequencies* prior for all four partitions.
3. A lognormal distribution with an offset of 0.0, a (log) mean of -18.42068 (corresponding to 1E-8 in real space) and a (log) standard deviation of 1.5 was used as the *clock rate* prior for all four partitions.
4. A gamma distribution with an offset of 0.0, a shape of 1.0 and a scale of 100,000 was used as the *root height* parameter. The gamma distribution was truncated using a lower bound of 50,000 and upper bound of 2,000,000.
5. A gamma distribution with an offset of 0.0, a shape of 2.0 and a scale of 100,000 was used as the *skyline population size* prior.

MCMC chain

For all runs the model parameters and trees were sampled every 5,000 iterations over 50,000,000 iterations. The first 10% of the recorded iterations were discarded as a burn-in period.

BEAST results

The MCMC chain convergence for all parameters was assessed using the Tracer (v1.6) program (Rambaut et al., 2014) and the sampled trees were summarized and the maximum clade credibility tree calculated using the program TreeAnnotator (v 1.8.0) (Rambaut and Drummond 2013).

For mitochondrial clock rate estimates see table 3.S4. For other parameter estimates, ESS values and convergences see a supplementary BEAST log (File 3.S2). File 3.S2 is too large to be included in the paper copy of the thesis, but is available upon request from L. Loog.

Partition	**Mean (Rate)**	**ESS**	**95% HPD interval**
tRNA_rRNA	3.38E-08	2119	[2.6621E-8, 4.0527E-8]
PCDS1	4.51E-08	2003	[2.6621E-8, 4.0527E-8]
PCDS2	4.73E-08	1809	[3.8539E-8, 5.6882E-8]
PCDS3	1.12E-07	1245	[9.5106E-8, 1.2969E-7]

Table 3.S4: Mitochondrial clock rate estimates from BEAST

Sample ID	**Mean Age in Years BP**	**ESS**	95% HPD interval
TH4	52153.715	520	[39259.1785, 65899.259]
TH6	29272.436	3572	[21900.1268, 36390.9274]
TH14	4802.368	7714	[-1077.3547, 11121.1716]
TU15	25694.856	6908	[16597.0261, 34901.8937]
CGG12	55643.388	645	[43151.1409, 68838.1615]
CGG29	67239.038	417	[50579.1862, 80836.7417]
CGG32	61110.94	450	[48920.877, 73682.795]

Table 3.S5: BEAST estimated molecular dates.

3.S3.2 Spatial Modelling Results

Model	Marginal Density	Nr Retrained	Likelihood	Bayes factor
Static	4.36E-09	535984	2.34E-03	0.124
Bottleneck	4.80E-09	463801	2.23E-03	0.118
Expansion_Europe	4.48E-09	747804	3.35E-03	0.178
Expansion_Central_North_Eurasia	3.45E-09	1821779	6.29E-03	0.334
Expansion_Beringia	3.71E-09	3467674	1.29E-02	0.682
Expansion_Middle-East	4.08E-09	1047509	4.28E-03	0.227
Expansion_East-Eurasia	3.47E-09	2613115	9.07E-03	0.481
Expansion_Arctic_North-America	6.95E-09	1089710	7.58E-03	0.402
Expansion_North-America	7.00E-09	1092975	7.65E-03	0.406
Bottleneck_Expansion Europe	4.97E-09	842708	4.19E-03	0.222
Bottleneck_Expansion Central_North_Eurasia	4.74E-09	1833150	8.68E-03	0.461
Bottleneck_Expansion Beringia	5.56E-09	3390358	1.88E-02	1.00
Bottleneck_Expansion Middle-East	5.04E-09	1169565	5.90E-03	0.313
Bottleneck_Expansion East-Eurasia	4.88E-09	2590882	1.27E-02	0.671
Bottleneck_Expansion Arctic_North-America	6.00E-09	664845	3.99E-03	0.212
Bottleneck_Expansion North-America	5.98E-09	667190	3.99E-03	0.212

Table 3.S6: ABC likelihoods and Bayes factors for all demographic scenarios tested.

	$\log_{10} m$	$\log_{10} K_1$	$\log_{10} K_2$	$\log_{10} K_3$	X	T	ΔT
mode	-1.21889	0.787876	-0.707106	0.41859	0.212122	24.091	0.202818
mean	-0.285358	0.126049	-0.145544	-0.048238	0.498321	0.680888	0.498127
median	-1.23045	0.603303	-0.632685	-0.125521	0.491106	23.914	0.489649
lower_95 quantile	-1.92422	-1.47999	-1.89776	-1.84251	0.034346	13.7236	0.035054
upper_95 quantile	-0.509983	1.86148	1.04406	1.33684	0.956468	33.4882	0.95642
HPD_95 lower	-1.91385	-1.15143	-1.99986	-1.87898	0.040521	14.1922	0.041432
HPD_95 upper	-0.523926	1.99991	0.747259	1.26501	0.949378	33.2827	0.959566

Table 3.S7: Posterior probability estimates for seven estimated parameters (ΔT, T, $\log_{10} K_1$, $\log_{10} K_2$, $\log_{10} K_3$, $\log_{10} m$, x) in the most likely model (Expansion out of Beringia with a population size change)

	$\log_{10} m$	$\log_{10} K_1$	$\log_{10} K_2$	$\log_{10} K_3$	X	T	ΔT
mode	-1.17463	0.747475	-0.424263	0.423481	0.363636	23.7376	0.21291
mean	-0.274114	0.124678	-0.108807	-0.050632	0.503041	0.674698	0.497701
median	-1.18503	0.5939	-0.479917	-0.137642	0.497858	23.6955	0.489209
lower_95 quantile	-1.86715	-1.48136	-1.88088	-1.84533	0.035648	12.2221	0.034849
upper_95 quantile	-0.449778	1.8593	1.33106	1.33419	0.957523	34.3488	0.956024
HPD_95 lower	-1.86938	-1.11098	-1.99988	-1.91915	0.0506204	12.7783	0.041480
HPD_95 upper	-0.479874	1.99987	1.03014	1.23124	0.95948	34.3433	0.94943

Table 3.S8: Posterior probability estimates for seven estimated parameters (ΔT, T, $\log_{10} K_1$, $\log_{10} K_2$, $\log_{10} K_3$, $\log_{10} m$, x) in the second most likely model (Expansion out of East Eurasia with a population size change).

3.S3.3 Bibliography

Drummond, A. J., A. Rambaut, B. Shapiro, and O. G. Pybus. 2005. Bayesian Coalescent Inference of Past Population Dynamics from Molecular Sequences. Molecular Biology and Evolution 22 (5): 1185–92. doi:10.1093/molbev/msi103.

Drummond, Alexei J., Marc A. Suchard, Dong Xie, and Andrew Rambaut. 2012. Bayesian Phylogenetics with BEAUti and the BEAST 1.7. Molecular Biology and Evolution 29 (8): 1969–73.

Kim, K. S., S. E. Lee, H. W. Jeong, and J. H. Ha. 1998. The Complete Nucleotide Sequence of the Domestic Dog (Canis Familiaris) Mitochondrial Genome. Molecular Phylogenetics and Evolution 10 (2): 210–20.

Lanfear, Robert, Brett Calcott, Simon Y. W. Ho, and Stephane Guindon. 2012. PartitionFinder: Combined Selection of Partitioning Schemes and Substitution Models for Phylogenetic Analyses. Molecular Biology and Evolution 29 (6): 1695–1701.

Rambaut, A., and A. J. Drummond. 2013. TreeAnnotator.

Rambaut, A., M. A. Suchard, D. Xie, and A. J. Drummond. 2014. Tracer (version 1.6.)

3.S4 Supplementary figures

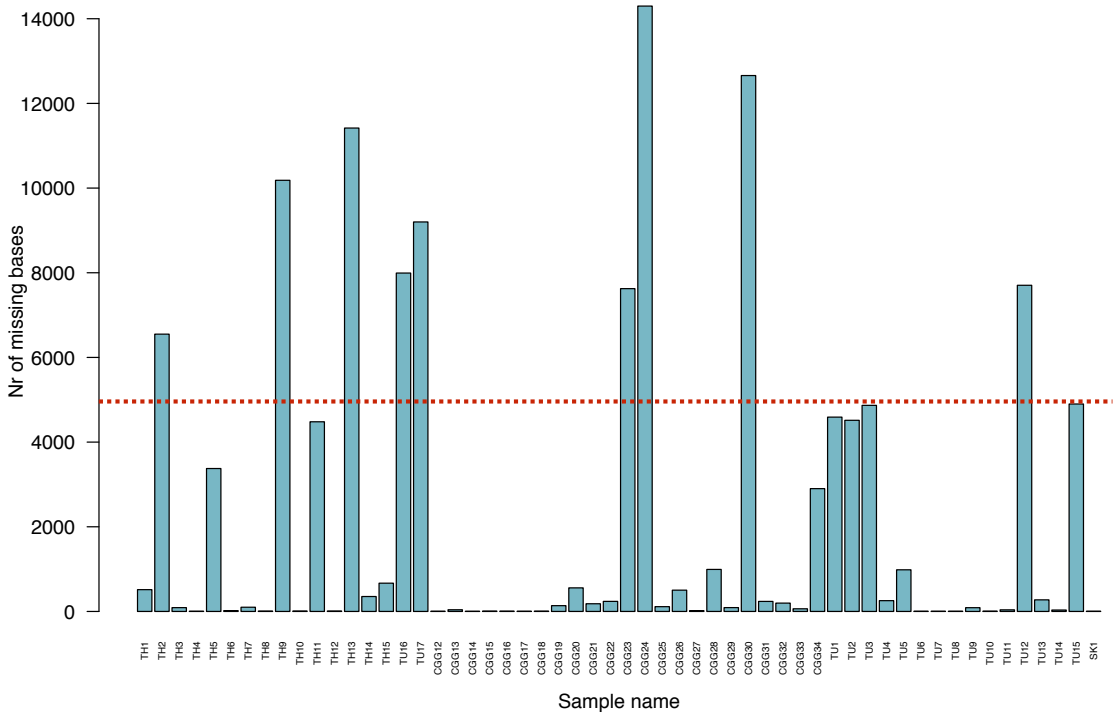

Fig. 3.S3: Number of bases missing from the complete mitochondrial genome (total of 15,463 base pairs - excluding the control region) (on y-axis) for each of the samples (x-axis). Nine sequences had more than 1/3 (5,150 bases) missing and were therefore excluded from all analyses (See supplementary table 1 for list of excluded samples). The red line represents the cut-off point (5,150 bases).

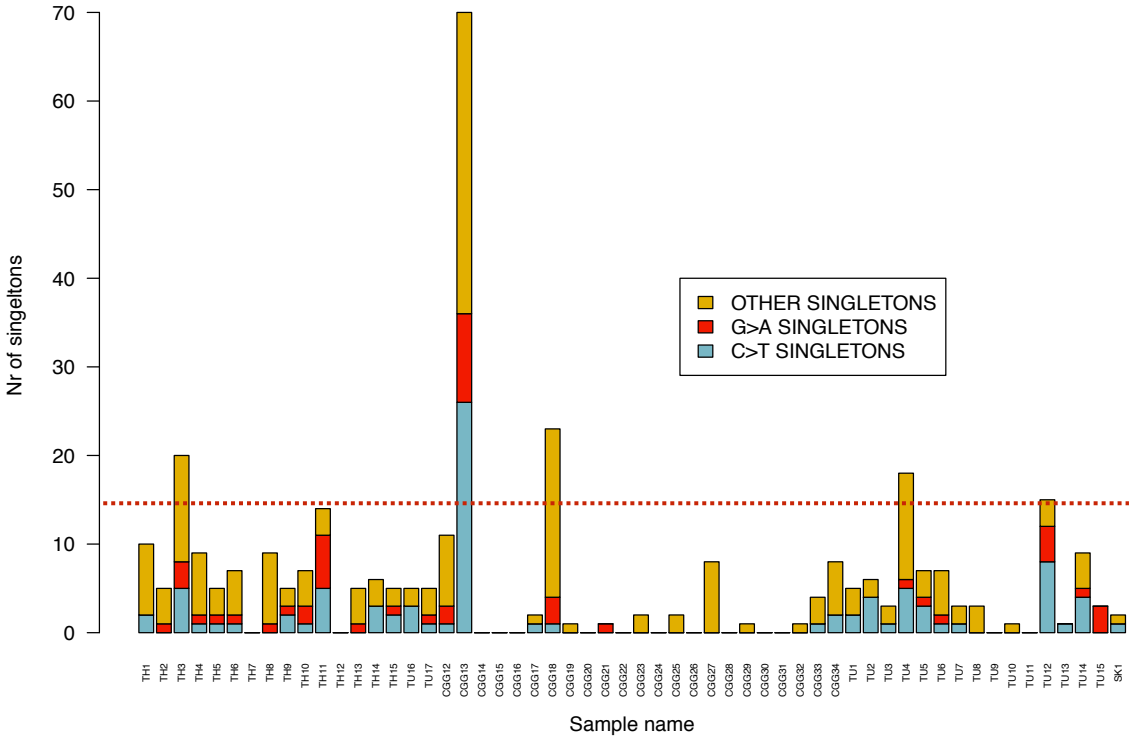

Fig. 3.S4: Number of singletons found in each of the sequences. Red represents G to A substitutions, blue represents C to T substitutions and yellow represents transversion substitutions. All ancient sequences that contained more than 0.1% (15 bases) of transition substitutions (C to T or A to G changes) were excluded from all analyses, as an excess of these substitutions indicate large amounts of DNA damage in the form of deamination. The red line represents the cut-off point (15 bases).

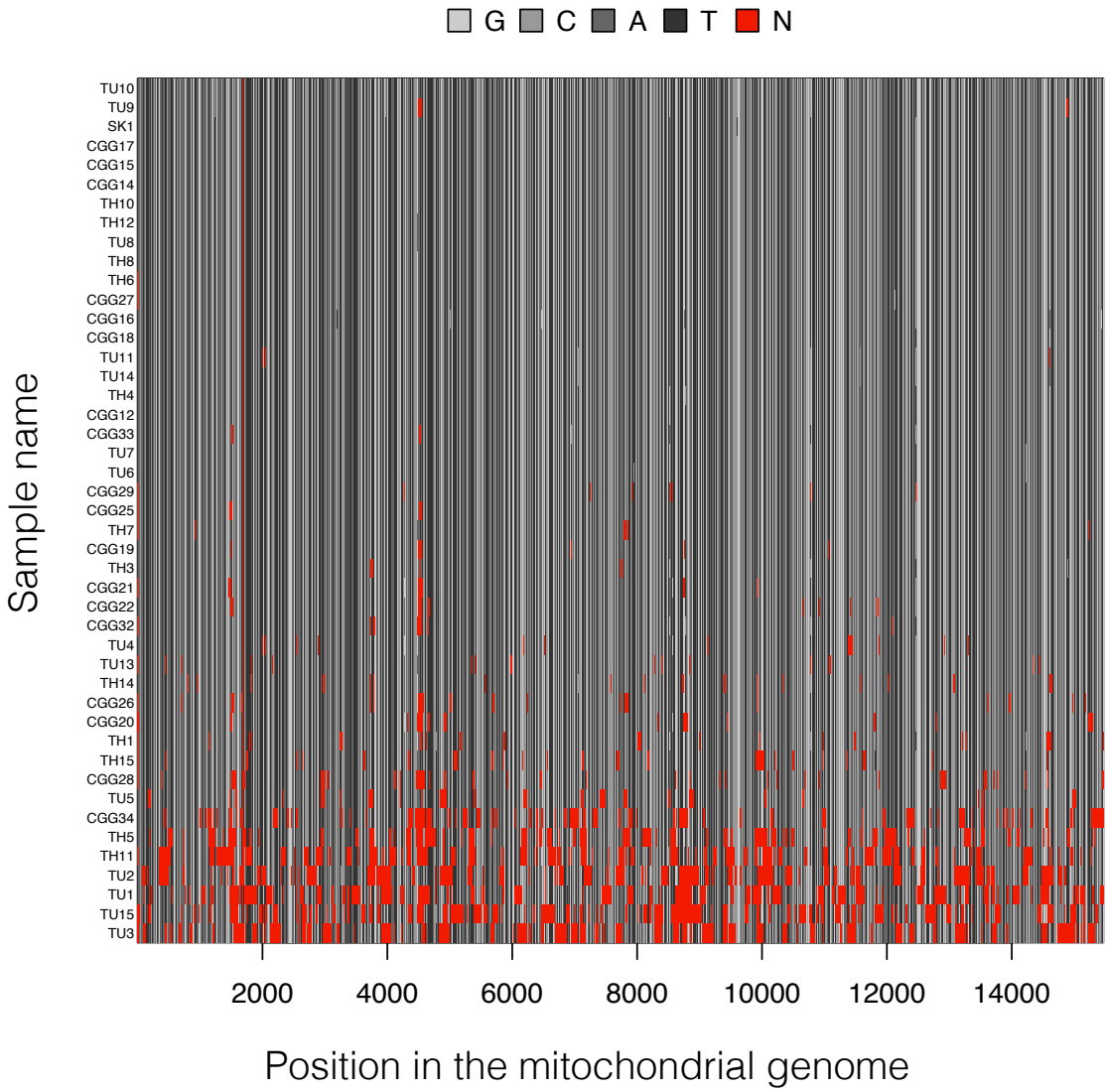

Fig. 3.S5: Positions where data is missing (red) for each sample (excluding the control region).

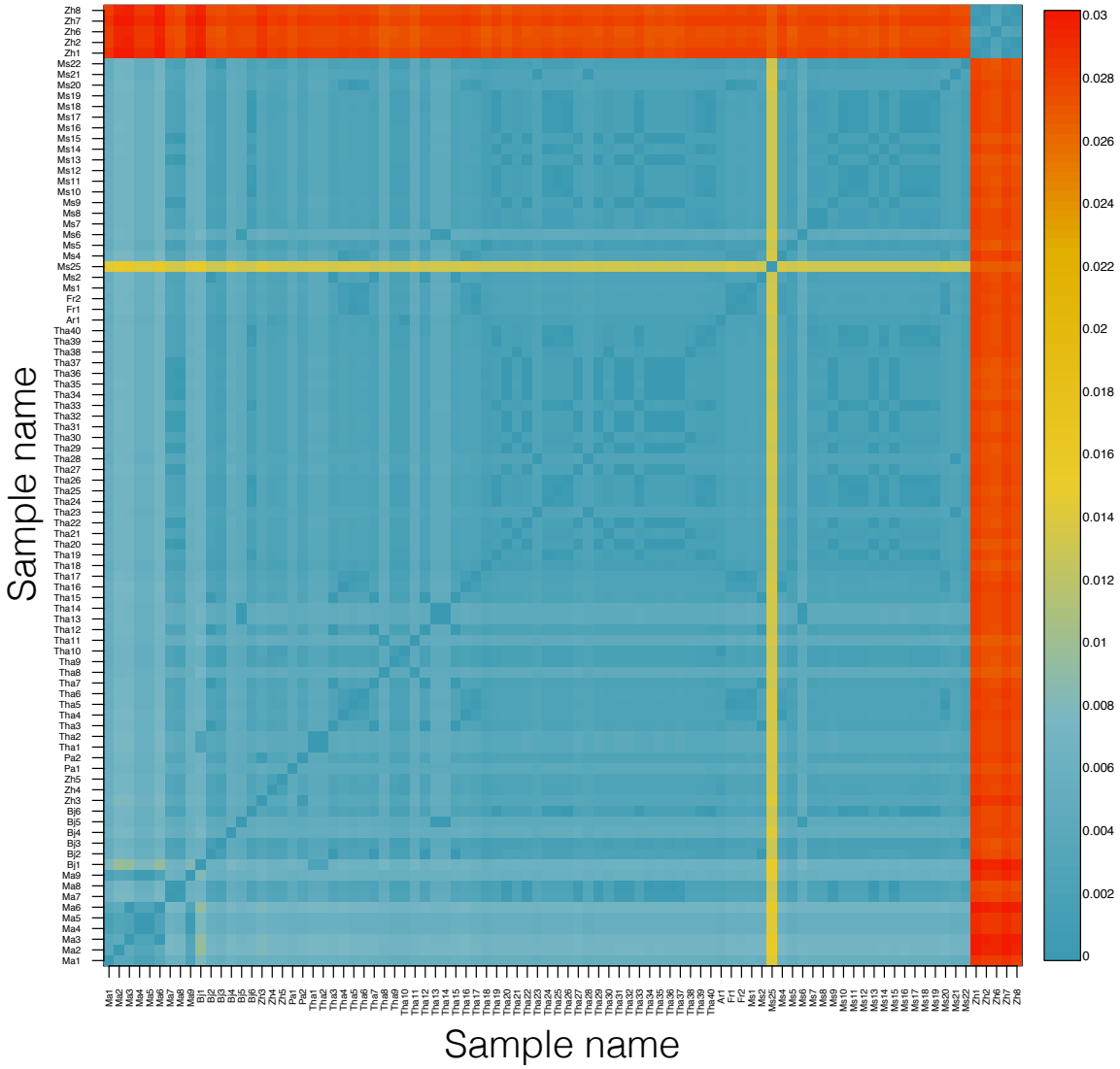

Fig. 3.S6: Pairwise genetic similarity (π), measured as proportion of sites that differ between pairs of samples. Values are colour coded, see colour bar on the right, with blue colours corresponding to small π and red colours corresponding to large π.

Fig. 3.S7: Neighbor-joining tree of all samples based on the pairwise genetic distance (π) matrix, measured as proportion of sites that differ between sequence pairs between samples, calculated using the Ape package in R. Modern northern Eurasian and North American wolves are represented with black labels. Ancient grey (age < 500 years) wolves are represented with blue labels. Modern Tibetan and Indian wolves are represented with red and yellow colours respectively.

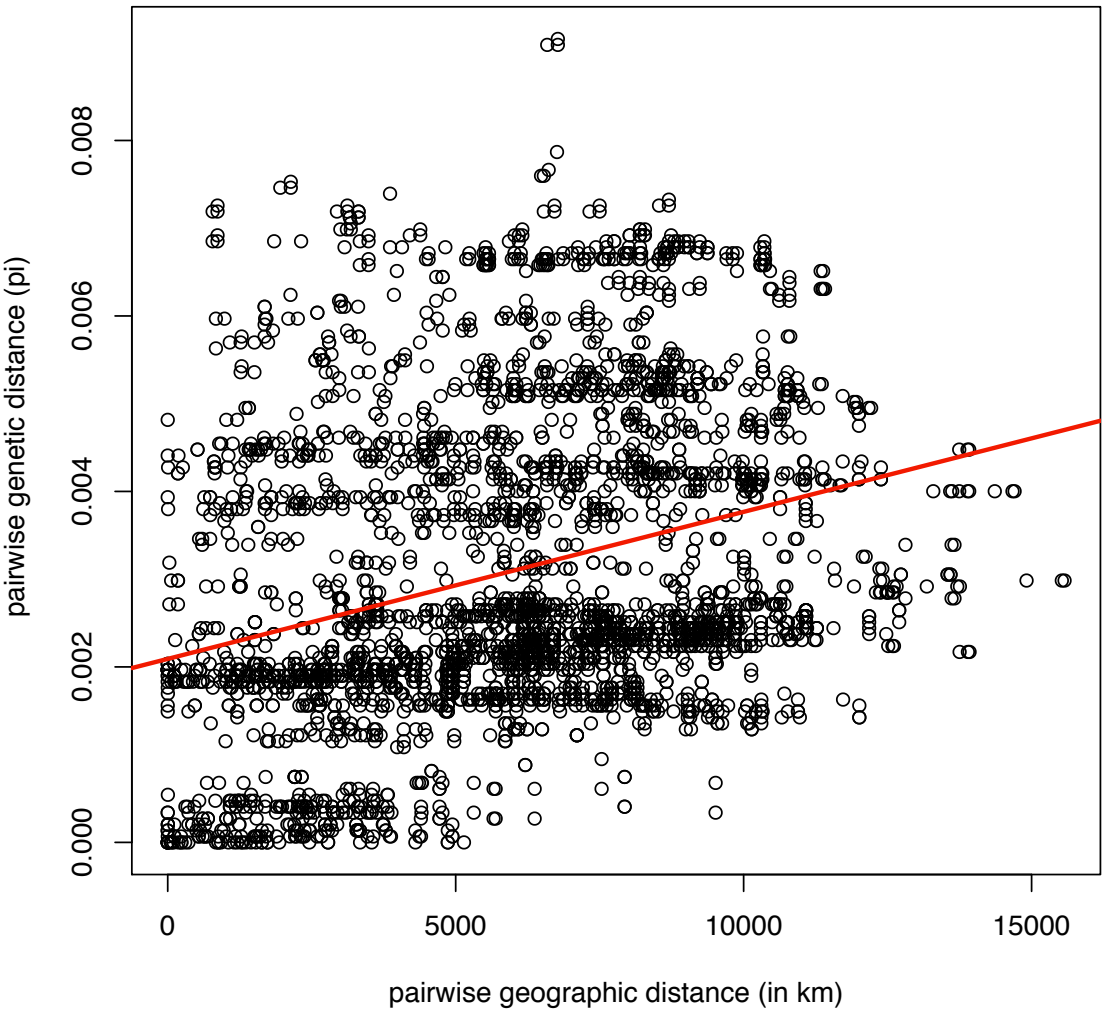

Fig. 3.S8: Pairwise geographic distances between all modern North Eurasian and North American wolf samples (N = 84) plotted against the pairwise genetic distances. □= 0.3 (Mantel $p < 0.0001$).

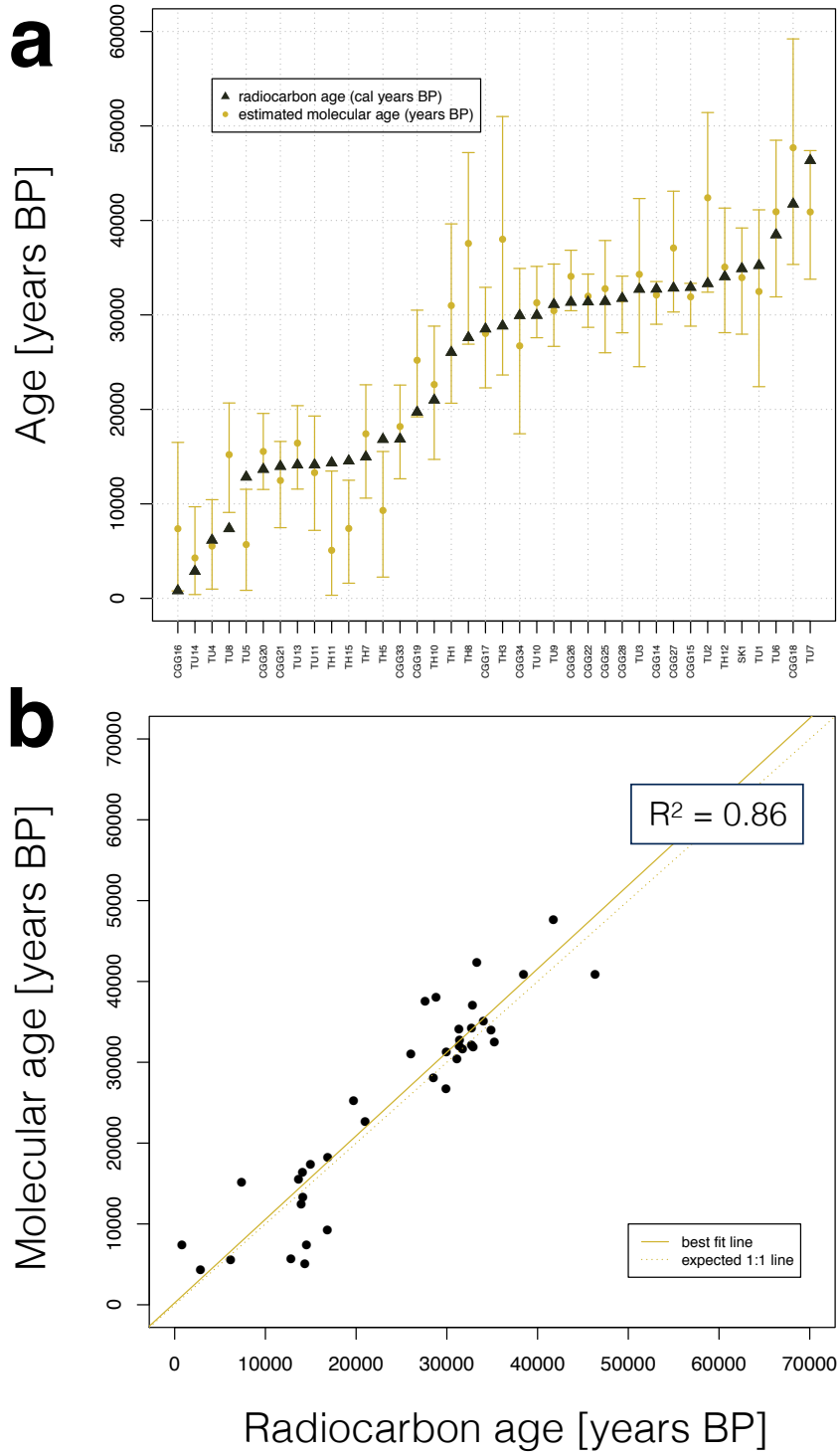

Fig. 3.S9: Validation of the molecular dating procedure. (A) Estimated molecular age distributions (yellow lines, yellow dot = median) from the leave-one-out analyses with BEAST and radiocarbon ages (black triangles) for each sample. (B) Linear fit (solid yellow line) between radiocarbon dates and esimated molecular dates from the leave-one-out analyses with BEAST. The dashed yellow line shows the 1:1 correspondence.

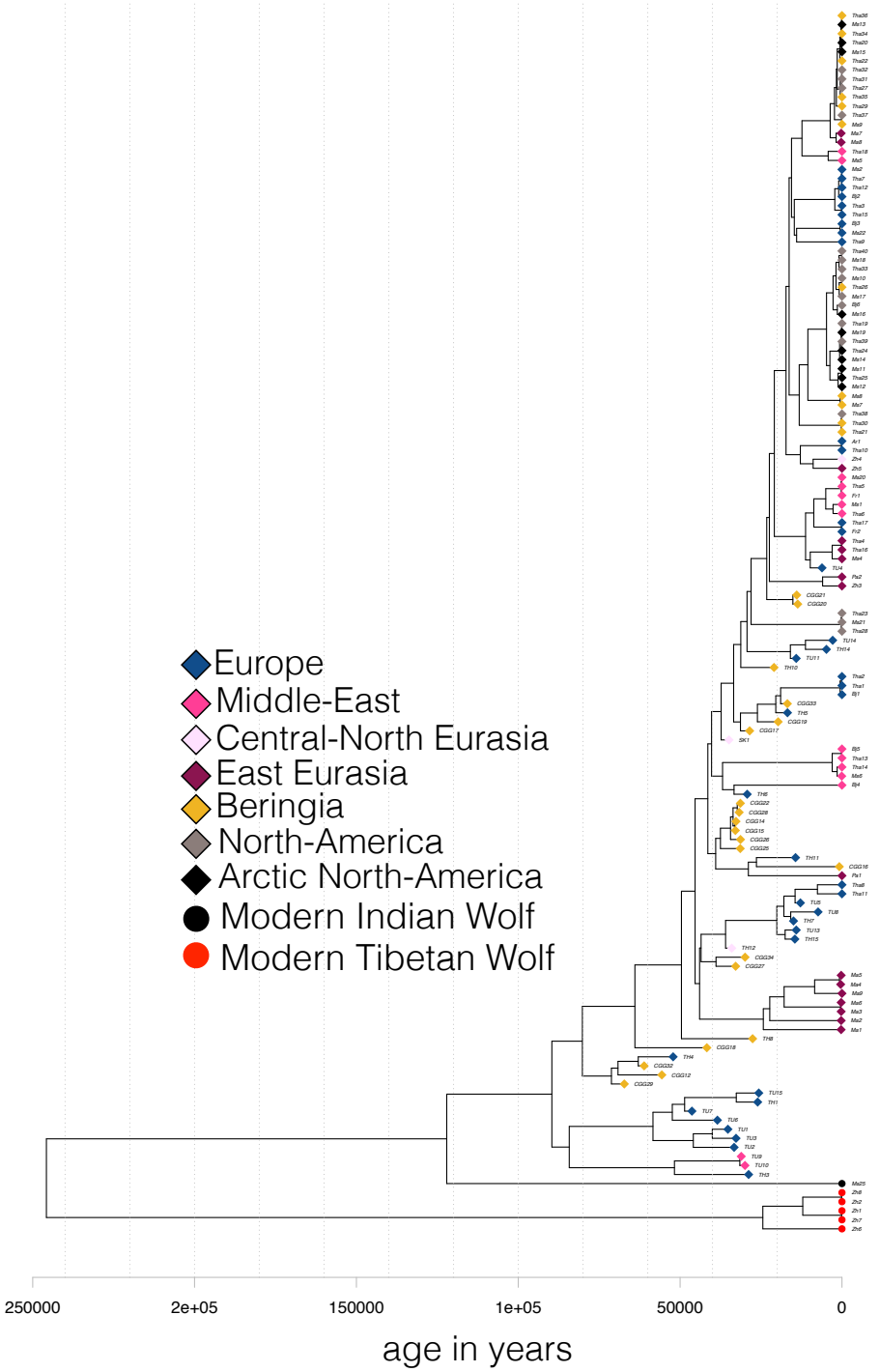

Fig. 3.S10: Tip calibrated BEAST tree of all 135 ancient and modern wolf sequences. Circles represent samples excluded from the demographic analyses (wolves from the Himalayas and the Indian subcontinent) and diamonds represent samples included in the demographic, colour coded by geographic regions (demes) used in the analyses.

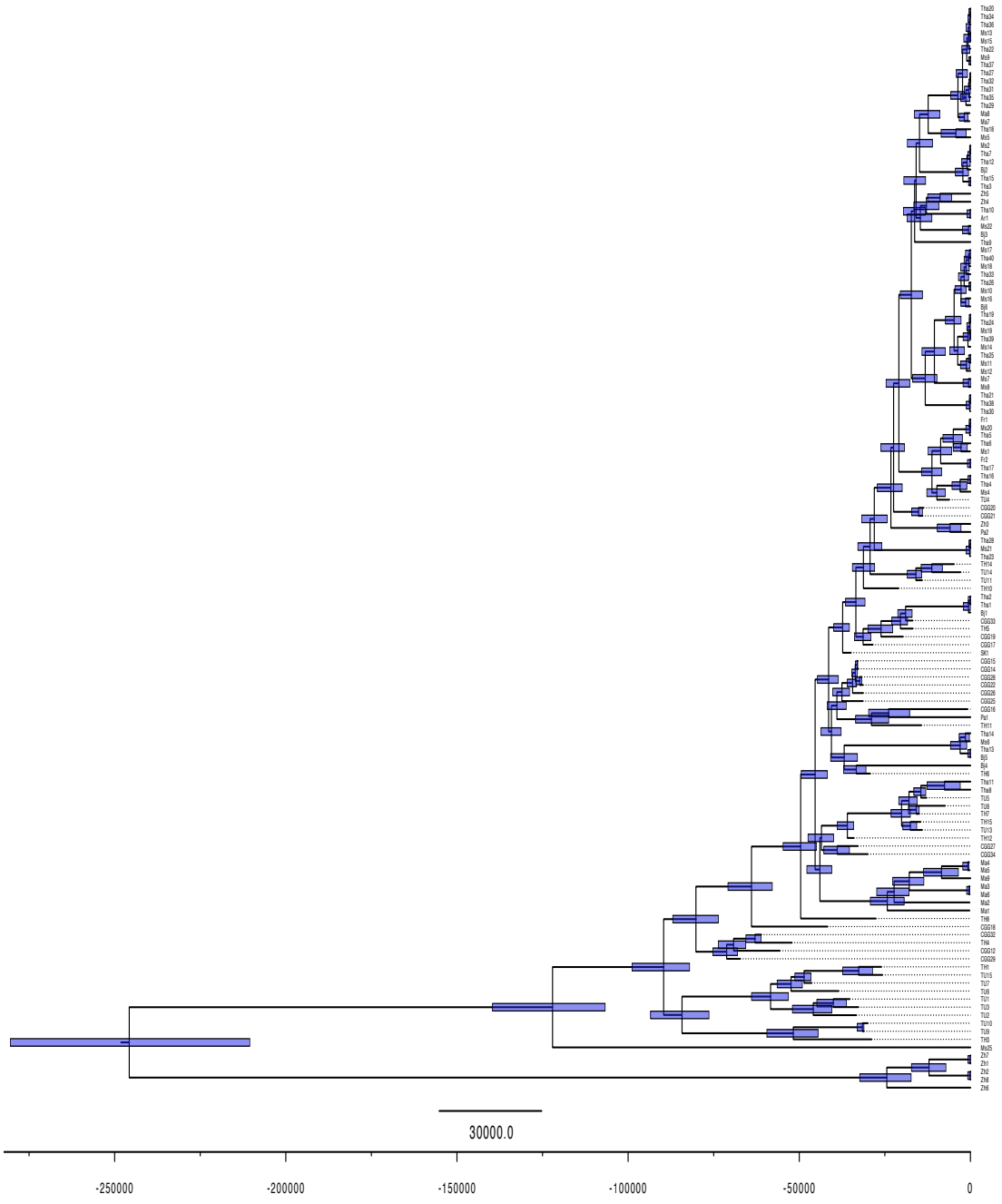

Fig. 3.S11: Tip calibrated BEAST tree of all 135 ancient and modern wolf sequences with 95% credibility intervals for all dated nodes indicated by the blue bars.

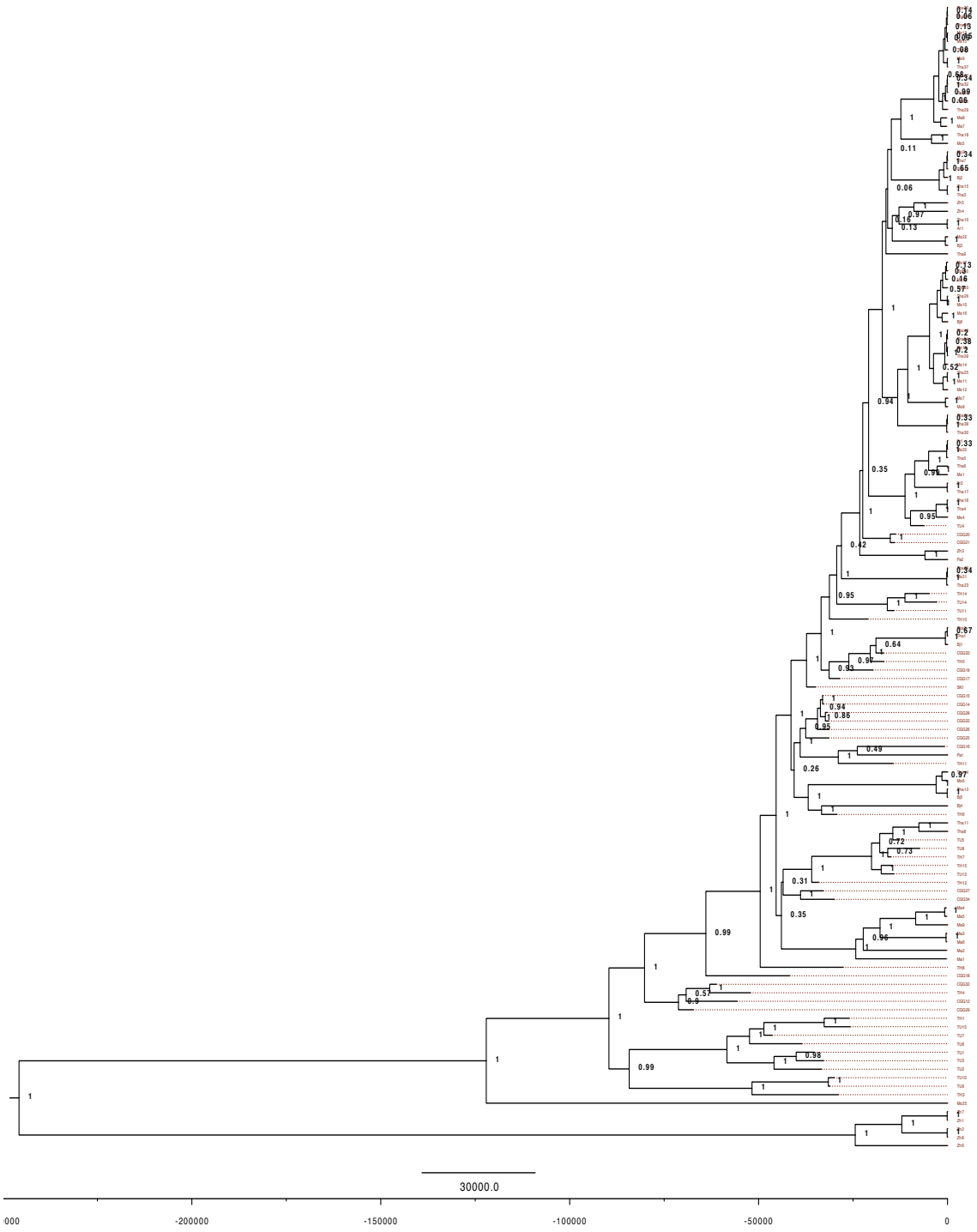

Fig. 3.S12: Tip calibrated BEAST tree of all 135 ancient and modern wolf sequences with support values depicted by each node of the tree.

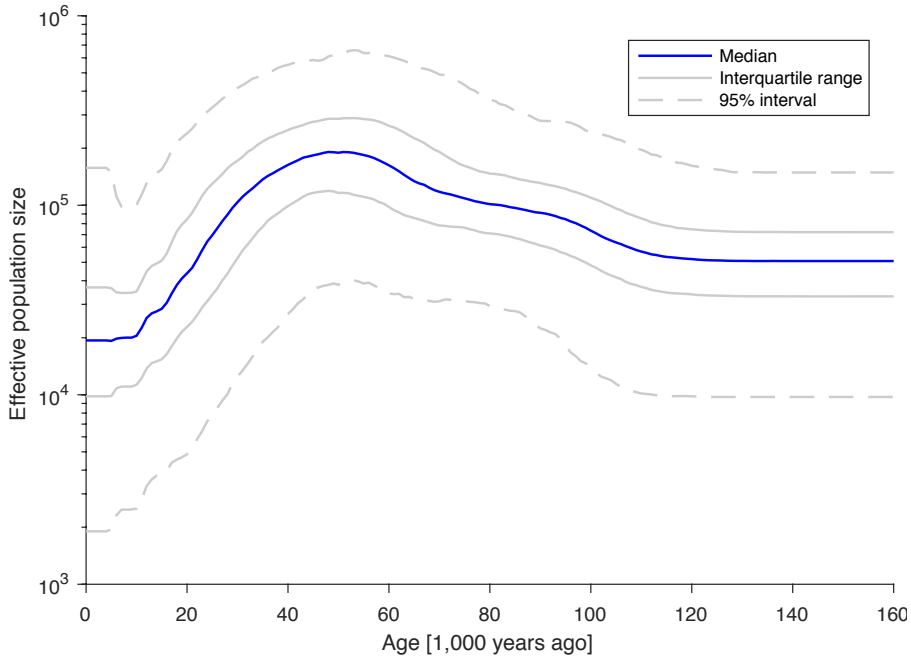

Fig. 3.S13: The effective population size through time from the BEAST analysis (Bayesian skyline plot). Solid blue line represents the median estimate and the grey lines represent the interquartile range (dashed line) and 95% intervals (solid line).

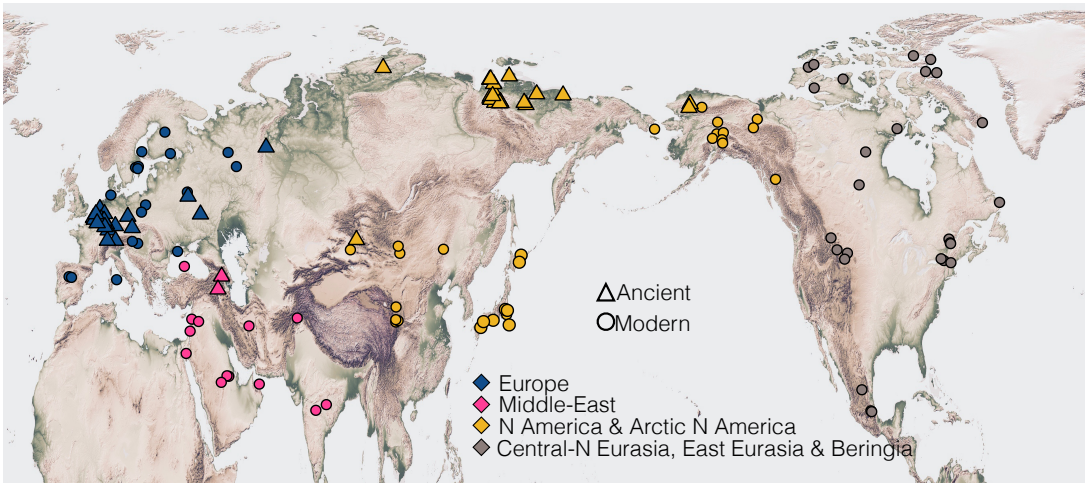

Fig. 3.S14: Geographic distribution of modern (circles) and ancient (triangles) samples, grouped by four super-demes used in the ABC analysis (colour coded).

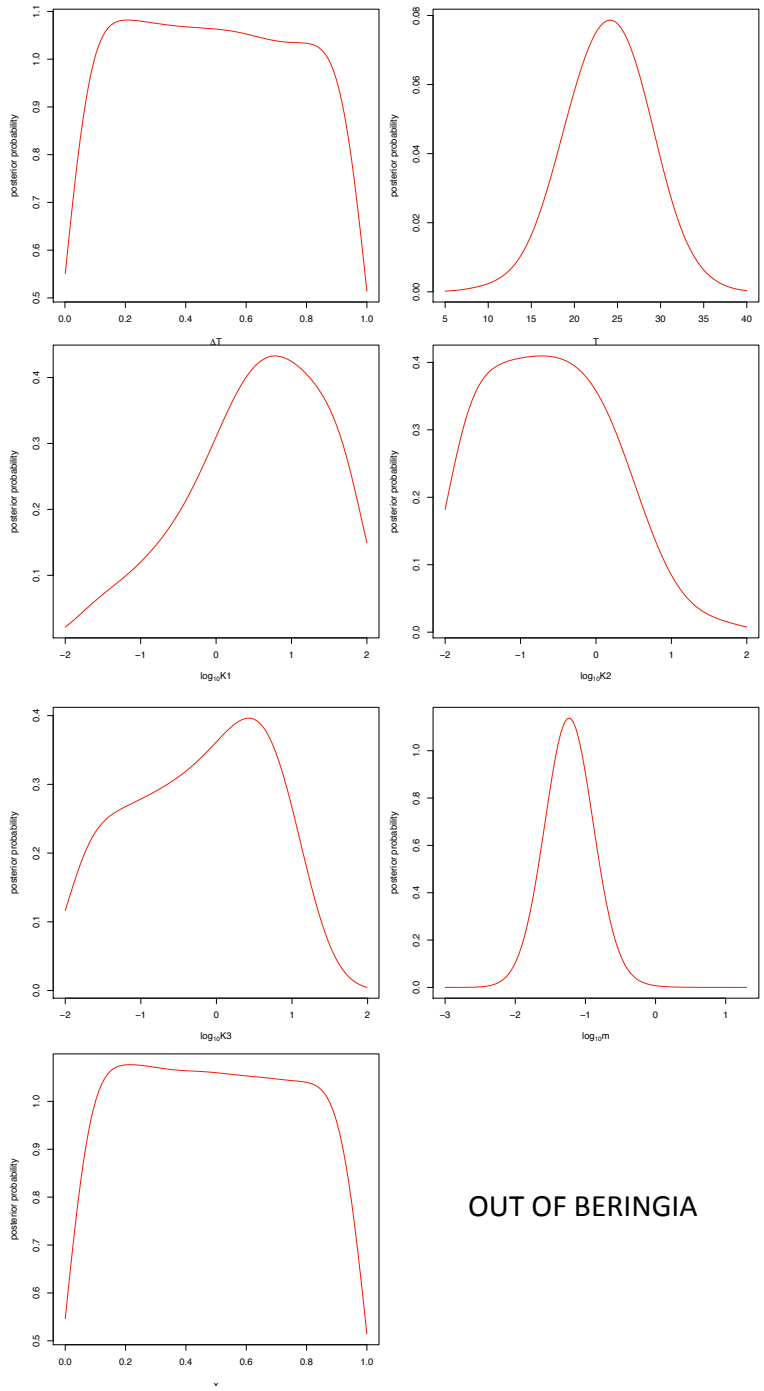

Fig. 3.S15: Posterior probability density distribution (on y-axis) for seven estimated parameters (ΔT, T, $\log_{10} K_1$, $\log_{10} K_2$, $\log_{10} K_3$, $\log_{10} m$, x) in the most likely model (Expansion out of Beringia with population size change).

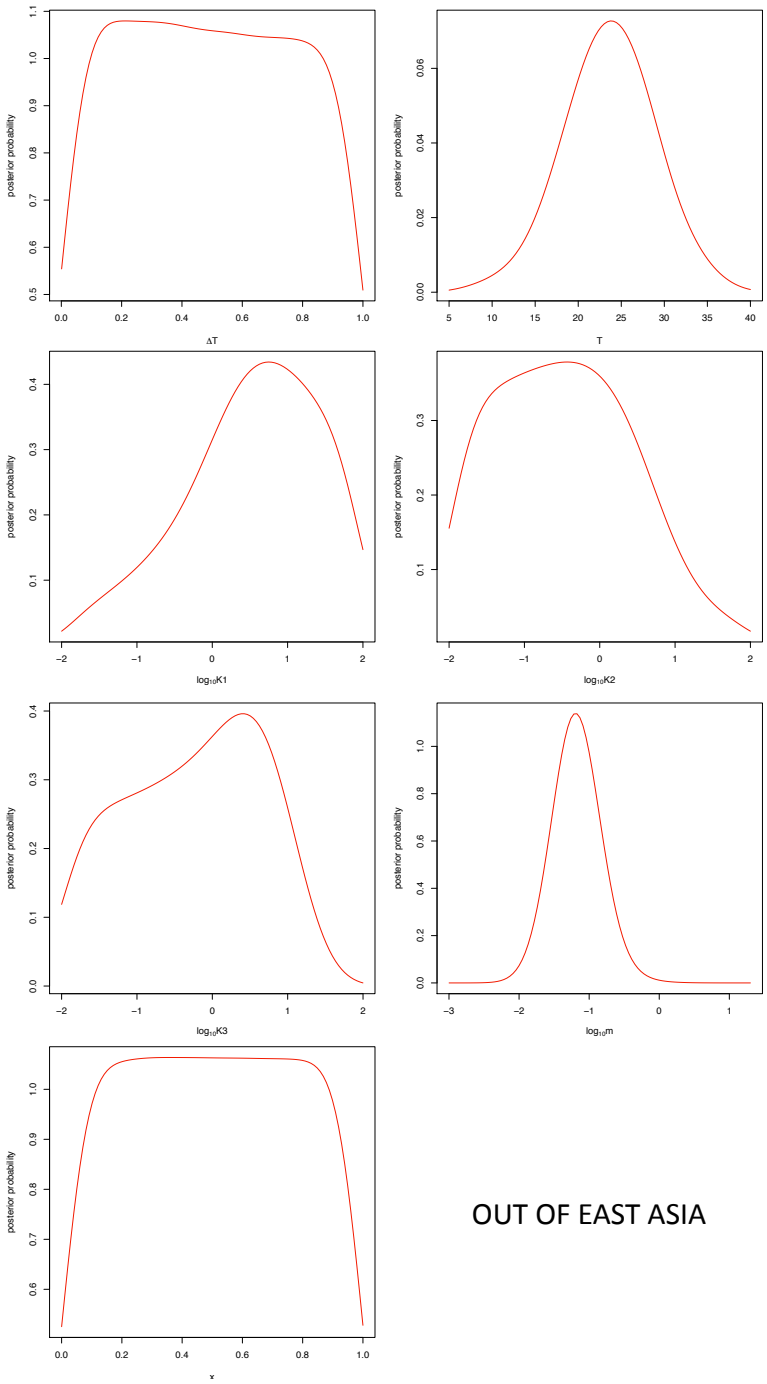

Fig. 3.S16: Posterior probability density distribution (on y-axis) for seven estimated parameters (ΔT, T, $\log_{10} K_1$, $\log_{10} K_2$, $\log_{10} K_3$, $\log_{10} m$, x) in the most likely model (Expansion out of East Eurasia with population size change) .

Chapter 4: Inferring allele frequency trajectories from ancient DNA indicates that selection on a chicken gene coincided with changes in medieval husbandry practices

This work was published in 2017 in the journal of Molecular Biology and Evolution 34(8):1981-1990

4.1 Annex to Chapter 4: Statement of my contribution

Original idea and design of research

I generated the idea behind the article and planned the research together with Professor G. Larson, Professor M.G. Thomas, and Dr A. Eriksson.

Statistical analysis

I curated the ancient and modern genetic and archaeological data. I calculated the chicken population size through time. I performed calculations for levels of past gene flow. I designed the statistical framework with Dr A. Eriksson. I implemented the statistical framework with input from Dr A. Eriksson. I performed the statistical analysis of the previously published and new (generated by my co-authors) data, various statistical analysis to test the sensitivity of the method and robustness of the results, and the statistical analysis of archaeological data. I interpreted the results of the statistical analysis with input from my co-authors.

Manuscript

I wrote the manuscript and generated all the tables and figures. I received input and comments from other co-authors to the manuscript.

4.2 List of authors and affiliations

Liisa Loog[1,2†], Mark G. Thomas[3], Ross Barnett[1], Richard Allen[1], Naomi Sykes[4], Ptolemaios D. Paxinos[5], Ophelie Lebrasseur[1], Keith Dobney[6,7], Joris Peters[5,8], Andrea Manica[2], Greger Larson[1*†], Anders Eriksson[9,2*†]

[†]Corresponding authors: L.L. (liisaloog@gmail.com), A.E. (anders.eriksson@kcl.ac.uk), G.L (greger.larson@arch.ox.ac.uk).

* These authors contributed equally

Affiliations

1. The Palaeogenomics and Bio-Archaeology Research Network, Research Laboratory for Archaeology, University of Oxford, Dyson Perrins Building, South Parks Road, Oxford OX1 3QY, UK
2. Department of Zoology, University of Cambridge, Downing Street, Cambridge CB2 3EJ, UK.
3. Research Department of Genetics, Evolution and Environment, University College London, Gower Street, London WC1E 6BT, UK.
4. 4Department of Archaeology, University of Nottingham, Nottingham, NG7 5RD, UK
5. Department of Veterinary Sciences, Institute of Palaeoanatomy, Domestication Research and the History of Veterinary Medicine, LMU Munich, Kaulbachstr. 37, D-80539 Munich, Germany
6. Department of Archaeology, School of Geosciences, University of Aberdeen, St. Mary's, Elphinstone Road, AB24 3UF, UK.
7. Department of Archaeology, Classics and Egyptology, University of Liverpool, 12-14 Abercromby Square, Liverpool L69 7WZ, UK.
8. Department of Archaeology, Simon Fraser University, Burnaby, B.C. V5A 1S6, 778-782-419, Canada
9. SNSB, Bavarian State Collection of Anthropology and Palaeoanatomy, Karolinenplatz 2a, D-80333 Munich, Germany
10. Department of Medical & Molecular Genetics, King's College London, Guys Hospital, London SE1 9RT, UK.

4.3 Abstract

Ancient DNA provides an opportunity to infer the drivers of natural selection by linking allele frequency changes to temporal shifts in environment or cultural practices. However, analyses have often been hampered by uneven sampling and uncertainties in sample dating, as well as being confounded by demographic processes. Here we present a Bayesian statistical framework for quantifying the timing and strength of selection using ancient DNA that explicitly addresses these challenges. We applied this method to time series data for two loci: *TSHR* and *BCDO2*, both hypothesised to have undergone strong and recent selection in domestic chickens. The derived variant in *TSHR*, associated with reduced aggression to conspecifics and faster onset of egg laying, shows strong selection beginning around 1,100 years ago, coincident with archaeological evidence for intensified chicken production and documented changes in egg and chicken consumption. To our knowledge, this is the first example of pre-industrial domesticate trait selection in response to a historically attested cultural shift in food preference. For *BCDO2*, we find support for selection, but demonstrate that the recent rise in allele frequency could also have been driven by gene flow from imported Asian chickens during more recent breed formations. Our findings highlight that traits found ubiquitously in modern domestic species may not necessarily have originated during the early stages of domestication. In addition our results demonstrate the importance of precise estimation of allele frequency trajectories through time for understanding the drivers of selection.

4.4 Introduction

A comprehensive understanding of the evolutionary responses to changing selection pressures can be achieved by reconstructing allele frequency trajectories through time and linking them to changes in the ecological context in which an organism has evolved. This association has typically only been possible in longitudinal genomic studies of laboratory organisms with relatively short generation times, whose environments can be easily and rapidly manipulated (Kawecki et al. 2012). Linking episodes of selection to their drivers in natural systems is more challenging. The most common approach has been to study large sets of modern genetic data from closely related species or sub-populations using various statistical approaches (e.g. genome wide scans for selection) (Storz 2005). However, these approaches typically lack the power to reliably estimate the timing and strength of selection, especially over short evolutionary time scales. Consequently, it is

challenging to associate past episodes of selection with specific drivers, especially when those drivers are not present in contemporary environments.

Ancient DNA data can provide direct information on changes in allele frequencies through time, and as such allows us to directly link past selection to contemporaneous ecological factors. However, ancient DNA sample sizes are typically small, and samples tend to be sparsely and unevenly distributed in space and time. Several methods exist for studying selection using ancient DNA (reviewed in Malaspinas 2016), but typically they lack the ability to model the confounding effects of gene flow – a process that could lead to over-estimation of selection coefficients (Mathieson et al. 2015). To overcome these challenges, we developed a Bayesian statistical framework that permits formal quantification of selection parameters using ancient allele frequency data, while explicitly taking into account both uncertainty in sample ages and gene flow from external sources, and apply this framework to genotype data from domestic chicken.

The domestication of chickens (*Gallus gallus domesticus*) from wild junglefowl took place over a relatively short evolutionary timeframe (Rubin et al. 2010). In addition, the genetic architectures underlying many of the phenotypic traits that distinguish domestic populations are well understood (Eriksson et al. 2008; Rubin et al. 2010). As such, chickens present an ideal opportunity to correlate the timing of allele frequencies shifts with changes in human imposed selective pressures over the past several thousand years. To do so, we focussed on two loci: thyroid-stimulating hormone receptor (*TSHR*) and β-carotene dioxygenase 2 (*BCDO2*), both previously identified as targets of selection in domesticated chickens (Rubin et al. 2010).

TSHR plays a role in growth, metabolic regulation and photoperiod control of reproduction in mammals and birds by stimulating the synthesis and release of thyroid hormones (Yoshimura et al. 2003; Hanon et al. 2008; Nakao et al. 2008; Follett 2015; Nishiwaki-Ohkawa and Yoshimura 2016). Modern chickens carry a derived recessive *TSHR* allele that is thought to cause loss of strict seasonal reproduction (Rubin et al. 2010) - a commonly observed difference between domesticated animals and their wild relatives (Belyaev 1979) - and has been shown to associate with faster onset of egg laying at sexual maturity (Karlsson et al. 2016). This allele has also been directly associated with reduced aggressive behaviors toward conspecifics and decreased fear of humans (Karlsson et al. 2015). It has, therefore, been suggested that these traits could have been selected to

increase egg yield and facilitate larger groups or higher bird densities in a domestic setting (Karlsson et al. 2015; Karlsson et al. 2016).

The *BCDO2* gene is expressed in the skin where it encodes an enzyme that cleaves colorful carotenoids into colorless apocarotenoids, and polymorphisms in the *BCDO2* gene have well-known effects on skin pigmentation in birds (Eriksson et al. 2008). Domestic chickens are known to possess both a dominant, ancestral *BCDO2* allele that results in white or grey skin, and a recessive derived allele that is associated with yellow skin (Eriksson et al. 2008) – the latter likely acquired by domestic chickens through admixture with grey jungle fowl (*Gallus sonneratii*) (Eriksson et al. 2008). The biological mechanism for selection at the *BCDO2* locus is less clear than for the *TSHR* locus, but it has been previously hypothesised that the yellow legs phenotype could have been used as a proxy for good nutritional status in chickens, or selected for purely cosmetic reasons (Eriksson et al. 2008).

Genome-wide comparison between domesticated chickens and their wild relatives provides a powerful method for identifying loci under selection since chickens were domesticated around 6,000 years ago (Peters et al. 2016). Given the ubiquity of the derived *TSHR* allele in modern domesticated chicken populations (Rubin et al. 2010), and its association with several hallmark domestication traits (Karlsson et al. 2015), it has been proposed that the derived *TSHR* allele was selected during the initial stages of the domestication process (Rubin et al. 2010; Karlsson et al. 2015). However, due to the low mutation and recombination rates in nuclear DNA, these studies lack the power to accurately estimate the timing and the strength of selection.

Flink et al. (2014) typed the *TSHR* and *BCDO2* loci in archaeological chicken samples from Europe, spanning the last 2,200 years, to further examine the hypothesis of selection during early domestication. They observed significantly lower derived allele frequencies in their ancient samples relative to the modern populations, which led them to reject the early selection hypotheses for both loci in favor of more recent selection. Given the sparseness and uneven temporal distribution of their data, they did not attempt to quantify the timing or strength of selection. A further complication to the analysis of selection comes from recent gene flow in domesticated chickens. During modern European chicken breed formation (beginning 100 – 150 years ago), Asian chickens were imported and bred with local European stock to improve existing birds and create novel breeds (Dana et al.

2011; Flink et al. 2014; Lyimo et al. 2015). In this study, we applied our statistical framework to the ancient DNA data reported by Flink et al. (Flink et al. 2014) and 16 additional samples (fig. 1 and Materials and Methods), and used forward simulations to test if genetic drift and gene flow, without invoking selection, could explain the observed allele frequency changes.

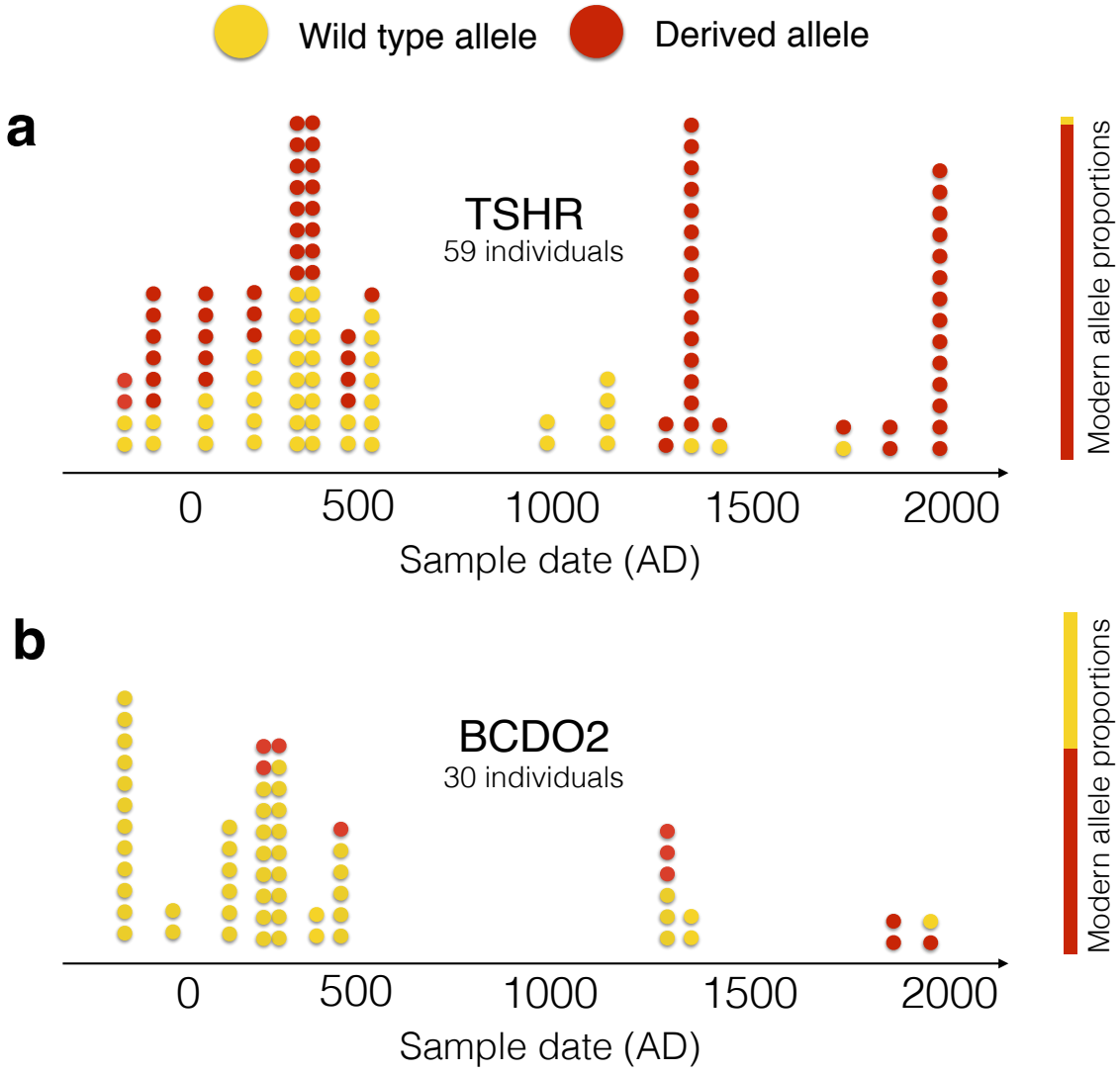

Fig. 4.1: Observed allele counts through time for the *TSHR* locus (a) and the *BCDO2* locus (b). Wild type alleles in ancient samples are represented by yellow dots and derived alleles by red dots. Modern allele proportions are shown as solid bars to the right of each panel.

4.5 New Approaches

4.5.1 A Bayesian framework to infer past episodic selection

We represented the European domesticated chickens as a randomly mating population (an assumption we test below) in which an allele is under selection, and that receives gene flow from an external source. To simplify the model, we assumed that the population size was large enough to ignore genetic drift on these time scales. This allowed us to treat allele frequency trajectories as deterministic, an assumption that we also tested. Combining the standard model for selection on a recessive trait with a term that corresponds to gene flow from an external population, we obtained a differential equation for the allele frequency trajectory of the selected allele,

$$\frac{df}{dt} = s(t)f^2(1-f) + m(t)(f_{\text{external}} - f), \qquad \text{(Eq. 4.1)}$$

where f is the frequency of the hypothesized selected alele, s is the selection coefficient, m is the rate of gene flow and f_{external} is the frequency of hypothesized selected allele in the external source population. The initial value for f(t) is the ancestral frequency ($f_{\text{ancestral}}$). The model has three additional parameters defining the starting time of selection ($t_{\text{selection}}$) and the beginning (g_{start}) and end (g_{end}) of gene flow from the external source. The selection coefficient s is constant after the starting time and is zero before. Similarly, m is constant in the gene flow interval and is zero at other times.

Using only the genotype information to estimate all seven parameters of the model would be challenging. However, because chickens are a relatively well-studied species, we were able to specify the values of four parameters by using historic information and mitochondrial DNA data, thus greatly reducing model search space. Gene flow from Asia is historically well-documented (Dana et al. 2011; Flink et al. 2014; Lyimo et al. 2015), beginning around 250 years ago ($g_{\text{start}} = 250$) and continuing until the present day ($g_{\text{end}} = 0$). The rate of gene flow m was estimated using modern and ancient mitochondrial haplotype frequencies, taking advantage of the fact that all ancient European chickens (i.e. prior to the gene flow from Asia) have the same mitochondrial haplotype (Materials and Methods). The frequency of the derived allele in the Asian population at the time of gene flow is currently unknown. To minimize the possibility of overestimating the role of selection in increasing the allele frequency over the effect of gene flow from Asia, we

made a conservative assumption that $f_{external} = 0.99$ (i.e. the selected allele is nearly fixed in Asian chickens).

The likelihood of the data is a function of the frequency curve of the selected allele in the population and is calculated as the product of the probabilities of all observed alleles:

$$L = \prod_i f(t_i)^{x_i}\left(1 - f(t_i)\right)^{1-x_i}. \quad \text{(Eq. 4.2)}$$

Here L is the likelihood of the data, $f(t)$ is the allele frequency at the time t, t_i is the age of the sample i, and $x_i = 1$ in case of observing the derived allele in sample i, and $x_i = 0$ when observing the wild type.

Eq. (4.2) assumes that sample ages are precisely known. However, archaeological samples often come with some age uncertainty. To account for this, we replace the likelihood of each genotype (each factor in Eq. 4.2) with its posterior likelihood given the distribution of sample age from archaeological dating (Materials and Methods).

4.6 Results

4.6.1 Timing and strength of selection, and past allele frequency trajectories for TSHR and BCDO2

The remaining parameters of the model – the starting time of selection ($t_{selection}$), the selection coefficient (s) and the ancestral frequency of the selected allele ($f_{ancestral}$) – were inferred by making a full parameter sweep where we calculated the deterministic allele frequency trajectory for each parameter combination. We then calculated the posterior probability density distribution for each parameter by numerically integrating the likelihood of the data over the remaining two parameters (assuming a uniform prior for starting time of selection, ancestral frequency, and the logarithm of the selection strength). In addition, to visualize the inferred allele frequency trajectories, we calculated the posterior distribution of allele frequency through time by weighting the allele frequency trajectory of each parameter combination (sampled from their prior distributions) by the likelihood of the data given the parameters.

For the *TSHR* locus, we estimated a selection coefficient of 0.0049 (95% CI: 0.0030-0.0069, fig. 4.S1), which would have generated a rapid increase in allele frequency (fig. 4.2a) starting 920 AD (95% CI: 290 AD – 1210 AD, fig. 4.S1). We also inferred that the frequency of the *TSHR* derived allele prior to selection in the ancestral chicken population

was 0.44 (95% CI: 0.34-0.54, fig. 4.S1), similar to that estimated in a red jungle fowl captive zoo population (frequency 0.35, 95% CI:0.22-0.50 (Rubin et al. 2010)).

For the *BCDO2* locus, we inferred a selection coefficient of 0.0036 (95% CI: 0.0001-0.0158, fig. 4.S2), similar in magnitude to that estimated for the *TSHR* locus. Despite supporting selection, the inferred allele frequency trajectories corresponding to the best fitting parameter combinations show only a very marginal increase in the *BCDO2* derived allele frequency prior to the time of gene flow (fig. 4.2b), therefore the observed rise in allele frequency can be largely attributed to recent Asian gene flow. This result is expected given the low inferred ancestral frequency of the derived allele ($f_{\text{ancestral}}$=0.14, 95% CI: 0.07–0.25, fig. 4.S2), as the efficacy of selection for a recessive adaptive allele is highly sensitive to its initial frequency. As a consequence of minimal increase in allele frequency prior to the period of Asian gene flow, the starting time of selection is poorly resolved in this analysis (fig. S2), and, therefore, has little effect on the allele frequency trajectory.

Analyses of selection usually focus on estimating the strength of selection, and on rejecting the null model of genetic drift as an explanation of the data (Malaspinas 2016). However, selection coefficients can be difficult to interpret as the inferred values do not necessary reflect the true rate of change in allele frequencies, especially for recessive alleles – we inferred similar selection coefficients for the *TSHR* and BCDO2 genes, but while the former shows a rapid increase in allele frequency, the latter results in only very marginal rate of change in allele frequencies. Thus, genotype data spanning an episode of selection, combined with statistical modeling, allow precise estimation of allele frequency trajectories though time (e.g. fig. 4.2). This in turn enables direct examination of both the timing as well as rate of adaptation, and greatly simplifies the biological interpretation of the effect of selection during the episode.

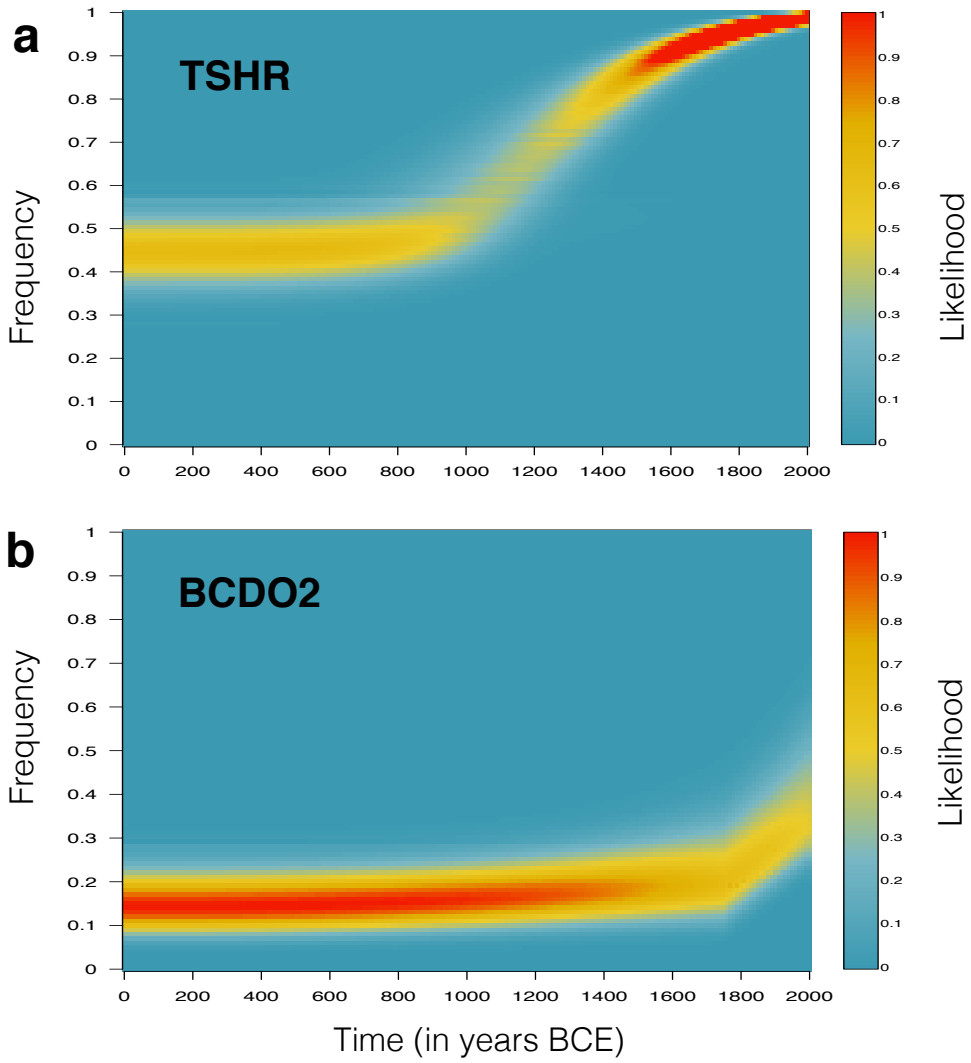

Fig. 4.2: Posterior distribution of the derived allele frequency as a function of time for the *TSHR* locus (a) and the BCDO2 locus (b). The likelihoods are color coded (see color bar) and are shown relative to the maximum likelihood in the plot.

4.6.2 Testing the confounding effect of genetic drift

To test if the observed data could be explained by purely demographic factors, such as the rate of genetic drift and recent Asian gene flow, we simulated 10,000 stochastic allele frequency trajectories under this model (Materials and Methods). We then estimated the proportion of likelihood values greater than or equal to the values from the deterministic model of selection and gene flow (for a formal significance test), as well as the average likelihood of the trajectories (for a formal likelihood ratio test). To minimize the possibility of underestimating the role of drift in increasing the allele frequency over that

of selection, we took a conservative approach and used BEAST (Drummond et al. 2012) to estimate the effective population size of the European chicken population based on mtDNA sequences from modern samples (Material and Methods). Since the male to female ratio in the ancient European chicken population is unknown, we assumed the size of the female effective population size as the effective populations size in our stochastic simulations.

For the *TSHR* locus, all of the stochastic trajectories from the drift model had a lower likelihood than the best fitting trajectory from the selection model. In addition, the formal likelihood ratio test estimates the selection model to be $3x10^{19}$ times more likely than the drift model. Consequently, the high frequency of the derived allele in the modern domesticated chicken populations cannot be explained by drift and gene flow alone, despite our conservative assumptions.

For the *BCDO2* derived allele, the best fitting selection model explains the data only marginally better than the drift model. Out of the 10,000 simulated allele frequency trajectories, 366 have a likelihood value as high or higher than the best fitting selection model, and the selection model is nine times more likely than the drift model. Thus, while it is possible to obtain the patterns observed in the ancient DNA under the drift model, it is rare and the selection model is still supported by the data.

Finally, to test the effect of gene flow on our ability to reject selection over genetic drift, we ran the deterministic and stochastic models without migration. As expected from the timing and strength of selection acting on the *TSHR* locus, removing gene flow from the stochastic model made little difference to our ability to reject the null-hypothesis of no selection ($p < 0.0001$). In contrast, selection for the *BCDO2* locus became highly significant ($s = 0.0060$, $p = 0.0005$) in models without migration, confirming that unaccounted gene flow can cause spurious effects in selection analyses.

4.6.3 Sensitivity analyses

As discussed in the introduction, sparseness of samples and geographic patterns could confound analysis of past selection. To assess whether geographic structure in the data could affect the analysis, we first applied a standard Hardy-Weinberg test to ancient samples predating the Medieval times, and fail to reject Hardy-Weinberg equilibrium for both *TSHR* (χ^2=0.057, p=0.81) and *BCDO2* (χ^2=0.20, p=0.66) (Materials and Methods).

This lack of structure is also consistent with the observation that European ancient chicken samples have the same mitochondrial haplotype (Flink et al. 2014). As an explicit test of spatial genetic and cultural differences across Europe, we restricted the data to locations from Northwest Europe and excluded samples from the Mediterranean region (Materials and Methods and fig. 4.S4). Analysis on this subset of the data yielded parameter ranges similar to the full dataset (table 4.S9), suggesting little or no effect of geographic structure on our estimates. The main difference between the two results is that the starting time and coefficient of selection are less well defined in the analyses with the restricted data compared to the analysis with the full dataset (tables 4.S9 and figs. 4.S5 and 4.S6). For *TSHR*, we also observed an increased uncertainty of inferred allele frequency trajectory between 1100 AD and 1600 AD (fig. 4.S7). This is mostly due to the fact that the analysis with the reduced dataset lacks most samples from this informative time period. However, the increase in allele frequency in the 10th century AD is still best supported, and we can confidently rule out a significant rise in allele frequency prior to 900AD due to the large number of samples predating the period (fig. 4.S7).

To explore the effect of sparseness of ancient samples, we picked a parameter combination similar to the best supported scenario for *TSHR*, simulated 50 replicate datasets with sample sizes ranging from 10 to 200 diploid individuals (Materials and Methods), and repeated the analysis for each dataset. Fig. 4.S8 shows the confidence intervals for the three estimated parameters in each dataset. As expected, we observe a trend of increasingly wide confidence intervals with decreasing sample size. However, the medians of the posterior distributions are scattered near the true value, indicating little or no bias in estimating the parameters even for relatively small number of sample sizes.

As illustrated above, a large sample size is important for accurate reconstruction of past selection, but more fundamentally, it is important that the samples used in the analysis represents the underlying allele frequency curve, i.e. to have data before, during and after the change in allele frequency due to selection. Nevertheless, as also demonstrated in the analyses above, temporal clustering of the data does not necessarily cause biased estimates but will instead result in a wider range of parameter combinations as plausible explanations for the data.

4.6.4 Selection at the TSHR locus coincides with medieval changes in chicken husbandry

Our analysis indicates that selection on the *TSHR* derived allele began around 920 AD (290 – 1210 AD at 95% level). Intriguingly, this period coincides with major changes in chicken husbandry witnessed in several archaeological assemblages across Northwestern Europe (Boessneck et al. 1979; Heinrich 1987; Pieper and Reichstein 1995; Heinrich 2006; Hüster Plogmann 2006; Serjeantson 2006; Sykes 2007; Holmes 2014). Analyses of data from 184 English archaeological faunal assemblages and 104 German archaeological faunal assemblages demonstrate a substantial increase in the frequency of chicken remains from the Early to the High Middle Ages (fig. 4.3 and Materials and Methods) and higher proportions of adult hens in the flocks, presumably to increase egg production (Serjeantson 2006; Sykes 2007; Holmes 2014).

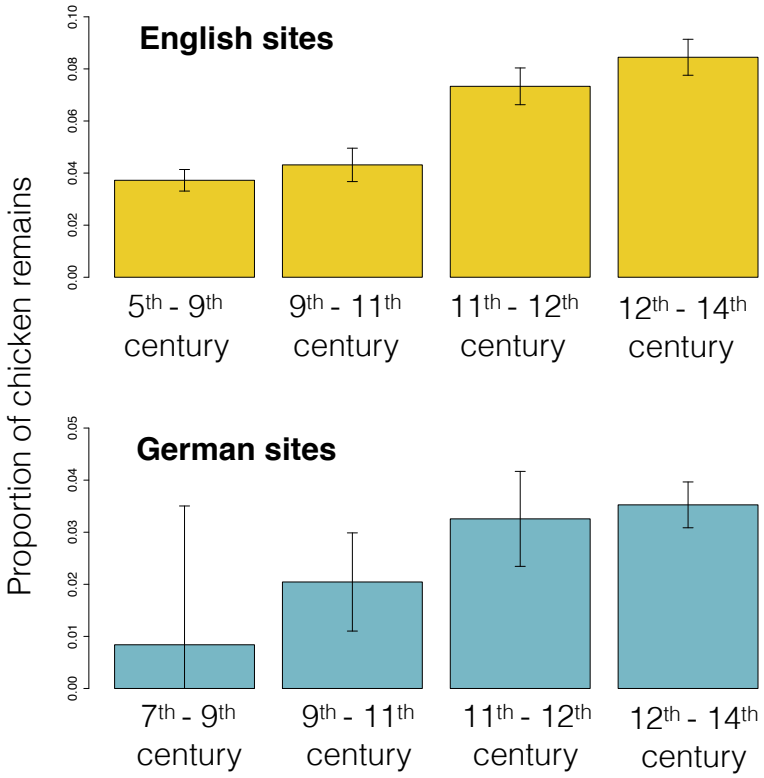

Fig. 4.3: Proportion of chicken remains (by number of identified specimens) from 184 English (top) and 104 German (bottom) archaeofaunal assemblages (Material and Methods)

4.7 Discussion

This study demonstrates how inferring allele frequency trajectories through time, using ancient DNA in a flexible Bayesian inference framework, has numerous advantages over previous approaches to studying selection. Firstly, our method provides a means of formally accommodating small sample sizes, uneven temporal distribution of samples and uncertainties in sample ages. Secondly, it allows for episodic selection and gene flow to be explicitly modeled, thus enabling formal integration of independent lines of evidence related to migration, admixture rates, past population sizes and the expression of alleles (dominant or recessive), all of which significantly enhance inferential power. Thirdly, the deterministic nature of our inference approach renders the method fast, flexible, and capable of handling any genotype or allele frequency data from samples before, during and after the hypothesized period of selection. Additionally, as demonstrated by our sensitivity analyses, the approach can also be used to (iteratively) identify the most informative time periods for selection analysis (the periods with the largest uncertainty in the reconstruction of the allele trajectory), and thereby be used as a tool for selecting samples for genetic sequencing.

Although determining the causal factors behind the inferred selection on the *TSHR* locus is beyond the scope of this paper, by combining ancient DNA with statistical modeling we can increase our ability to identify specific ecological or socio-cultural drivers behind selection. Rather than relying purely on knowledge of the biological function of genes to infer causes of selection, our method allows to also include factors such as known climatic or socio-cultural developments inferred, from geological, archeological or historical records that are broadly contemporaneous with the time of inferred allele frequency changes.

For example, our inferred timing of the onset of selection on the *TSHR* derived allele brackets a key period of changes in dietary preferences and chicken husbandry practices across northwestern Europe between the 9th and 12th centuries AD (fig. 4.3). The significant intensification of chicken and egg production, evident in the Medieval European archaeological record, has been linked to Christian fasting practices which forbade the consumption of meat from four-legged animals during fasting periods, but allowed for the consumption of birds, eggs and fish (Venarde 2011). These rules, which originated in the Benedictine Monastic Order, became widely adopted across Europe due

to increasing political influence of the Catholic church and applied to all segments of society ca. 1000 AD (Sykes 2007). An increase in chicken consumption has also been observed in Viking sites in present-day Scandinavia and Northern Germany (Boessneck et al. 1979; Pieper and Reichstein 1995; Hüster Plogmann 2006), coinciding with Christianization of these areas (starting in the late 10^{th}-11^{th} and the mid-9^{th} centuries AD respectively) (Näsman 1976; Sanmark 2004).

Religiously inspired dietary preferences are not the only factors potentially affecting medieval poultry consumption. The observed increase in chicken production could also have been driven by urbanization and population growth (Bartlett 1994), facilitated by the widespread introduction of the more efficient agricultural practices including the three-field system with crop rotation and new tools such as the heavy plough (White 1967; Andersen et al. 2016) as well as favorable climatic conditions (Mann et al. 2009) in the High Middle Ages. Although heavily reliant on the agricultural land surrounding the towns and the cities (Keene 1995), the urban population likely secured some of its own needs by keeping single animals such as goats, pigs and small flocks of chickens in the domestic space in order to have predictable access to milk, eggs and occasionally meat. These factors could, individually or in combination, explain the observed medieval increase in poultry consumption, which would most likely have resulted in intensified production of poultry. This could have been achieved either through increasing chicken flock sizes or (in an urban setting) flock densities, which could have been facilitated by selection on reduced aggression within the flocks (Karlsson et al. 2015) or faster onset of egg laying at sexual maturity (Karlsson et al. 2016), both demonstrated effects of the derived *TSHR* allele.

For *BCDO2* we also find some support of selection. However, our analysis suggests that the significant rise in allele frequency between ancient and modern non-commercial chicken breeds can be attributed to recent gene flow from Asia. It is also possible that the commercial chicken lines (excluded from this study) have experienced additional strong selection at the *BCDO2* locus. This is supported by observation that the frequency of the derived *BCDO2* allele is much higher in commercial chicken lines compared to the local chicken breeds used in this study (Rubin et al. 2010).

To our knowledge, the spread of the *TSHR* derived allele is the first example of a pre-industrial domesticate trait selection in response to a historically attested cultural shift in

food preference. This result supports the view (Allaby et al. 2008) that domestication is an ongoing process where numerous traits that have been traditionally associated with domestication underwent selection long after the initial domestication phases, and that domestic populations have experienced highly variable selective regimes in response to shifting cultural preferences. More generally, humans and their domestic plants and animals have undergone radical shifts in allele frequencies as they have each responded to alterations in natural and artificial selective pressures over the past 15,000 years. The ability to infer allele frequency trajectories and the timing and strength of selection episodes, based upon time-stamped genetic data, allows for those episodes to be correlated with specific ecological and cultural drivers, especially for drivers that are not present in contemporary populations. This in turn can reveal both the processes and causative mechanisms responsible for generating the patterns of genomic variation in humans and their co-dependent domestic plants and animals found today.

4.8 Materials and Methods

4.8.1 Ancient genotypes

We use genotype data from two loci, *TSHR* (position 43,250,347 on chromosome 5) and *BCDO2* (position 6,273,428 on chromosome 24), both argued to have undergone selection in domestic chickens. The two loci are typed, respectively, in 59 and 30 non-modern West Eurasian and Moroccan chickens, temporally raging approximately from 2,200 years ago to present day. The genotypes of ancient West Eurasian individuals as well as their approximate ages are taken from Flink et al. (2014). We increased the size of dataset for both *TSHR* and *BCDO2* locus by 14 and 4 individuals respectively. These additional samples were genotyped using the same protocol as reported in Flink et al. (2014) (Supplementary Information for details). Six ancient samples (four samples out of the 14 samples newly presented in this study) were directly radiocarbon dated (table 4.S7). The rest of the samples were dated by stratigraphic association. In order to minimize the possibility of intrusion from more recent periods all indirectly dated samples originate from sites with no following occupational layers (e.g. no building structures or archaeological strata). See table 4.S2 and 4.S3 for list of all samples used in the analyses, as well as their genotypes at the two loci and ages, for *TSHR* and *BCDO2* respectively.

4.8.2 Modern allele frequencies

The modern allele frequencies for *TSHR* locus is calculated from the total frequency of selected allele in sampled 167 non-industrial European chickens, representing 24 breeds. Data presented in (Rubin et al. 2010) (see table 4.S4 for breeds included and the *TSHR* allele frequencies in those breeds).

As the allele frequencies at the *BCDO2* locus in modern populations are unknown we use the phenotypes of 18 modern non-industrial European chicken breeds, reported in European collaboration project on chicken biodiversity database (AVIANDIV: http://w3.tzv.fal.de/aviandiv, accessed on 1 November 2015) (table 4.S5) for breeds included, typical phenotypes and estimated average population sizes). As the hypothesized selected *BCDO2* allele is recessive, the birds from breeds reported to be yellow legged were considered to carry two copies of the selected allele. For birds from breeds reported to be predominantly white legged the frequency of the proposed selected allele was assumed to be 0.016, based on the estimates of frequency in the white legged European breeds in (Eriksson et al. 2008) (see table 4.S6 for the breeds included) and assuming Hardy-Weinberg equilibrium.

To factor in the uncertainty rising from the fact that the *BCDO2* allele counts are not independent observations but estimates themselves, we used bootstrapping at the level of breeds to estimate the uncertainty in the population wide frequency. We then approximate this distribution with a binomial distribution by fitting the mean and the variance of the binomial distribution to the bootstrapped distribution, yielding an effective sample size of 18.4 individuals. This approximation allows us to give the estimate an equal weight to the ancient samples when calculating the likelihoods in the model.

4.8.3 Fixed parameters

Timing of gene flow from Asia

The starting time of gene flow from Asia is historically well documented (Dana et al. 2011; Flink et al. 2014; Lyimo et al. 2015) and as a result, is fixed to start at 250 years ago and lasts until the present.

Rate of gene flow from Asia

The rate of gene flow was estimated using modern and ancient mitochondrial haplogroup frequencies: Based on all samples currently available, all European chickens prior to

historically documented gene flow from Asia belonged to mitochondrial haplogroup E (Flink et al. 2014). Today 90% of European chickens belong to haplogroup E while the rest are assigned to haplogroups A, B and C. Haplogroup E is also most common among Asian chicken populations, however only 30% of the sampled Asian Chickens belong to this haplogroup. Assuming that the change in the frequency of haplogroup E is the direct result of gene flow from Asia and that this gene flow has not been sex biased, we can estimate that approximately 15% of the modern European chickens have Asian origin. As a result, the rate of gene flow per year in the model is assumed to be equal to the proportion of European chickens with Asian ancestry (15%) divided by the length of the admixture period (250 years).

Allele frequencies in the source population

The frequency of the selected allele in the Asian population at the time of the gene flow is unknown. Therefore we used a conservative estimate of ($f_{external} = 1$) i.e. the selected allele is fixed in Asian chickens. We chose this conservative approach to minimize the possibility of overestimating the role of selection at increasing the allele frequency over the effect of gene flow from Asia. As a result, lower frequency in Asian population during the period of the gene flow could result in later estimates of the starting times of selection and higher estimates of selection coefficients in the two loci considered. However, for *TSHR* we observe that selection brings the frequency to near fixation before the onset of gene flow, and therefore the precise frequency of the derived allele in Asia is not very important for the allele frequency trajectory. For *BCDO2*, a lower frequency of the derived allele in Asia could lead to slightly higher levels of selection.

4.8.4 Model fitting

In order to infer starting time of selection, selection coefficient and ancestral frequency of a selected allele, we perform a full sweep of those parameters and calculate the deterministic allele frequency trajectory for each parameter combination. The deterministic allele frequency curves were calculated using *lsoda* function in R package *deSolve* (Soetaert et al.).

Value ranges considered for estimated parameters

Parameter values considered for starting time of selection are between 0 to 2000 years ago in uniformly spaced steps of ten years. For the selection coefficient, we considered 100 uniformly spaced points between 10^{-4} and 1 on a log scale. Parameter values

considered for ancestral frequency of a selected allele ranged from 0.01 to 1 in 100 steps. We derive the marginal likelihoods for each of the parameters (starting time of selection, selection coefficient and the starting time of selection) by averaging over the likelihoods of the remaining two parameters.

Incorporating sample age uncertainty

Following the Bayesian principle, we treat the age of each sample as a random variable with uniform distribution over its age range (see tables 4.S2 and 4.S3 for age ranges), and calculate the posterior likelihood of the sample data given this distribution (numerically approximating the continuous distribution within each interval by ten equally spaced time points)

4.8.5 Test of significance

Stochastic Simulations

In the model described above the change in the allele frequency is assumed to be a result of selection and gene flow, and that the effective population size is large enough to ignore genetic drift. To test if selection is needed to explain the change in the allele frequency through time we explicitly test whether the selection models are statistically different from models including drift and gene flow alone. We do this by simulating allele frequency trajectories with drift, under the assumption of no selection but the same gene flow parameter values as in the deterministic allele frequency trajectories above.

We use the *sde.sim* function in the R package *sde* (Iacus 2008) to simulate 10,000 allele frequency trajectories using the stochastic differential equation corresponding to Eq. 4.1 without selection and including genetic drift in a population of size N_e:

$$\frac{df}{dt} = m(t)(f_{\text{external}} - f) + \sqrt{f(1-f)/2N_e}\xi(t), \qquad \text{(Eq. 4.3)}$$

To match the selection model described above, ancestral allele frequency is sampled from a uniform distribution over the interval [0,1]. The population size N_e is sampled from the posterior distribution of population size estimates from BEAST (Drummond et al. 2012) (see below), with a median value of 1.8×10^5 and 95% HPD interval ranging from 26000 to 4.6×10^5. Since this population size estimate is based on a non-recombining and maternally inherited locus, the total effective population size should be four times that. However, as male to female ratio in ancient European chicken population is unknown,

we take a conservative approach and use the minimum effective population size, which roughly corresponds to the size of the female effective population size. Therefore, we multiply the posterior distribution of population size by factor of two to get an estimate of a minimum effective population size. This approach is conservative since the power of genetic drift to influence allele frequencies decreases with increasing population size. To formally evaluate whether the model with selection provides a significantly better fit for the data we calculate the proportion of log likelihood values from the stochastic simulations that are as high or higher than the log likelihood of the selection model.

Chicken population size estimation using BEAST

We estimated an order of magnitude effective population size for chickens through time using Bayesian Phylogenetic tool BEAST (Drummond et al. 2012) and a 200 base pairs long mitochondrial control region fragment from 194 modern European chickens and 39 ancient European individuals with known ages and a uniform prior for constant population size ranging [0, 10^{-7}], (the full BEAST input file is too large to be included in the printed version of this thesis, but is available upon request from L. Loog).

4.8.6 Sensitivity analyses

Hardy-Weinberg analysis

We selected samples dating to before 300AD to test for deviation from Hardy-Weinberg equilibrium. Due to the large sample size (n=37 for *TSHR* and n=24 for *BCDO2*) we used the standard χ^2 test (with one degree of freedom) to investigate whether the genotype frequencies are binomially distributed.

North-Western subset of the data (sensitivity to potential geographic structure)

We generated a reduced data set covering North-West Europe by excluding ancient samples from Turkey, Greece and Morocco, resulting in 42 ancient samples for *TSHR* locus and 30 ancient samples for *BCDO2* locus (fig. 4.S4) for the temporal distribution of these samples). For consistency, all data points from Italy and Spain (*BCDO2*) and Italy and Israel (*TSHR*) were also excluded from the calculation of modern allele frequencies (but this did not affect the modern frequencies).

Simulated data (sensitivity to sample size)

We chose a combination of parameters similar to that found for *TSHR* (starting time of selection=1000AD, selection coefficient=0.005 and ancestral frequency=0.4). For

simplicity, we assume no gene flow from Asia ($m = 0$). We simulated 10 replicate data sets each of 10, 20, 50, 100 and 200 ancient diploid samples (and 150 modern samples). Simulated ancient samples were given randomly chosen dates (uniformly distributed from year 0 to 2000AD) and 100 years age uncertainty (on both sides of the assigned age). For each individual we generated random diploid genotypes according to the derived allele frequency given by the model at the sample age.

4.8.7 Archaeological chicken remains frequency calculation

We used data from Appendix Ia in Sykes (2007) on the faunal number of identified specimens (NISP) from 184 English archaeological faunal assemblages and compiled information (table 4.S10) on faunal NISP from 104 German archaeological faunal assemblages to estimate the relative frequency of chicken remains at each of the four time periods for English and German sites respectively. We calculated the relative frequency by dividing the number of identified chicken specimens by the total faunal NISP for the same time period (fig. 4.3 and table 4.S1) The 95% confidence intervals were calculated using the normal distribution approximation (justified by the large sample sizes).

The framework described above is implemented in the statistical environment R. The R code is available to download from GitHub (https://github.com/LiisaLoog/Selection-Framework) and from L.L upon request.

4.9 Acknowledgements

The authors are grateful to Brian Follett for his comments on the biological functions of the *TSHR* gene. L.L., R.A., K.D. & G.L. were supported by Natural Environment Research Council, UK (grant numbers NE/K005243/1, NE/K003259/1). M.G.T. was supported by Wellcome Trust Senior Investigator Award (grant number 100719/Z/12/Z) and Leverhulme Trust (grant number RP2011-R-045). A.M. & A.E. were supported by the European Research Council Consolidator grant (grant number 647787-LocalAdaptation). R.A., N.S. & G.L. were supported by Arts and Humanities Research Council (grant number AH/L006979/1). R.A. & G.L. were supported by European Research Council (grant number ERC-2013-StG 337574-UNDEAD).

4.10 References

Allaby RG, Fuller DQ, Brown TA. 2008. The genetic expectations of a protracted model for the origins of domesticated crops. Proc. Natl. Acad. Sci. 105:13982–13986.

Andersen TB, Jensen PS, Skovsgaard CV. 2016. The heavy plow and the agricultural revolution in Medieval Europe. J. Dev. Econ. 118:133–149.

Bartlett R. 1994. The Making of Europe: Conquest, Colonization and Cultural Change 950 - 1350. Penguin UK

Belyaev DK. 1979. Destabilizing selection as a factor in domestication. J. Hered. 70:301–308.

Boessneck J, Driesch A von den, Stenberger L. 1979. Eketorp: Befestigung und Siedlung auf Öland, Schweden : die Fauna. Almqvist & Wiksell International

Dana N, Megens H-J, Crooijmans RPMA, Hanotte O, Mwacharo J, Groenen M a. M, van Arendonk J a. M. 2011. East Asian contributions to Dutch traditional and western commercial chickens inferred from mtDNA analysis. Anim. Genet. 42:125–133.

Drummond AJ, Suchard MA, Xie D, Rambaut A. 2012. Bayesian Phylogenetics with BEAUti and the BEAST 1.7. Mol. Biol. Evol. 29:1969–1973.

Eriksson J, Larson G, Gunnarsson U, Bed'hom B, Tixier-Boichard M, Strömstedt L, Wright D, Jungerius A, Vereijken A, Randi E, et al. 2008. Identification of the Yellow Skin Gene Reveals a Hybrid Origin of the Domestic Chicken. PLoS Genet 4(2):e1000010

Flink LG, Allen R, Barnett R, Malmström H, Peters J, Eriksson J, Andersson L, Dobney K, Larson G. 2014. Establishing the validity of domestication genes using DNA from ancient chickens. Proc. Natl. Acad. Sci. 111:6184–6189.

Follett BK. 2015. "Seasonal changes in the neuroendocrine system": Some reflections. Front. Neuroendocrinol. 37:3–12.

Hanon EA, Lincoln GA, Fustin J-M, Dardente H, Masson-Pévet M, Morgan PJ, Hazlerigg DG. 2008. Ancestral TSH Mechanism Signals Summer in a Photoperiodic Mammal. Curr. Biol. 18:1147–1152.

Heinrich D. 1987. Untersuchungen an mittelalterlichen Fischresten aus Schleswig: Ausgrabung Schild 1971-1975. Wachholtz

Heinrich D. 2006. Die Fischreste aus dem Hafen von Haithabu - Handaufgelesene Funde. In: Untersuchungen an Skelettresten von Tieren aus dem Hafen von Haithabu. Neumünster: Wachholtz. p. 157–194.

Holmes M. 2014. Animals in Saxon and Scandinavian England: Backbones of Economy and Society. Sidestone Press

Hüster Plogmann H. 2006. Untersuchungen an den Skelettresten von Säugetieren und Vögeln aus dem Hafen von Haithabu. In: Schietzel K, editor. Berichte über die Ausgrabungen in Haithabu. Vol. 35. Neumünster: Wachholtz. p. 25–156.

Iacus SM. 2008. Simulation and Inference for Stochastic Differential Equations With R Examples. Springer NY

Karlsson A-C, Fallahshahroudi A, Johnsen H, Hagenblad J, Wright D, Andersson L, Jensen P. 2016. A domestication related mutation in the thyroid stimulating hormone receptor gene (*TSHR*) modulates photoperiodic response and reproduction in chickens. Gen. Comp. Endocrinol. 228:69–78.

Karlsson A-C, Svemer F, Eriksson J, Darras VM, Andersson L, Jensen P. 2015. The Effect of a Mutation in the Thyroid Stimulating Hormone Receptor (*TSHR*) on Development, Behaviour and TH Levels in Domesticated Chickens. PLOS ONE 10:e0129040.

Kawecki TJ, Lenski RE, Ebert D, Hollis B, Olivieri I, Whitlock MC. 2012. Experimental evolution. Trends Ecol. Evol. 27:547–560.

Keene D. 1995. Small towns and the metropolis : the experience of medieval England. In: Duvosquel JM, Thoen E, Verhulst AE, editors. Peasants & townsmen in medieval Europe: studia in honorem Adriaan Verhulst. Gent: Snoeck-Ducaju & Zoon. p. 223–238.

Lyimo CM, Weigend A, Msoffe PL, Hocking PM, Simianer H, Weigend S. 2015. Maternal genealogical patterns of chicken breeds sampled in Europe. Anim. Genet. 46:447–451.

Malaspinas A-S. 2016. Methods to characterize selective sweeps using time serial samples: an ancient DNA perspective. Mol. Ecol. 25:24–41.

Mann ME, Woodruff JD, Donnelly JP, Zhang Z. 2009. Atlantic hurricanes and climate over the past 1,500 years. Nature 460:880–883.

Mathieson I, Lazaridis I, Rohland N, Mallick S, Patterson N, Roodenberg SA, Harney E, Stewardson K, Fernandes D, Novak M, et al. 2015. Genome-wide patterns of selection in 230 ancient Eurasians. Nature 528:499–503.

Nakao N, Ono H, Yamamura T, Anraku T, Takagi T, Higashi K, Yasuo S, Katou Y, Kageyama S, Uno Y, et al. 2008. Thyrotrophin in the pars tuberalis triggers photoperiodic response. Nature 452:317–322.

Näsman U. 1976. Introduction to the Descriptions of Eketorp-I, -II and –III. In: Eketorp – Fortification and Settlement on Öland/Sweden. Stockholm: Almqvist & Wiksell

Nishiwaki-Ohkawa T, Yoshimura T. 2016. Molecular basis for regulating seasonal reproduction in vertebrates. J. Endocrinol.229:R117-27.

Peters J, Lebrasseur O, Deng H, Larson G. 2016. Holocene cultural history of Red jungle fowl (Gallus gallus) and its domestic descendant in East Asia. Quat. Sci. Rev. 142:102–119.

Pieper H, Reichstein H. 1995. Untersuchungen an Skelettresten von Vögeln aus dem mittelalterlichen Schleswig. In: Vogel V, editor. Ausgrabungen in Schleswig, Berichte und Studien. Vol. 11. p. 9–114.

Rubin C-J, Zody MC, Eriksson J, Meadows JRS, Sherwood E, Webster MT, Jiang L, Ingman M, Sharpe T, Ka S, et al. 2010. Whole-genome resequencing reveals loci under selection during chicken domestication. Nature 464:587–591.

Sanmark A. 2004. Power and Conversion: A Comparative Study of Christianization in Scandinavia. Department of Archaeology and Ancient History, Uppsala University, Occasional Papers in Archaeology

Serjeantson D. 2006. Birds: food and a mark of status. In: Woolgar CM, Serjeantson D, Waldron T, editors. Food in Medieval England: Diet and Nutrition. Oxford University Press. p. 131–147. Available from: http://eprints.soton.ac.uk/342285/

Soetaert K, Petzoldt T, Setzer RW. 2010. Solving Differential Equations in R: Package deSolve. Available from: https://core.ac.uk/display/6287976/tab/similar-list

Storz JF. 2005. Using genome scans of DNA polymorphism to infer adaptive population divergence. Mol. Ecol. 14:671–688.

Sykes NJ. 2007. The Norman Conquest: A Zooarchaeological Perspective. British Archaeological Reports.International Series 1656.

Venarde BL. 2011. The Rule of Saint Benedict. Harvard University Press

White LJ. 1967. The Life of the Silent Majority. In: Hoyt RS, editor. Life and Thought in the Early Middle Ages. Minneapolis: University of Minnesota Press. p. 85–100.

Yoshimura T, Yasuo S, Watanabe M, Iigo M, Yamamura T, Hirunagi K, Ebihara S. 2003. Light-induced hormone conversion of T4 to T3 regulates photoperiodic response of gonads in birds. Nature 426:178–181.

4.11 Permission from all co-authors to use our joint work as a contribution towards this thesis

I hereby give permission to Liisa Loog to use our joint work *"Inferring allele frequency trajectories from ancient DNA indicates that selection on a chicken gene coincided with changes in medieval husbandry practices. Molecular Biology and Evolution (2017), 34(8):1981-1990"* as contribution towards her D. Phil. thesis to be submitted for examination at Oxford University.

I confirm that to the best of my knowledge, the author contribution statement below is accurate and Liisa Loog's contribution towards the work is greater than that of any other co-author.

Article author contribution statement: M.G.T. & G.L. initiated the project; L.L., M.G.T. & A.E. designed the research; A.E. & L.L. designed the statistical framework; L.L. implemented the framework and performed statistical analysis with input from A.E.; R.B. & R.A. generated the new data; J.P. provided sample material; P.D.P compiled the archaeological faunal data from German sites; O.L. researched information about historic chicken population sizes; N.S., K.D. & J.P. interpreted the TSHR results within an archaeological and historical context; L.L., M.G.T., A.M., G.L. & A.E. wrote the paper with input from N.S., K.D. & J.P.

Date: 11/02/2018

Name(s): Greger Larson Naomi Sykes

Signature(s):

Date: 16/02/2018

Name(s): RICHARD BALLEN

Signature(s):

Date: 15th February 2018

Name(s): Dr Ophélie Lebrasseur

Signature(s):

Date: 11/02/18

Name(s): Prof Keith Dobney

Signature(s):

Date: 11th Feb 2018

Name(s): Ross Barnett

Signature(s):

Date: 11/2/2018

Name(s): Anders Eriksson

Signature(s):

Date: 12/2/18

Name(s): Andrea Manica

Signature(s):

Date: 11/2/18

Name(s): Mark G Thomas (M.G.T.)

Signature(s):

LMU LUDWIG-MAXIMILIANS-UNIVERSITÄT MÜNCHEN — TIERÄRZTLICHE FAKULTÄT — LEHRSTUHL FÜR PALÄOANATOMIE, DOMESTIKATIONSFORSCHUNG UND GESCHICHTE DER TIERMEDIZIN

LMU - Lehrstuhl f. Paläoanatomie - Kaulbachstr. 37 - 80539 München

Vorstand
Univ.-Prof. Dr. Dr. habil. Joris Peters

Telefon +49 (0)89 2180-9110
Telefax +49 (0)89 2180-9219

joris.peters@lmu.de

www.palaeo.vetmed.uni-muenchen.de

Postanschrift:
Kaulbachstraße 37, III. Stock
D-80539 München

We hereby give permission to Liisa Loog to use our joint work *"Inferring allele frequency trajectories from ancient DNA indicates that selection on a chicken gene coincided with changes in medieval husbandry practices. Molecular Biology and Evolution (2017), 34(8):1981-1990"* as contribution towards her Dr. Phil. thesis to be submitted for examination at Oxford University.

We confirm that to the best of our knowledge, the author contribution statement below is accurate and Liisa Loog's contribution towards the work is greater than that of any other co-author.

Article author contribution statement: M.G.T. & G.L. initiated the project; L.L., M.G.T. & A.E. designed the research; A.E. & L.L. designed the statistical framework; L.L. implemented the framework and performed statistical analysis with input from A.E.; R.B. & R.A. generated the new data; J.P. provided sample material; P.D.P compiled the archaeological faunal data from German sites; O.L. researched information about historic chicken population sizes; N.S., K.D. & J.P. interpreted the TSHR results within an archaeological and historical context; L.L., M.G.T., A.M., G.L. & A.E. wrote the paper with input from N.S., K.D. & J.P.

Date: 12 February 2018

Name(s): Ptolemaios Dimitrios Paxinos Joris Peters

Signature(s):

Dienstgebäude
Kaulbachstr. 37, III. Stock
80539 München

Öffentliche Verkehrsmittel
U-Bahn U3, U6
Haltestelle Universität

Bayerische Landesbank München
IBAN: DE 5570 2500 0000 0302 4868
BIC/SWIFT: BYLADEMM
USt-IdNr.: DE 811 265 105

4.S1 Wet Laboratory Procedures and Protocols

4.S1.1 Ancient DNA Laboratories and Experimental Set-Up

DNA extractions and PCR amplifications were performed in a dedicated ancient DNA laboratory in the Department of Archaeology (Durham Evolution and Ancient DNA) at Durham University, United Kingdom. We followed strict laboratory procedures according commonly used guidelines (Cooper and Poinar 2000; Gilbert et al. 2005). All equipment and work surfaces were cleaned before and after each use with a dilute solution of bleach [5–10% (wt/vol) active sodium hypochlorite] followed by ddH2O and ethanol [99% (vol/vol)]. Pipettes and plastic racks were UV-irradiated in a dedicated cross-linker (at <15 cm for at least 30 min at 254-nm wavelength) before and after use. Pre- and post-PCR laboratories are physically isolated; access to the pre-PCR laboratories is restricted to Ancient DNA laboratory users only and access is also prohibited if the laboratory user had entered post-PCR areas the same day. Ancient DNA laboratory users wear clean laboratory coats, double layer of gloves (nitrile and latex), and overshoes to avoid introducing contaminants from post-PCR areas.

4.S1.2 Ancient DNA Extraction

The ancient chicken bones were prepared for DNA extraction by removing an approximately 1-mm layer of outer bone surface by abrasion using a Dremel drill with clean, single-use cut-off wheels (Dremel no. 409). A subsection of the bone was subsequently isolated and pulverized in a Micro-Dismembrator (Sartorious- Stedim Biotech), followed by collection in 15-mL Grainer tubes. Milling containers and grinding balls were subsequently suspended and cleaned in 1% virkon, and rinsed in absolute [99% (vol/vol)] ethanol.

Next, 50- to 100-mg bone powder/specimen was digested in 0.425M EDTA (pH 8), 0.05% SDS, 0.05M Tris·HCI and 400 μg Proteinase K, and incubated overnight on a rotator at 50 °C until fully dissolved. Once dissolved overnight, 2 mL of solution was concentrated in a Millipore Amicon Ultra-4 30 kDa molecular weight cut-off to a final volume of 100 μL. The concentrated DNA extract was purified using the QIAquick PCR Purification Kit (Qiagen) following manufacturers recommendations, except that the final elution step was performed twice (2 × 50 μL) to produce a final volume of 100 μL. Approximately 1 in 10 DNA extractions were blank negative controls containing only extraction buffer and Proteinase K.

PCR Amplification. PCR set-up was performed in a fume hood in a dedicated facility adjacent to the dedicated ancient DNA extraction facility. The PCR set-up facility is subject to positive air pressure that minimizes the risk of introducing contaminant DNA. Approximately 1 in 11 PCR reactions were negative controls.

BCDO2: PCRs were set up in 25-μL reactions using 1.0–1.25 U Taq GOLD (Applied Biosystems), 1× Gold buffer (Applied Bio- systems), 2.5 mM MgCl2, 0.5 μg/μL BSA, 1 M betaine, 200 μM of each dNTP, 0.4 μM of each primer, and 2–5 μL of ancient DNA extract. PCR cycling conditions were 95 °C for 5 min, 50 cycles of 94°C for 30 s, 57 °C for 30 s, and 72 °C for 30 s, followed by 72 °C for 10 min.

TSHR: PCRs were set up in 25 μL reactions using 1.0–1.25 U Taq GOLD (Applied Biosystems), 1× Gold buffer (Applied Bio- systems), 2.5 mM MgCl2, 0.5 μg/μL BSA, 200 μM of each dNTP, 0.6 μM of the biotinylated forward primer, and 0.8 μM of the reverse primer, and 2–5 μL of aDNA extract. PCR cycling conditions were 95 °C for 5 min, 50 cycles of 94 °C for 30 s, 56 °C for 30 s, and 72 °C for 30 s, followed by 72 °C for 10 min. PCRs were visualized on a 1–2% (wt/vol) agarose gel using GelRed and UV illumi- nation. PCR products were purified using ExoSAP-IT (USB Affymetrix) and stored at −20 °C before sequencing.

4.S1.3 DNA Genotyping

Pyrosequencing was performed in-house at the Archaeology department in Durham using the PyroMark Q24 (Qiagen) following manufacturers guidelines, and using Qiagen Q24 sequencing reagent kits. Results, sequences, and genotypes were analyzed in the PyroMark Q24 software (Qiagen) using modified settings: accepted peak deviation and minimum peak heights were set to less strict to account for low signal intensity and slight deviations in peak heights (which, if observed, could be the result of Type-2 C→U deamination/error). Dispensation order was automatically generated using the PyroMark Q24 software (Qiagen) (Table S8).

To account for allelic dropout that is common in ancient DNA studies (Svensson et al. 2007), each SNP/genotype was confirmed by repeated genotyping from two to eight independent PCRs (at least two independent replications for heterozygous specimens, but up to eight replications in for homozygous specimens and heterozygous specimens for which we repeatedly observed allelic drop- out). The probability of falsely assigning a

heterozygous individual as homozygous was calculated as follows: P(false homozygote) = K × (K/2)n − 1, where n is the number of replicates and K is the observed number of allelic dropouts divided by the total number of genotypings of heterozygous individuals (Gagneux et al. 1997; Svensson et al. 2007)

4.S2 Archeological background for newly genotyped samples

The 14 new samples come from three different archaeological sites located in Morocco and Turkey.

Mogador

Four samples (RB579; RB585; RB585; RB587) come from the site of Île de Mogador in Morocco. The site has three main occupational periods: The first corresponds to a Phoenician inhabitation between the 7th and 5th century BC. The second major occupation phase dates to the Roman period and lasted from the 1st till the 3rd century CE. The chicken samples newly genotyped for this study come from a third period, corresponding to a modern re-occupation, which started in the 17th/18th century and lasted into the 20th century CE. The chicken samples, newly genotyped for this study, are dated to be not older than 50 years (Table S7). General information about the site together with a detailed study of its fauna is available in Becker et al. (2012).

Doliche/Dülük Baba Tepes

Three samples (RB593; RB594; RB595) come from a hill-top site of Doliche/Dülük Baba Tepesi near modern Gaziantep in Southern Anatolia, Turkey. The site, famous for being the place where the cult of Iupiter Dolichenus originated, was occupied from the 6th century BC until the 13th century AD. In modern times (until recently) the site witnessed civilian and military use. The chicken samples, newly genotyped for this study, come from modern refuse overlying antique occupation and are dated to be not older than 50 years (Table S7). Archaeological background of the site and a detailed report containing information about the faunal assemblage can be found in Pöllath and Peters (2011).

Korucutepe/Elazig

Seven samples (RB598; RB599; RB600; RB601; RB602; RA26; RA27) come from the site on Korucutepe/Elâzığ located in Eastern Anatolia, Turkey. Site occupation started in the second half of the 4th millennium BC and continued during the Bronze and early Iron Ages. Around 800 BC the site was abandoned until its resettlement by Seljuqs some two

thousand years later (between 1200 and 1400 AD). After this time period occupation ceased at the site. Samples genotyped for this study have been dated to be around 700 years old (Table S7), thus coinciding with the Seljuk occupation. General information about the site can be found in Boessneck and von den Driesch (1975).

4.S3 Supplementary bibliography

Becker C, von den Driesch A, Küchelmann HC. 2012. Mogador, eine Handelsstation am westlichen Rand der phönizischen und römischen Welt - die Tierreste. In: Grupe G, McGlynn G, Peters J, editors. Documenta Archaeobiologiae. 10. Rahden/Westfalen: Leidorf. p. 11–160.

Boessneck J, von den Driesch A. 1975. Tierknochenfunde vom Korucutepe bei Elâzığ in Ostanatolien (Fundmaterial der Grabungen 1968 und 1969). In: van Loon MN, editor. Korucutepe. Vol. 1. Amsterdam/Oxford/New York: North-Holland Publishing Company and American Elsevier Publishing Company. p. 1–220.

Cooper A, Poinar HN. 2000. Ancient DNA: Do It Right or Not at All. Science 289:1139–1139.

Eriksson J, Larson G, Gunnarsson U, Bed'hom B, Tixier-Boichard M, Strömstedt L, Wright D, Jungerius A, Vereijken A, Randi E, et al. 2008. Identification of the Yellow Skin Gene Reveals a Hybrid Origin of the Domestic Chicken. PLoS Genet. 4(2): e1000010.

Gagneux P, Boesch C, Woodruff DS. 1997. Microsatellite scoring errors associated with noninvasive genotyping based on nuclear DNA amplified from shed hair. Mol. Ecol. 6:861–868.

Gilbert MTP, Bandelt H-J, Hofreiter M, Barnes I. 2005. Assessing ancient DNA studies. Trends Ecol. Evol. 20:541–544.

Pöllath N, Peters J. 2011. "Smoke on the Mountain" - Animal Sacrifices for the Lord of Doliche. In: Winter E, editor. Von Kummuh nach Telouch. Asia Minor Studien. 64. Bonn: Habelt. p. 47–68.

Rubin C-J, Zody MC, Eriksson J, Meadows JRS, Sherwood E, Webster MT, Jiang L, Ingman M, Sharpe T, Ka S, et al. 2010. Whole-genome resequencing reveals loci under selection during chicken domestication. Nature 464:587–591.

Svensson EM, Anderung C, Baubliene J, Persson P, Malmström H, Smith C, Vretemark M, Daugnora L, Götherström A. 2007. Tracing genetic change over time using nuclear SNPs in ancient and modern cattle. Anim. Genet. 38:378–383.

4.S4 Supplementary Figures

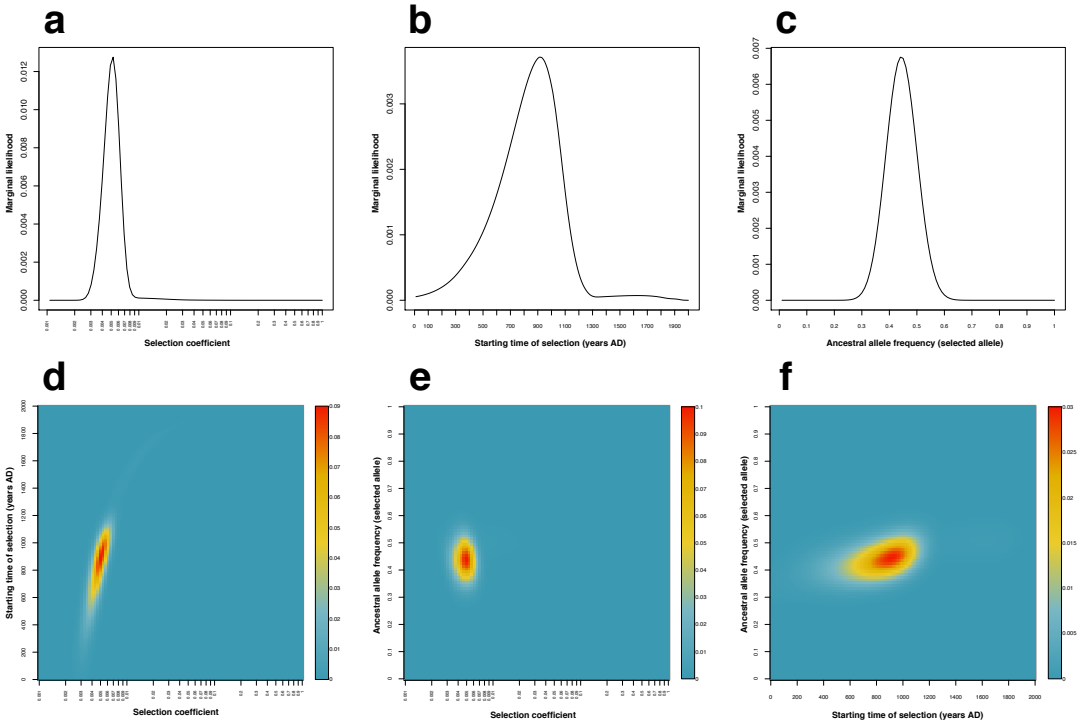

Figure 4.S1: Marginal posterior distribution of parameters for the *TSHR* locus: selection coefficient (a), starting time of selection (b) and ancestral allele frequency (c). Panels d-f show joint marginal posterior distribution of pairs of parameters.

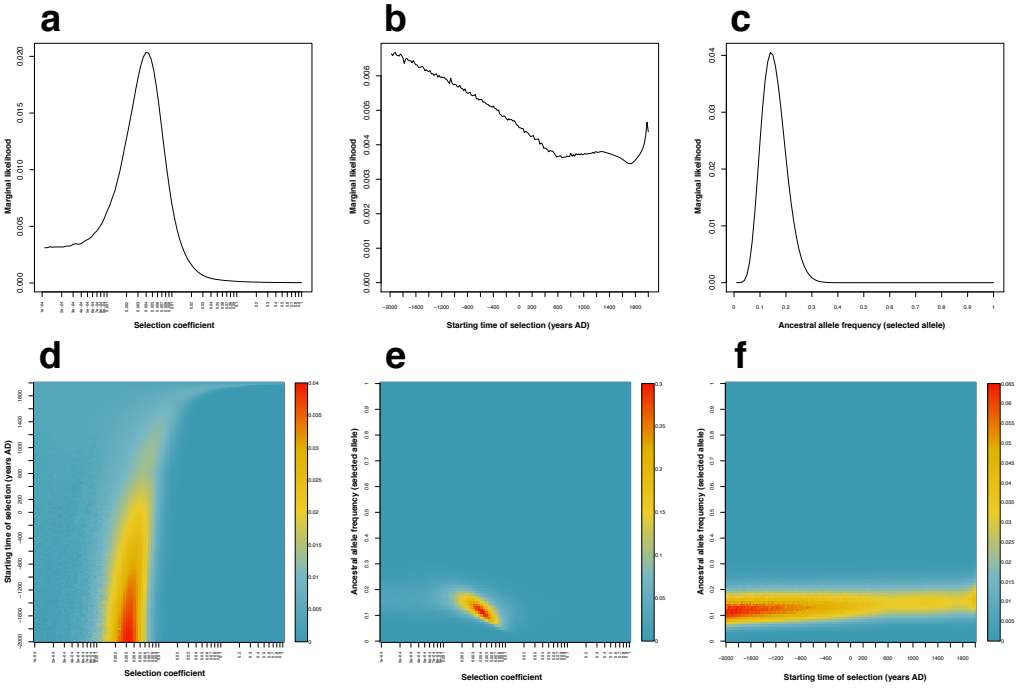

Figure 4.S2: Marginal posterior distribution of parameters for the *BCDO2* locus: selection coefficient (a), starting time of selection (b) and ancestral allele frequency (c). Panels d-f show the joint marginal posterior distribution of pairs of parameters.

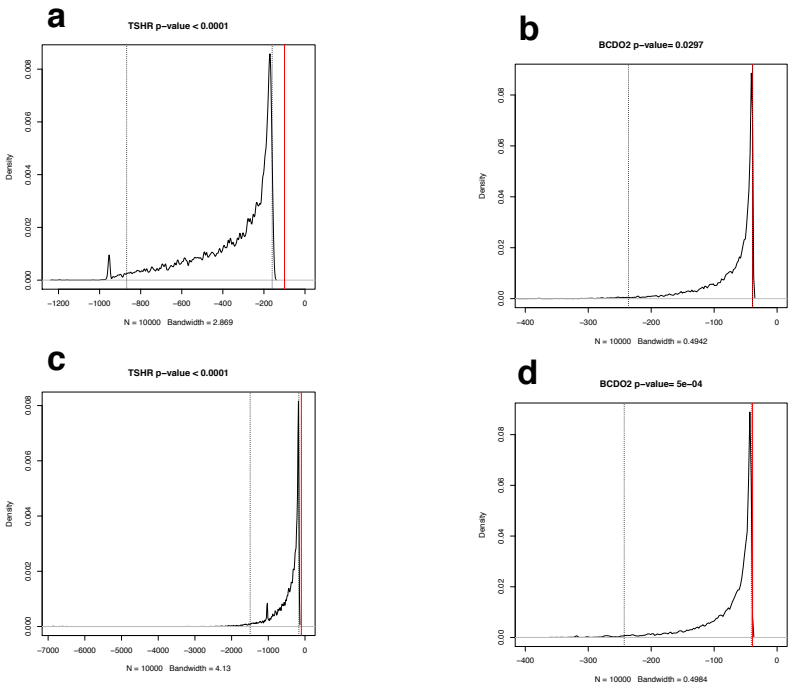

Figure 4.S3: Distribution of data likelihoods for the *TSHR* locus from 10,000 simulations of random genetic drift with (a) and without (c) gene flow from imported Asian jungle fowl. Panels b and d show the corresponding results for the *BCDO2* locus.

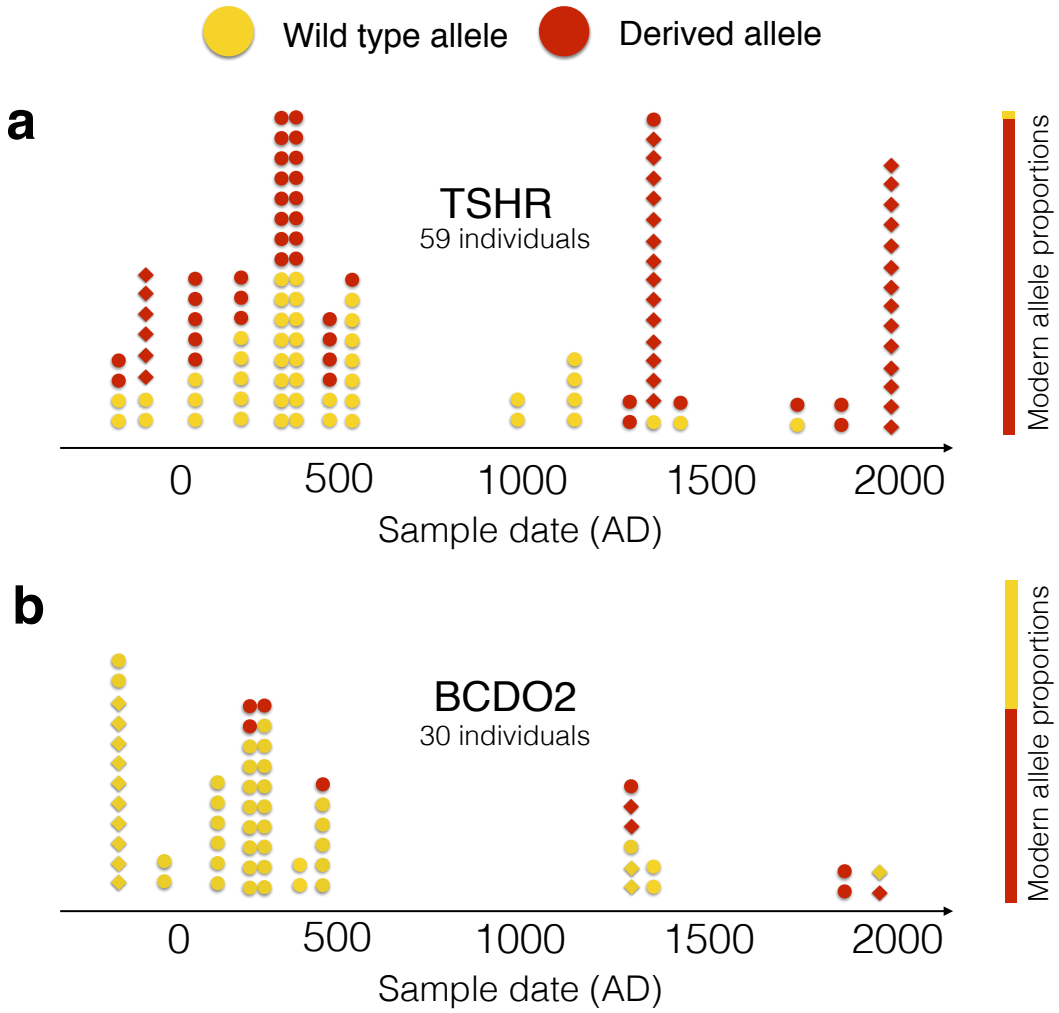

Figure 4.S4: Observed allele counts through time for the *TSHR* locus (**a**) and the *BCDO2* locus (**b**). Wild type alleles in ancient samples are represented by yellow dots and derived alleles by red dots. Modern allele proportions are shown as solid bars to the right of each panel. Circles represent ancient samples from North-Western Europe and diamonds represent ancient samples from the Mediterranean region.

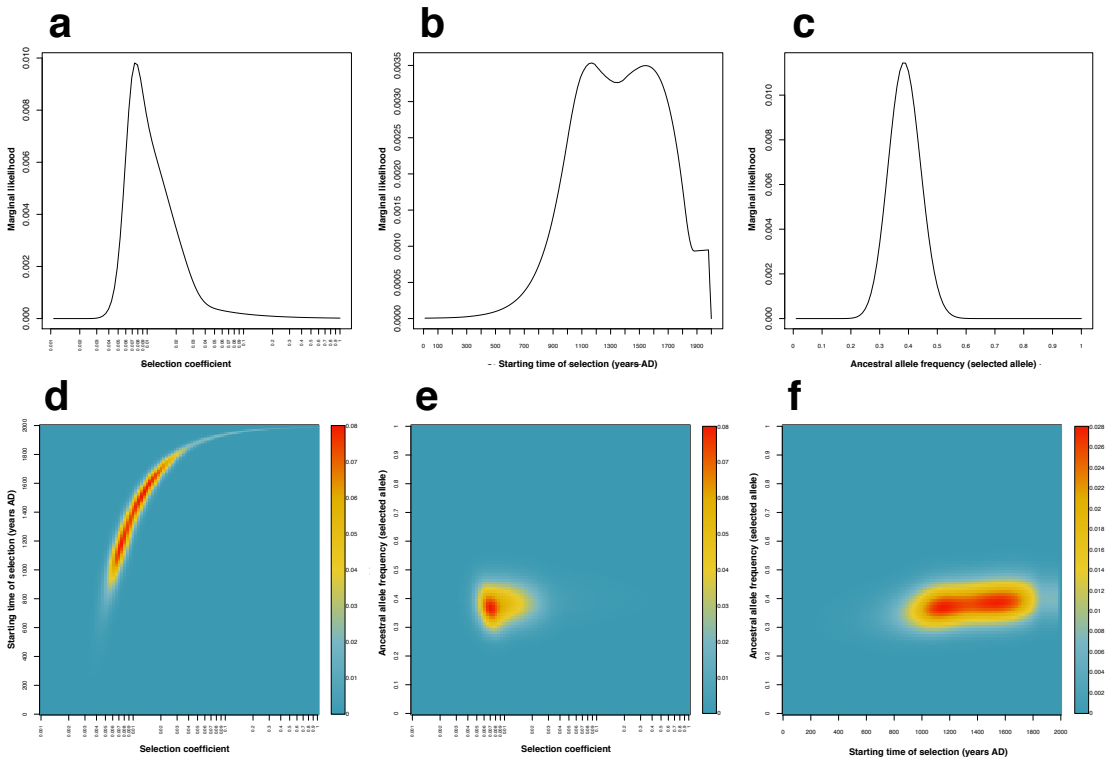

Figure 4.S5: Marginal posterior distribution of parameters for the *TSHR* locus in the North-Western Europe subset of the data: selection coefficient (**a**), starting time of selection (**b**) and ancestral allele frequency (**c**). Panels **d-f** show joint marginal posterior distribution of pairs of parameters.

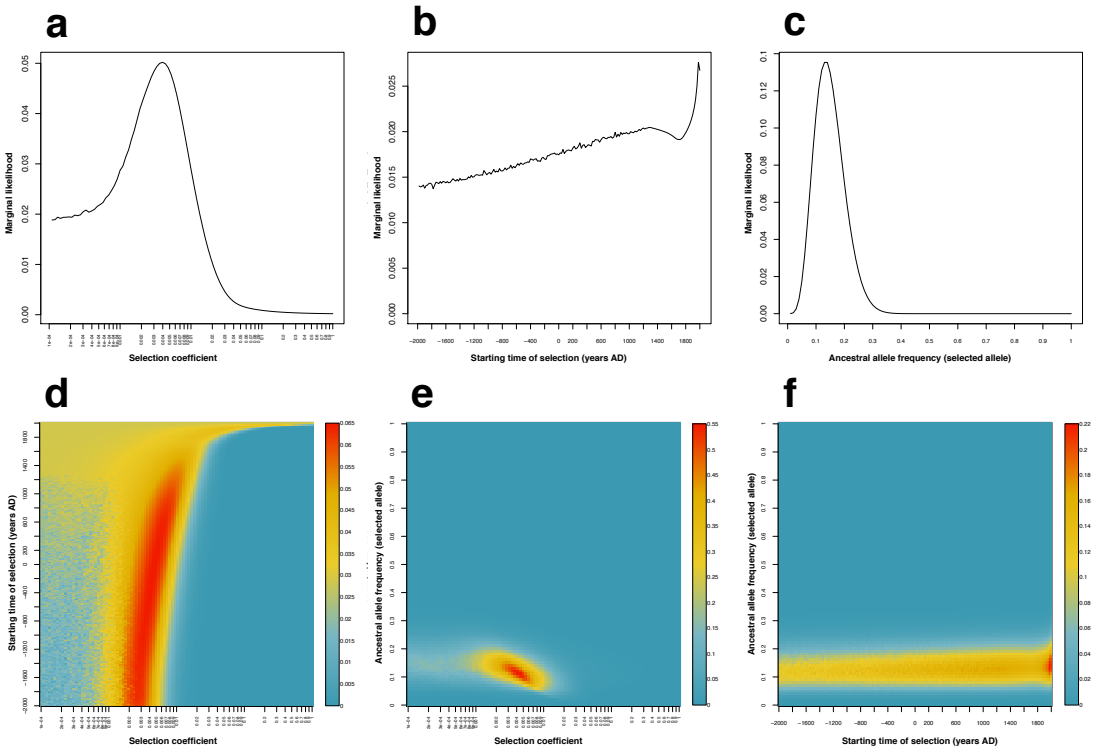

Figure 4.S6: Marginal posterior distribution of parameters for the *BCDO2* locus in the North-Western Europe subset of the data: selection coefficient (a), starting time of selection (b) and ancestral allele frequency (c). Panels d-f show the joint marginal posterior distribution of pairs of parameters.

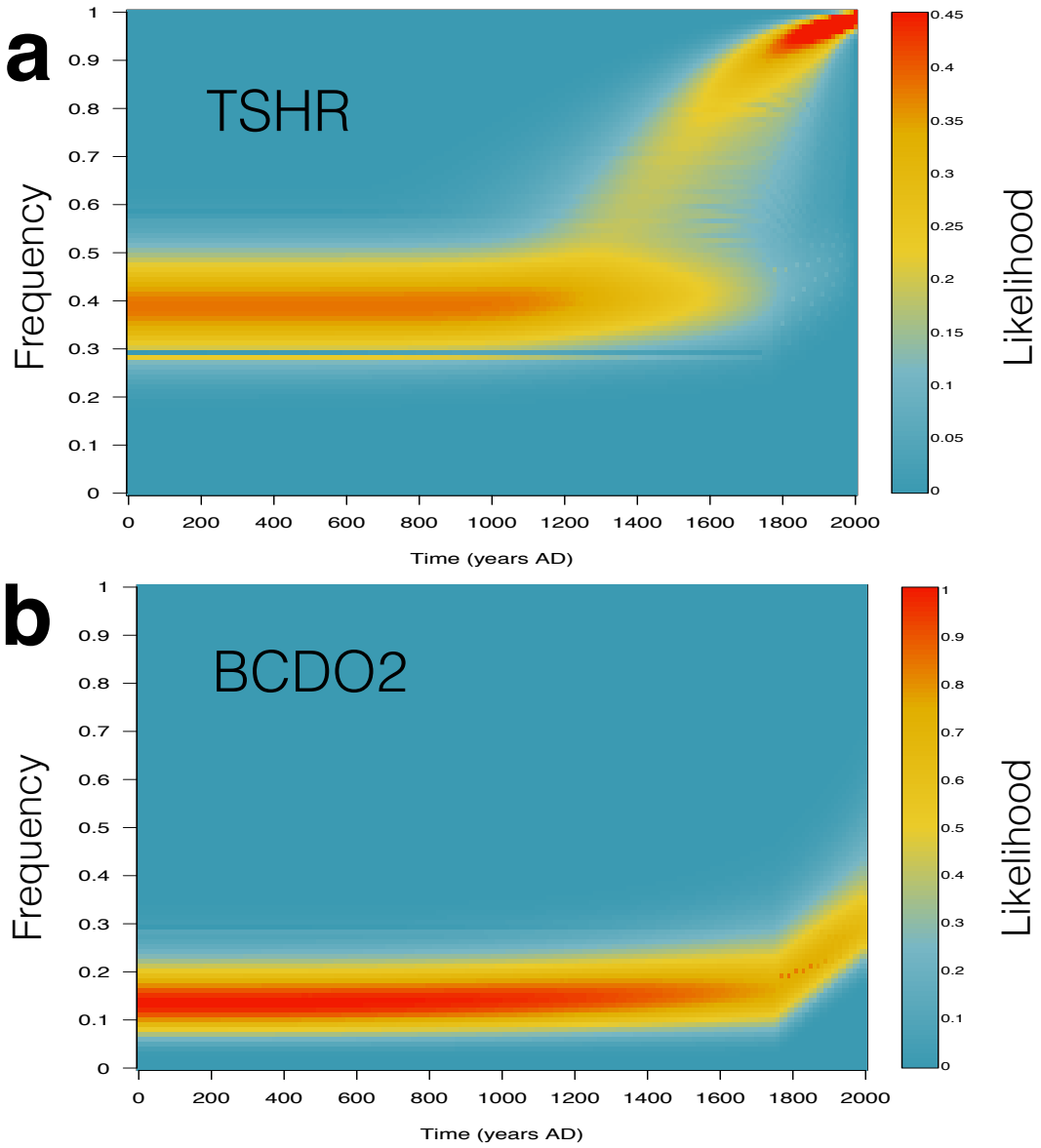

Figure 4.S7: Posterior distribution of the derived allele frequency as a function of time for the *TSHR* locus (a) and the *BCDO2* locus (b) in the North Western Europe subset of the data. The likelihoods are color coded (see color bar) and are shown relative to the maximum likelihood in the plot.

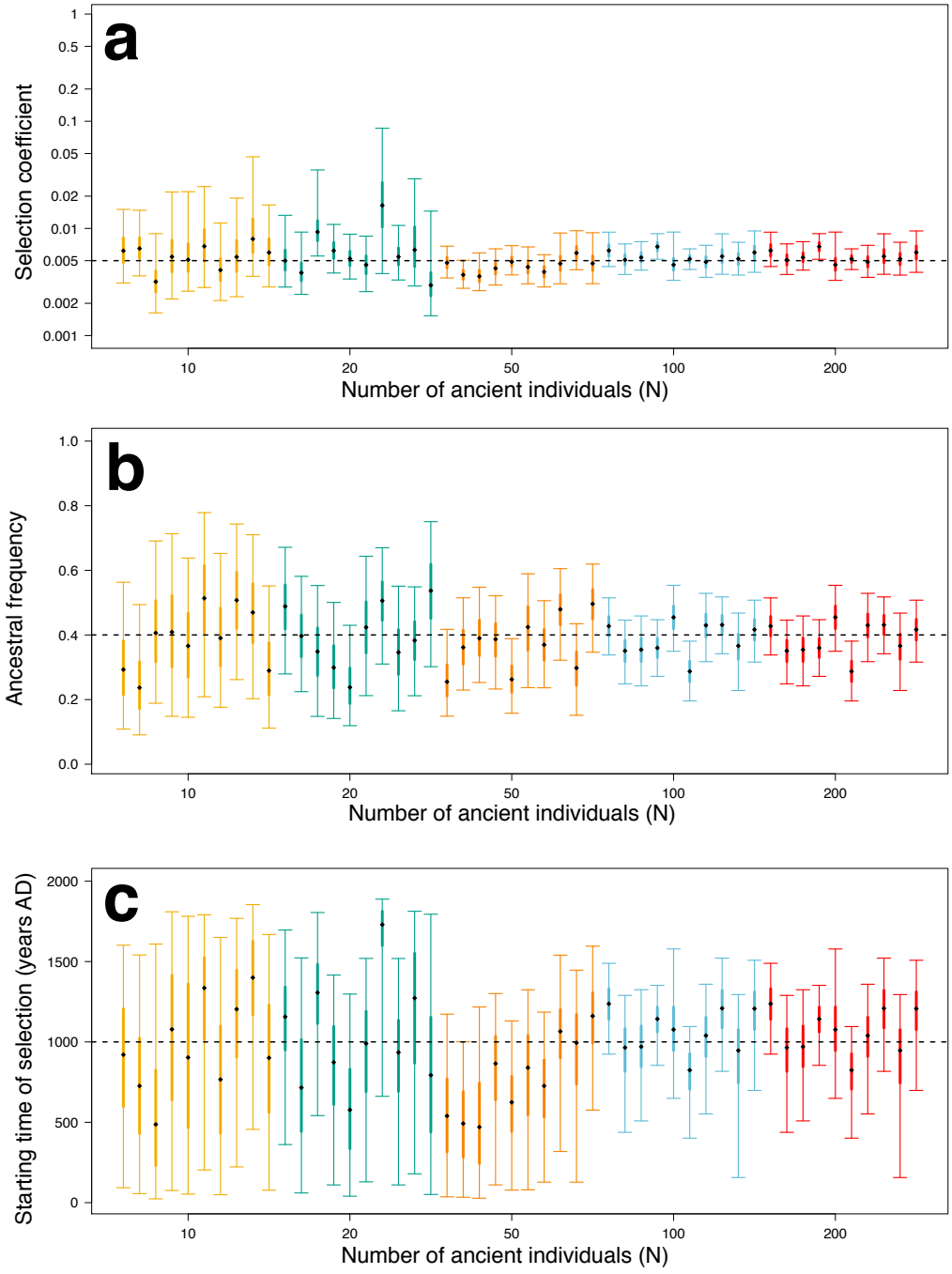

Figure 4.S8: Effect of sample size on the parameter estimates in simulated data. Marginal estimated parameter distributions for selection coefficient (a), ancestral derived allele frequency (b) and starting time of selection (c, in years AD). For each simulated dataset, we show the median (black dot), inter-quartile range (thick line) and symmetric 95% confidence intervals (thin line). Data sets are grouped according to number of simulated ancient individuals (N) and coloured by size: N=10 (yellow), N=20 (green), N=50 (orange), N=100 (blue) and N=200 (red).

4.S4 Supplementary Tables

Table 4.S1a

Period (century AD)	Total number of chicken remains	Total number animal remains	Proportion of chicken remains	95% Confidence Intervals	
5th to 9th	8029	215655	0.037230762	0.04137207	0.03308946
9th to 11th	3856	89374	0.043144539	0.04955772	0.03673136
11th to 12th	5237	71435	0.073311402	0.0803708	0.06625201
12th to 14th	6228	73729	0.084471511	0.09137825	0.07756478

Table 4.S1b

Period (century AD)	Total number of chicken remains	Total number animal remains	Proportion of chicken remains	95% Confidence Intervals	
7th to 9th	45	5364	0.008389262	-0.01825982	0.03503835
9th to 11th	866	42353	0.020447194	0.01102118	0.0298732
11th to 12th	1456	44713	0.032563237	0.02344627	0.04168021
12th to 14th	6754	191586	0.035253098	0.03085484	0.03965136

Table 4.S1: Relative frequency of domestic chicken remains (by number of identified specimens) from 184 English archaeological faunal assemblages (Table S1a) and 104 German archaeological faunal assemblages (Table S1b).

ID	Country	Genotype	From (Years AD)	To (Years AD)	Dating Method	Reference
Ch37	Germany	GA	-280	-15	Context	Flink et al. 2014
Ch40	Germany	GA	-280	-15	Context	Flink et al. 2014
RA6	Greece	AA	-200	-40	Context	Flink et al. 2014
RA18	Greece	AA	-200	-40	Context	Flink et al. 2014
RA22	Greece	AA	-200	-40	Direct	Flink et al. 2014
Ch31	Germany	GG	-200	-30	Context	Flink et al. 2014
Ch33	Austria	GA	-100	50	Context	Flink et al. 2014
Ch34	Austria	GA	-100	50	Context	Flink et al. 2014
Ch35	Austria	AA	-100	50	Context	Flink et al. 2014
Ch36	Austria	GA	-100	50	Context	Flink et al. 2014
RB373	England	GG	69	96	Context	Flink et al. 2014
RB374	England	GA	69	96	Context	Flink et al. 2014
RB375	England	GA	69	96	Context	Flink et al. 2014
RB376	England	GA	69	96	Context	Flink et al. 2014
Ch3	Germany	GG	100	300	Context	Flink et al. 2014
Ch4	Germany	AA	100	300	Context	Flink et al. 2014
Ch7	Germany	AA	100	300	Context	Flink et al. 2014
Ch10	Germany	GG	100	300	Context	Flink et al. 2014
Ch12	Germany	GA	100	300	Context	Flink et al. 2014
Ch13	Germany	GA	100	300	Context	Flink et al. 2014
Ch14	Germany	GG	100	300	Context	Flink et al. 2014
Ch15	Germany	GA	100	300	Context	Flink et al. 2014
Ch16	Germany	GA	100	300	Context	Flink et al. 2014
Ch17	Germany	GA	100	300	Context	Flink et al. 2014
Ch19	Germany	AA	100	300	Context	Flink et al. 2014
Ch20	Germany	GA	100	300	Context	Flink et al. 2014
Ch21	Germany	GG	100	300	Context	Flink et al. 2014
Ch22	Germany	GA	100	300	Context	Flink et al. 2014
Ch23	Germany	GG	100	300	Context	Flink et al. 2014
Ch24	Germany	GA	100	300	Context	Flink et al. 2014
Ch25	Germany	GA	0	500	Context	Flink et al. 2014
Ch26	Germany	GG	0	500	Context	Flink et al. 2014
Ch27	Germany	GA	0	500	Context	Flink et al. 2014
RB368	England	GG	120	400	Context	Flink et al. 2014
RB369	England	GG	120	400	Context	Flink et al. 2014
RB370	England	GG	120	400	Context	Flink et al. 2014
RB372	England	GA	120	400	Context	Flink et al. 2014
RB383	England	GG	900	1100	Context	Flink et al. 2014
RB378	England	GG	1000	1200	Context	Flink et al. 2014
RB381	England	GG	1000	1200	Context	Flink et al. 2014
RB384	England	AA	1100	1400	Context	Flink et al. 2014
RB388	England	GA	1100	1500	Context	Flink et al. 2014
RB599	Turkey	AA	1272	1334	Direct	This study
RB600	Turkey	AA	1275	1337	Context	This study

RB601	Turkey	AA	1275	1337	Context	This study
RB602	Turkey	AA	1275	1337	Context	This study
RA26	Turkey	AA	1275	1337	Context	This study
RA27	Turkey	AA	1275	1337	Context	This study
RB598	Turkey	AA	1278	1340	Direct	This study
RB380	England	GA	1300	1500	Context	Flink et al. 2014
RB385	England	GA	1500	1800	Context	Flink et al. 2014
Ch38	Germany	AA	1820	1880	Direct	Flink et al. 2014
RB579	Morocco	AA	1950	2000	Direct	This study
RB585	Morocco	AA	1950	2000	Context	This study
RB586	Morocco	AA	1950	2000	Direct	This study
RB587	Morocco	AA	1950	2000	Context	This study
RB593	Turkey	AA	1950	2000	Context	This study
RB594	Turkey	AA	1950	2000	Context	This study
RB595	Turkey	AA	1950	2000	Context	This study

Table 4.S2: List of ancient samples used in the analysis of the *TSHR* locus (position 43,250,347 on chromosome 5). G is the ancestral allele and A is the derived allele.

ID	Country	Genotype	From (Years AD)	To (Years AD)	Dating Method	Reference
RA6	Greece	AA	-200	-40	Context	Flink et al. 2014
RA11	Greece	AA	-200	-40	Context	Flink et al. 2014
RA14	Greece	AA	-200	-40	Context	Flink et al. 2014
RA18	Greece	AA	-200	-40	Context	Flink et al. 2014
RA22	Greece	AA	-200	-40	Context	Flink et al. 2014
Ch31	Germany	AA	-200	-30	Context	Flink et al. 2014
Ch36	Austria	AA	-100	50	Context	Flink et al. 2014
RB374	England	GA	69	96	Context	Flink et al. 2014
RB375	England	AA	69	96	Context	Flink et al. 2014
RB376	England	AA	69	96	Context	Flink et al. 2014
Ch3	Germany	GA	100	300	Context	Flink et al. 2014
Ch4	Germany	AA	100	300	Context	Flink et al. 2014
Ch10	Germany	AA	100	300	Context	Flink et al. 2014
Ch12	Germany	GA	100	300	Context	Flink et al. 2014
Ch13	Germany	AA	100	300	Context	Flink et al. 2014
Ch15	Germany	AA	100	300	Context	Flink et al. 2014
Ch16	Germany	AA	100	300	Context	Flink et al. 2014
Ch19	Germany	GA	100	300	Context	Flink et al. 2014
Ch20	Germany	AA	100	300	Context	Flink et al. 2014
Ch21	Germany	AA	100	300	Context	Flink et al. 2014
Ch27	Germany	AA	0	500	Context	Flink et al. 2014
RB368	England	GA	120	400	Context	Flink et al. 2014

RB369	England	AA	120	400	Context	Flink et al. 2014
RB370	England	AA	120	400	Context	Flink et al. 2014
RA26	Turkey	AA	1275	1337	Context	This study
RA27	Turkey	GG	1275	1337	Context	This study
RB598	Turkey	GA	1278	1340	Context	This study
RB380	England	AA	1300	1500	Context	Flink et al. 2014
Ch38	Germany	GG	1820	1880	Context	Flink et al. 2014
RB579	Morocco	GA	1950	2000	Context	This study

Table 4.S3: List of ancient samples used in the analysis of the *BCDO2* locus (position 6,273,428 on chromosome 24). A is the ancestral allele and G is the derived allele.

Breed	**Origin**	**Samples in pool**	**Frequency**
White Leghorn Line 13 (WL-A)	Sweden	11	1
Rhode Island Red	Netherlands	10	1
Rhode Island Red (RIR)	France	8	1
Jaärhöns	Norway	8	1
Poltava clay	Ukraine	8	1
Dorking	UK	3	0.67
Broiler Dam Line B (CB-2	France	9	1
Broiler Sire Line B	France	10	1
Bourbonnaise	France	8	1
Coucou de Rennes	France	7	1
Czech Golden Pencilled	Czech Republic	5	1
Finnish Landrace	Finland	5	1
Friesian fowl	Netherlands	5	1
Houdan	France	5	1
Marans	France	8	1
Owl-bearded	Netherlands	8	1
Red Villafranquina	Spain	5	1
Transsylvanian Naked Neck	Hungary	5	1
Westfa_lischer Totleger	Germany	3	0.67
Yurlov crower	Russia	4	1
Icelandic	Iceland	12	0.92
Inhibition of Gold	France	3	1
Coucou du Vercors	France	5	1
SASSO	France	12	1
Total nr of individuals:	**167**	**Total frequency:**	**0.98**

Table 4.S4: Frequency of the *TSHR* derived allele (position 43,250,347 on chromosome 5) in modern European breeds. (Data from (Rubin et al. 2010)).

Breed	Area of breed origin	Sampling country	Skin colour
Bedouin	Middle east	Israel	White
Owl-bearded (Uilenbaarder)	Netherlands	Netherlands	White
Friesian fowl	Netherlands	Netherlands	White
Bresse noire	France	France	White
Houdan	France	France	White
Marans	France	France	White
Dorking	England	England	White
Finnish Landrace	Finland	Finland	White
Sicilienne Buttercup	Italia	Italia	White
Yurlov crower, Russia	Russia	Russia	White
Westfaeliche Totleger	Germany	Germany	White
Sundheimer	Germany	Germany	Yellow
Old Scand. Ref. Pop	Scandinavia	n/a	Yellow
Green-legged Partridge	Poland	Poland	Yellow
Orlov	Russia	Russia	Yellow
Ukrainian bearded	Ukraine	Ukraine	Yellow
Poltava clay	Ukraine	Ukraine	Yellow
Yurlov crower,Ukraine	Russia	Russia	Yellow

Table 4.S5: List of modern European breeds included for *BCDO2* derived allele frequency calculation. (Data from AVIANDIV (https://aviandiv.tzv.fal.de) database).

Breed	Origin	Breed phenotype	Sample size	Frequency of the derived allele in breeds
Friesian Fowl	Netherlands	white skin	6	0
Padova	Italia	white skin	4	0
Westfa¨lischer Totleger	Germany	white skin	3	0
Houdan	France	white skin	5	0
Dorking	England	white skin	4	0
Red Villafranquina	Spain	white skin	5	0.1
Czech Golden Pencilled	Czech Republic	white skin	5	0
			Total:	**Total frequency:**
			32	**0.015625**

Table 4.S6: Frequency of *BCDO2* derived allele (position 6,273,428 on chromosome 24) in modern European breeds. (Data from (Eriksson et al. 2008)

Sample_ID	Reference	Lab_code	Radiocarbon_Age(BP)	
RB599	This study	OxA-X-2504	754	± 27
RB598	This study	OxA-27436	738	± 24
Ch38	Flink et al.2014	Beta-356195	80	± 30
RB579	This study	OxA-27588	1.12172	± 0.00631
RB586	This study	OxA-27435	1.28372	± 0.00326
RA22	Flink et al.2014	Beta-351382	2030	± 30

Table 4.S7: Radiocarbon ages (BP) for directly dated samples used in the analyses.

Locus	Primer sequence (5'–3')	Primer name	Source	Sequence to analyze
TSHR	CTTTCTTCTTGCCCTTTT	TSHR-F (biotin)	Flink et al. 2014	
TSHR	GATGCTGACTTTGCTGTA	TSHR-R	Flink et al. 2014	
TSHR	TGCTGTAGCTGCTGACTC	TSHR-S	Flink et al. 2014	C/TAACCAGTGG
BCDO2	ACTCTTGCATGGATCTGG	BCDO2-F (biotin)	Flink et al. 2014	
BCDO2	TGTGGTCTCAGAATTTGG	BCDO2-R	Flink et al. 2014	
BCDO2	TCAGAATTTGGGACG	BCDO2-S	Flink et al. 2014	C/TTGGCAATGC

Table 4.S8: Polymerase Chain Reaction and sequencing primers used for *TSHR* and *BCDO2*.

Table 4.S9a

BCDO2	**s**	**f.anc**	***TSHR***	**s**	**t.sel.start**	**f.anc**
CI.lower (95%)	0.000131826	0.07	CI.lower(0.025)	0.003019952	290	0.34
CI.upper (95%)	0.01584893	0.25	CI.upper(0.975)	0.00691831	1210	0.54
Max	0.003630781	0.14	Max	0.004897788	920	0.44

Table 4.S9b

BCDO2	**s**	**f.anc**	***TSHR***	**s**	**t.sel.start**	**f.anc**
CI.lower (95%)	0.000120226	0.06	CI.lower(0.025)	0.004570882	750	0.28
CI.upper(95%)	0.02089296	0.25	CI.upper(0.975)	0.05495409	1900	0.49
Max	0.003630781	0.13	Max	0.00691831	1170	0.38

Table 4.S9: Marginal likelihoods for the selection coefficient(s); ancestral allele frequency (f.anc) and starting time of selection (t.sel.start) estimated for the *TSHR* and *BCDO2* loci. Table 4.S9a contains the estimates and the 95% confidence intervals (CIs) from the analysis with the full dataset. Table 4.S9b contains the estimates and the confidence intervals (CIs, calculated at the 0.025 and 0.975 quintiles))from the analysis with the subset of full dataset containing samples from North Western Europe Only.

Site	Type of site	BOS	SUS	OVIS/CAPRA	GALLUS	ANSER	Total	Reference
Karlburg, Dorf	Village	218	443	92	9	0	762	Vagedes (1994; 2001)
Hitzacker	Castle	543	2643	1220	35	17	4458	Kocks (1978); Walcher (1978)
Dannenberg	Castle	68	60	13	1	2	144	Kocks (1978); Walcher (1978)
Total		829	3146	1325	45	19	5364	

9th-11th century AD

Site	Type of site	BOS	SUS	OVIS/CAPRA	GALLUS	ANSER	Total	Reference
Karlburg, Dorf	Village	71	111	62	1	2	247	Vagedes (1994; 2001)
Roßtal (insgesamt)	Castle	2490	7918	3401	345	39	14193	Vagedes/Peters (2001)
Oberammerthal	Castle	131	702	348	12	1	1194	Kerth/Landgraf (2001)
Alt-Muehlhausen	Village	352	572	239	22	5	1190	Barthel (1981)
Frauenkloster Herford	Cloister	50	125	63	9	10	257	Reichstein (1993a)
Sulzbach	Castle	174	3680	3642	198	98	7792	Pasda (2004)
Alt-Luebeck	Castle	1300	833	223	14	3	2359	Nobis (1957); Schröder (1984)
Helfta, Königshof	Castle	647	1003	587	86	12	2335	Müller (1996)
Hildesheim, Leunishof	Town	225	766	431	9	0	1431	Schoon (2000)
Hitzacker	Castle	2018	6167	2850	183	40	11258	Kocks (1978); Walcher (1978)
Dannenberg	Castle	158	141	40	2	3	344	Kocks (1978); Walcher (1978)
Total		**7545**	**21907**	**11824**	**866**	**211**	**42353**	

11th-12th century AD

Site	Type of site	BOS	SUS	OVIS/CAPRA	GALLUS	ANSER	Total	Reference
Hl. Berg	Castle	16	73	9	1	0	99	Obermaier (2009)
Regensburg, Lederergasse 1	Town	1213	171	377	3	0	1764	Sachenbacher-Palavestra (1999)
Nürnberg, Burgamtmannsgebäude	Castle	190	709	185	179	76	1339	Pasda (2004)
Nürnberg, Palas	Castle	44	526	128	40	6	744	Pasda (2004)
Nürnberg, Palas-alt	Castle	27	569	149	34	0	779	Boessneck/von den Driesch-Karpf (1968)
Karlburg, Dorf	Village	40	32	18	1	2	93	Vagedes (1994; 2001)
Rotenhain, Alte-Burg	Castle	6	39	33	2	0	80	Wustrow (2004)
Altenberg, Burg Berge	Castle	64	820	730	228	11	1853	Nobis (1985)
Hoexter, An der Kiliankirche 14	Town	274	125	122	1	0	522	Doll (2001)
Hoexter, Grubestr. 12-14	Town	27	43	12	2	0	84	Doll (2001)
Hoexter, Grubestr. 40	Town	637	316	342	93	2	1390	Doll (2001)
Hoexter, Rodewiekstr. 1	Town	124	34	31	12	3	204	Doll (2001)
Hoexter, Weserstr. 3-5	Town	178	84	38	3	0	303	Doll (2001)
Burg Plesse	Castle	148	1050	341	75	9	1623	Schoon (1998b)
Sulzbach	Castle	364	3816	1377	110	48	5715	Pasda (2004)
Alt-Luebeck	Castle	978	823	255	26	7	2089	Nobis (1957); Schröder (1984)
Wiprechtsburg bei Groitzsch	Castle	2378	2952	523	97	157	6107	Müller (1977)
Emden, Rosenstraße	Town	845	49	365	2	1	1262	Grimm (2010)
Emden, Schulstraße	Town	870	74	546	0	2	1492	Grimm (2010)
Braunschweig, Turnierstraße	Town	158	411	126	69	0	764	Oehlmann (1989)
Hitzacker	Castle	2455	8247	3958	458	98	15216	Kocks (1978); Walcher (1978)
Dannenberg	Castle	498	562	102	20	9	1191	Kocks (1978); Walcher (1978)
Total		**11534**	**21525**	**9767**	**1456**	**431**	**44713**	

12th-14th century AD

Site	Type of site	BOS	SUS	OVIS/CAPRA	GALLUS	ANSER	total	Reference
Sulzberg	Castle	143	96	46	7	2	294	von den Driesch (1995)
Burg von Hütte	Castle	32	322	48	23	0	425	Becker (2003)
Konstanz, Fischmarkt	Town	8080	467	1992	54	10	10603	Prilloff (2000)
Konstanz, Fischmarkt	Town	1234	500	1313	150	43	3240	Prilloff (2000)
Schloss Murnau	Castle	887	748	291	0	0	1926	von den Driesch/Manhart (1994)
Schloss Murnau	Castle	1480	1000	586	0	0	3066	von den Driesch/Manhart (1994)
Augsburg, Beim Märzenbad 9	Town	2218	489	540	29	15	3291	Pöllath/von den Driesch (2000)
Regensburg, Lederergasse 1	Town	135	14	40	1	3	193	Sachenbacher-Palavestra (1999)
Aholming	Village	253	104	44	4	0	405	Pöllath et al. (2010)
Karlburg, Dorf	Village	130	165	51	5	4	355	Vagedes (1994; 2001)
St. Arnual	Cloister	40	123	46	77	7	293	Deschler-Erb et al. (2007)
Einbeck, Negenborner Weg	Town	319	300	108	8	2	737	Schulze-Rehm (1998)
Erfurt, Marktstr. 50	Town	55	13	5	2	1	76	Barthel (1979)
Wartburg	Castle	80	437	94	24	0	635	Prilloff (2004)
Warberg	Castle	273	245	33	6	0	557	Pasda (2004)
Rauenwörth	Castle	848	485	142	36	2	1513	Sachenbacher-Palavestra (1992)
Treuchtlingen	Castle	92	141	18	33	0	284	Pasda (2004)

Treuchtlingen	Castle	227	184	57	70	22	560	Pasda (2004)
Ulm, Nikolauskapelle auf dem Grünen Hof	Town	39	8	21	1	0	69	Schmidt/Scholkmann (1981)
Burg Thann	Castle	367	274	93	258	20	1012	Pasda (2004)
Burg Thann	Castle	1040	551	200	270	22	2083	Pasda (2004)
Nürnberg, Burgamtmannsgebäude	Castle	191	577	152	122	19	1061	Pasda (2004)
Nürnberg, Palas	Castle	164	522	145	118	13	962	Pasda (2004)
Schloss Marbach	Castle	1199	316	255	33	16	1819	Doll (2003)
Schloss Marbach	Castle	1711	722	595	91	29	3148	Doll (2003)
Schloss Marbach	Castle	277	168	144	28	11	628	Doll (2003)
Burg Schnellerts	Castle	965	523	175	171	45	1879	Harre (1994)
Dreieichenhain, Fahrgasse	Town	9	12	3	0	1	25	Blänkle (1996)
Oberursel-Bommersheim	Castle	2478	5016	920	949	397	9760	von Waldstein (1992)
Isenburg, Hattingen	Castle	376	826	152	206	26	1586	Reichstein (1981)
Altenberg	Village	113	27	16	0	0	156	Doll (1998)
Erfurt, Ecke Krämpferstraße	Town	772	721	929	107	35	2564	Barthel et al. (1979); Barthel (1981)
Posteburg	Castle	190	293	40	1	1	525	Schoon (1998a)
Frauenkloster Herford	Cloister	219	574	513	179	89	1574	Reichstein (1993a)
Sulzbach	Castle	302	750	308	128	43	1531	Pasda (2004)
Köln, Dom	Town	293	314	192	39	11	849	Paxinos (unpublished Dissertation)
Köln, Dom	Town	3395	1394	951	58	0	5798	Paxinos (unpublished Dissertation)
Haus Horst, Gelsenkirchen	Castle	669	476	377	39	2	1563	Doll (2010)
Haus Meer	Castle	918	2096	639	27	50	3730	Clason (1968); Reichstein (1999b)
Emden, Kirchstraße	Town	1181	126	995	30	1	2333	Grimm (2010)
Wiprechtsburg bei Groitzsch	Castle	1685	1118	595	129	37	3564	Müller (1977)
Hildesheim, Leunishof	Town	99	598	138	20	3	858	Schoon (2000)
Diderikeshusen	Village	32	84	47	18	3	184	Reichstein (1993b)
Kloster Norden	Cloister	3	12	26	17	0	58	Küchelmann (2010)
Emden, Rosenstraße	Town	1373	151	459	5	4	1992	Grimm (2010)
Emden, Schulstraße	Town	1768	123	776	5	16	2688	Grimm (2010)
Emden, Kirchstraße	Town	1205	206	681	24	2	2118	Grimm (2010)
Bremen, Marktplatz	Town	598	310	154	5	0	1067	Küchelmann (2014)
Braunschweig, Turnierstraße	Town	329	711	190	36	0	1266	Oehlmann (1989)
Braunschweig, Packhof	Town	37	31	49	10	0	127	May (1985)
Burg Bodenteich	Castle	34	525	98	121	4	782	Reichstein (1999a)
Schleswig, Schild	Town	16797	8821	8197	1180	1120	36115	Hüster (1990); Heinrich (1995); Pieper/Reichstein (1995); Spahn (1986); Heinrich (1991)
Schleswig, Schild	Town	3273	2022	1844	371	294	7804	Hüster (1990); Heinrich (1995); Pieper/Reichstein (1995); Spahn (1986); Heinrich (1991)
Lübeck, Dr.-Julius-Leber-Str. 58	Town	1109	530	355	56	17	2067	Pyrozok/Reichstein (1991)
Lübeck, Koenigsstrasse 59	Town	2409	394	339	37	10	3189	Paul (1978; 1980)
Kiel	Town	372	141	66	5	6	590	Johansson/Reichstein (1979)
Starigard, Oldenburg i.H.	Castle	1954	2203	220	121	108	4606	Prümmel (1984)
Stralsund, Katharinenkloster	Cloister	9	0	33	1	0	43	Grimm (2005)
Freyenstein	Town	676	770	523	104	26	2099	Benecke (1989)
Berlin, Alt-Koepenick 17-19	Town	193	205	118	25	2	543	Benecke (2010)
Berlin, Breite Straße 21-29	Town	145	313	89	54	8	609	Benecke (2010)
Berlin, Fischerinsel 12/ Getraudenstraße	Town	230	149	121	9	7	516	Benecke (2010)
Berlin, Gruenstraße 18/19	Town	63	33	30	5	2	133	Benecke (2010)
Gliechow	Castle	43	51	38	20	0	152	Müller (1990)
Gliechow	Castle	19	18	16	1	0	54	Müller (1990)
Salzwedel	Village	296	169	155	15	0	635	Prilloff (1988)
Hitzacker	Castle	11099	23623	7944	956	326	43948	Kocks (1978); Walcher (1978)
Dannenberg	Castle	290	289	68	20	4	671	Kocks (1978); Walcher (1978)
Total		**79534**	**65719**	**36638**	**6754**	**2941**	**191586**	

Table 4.S10: Faunal number of identified specimens from 104 German archaeological faunal assemblages (for references, see associated bibliography below).

Bibliography for Table 4.S10

Barthel H-J. 1979. Tierknochenreste einer mittelalterlichen Grube in Erfurt, Marktstraße 50. Ausgrabungen und Funde. Nachrichtenblatt für Vor- und Frühgeschichte 24: 254-259.

Barthel H-J, Stecher H, Timpel W. 1979. Eine mittelalterliche Produktionsstätte für Knochenspielwürfel. Alt-Thüringen 16: 137-171.

Barthel H-J. 1981. Untersuchungen an Tierknochen aus mittelalterlichen Siedlungen. In: Rudolf F (ed), Beiträge zur Archäozoologie I. Weimarer Monographien zur Ur- und Frühgeschichte 4: 39-100.

Becker V. 2003. Tierknochen- und Flötenfunde aus dem hochmittelalterlichen Burgstall von Hütt, Markt Eichendorf, Lkr. Dingolfing-Landau. In: Schmotz K (ed), Vorträge des 21. Niederbayerischen Archäologentages, pp. 201-212. Rahden/Westf.: Leidorf.

Benecke N. 1989. Die Tierknochen aus der Stadtwüstung des 13. Jahrhunderts von Freyenstein, Kr. Wittstock. Zeitschrift für Archäologie 23: 101-122.

Benecke N. 2010. Mittelalterliche Tierknochenfunde aus neuen Ausgrabungen in Berlin. In: Haspel J, Wemhof M (eds), Miscellanea Archaeologica IV. Festschrift für Wilfried Menghin. Beiträge zur Denkmalpflege in Berlin 32: 196-209.

Blänkle P. H. 1996. Überreste von zwei spätmittelalterlichen Pferdeschädeln und von weiteren Tierknochen aus der Fahrgasse in Dreieichenhain. Bericht des Offenbacher Vereins für Naturkunde 96: 3-13.

Boessneck J, von den Driesch-Karpf, A. 1968. Tierknochenfunde von der Burg Nürnberg. Jahrbuch für fränkische Landesforschung 28: 73-92.

Clason AT, 1968. Die Tierreste aus der Motte bei Haus Meer, Gemeinde Büderich. Rheinische Ausgrabungen 1: 101-130.

Deschler-Erb S, Bopp-Ito M, Plogmann, HH. 2007. Die mittelalterlichen Tierknochen aus dem Keruzgangsbereich des Stiftes St. Arnual. In: Hermann H-W, Selmer J (eds). Leben und Sterben in einem mittelalterlichen Kollegialstift. Archäologische und baugeschichtliche Untersuchungen im ehemaligen Stift St. Arnual in Saarbrücken, pp. 523-538.

Doll M. 1998. Tierknochen. In: Dahm C, Lobbedey U, Weisgerber G (eds), Der Altenberg. Bergwerk und Siedlung aus dem 13. Jahrhundert im Siegerland. Denkmalpflege und Forschung in Westfalen 34: 169-179.

Doll M. 2001. Hochmittelalterliche Haustierhaltung in Höxter an der Weser. In: Pfrommer J, Schreg R (eds), Zwischen den Zeiten. Archäologische Beiträge zur Geschichte des Mittelalters in Mitteleuropa. Festschrift für Barbara Scholkmann, pp. 19-41.

Doll M. 2003. Haustierhaltung und Schlachtsitten des Mittelalters und der Neuzeit. Eine Synthese aus archäozoologischen, bildlichen und schriftlichen Quellen Mitteleuropas. Internationale Archäologie 78. Rahden/Westfalen: Leidorf.

Doll M. 2010. Forschungen zu Haus Horst in Gelsenkirchen. Tierknochen aus acht Jahrhunderten. Denkmalpflege und Forschung in Westfalen 49(4). Mainz: von Zabern.

Grimm J. 2005. Keine Lust zum Geschirrspülen? Auswertung der spätmittelalterlichen Tierknochen und der botanischen Reste aus der Remternische des Katharinenklosters in Stralsund. Mit einer baugeschichtlichen Einleitung. In: Ericsson I, Atzbach R(eds), Depotfunde aus Gebäuden Zentraleuropas = Concealed finds from buildings in Central Europe. Bamberger Kolloquien zur Archäologie des Mittelalters und der Neuzeit 1: 173-180.

Grimm J. 2010. Animal keeping and the use of animal products in medieval Emden (Lower Saxony, Germany). PhD Thesis, Universiteit Groningen. Available from: http://dissertations.ub.rug.nl/faculties/arts/2010/j.m.grimm/

Harre N. 1994. Die Nutzung der Tiere im Spätmittelalter-untersucht anhand der Tierknochenfunde der Burgruine Schnellerts bei Brensbach, Odenwaldkreis. In: Kokabi M, Wahl J (eds), Beiträge zur Archäozoologie und Prähistorischen Anthropologie. 8. Arbeitstreffen der Osteologen Konstanz 1993 im Andenken an Joachim Boessneck. Forschungen und Berichte zur Vor- und Frühgeschichte in Baden-Württemberg 53: 397-419. Stuttgart: Theiss.

Heinrich D. 1991. Untersuchungen an Skelettresten wildlebender Säugetiere aus dem mittelalterlichen Schleswig, Ausgrabung Schild 1971-1975. Ausgrabungen in Schleswig, Berichte und Studien 9. Neumünster: Karl-Wachholtz.

Heinrich D. 1995. Untersuchungen an Skelettresten von Pferden aus dem mittelalterlichen Schleswig. Ausgrabungen in Schleswig, Berichte und Studien 11: 115-177.

Hüster H. 1990. Untersuchungen an Skelettresten von Rindern, Schafen, Ziegen und Schweinen aus dem mittelalterlichen Schleswig, Ausgrabung Schild 1971-1975. Ausgrabungen in Schleswig. Berichte und Studien 8. Neumünster: Karl-Wachholtz.

Johansson F, Reichstein H. 1979. Einige Angaben zu Tierknochenfunden aus der Altstadt von Kiel. Offa 36: 152-162.

Kerth K, Landgraf I. 2001. Die Haustier- und Jagdwildreste auf der Burg Oberammerthal, Landkreis Amberg. In: Ettel P(ed), Karlburg-Rosstal-Oberammerthal. Studien zum frühmittelalterlichen Burgenbau in Nordbayern .Frühgeschichtliche und Provinzialrömische Archäologie. Materialien und Forschungen 5: 251-257.

Kocks B-M. 1978. Die Tierknochenfunde aus den Burgen auf dem Weinberg in Hitzacker/Elbe und in Dannenberg (Mittelalter). I. Die Nichtwiederkäuer. Diss. med. vet., Ludwig-Maximilians-Universität München.

Küchelmann C. 2010. Vornehme Mahlzeiten: Tierknochen aus dem Dominikanerkloster Norden. Nachrichten aus Niedersachsens Urgeschichte 79: 155-200.

Küchelmann C. 2014. Mit Knochen gepflastert-Tierknochenfunde vom Bremer Marktplatz. Schriften des Naturwissenschaftlichen Vereins für Schleswig-Holstein 73: 23-64

May E. 1985. Zu den Tierknochen aus mittelalterlichen Grabungskomplexen der Packhofgrabung in Braunschweig. In: Rötting H (ed), Stadtarchäologie in Braunschweig. Ein fachübergreifender Arbeitsbericht zu den Grabungen 1976-1984. Forschungen der Denkmalpflege in Niedersachsen 3: 307-313.

Müller H-H. 1977. Die Tierreste aus der Wiprechtsburg bei Groitzsch, Kr. Bona. Arbeits- und Forschungsberichte zur Sächsischen Bodendenkmalpflege 22: 101-170.

Müller H-H. 1990. Die Tierknochenfunde aus dem hochmittelalterlichen Herrensitz von Gliechow, Kr. Calau. Veröffentlichungen des Museums für Ur- und Frühgeschichte Potsdam 24: 233-241.

Müller H-H. 1996. Die Tierreste aus dem ehemaligen Königshof von Helfta. Jahresschrift für mitteldeutsche Vorgeschichte 78: 159-264.

Nobis G. 1957. Haustiere im frühgeschichtlichen Alt Lübeck. Der Stand der Forschung an den Tierknochen. Zeitschrift des Vereins für Lübeckische Geschichte und Altertumskunde 37: 145-154.

Nobis G. 1985. Untersuchung an Tierknochen aus den Grabungen auf der Burg Berge (Mons) - Altenberg (Rheinisch-Bergischer Kreis). Beiträge zur Archäologie des Mittelalters 3: 152-169.

Obermaier H. 2009. Tierknochenfunde vom "Hl. Berg" in Oberelchingen, Gem. Elchingen aus dem 11./12. und 16. Jh. Geschichte im Landkreis Neu-Ulm. Jahrbuch des Landkreises Neu-Ulm 15: 43-52.

Oehlmann B. 1989. Zur Bestimmung hochmittelalterlicher Tierknochen-Fundkomplexe unterschiedlicher Herkunft in Braunschweig. Nachrichten aus Niedersachsens Urgeschichte 58: 273-278.

Pasda K. 2004. Tierknochen als Spiegel sozialer Verhältnisse. Erlangen: Praehistorika archäologischer Verlag.

Paul A. 1978. Untersuchungen an Tierknochenfunden aus dem mittelalterlichen Lübeck: Grabung Königstraße 59-63. Lübecker Schriften zur Archäologie und Kulturgeschichte 1: 174-175.

Paul A. 1980. Untersuchungen an Tierknochen aus dem mittelalterlichen Lübeck (Grabung Königsstraße 59-63). Lübecker Schriften zur Archäologie und Kulturgeschichte 2: 7-104.

Paxinos PD. 2017. Die Archäozoologie der Pest. Die Auswirkungen des Schwarzen Todes (1347-1350) auf Viehnutzung, Wirtschaft und Handel in Deutschland. Unpublished PhD Thesis, Ludwig-Maximilians-Universität München.

Pieper H, Reichstein H. 1995. Untersuchungen an Skelettresten von Vögeln aus dem mittelalterlichen Schleswig. Ausgrabungen in Schleswig. Berichte und Studien 11: 9-113.

Pöllath N, Dohr A, Kaminski S, Kriegmair R, Scharafin U, Trixl S. 2010. Schindmähren und Knochenschlicker. Tierknochenfunde aus Aholming, Lkr. Deggendorf. In: Schmotz K (ed), Vorträge des 29. Niederbayerischen Archäologentages; pp. 211-234. Rahden/Westf.: Leidorf.

Pöllath N, von den Driesch A. 2000. Die Tierknochen aus Augsburg, "Beim Märzenbad 9". Zeugnisse für Ernährungsgewohnheiten und Handwerk im Hochmittelalter. Augsburger Beiträge zur Archäologie 3: 225-238.

Prilloff R-J. 1988. Untersuchungen mittelalterlicher Tierreste aus der Altmark. In: Rudolf F (ed), Beiträge zur Archäozoologie VII. Weimarer Monographien zur Ur- und Frühgeschichte 22: 58-82.

Prilloff R-J. 2000. Tierknochen aus dem mittelalterlichen Konstanz. Eine archäozoologische Studie zur Ernährungswirtschaft und zum Handwerk im Hoch- und Spätmittelalter. Materialhefte zur Archäologie in Baden-Württemberg 50. Stuttgart: Theiss.

Prilloff R-J. 2004. Hoch- und spätmittelalterliche Tierreste aus der Wartburg bei Eisenach, Grabung Palas-Sockelgeschoss. Wartburg-Jahrbuch 2003: 211-237.

Prümmel W. 1993. Starigard/Oldenburg. Hauptburg der Slawen in Wagrien. IV. Die Tierknochenfunde unter Berücksichtigung der Beizjagd. Offa 74. Neumünster: Karl Wachholtz.

Putzar R, Reichstein H. 1977. Frühneuzeitliche Tierknochenfunde aus der Curia Eckhorst bei Lübeck. Die Heimat. Zeitschrift für Natur- und Landeskunde von Schleswig-Holstein und Hamburg 4-5: 144-154.

Pyrozok A, Reichstein H. 1991. Tierknochenfunde aus hochmittelalterlichen Siedlungsablagerungen in Lübeck (Grabung Dr.-Julius-Leber-Strasse 58). Lübecker Schriften zur Archäologie und Kulturgeschichte 21: 183-202.

Reichstein H. 1981. Untersuchung an Tierknochen von der Isenburg bei Hattingen/Ruhr. Ein Beitrag zur Nahrungswirtschaft auf hochmittelalterlichen Burgen. Hattingen.

Reichstein H. 1993a. Tierknochen aus mittelalterlichen und frühneuzeitlichen Fundkomplexen aus dem Herforder Stiftsbereich. In: Grunsky E, Trier B (eds,. Das Damenstift Herford. Die archäologischen Ergebnisse zur Geschichte der Profan- und Sakralbauten seit dem späten 8. Jahrhundert. Band I, pp. 251-267.

Reichstein H. 1993b. Tierknochen aus der Ortswüstung Diderikeshusen bei Büren, Kr. Paderborn. In: Trier B(ed), Zwischen Pflug und Fessel. Mittelalterliches Landleben im Spiegel der Wüstungsforschung, pp. 119-129.

Reichstein H. 1999a. Die Nahrungsversorgung auf Burg Bodenteich, Kr. Uelzen, im Spiegel der Tierknochenfunde. In: Becker C, Manhart H, Peters J, Schibler J (eds). Historia Animalium ex Ossibus. Festschrift für Angela von den Driesch. Studia Honoraria 8, pp. 379-388. Rhden/Westf.: Leidorf.

Reichstein H. 1999b. Untersuchungen an Tierknochen. In: Janssen W, Janssen B (eds), Die frühmittelalterliche Niederungsburg bei Haus Meer, Kreis Neuss. Rheinische Ausgrabungen 46: 225-249.

Sachenbacher-Palavestra M. 1992. Tierknochenfunde aus der Wasserburg Rauenwörth bei Gungolding. Sammelblatt des Historischen Vereins Ingolstadt 101: 134-138.

Sachenbacher-Palavestra M. 1999. Tierknochenfunde aus der Lederergasse in Regensburg (11.-18. Jahrhundert). Materialhefte zur Archäologie des Mittelalters und der Neuzeit 4: 128-137.

Schmidt E, Scholkmann B. 1981. Die Nikolauskapelle auf dem Grünen Hof in Ulm. Ergebnisse einer archäologischen Untersuchung. Mit Beiträgen von Stefan Kummer und Franz Quarthal. Forschungen und Berichte der Archäologie des Mittelalters in Baden-Württemberg 7: 303-370.

Schoon R. 1998a. Die Tierknochenfunde von der Posteburg bei Schmarrie, Gde. Hülsede, Ldkr. Schaumburg (um 1400 n.Chr.). Nachrichten aus Niedersachsens Urgeschichte 67: 151-170.

Schoon R. 1998b. Untersuchungen an Tierknochenfunden von der Burg Plesse, Gem. Bovenden, Landkreis Göttingen (12.-17. Jahrhundert). Plesse-Archiv 32: 7-180.

Schoon R. 2000. Untersuchungen an Tierknochenfunden des 9. bis 20. Jahrhunderts vom Domhof in Hildesheim. In: Kruse KB (ed). Der Hildesheimer Dom. Von der Kaiserkapelle und den Karolingischen Kathedralkirchen bis zur Zerstörung 1945. Grabungen und Bauuntersuchungen auf dem Domhügel 1988 bis 1999. Materialhefte zur Ur- und Frühgeschichte Niedersachsens 27: 453-507.

Schröder B. 1984. Untersuchung an Tierknochenfunden aus alt- und jungslawischen Siedlungsschichten des Burgwalls Alt Lübeck. In: Amt für Vor- und Frühgeschichte (Bodendenkmalpflege) der Hansestadt Lübeck (ed), Forschungsprobleme um den slawischen Burgwall Alt Lübeck, pp. 47-87.

Schulze-Rehm C. 1998. Einbeck, Negenborner Weg. Die Tierknochen aus der mittelalterlichen Töpferei. In: Heege A(ed), Einbeck, Negenborner Weg. Band 1: Naturwissenschaftliche Studien zu einer Töpferei des 12. und frühen 13. Jahrhunderts. Keramiktechnologie, Paläoethnobotanik, Pollenanalyse, Archäozoologie, pp. 189-224.

Spahn N. 1986. Untersuchungen an Skelettresten von Hunden und Katzen aus dem mittelalterlichen Schleswig, Ausgrabung Schild 1971-1975. Ausgrabungen in Schleswig, Berichte und Studien 5. Neumünster: Karl-Wachholtz.

Vagedes K. 1994. Die Tierknochenfunde aus Karlburg. Diss. med. vet., Ludwig-Maximilians-Universität München.

Vagedes K. 2001. Die Tierknochenfunde aus Karlburg. Ein Vergleich zwischen Burg und Talsiedlung. In. Ettel P (ed), Karlburg-Rosstal-Oberammerthal. Studien zum

frühmittelalterlichen Burgenbau in Nordbayern. Frühgeschichtliche und Provinzialrömische Archäologie. Materialien und Forschungen 5: 305-315.

Vagedes K, Peters J. 2001. Die Faunenreste aus der karolingisch-ottonischen Reichsburg in Roßtal, Landkreis Fürth. In. Ettel P (ed), Karlburg-Rosstal-Oberammerthal. Studien zum frühmittelalterlichen Burgenbau in Nordbayern. Frühgeschichtliche und Provinzialrömische Archäologie. Materialien und Forschungen 5: 317-339.

von den Driesch A. 1995. Tierhaltung und Jagd. Aspekte der Ernährung auf der Burg Sulzberg. In: Behrer C, von den Driesch A, Kata B, Pfister P, Burg Sulzberg. Von der Turmburg zum Jagdschloss, pp. 193-201.

von den Driesch A, Manhart H. 1994. Schloß Murnau. Die Tierknochenfunde (13. - 18. Jahrhundert). In: Schloßmuseum Murnau (ed), Schloß Murnau. Ein Bauwerk der Stauferzeit und seine Geschichte. Forschungen zur Archäologie des Mittelalters und der Neuzeit in Bayern 1: 280-290.

von Waldstein C. 1992. Die Tierknochenfunde von der spätmittelalterlichen Wasserburg in Oberursel-Bommersheim/Hochtaunuskreis. Diss. med. vet., Ludwig-Maximilians-Universität München.

Walcher HF. 1978. Die Tierknochenfunde aus den Burgen auf dem Weinberg in Hitzacker/Elbe und in Dannenberg (Mittelalter). II. Die Wiederkäuer. Diss. med. vet., Ludwig-Maximilians-Universität München.

Wustrow C. 2004. Die Tierknochen aus der Alte-Burg von Rotenhain. Berichte zur Archäologie an Mittelrhein und Mosel 9: 230-233.

Conclusions

Population genetic inference using ancient DNA has traditionally suffered from several methodological challenges. Sample quality is low and non-uniform, and samples are distributed sparsely across space and time, rendering traditional population genetic approaches inadequate. As a result, inference using ancient DNA data has often relied on more informal and interpretive approaches, which do not allow explicit and rigorous hypothesis testing and where results are open to subjective interpretation of individual researchers. Although there are methods designed to test specific population genetic models (using the assumption that population history can be viewed as a species trees), as a general rule they do not accommodate spatially and temporally explicit hypothesis testing. Consequently, the results of such analyses are difficult to interpret within the archaeological and palaeoecological context. In this thesis I have provided three approaches specifically tailored to using ancient DNA data for testing hypothesis of spatially and temporally explicit demographic and evolutionary histories. Below I summarise the main analytical challenges, how the approaches presented above have overcome them, and the some theoretical advantages they bring to the evolutionary inference from ancient DNA data. Finally I outline some of the outstanding methodological challenges and future directions for the evolutionary inference using ancient DNA.

Sparseness of samples in space and in time

One of the key advantages ancient DNA brings to the population genetic inference is the possibility to directly observe of how evolution and other population genetic processes have acted in the past. However, traditional population genetic approaches are tailored to population level samples – rarely achievable in most archaeological and fossil contexts. To overcome the problem of temporal sparseness of data, samples are frequently grouped based on temporal proximity (which in some cases can be up to thousands of years) and treated as a temporally homogeneous sample. As discussed in Chapters 2 and 4, this usually results in a substantial loss in temporal resolution in the analysis. This issue is compounded by the fact that samples of different ages are not equivalent because evolutionary processes, such as genetic drift and mutations, have acted more on younger samples than older ones. Ignoring this heterogeneity further increases the level of noise

in the analysis and can potentially bias the inference (Depaulis et al. 2009; Skoglund, Sjödin, et al. 2014).

In Chapter 4 I addressed the issue of temporal sparseness when inferring the action of natural selection in the European domestic chicken population. This example illustrates a classic ancient DNA dataset where inference is complicated by the sparse sample distribution over time and sample date uncertainty. Here ancient DNA data from the *TSHR* gene from c.a. 60 samples (with dates spanning the last 2,500 years) suggest that the average frequency of the derived allele was substantially lower in ancient populations compared to the contemporary ones. This is consistent with the footprint of strong and recent selection found around this locus in present-day populations. Knowing the exact allele frequency through time would allow direct observation of selection, its starting time and its strength. Although it would, in principle, be possible to use the ancient DNA data to directly estimate allele frequencies through time in windows across the time period, in practice this is not feasible as the data is too scattered to obtain any meaningful temporal accuracy.

To overcome this problem, I have taken advantage of the fact that although samples are distributed too sparsely for direct calculation of allele frequencies through time, each samples carries some information about the allele frequency in the population at its sampling point. By modelling the allele frequency trajectory through time, it is possible to link the samples to an underlying allele frequency curve: in particular, if each data point represents a sample randomly drawn from the population, the probability of observing a particular allele is given by its frequency in the population at the time. Thus, even though each single sample provides only a modest amount of evidence in support (or lack of support) for a given curve, when considered together the temporally sparse samples can provide powerful means for comparing different allele frequency trajectories. In Chapter 4 this approach allowed, despite a relatively modest sample size, to estimate the starting time of selection and its strength with remarkable precision. Vital to this was having few samples distributed across the period of change rather than great number of samples at few time points. This example shows that not only can the noise be reduced by explicitly accounting for heterogeneous sample distribution in time but also inference can gain considerable additional power by doing so.

The genetic selection example in Chapter 4 dealt with temporal heterogeneity, but many demographic processes involve both space and time. In this case, samples are typically not only sparse in time, but also scattered across different locations for different time periods, making inference about demographic processes challenging. In Chapter 2 I present a novel method for estimating mobility within archaeological populations (or regions). This approach builds on classical population genetic methods, that link genetic differences to geographic distances in contemporary populations, and extends them to explicitly consider both space and time. In Chapter 2 I show that ignoring time differences and using classical methods on (temporally sparse) samples compressed into discrete time slices results in a significant loss of power to infer past changes in movement rates. A key contributing factor to this loss of information is that movement (mobility) affects not only the geographic distribution of genetic variation but also genetic differences between samples from the same location but different time points. This is a problem when ignoring temporal information, as it confounds the link between genetic variation and space within a time slice. In Chapter 2, I show that the classical approach can be generalised to compare genetic differences to differences in space-time, thus explicitly taking advantage of the extra information provided by temporal differences. Converting time into space introduces a parameter with the physical dimension of speed. I show using spatially explicit simulations that the parameter estimated using this approach is indeed proportional to the level of mobility used in the simulations, allowing the statistic to be interpreted in physical terms and quantifying mobility through time. However, it is not possible to estimate an absolute level as the constant of proportionality depends on various properties of the populations, such as its size, that is not readily available in most applications.

Explicitly taking spatial and temporal information into account is even more important when considering complex demographic scenarios as these often leave subtle differences in genetic patterns over space and time. In Chapter 3 I reconstruct the demographic history of Grey wolves using mtDNA. As discussed in Chapter 1, analysis of mitochondrial DNA is challenging as it represents a single outcome of a highly stochastic process. However, as mitochondrial DNA is more easily retrievable from ancient samples, significantly better spatial and temporal coverage can be achieved. This

illustrates further how scant or noisy information can contribute to analysis when its geographic and temporal location is explicitly taken into account.

Date Uncertainty

Not only are ancient DNA samples sparsely distributed in space and in time but challenges also stem from uncertainty associated sample dates: unlike sampling times for genetic data from contemporary individuals, it is rarely possible to directly observe the age of ancient DNA samples. The level of uncertainty can depend on sample preservation, its archaeological context and available dating methods, and can therefore vary substantially between samples. In the ancient DNA context, direct radiocarbon dating of the sample typically yields the narrowest time estimates, but is not always available (e.g. due to lack of sample material) or feasible or appropriate (e.g. due to contamination, or age of the sample). In some cases, it may be possible to obtain a date from the archaeological context of the sample, but at the expense of additional uncertainty.

Above, I discussed the importance of explicitly accounting for sample ages, as they can strongly affect the analysis. Thus, to avoid bias it is also important to account for date uncertainty. In population genetic models that explicitly take temporal information into account, such as those presented in this thesis, this is relatively straightforward to do so: in Chapters 2 and 4 I have simply sampled dates from available date range for each sample when calculating the statistic (in Chapter 2) or when computing the likelihoods of the curves (in Chapter 4). This produces probability density distributions that explicitly account for sample age uncertainty. In demographic analysis presented in Chapter 3 majority of samples were directly radiocarbon dated resulting in very small sample date uncertainty relative to the time scales considered in the analysis. As a result, it was justified to use point estimates instead of age intervals and by doing so reduced the computational complexity of an otherwise computationally demanding analysis.

In certain cases, no temporal information is available or covers too large time period to be of any practical use for temporally explicit inference. In such cases, approximate dates can be obtained using a molecular clock based on genetic information, where the clock is calibrated using a panel of ancient DNA samples with directly estimated dates (Fu et al. 2014; Rieux et al. 2014). In Chapter 3, I have estimated the mitochondrial mutation rate for wolves and used this to date samples that otherwise lack date estimates. Using a leave-one-out analysis on directly dated samples I also show that the date estimates obtained

using this method are statistically unbiased. However, the confidence intervals of the obtained dates are much larger compared to intervals obtained by direct radiocarbon dating of samples.

Formal hypothesis testing

Reconstructing the past demographic and evolutionary processes is inherently challenging as there is, in principle, an infinite number of histories that could have led to the present. Archaeological and ancient DNA data provide observations of the past that in principle can be used to reject the most unlikely scenarios and hypotheses. However, such information is rarely directly informative of the past and the data is only weakly constrained by the underlying histories. Therefore, not only can many different histories result in similar present-day patterns, but also in similar patterns of past variation.

As discussed above, this problem is magnified by the inherent sparseness of ancient DNA data in combination with the lack of tools that explicitly account for it. As a result, researchers have often resorted to more descriptive and interpretive approaches to studying the past (reviewed in Chapter 1). But as these approaches do not explicitly consider a range of alternative scenarios, there is great potential for subjective biases to affect the interpretation, not the least the temptation to weave a compelling story from the patterns without formally testing if the same pattern could be explained by another *a priory* equally likely scenario. Although the story can be true, without proper hypothesis testing it is impossible to tell how strongly the evidence speak in its favour or against it. Thus, in order to avoid such biases and a false sense of accuracy, a range of plausible scenarios needs to be identified and then explicitly compared using formal statistical and analytical techniques.

Using models to formally describe demographic scenarios makes assumptions explicit and thereby avoids subjective and unintentional biases (Gerbault et al. 2014). However, this often comes at a cost of making the inference analytically more challenging and computationally costly. Also, the use of models does not itself guarantee that the correct scenario will be identified by the analysis: the use of incorrect assumptions or exclusion of certain key assumptions can lead to model biases, while analysis based on overly complex models can be led astray by noise in the data (i.e. over-fitting). Thus, it is important that the models tested are as simple as possible, while still representing the key processes resulting in observed patterns of variation. Bayesian analysis enables

quantification of the information gained from using additional parameters and can therefore help to limit model complexity to a level where only informative parameters are used in the analysis. Such demographic models are also flexible in the sense that they can be re-evaluated as new data becomes available, and the analysis can be tailored to the data that is available (such as different kinds of genetic markers) without changing the underlying demographic model.

In chapter 4, a wide range of selection scenarios that reflect different starting times, selection strengths and levels of long-range gene flow could potentially explain the observed genotypes through time. With only a limited amount of data scattered over a 2,500 year time period, attempting to reconstruct the history of this population may seem futile. However, by explicitly calculating how likely the data is to be observed under each scenario, I was able to show that only a narrow sub-set of scenarios have a high likelihood for generating the observed data. From this analysis it is also clear which time periods are well resolved by the data and where it is less precise, thereby avoiding a false sense of accuracy where it is not merited. By allowing identification of less well-resolved time periods, such models can also guide additional sampling strategies.

Chapter 3 shows how hypothesis testing is vital when data is noisy and sparse, the possible scenarios are complex, and only subtle differences in genetic patterns are available to tell them apart; in such cases intuition can often fail and it can be tempting to over-interpret details in the patterns that are largely the result of chance.

Linking genetic evolution to environmental and cultural drivers

Pinpointing the timing of evolutionary events in a population allows identifying their potential causes and consequences. In Chapter 4 I achieved narrow enough time estimates to allow directly link the changes in selection on chickens to historical and archaeological data, thereby giving direct insight to the potential drivers of selection.

In addition to time, geographic location carries information about ecology, climate, geography and other environmental or cultural factors that could play important roles in shaping processes affecting past populations. However, reconstructing the geographic locations of past populations from genetic information is challenging. Although several approaches exist that allow explicit testing of different demographic scenarios using ancient DNA data, they rarely explicitly account for spatial variation between each

sample. This renders the demographic models abstract and leave the ancestral populations within them, and the inferred events and process that affect them, without explicit geographic interpretation. As a result, it is not possible to directly link inferred demographic histories to external information such as archaeological, historical and climatic data. This severely limits the ability to reconstruct the environments and properties of these past population and to identify potential ecological, cultural and climatic drivers behind the inferred processes.

Spatially and temporally explicit models can overcome this limitation. For example, Chapter 3 uses a spatially explicit model of Grey wolf demography to reconstruct their history from the late Pleistocene to present day. Within this framework I tested a range of different demographic scenarios that were motivated by the morphological evidence in fossil record as well as present-day genetic variation of wolves across the Northern Hemisphere. This analysis identified a range expansion around the Last Glacial Maximum that replaced the local populations in Eurasia and the Americas. Because of the spatially explicit nature of the model, I was able to pinpoint Beringia as the source of this expansion and to link the findings of the genetic analysis to the fossil record to interpret observed changes in wolf fossil morphology during this time period.

In addition to allowing direct interpretation of the genetic patterns within the archaeological, climatic, fossil and historical contexts, spatially and temporally explicit models enable information from external sources to be explicitly incorporated into the analysis. For example, in Chapter 3 I used known geographical features as likely barriers to gene flow to inform the spatial model of wolf demography, and in Chapter 4 I was able to take advantage of the historically well documented gene-flow from Asia at the time of formation of modern chicken breeds to inform the analysis. In a similar fashion, spatially and temporally explicit models can take advantage of range of external information, including reconstructions of past climate e.g. (Eriksson et al. 2012; Timmermann and Friedrich 2016), species and other resource distributions, availability of raw material, just to name a few.

Future Challenges

The recent increase in availability and quality of ancient DNA data has fuelled a drive to address ever more detailed archaeological and anthropological hypotheses, which entails increasingly complex and multifactorial analysis. I have shown that inference from

ancient DNA can greatly benefit from analyses that formally compare different evolutionary and demographic scenarios, both because of the increased power that comes from considering the full information in the data and from the reduced risk of subjective biases that comes with formal hypothesis testing. I have argued in this thesis that as archaeological and historic hypotheses are traditionally formulated as processes across space and time, analysis frameworks that can explicitly represent such processes offer significant advantages for formal hypothesis testing. Despite several ongoing interdisciplinary projects (e.g. Knipper et al. 2017), existing methods lack the ability to formally combine different lines of evidence such as different types of genetic, isotope and artefact data. This would greatly facilitate the study of and comparison between cultural and demographic processes and would enable researchers to formally test a wider range of archaeological and historical hypotheses. Furthermore, analysis frameworks that are able to incorporate genetic, osteological and fossil morphology data would allow extending analyses and reconstruction of past demographic processes to geographic regions and time periods for which we currently lack ancient DNA, and explore long-standing areas of research such as the relationships between different Middle-Pleistocene hominin groups and the origins of Neanderthals and Anatomically Modern Humans.

Reconstructing past demographic processes is important for formulating new as well as testing existing hypothesis about the past. Nevertheless, understanding how different traits have evolved in response to shifts in environments and cultural practices are central to anthropological and archaeological research. Although, ancient DNA has transformed our ability to study past genetic selection, current analysis has been largely limited to single genetic variants with strong effects. The traits most relevant to anthropological and archaeological research (e.g. physical characteristics, dietary adaptations, and susceptibility to diseases), however, are commonly controlled by many genes working together in interconnected networks that are partly overlapping across different traits. In order to understand the evolution of such traits it is necessary to extend the selection analysis to networks of different genes and their expression and regulation patterns. This could be done, for example, by including known expression quantitative trait loci (eQTLs) and predicted gene activity from methylation patterns that has only recently become possible on a genome-wide scale thanks to large-scale efforts to map regulatory variants in the human genome (such as ENCODE and GTEx). This analysis is challenged

in ancient DNA data by the reduced quality and variable coverage across the genome stemming from DNA degradation. Perhaps even more problematic for analysis of complex trait evolution is that most ancient DNA data is only available in the form of targeted enrichment and capture of specific loci (the most prevalent being the genome-wide panel of 1.2 million SNPs first published in Mathieson et. al. 2015), meaning that that some genetic loci associated with complex traits are likely to be missing from the datasets. A great challenge facing the field of ancient DNA is to combine this type of data with whole genome data to maximize the amount of information available for analysis. Currently, a common approach to solve these problems is to use imputation, a statistical approach using large reference panels of modern whole genome sequences to estimate the missing genetic variants. However, as genetic variant get shuffled around at every generation this approach becomes increasingly problematic with increasing age of the samples. This is especially true of genetic variants subject to positive selection, as recently demonstrated by Mathieson & Mathieson (2018). There is therefore a great need for alternative approaches tailored to ancient DNA and robust to these biases.

Although there are number of methodological and computational hurdles that need to be overcome for formal evolutionary inference using ancient DNA to reach its full potential, the greatest problem by far is that despite obvious analytical advantages, the frameworks for spatiotemporally explicit analysis using ancient DNA have not spread far beyond the laboratories where they were initially developed. A key reason for the limited uptake of these approaches among laboratories specialized in ancient DNA data generation is that the analytical frameworks are usually tailored to testing specific evolutionary scenarios using specific data sets. The lack of separation between the mathematical inference models and types of genetic data used, the details of the demographic scenarios, and environmental and other external factors that affect demography and selection makes it difficult to make changes to the analysis without fundamentally changing the computer code. Thus, a front end to the simulation programmes in which demographic and evolutionary scenarios can be designed, tested and visualised without explicit knowledge of the internal workings of the code could go a long way towards increasing the adoption of this type of analysis.

In summary, in this thesis I have presented approaches to overcome some of the most outstanding analytical challenges that currently exist in the field of ancient DNA research,

and applied them to cases that cover a wide range of demographic histories and evolutionary questions spanning different time-scales, species and types of data. I have shown that inference from ancient DNA can greatly benefit from analyses that formally compare different evolutionary and demographic scenarios, both because of the increased power that comes from considering the full information in the data and from the reduced risk of subjective biases that comes with formal hypothesis testing. I have also shown that analysis of ancient DNA data can not only benefit from spatially and temporally explicit model testing but this type of framework is crucial for being able to directly test archaeological hypothesis using genetic data.

Bibliography

Adler CJ, Dobney K, Weyrich LS, Kaidonis J, Walker AW, Haak W, Bradshaw CJA, Townsend G, Sołtysiak A, Alt KW, et al. 2013. Sequencing ancient calcified dental plaque shows changes in oral microbiota with dietary shifts of the Neolithic and Industrial revolutions. Nat. Genet. 45:450–455.

Alexander DH, Novembre J, Lange K. 2009. Fast model-based estimation of ancestry in unrelated individuals. Genome Res. 19:1655–1664.

Allentoft ME, Collins M, Harker D, Haile J, Oskam CL, Hale ML, Campos PF, Samaniego JA, Gilbert MTP, Willerslev E, et al. 2012. The half-life of DNA in bone: measuring decay kinetics in 158 dated fossils. Proc. R. Soc. B Biol. Sci. 279:4724–4733.

Allentoft ME, Sikora M, Sjögren K-G, Rasmussen S, Rasmussen M, Stenderup J, Damgaard PB, Schroeder H, Ahlström T, Vinner L, et al. 2015. Population genomics of Bronze Age Eurasia. Nature 522:167–172.

Andrades Valtueña A, Mittnik A, Key FM, Haak W, Allmäe R, Belinskij A, Daubaras M, Feldman M, Jankauskas R, Janković I, et al. 2017. The Stone Age Plague and Its Persistence in Eurasia. Curr. Biol. 27:3683–3691.e8.

Ballard JWO, Whitlock MC. 2004. The incomplete natural history of mitochondria. Mol. Ecol. 13:729–744.

Balloux F. 2010. The worm in the fruit of the mitochondrial DNA tree. Heredity 104:419.

Bollback JP, York TL, Nielsen R. 2008. Estimation of 2Nes From Temporal Allele Frequency Data. Genetics 179:497–502.

Bollongino R, Vigne J-D. 2008. Temperature monitoring in archaeological animal bone samples in the Near East arid area, before, during and after excavation. J. Archaeol. Sci. 35:873–881.

Carpenter ML, Buenrostro JD, Valdiosera C, Schroeder H, Allentoft ME, Sikora M, Rasmussen M, Gravel S, Guillén S, Nekhrizov G, et al. 2013. Pulling out the 1%: Whole-Genome Capture for the Targeted Enrichment of Ancient DNA Sequencing Libraries. Am. J. Hum. Genet. 93:852–864.

Castelo R, Roverato A. 2012. Inference of regulatory networks from microarray data with R and the bioconductor package qpgraph. Methods Mol. Biol. Clifton NJ 802:215–233.

Collins MJ, Nielsen-Marsh CM, Hiller J, Smith CI, Roberts JP, Prigodich RV, Wess TJ, Csapo J, Millard AR, Turner-Walker G. 2002. The survival of organic matter in bone: a review. Archaeometry 44:383–394.

Currat M, Excoffier L. 2011. Strong reproductive isolation between humans and Neanderthals inferred from observed patterns of introgression. Proc. Natl. Acad. Sci. 108:15129–15134.

Dabney J, Meyer M, Pääbo S. 2013. Ancient DNA Damage. Cold Spring Harb. Perspect. Biol. 5(7): a012567.

Dalén L, Lagerholm VK, Nylander JAA, Barton N, Bochenski ZM, Tomek T, Rudling D, Ericson PGP, Irestedt M, Stewart JR. 2017. Identifying Bird Remains Using Ancient DNA Barcoding. Genes 8:169.

Depaulis F, Orlando L, Hänni C. 2009. Using Classical Population Genetics Tools with Heterochroneous Data: Time Matters! PLoS ONE 4:e5541.

Eriksson A, Betti L, Friend AD, Lycett SJ, Singarayer JS, Cramon-Taubadel N von, Valdes PJ, Balloux F, Manica A. 2012. Late Pleistocene climate change and the global expansion of anatomically modern humans. Proc. Natl. Acad. Sci. 109:16089–16094.

Eriksson A, Manica A. 2012. Effect of ancient population structure on the degree of polymorphism shared between modern human populations and ancient hominins. Proc. Natl. Acad. Sci. 109:13956–13960.

Excoffier L, Dupanloup I, Huerta-Sánchez E, Sousa VC, Foll M. 2013. Robust Demographic Inference from Genomic and SNP Data. PLOS Genet. 9:e1003905.

Feder AF, Kryazhimskiy S, Plotkin JB. 2014. Identifying signatures of selection in genetic time series. Genetics 196:509–522.

Fu Q, Li H, Moorjani P, Jay F, Slepchenko SM, Bondarev AA, Johnson PLF, Aximu-Petri A, Prüfer K, de Filippo C, et al. 2014. Genome sequence of a 45,000-year-old modern human from western Siberia. Nature 514:445–449.

Fu Q, Posth C, Hajdinjak M, Petr M, Mallick S, Fernandes D, Furtwängler A, Haak W, Meyer M, Mittnik A, et al. 2016. The genetic history of Ice Age Europe. Nature 534:200–205.

Gamba C, Jones ER, Teasdale MD, McLaughlin RL, Gonzalez-Fortes G, Mattiangeli V, Domboróczki L, Kővári I, Pap I, Anders A, et al. 2014. Genome flux and stasis in a five millennium transect of European prehistory. Nat. Commun. 5:5257.

Gerbault P, Allaby RG, Boivin N, Rudzinski A, Grimaldi IM, Pires JC, Vigueira CC, Dobney K, Gremillion KJ, Barton L, et al. 2014. Storytelling and story testing in domestication. Proc. Natl. Acad. Sci. 111:6159–6164.

Gilbert MTP, Tomsho LP, Rendulic S, Packard M, Drautz DI, Sher A, Tikhonov A, Dalén L, Kuznetsova T, Kosintsev P, et al. 2007. Whole-Genome Shotgun Sequencing of Mitochondria from Ancient Hair Shafts. Science 317:1927–1930.

Girdland Flink L, Allen R, Barnett R, Malmstrom H, Peters J, Eriksson J, Andersson L, Dobney K, Larson G. 2014. Establishing the validity of domestication genes using DNA from ancient chickens. Proc. Natl. Acad. Sci. 111:6184–6189.

Green RE, Krause J, Briggs AW, Maricic T, Stenzel U, Kircher M, Patterson N, Li H, Zhai W, Fritz MH-Y, et al. 2010. A Draft Sequence of the Neandertal Genome. Science 328:710–722.

Gronau I, Hubisz MJ, Gulko B, Danko CG, Siepel A. 2011. Bayesian inference of ancient human demography from individual genome sequences. Nat. Genet. 43:1031–1034.

Gutenkunst RN, Hernandez RD, Williamson SH, Bustamante CD. 2009. Inferring the Joint Demographic History of Multiple Populations from Multidimensional SNP Frequency Data. PLOS Genet. 5:e1000695.

Haak W, Lazaridis I, Patterson N, Rohland N, Mallick S, Llamas B, Brandt G, Nordenfelt S, Harney E, Stewardson K, et al. 2015. Massive migration from the steppe was a source for Indo-European languages in Europe. Nature 522:207–211.

Haile J, Froese DG, MacPhee RDE, Roberts RG, Arnold LJ, Reyes AV, Rasmussen M, Nielsen R, Brook BW, Robinson S, et al. 2009. Ancient DNA reveals late survival of mammoth and horse in interior Alaska. Proc. Natl. Acad. Sci. 106:22352–22357.

Hey J, Nielsen R. 2007. Integration within the Felsenstein equation for improved Markov chain Monte Carlo methods in population genetics. Proc. Natl. Acad. Sci. 104:2785–2790.

Horsburgh KA. 2008. Wild or domesticated? An ancient DNA approach to canid species identification in South Africa's Western Cape Province. J. Archaeol. Sci. 35:1474–1480.

Jónsson H, Ginolhac A, Schubert M, Johnson PLF, Orlando L. 2013. mapDamage2.0: fast approximate Bayesian estimates of ancient DNA damage parameters. Bioinforma. Oxf. Engl. 29:1682–1684.

Knapp M, Hofreiter M. 2010. Next Generation Sequencing of Ancient DNA: Requirements, Strategies and Perspectives. Genes 1:227–243.

Knipper C, Mittnik A, Massy K, Kociumaka C, Kucukkalipci I, Maus M, Wittenborn F, Metz SE, Staskiewicz A, Krause J, et al. 2017. Female exogamy and gene pool diversification at the transition from the Final Neolithic to the Early Bronze Age in central Europe. PNAS:201706355.

Korneliussen TS, Albrechtsen A, Nielsen R. 2014. ANGSD: Analysis of Next Generation Sequencing Data. BMC Bioinformatics 15:356.

Krause J, Lalueza-Fox C, Orlando L, Enard W, Green RE, Burbano HA, Hublin J-J, Hänni C, Fortea J, de la Rasilla M, et al. 2007. The Derived FOXP2 Variant of Modern Humans Was Shared with Neandertals. Curr. Biol. 17:1908–1912.

Lacerda M, Seoighe C. 2014. Population Genetics Inference for Longitudinally-Sampled Mutants Under Strong Selection. Genetics 198:1237–1250.

Lalueza-Fox C, Römpler H, Caramelli D, Stäubert C, Catalano G, Hughes D, Rohland N, Pilli E, Longo L, Condemi S, et al. 2007. A Melanocortin 1 Receptor Allele Suggests Varying Pigmentation Among Neanderthals. Science 318:1453–1455.

Larson G, Albarella U, Dobney K, Rowley-Conwy P, Schibler J, Tresset A, Vigne J-D, Edwards CJ, Schlumbaum A, Dinu A, et al. 2007. Ancient DNA, pig domestication, and the spread of the Neolithic into Europe. Proc. Natl. Acad. Sci. 104:15276–15281.

Lawson DJ, Hellenthal G, Myers S, Falush D. 2012. Inference of Population Structure using Dense Haplotype Data. PLOS Genet. 8:e1002453.

Lazaridis I, Nadel D, Rollefson G, Merrett DC, Rohland N, Mallick S, Fernandes D, Novak M, Gamarra B, Sirak K, et al. 2016. Genomic insights into the origin of farming in the ancient Near East. Nature 536:419–424.

Leonardi M, Librado P, Der Sarkissian C, Schubert M, Alfarhan AH, Alquraishi SA, Al-Rasheid KAS, Gamba C, Willerslev E, Orlando L. 2017. Evolutionary Patterns and Processes: Lessons from Ancient DNA. Syst. Biol. 66:e1–e29.

Li H, Durbin R. 2011. Inference of human population history from individual whole-genome sequences. Nature 475:493–496.

Librado P, Orlando L, Hernandez R. 2018. Detecting Signatures of Positive Selection along Defined Branches of a Population Tree Using LSD. Mol Biol Evol 35:1520–1535.

Liepelt S, Sperisen C, Deguilloux M-F, Petit RJ, Kissling R, Spencer M, De Beaulieu J-L, Taberlet P, Gielly L, Ziegenhagen B. 2006. Authenticated DNA from Ancient Wood Remains. Ann Bot 98:1107–1111.

Lindahl T. 1993. Instability and decay of the primary structure of DNA. Nature 362:709–715.

Liu H, Prugnolle F, Manica A, Balloux F. 2006. A Geographically Explicit Genetic Model of Worldwide Human-Settlement History. Am. J. Hum. Genet. 79:230–237.

Llorente MG, Jones ER, Eriksson A, Siska V, Arthur KW, Arthur JW, Curtis MC, Stock JT, Coltorti M, Pieruccini P, et al. 2015. Ancient Ethiopian genome reveals extensive Eurasian admixture in Eastern Africa. Science 350:820–822.

Ludwig A, Pruvost M, Reissmann M, Benecke N, Brockmann GA, Castanos P, Cieslak M, Lippold S, Llorente L, Malaspinas A-S, et al. 2009. Coat Color Variation at the Beginning of Horse Domestication. Science 324:485–485.

Malaspinas A-S, Malaspinas O, Evans SN, Slatkin M. 2012. Estimating Allele Age and Selection Coefficient from Time-Serial Data. Genetics 192:599–607.

Malaspinas A-S. 2016. Methods to characterize selective sweeps using time serial samples: an ancient DNA perspective. Molecular Ecology 25:24–41.

Malaspinas A-S, Westaway MC, Muller C, Sousa VC, Lao O, Alves I, Bergström A, Athanasiadis G, Cheng JY, Crawford JE, et al. 2016. A genomic history of Aboriginal Australia. Nature 538:207–214.

Marchini J, Howie B. 2010. Genotype imputation for genome-wide association studies. Nat. Rev. Genet. 11:499–511.

Marciniak S, Perry GH. 2017. Harnessing ancient genomes to study the history of human adaptation. Nature Reviews Genetics 18:659–674.

Mathieson I, Alpaslan-Roodenberg S, Posth C, Szécsényi-Nagy A, Rohland N, Mallick S, Olalde I, Broomandkhoshbacht N, Candilio F, Cheronet O, et al. 2018. The genomic history of southeastern Europe. Nature [Internet]. Available from: https://www.nature.com/articles/nature25778

Mathieson I, Lazaridis I, Rohland N, Mallick S, Patterson N, Roodenberg SA, Harney E, Stewardson K, Fernandes D, Novak M, et al. 2015. Genome-wide patterns of selection in 230 ancient Eurasians. Nature 528:499–503.

Mathieson I, McVean G. 2013. Estimating Selection Coefficients in Spatially Structured Populations from Time Series Data of Allele Frequencies. Genetics 193:973–984.

Mathieson S, Mathieson I. 2018. FADS1 and the timing of human adaptation to agriculture. bioRxiv:337998.

McDonald JH, Kreitman M. 1991. Adaptive protein evolution at the Adh locus in Drosophila. Nature. 351:652–654

McRae BH, Beier P. 2007. Circuit theory predicts gene flow in plant and animal populations. Proc. Natl. Acad. Sci. 104:19885–19890.

McRae BH, Dickson BG, Keitt TH, Shah VB. 2008. Using Circuit Theory to Model Connectivity in Ecology, Evolution, and Conservation. Ecology 89:2712–2724.

Meyer M, Arsuaga J-L, de Filippo C, Nagel S, Aximu-Petri A, Nickel B, Martínez I, Gracia A, de Castro JMB, Carbonell E, et al. 2016. Nuclear DNA sequences from the Middle Pleistocene Sima de los Huesos hominins. Nature 531:504–507.

Nielsen R. 2004. Population genetic analysis of ascertained SNP data. Hum. Genomics 1:218.

Nielsen R, Beaumont MA. 2009. Statistical inferences in phylogeography. Mol. Ecol. 18:1034–1047.

Nielsen R, Korneliussen T, Albrechtsen A, Li Y, Wang J. 2012. SNP Calling, Genotype Calling, and Sample Allele Frequency Estimation from New-Generation Sequencing Data. PLOS ONE 7:e37558.

Novembre J, Johnson T, Bryc K, Kutalik Z, Boyko AR, Auton A, Indap A, King KS, Bergmann S, Nelson MR, et al. 2008. Genes mirror geography within Europe. Nature 456:98–101.

Olalde I, Allentoft ME, Sánchez-Quinto F, Santpere G, Chiang CWK, DeGiorgio M, Prado-Martinez J, Rodríguez JA, Rasmussen S, Quilez J, et al. 2014. Derived immune and ancestral pigmentation alleles in a 7,000-year-old Mesolithic European. Nature 507:225–228.

Oppenheimer S. 2012. Out-of-Africa, the peopling of continents and islands: tracing uniparental gene trees across the map. Philos. Trans. R. Soc. Lond. B Biol. Sci. 367:770–784.

Orlando L, Ginolhac A, Zhang G, Froese D, Albrechtsen A, Stiller M, Schubert M, Cappellini E, Petersen B, Moltke I, et al. 2013. Recalibrating Equus evolution using the genome sequence of an early Middle Pleistocene horse. Nature 499:74–78.

Oskam CL, Haile J, McLay E, Rigby P, Allentoft ME, Olsen ME, Bengtsson C, Miller GH, Schwenninger J-L, Jacomb C, et al. 2010. Fossil avian eggshell preserves ancient DNA. Proc. R. Soc. Lond. B Biol. Sci.:rspb20092019.

Pagani L, Lawson DJ, Jagoda E, Mörseburg A, Eriksson A, Mitt M, Clemente F, Hudjashov G, DeGiorgio M, Saag L, et al. 2016. Genomic analyses inform on migration events during the peopling of Eurasia. Nature 538:238–242.

Palkopoulou E, Mallick S, Skoglund P, Enk J, Rohland N, Li H, Omrak A, Vartanyan S, Poinar H, Götherström A, et al. 2015. Complete Genomes Reveal Signatures of Demographic and Genetic Declines in the Woolly Mammoth. Curr. Biol. 25:1395–1400.

Parducci L, Suyama Y, Lascoux M, Bennett KD. 2005. Ancient DNA from pollen: a genetic record of population history in Scots pine. Mol. Ecol. 14:2873–2882.

Patterson N, Moorjani P, Luo Y, Mallick S, Rohland N, Zhan Y, Genschoreck T, Webster T, Reich D. 2012. Ancient Admixture in Human History. Genetics 192:1065–1093.

Peltzer A, Jäger G, Herbig A, Seitz A, Kniep C, Krause J, Nieselt K. 2016. EAGER: efficient ancient genome reconstruction. Genome Biol. 17:60.

Petkova D, Novembre J, Stephens M. 2016. Visualizing spatial population structure with estimated effective migration surfaces. Nat. Genet. 48:94–100.

Pickrell JK, Reich D. 2014. Toward a new history and geography of human genes informed by ancient DNA. Trends Genet. 30:377–389.

Pinhasi R, Fernandes D, Sirak K, Novak M, Connell S, Alpaslan-Roodenberg S, Gerritsen F, Moiseyev V, Gromov A, Raczky P, et al. 2015. Optimal Ancient DNA Yields from the Inner Ear Part of the Human Petrous Bone. PLoS ONE 10:e0129102.

Poinar H, Kuch M, McDonald G, Martin P, Pääbo S. 2003. Nuclear Gene Sequences from a Late Pleistocene Sloth Coprolite. Curr. Biol. 13:1150–1152.

Posth C, Renaud G, Mittnik A, Drucker DG, Rougier H, Cupillard C, Valentin F, Thevenet C, Furtwängler A, Wißing C, et al. 2016. Pleistocene Mitochondrial Genomes Suggest a Single Major Dispersal of Non-Africans and a Late Glacial Population Turnover in Europe. Curr. Biol. 26:827–833.

Pritchard JK, Stephens M, Donnelly P. 2000. Inference of Population Structure Using Multilocus Genotype Data. Genetics 155:945–959.

Raghavan M, Steinrücken M, Harris K, Schiffels S, Rasmussen S, DeGiorgio M, Albrechtsen A, Valdiosera C, Ávila-Arcos MC, Malaspinas A-S, et al. 2015.

Genomic evidence for the Pleistocene and recent population history of Native Americans. Science:aab3884.

Ramachandran S, Deshpande O, Roseman CC, Rosenberg NA, Feldman MW, Cavalli-Sforza LL. 2005. Support from the relationship of genetic and geographic distance in human populations for a serial founder effect originating in Africa. Proc. Natl. Acad. Sci. U. S. A. 102:15942–15947.

Rasmussen M, Anzick SL, Waters MR, Skoglund P, DeGiorgio M, Stafford Jr TW, Rasmussen S, Moltke I, Albrechtsen A, Doyle SM, et al. 2014. The genome of a Late Pleistocene human from a Clovis burial site in western Montana. Nature 506:225–229.

Rasmussen M, Guo X, Wang Y, Lohmueller KE, Rasmussen S, Albrechtsen A, Skotte L, Lindgreen S, Metspalu M, Jombart T, et al. 2011. An Aboriginal Australian Genome Reveals Separate Human Dispersals into Asia. Science 334:94–98.

Rasmussen M, Li Y, Lindgreen S, Pedersen JS, Albrechtsen A, Moltke I, Metspalu M, Metspalu E, Kivisild T, Gupta R, et al. 2010. Ancient human genome sequence of an extinct Palaeo-Eskimo. Nature 463:757–762.

Rasmussen S, Allentoft ME, Nielsen K, Orlando L, Sikora M, Sjögren K-G, Pedersen AG, Schubert M, Van Dam A, Kapel CMO, et al. 2015. Early Divergent Strains of Yersinia pestis in Eurasia 5,000 Years Ago. Cell 163:571–582.

Ray N, Currat M, Foll M, Excoffier L. 2010. SPLATCHE2: a spatially explicit simulation framework for complex demography, genetic admixture and recombination. Bioinformatics 26:2993–2994.

Reich D, Green RE, Kircher M, Krause J, Patterson N, Durand EY, Viola B, Briggs AW, Stenzel U, Johnson PLF, et al. 2010. Genetic history of an archaic hominin group from Denisova Cave in Siberia. Nature 468:1053–1060.

Reich D, Thangaraj K, Patterson N, Price AL, Singh L. 2009. Reconstructing Indian population history. Nature 461:489–494.

Rieux A, Eriksson A, Li M, Sobkowiak B, Weinert LA, Warmuth V, Ruiz-Linares A, Manica A, Balloux F. 2014. Improved calibration of the human mitochondrial clock using ancient genomes. Mol. Biol. Evol.:msu222.

Renaud G, Hanghøj K, Willerslev E, Orlando L, Birol I. 2017. gargammel: a sequence simulator for ancient DNA. Bioinformatics 33:577–579.

Rollo F, Ubaldi M, Ermini L, Marota I. 2002. Ötzi's last meals: DNA analysis of the intestinal content of the Neolithic glacier mummy from the Alps. Proc. Natl. Acad. Sci. 99:12594–12599.

Rosenberg NA, Nordborg M. 2002. Genealogical trees, coalescent theory and the analysis of genetic polymorphisms. Nat. Rev. Genet. 3:380–390.

Sabeti PC, Reich DE, Higgins JM, Levine HZP, Richter DJ, Schaffner SF, Gabriel SB, Platko JV, Patterson NJ, McDonald GJ, et al. 2002. Detecting recent positive selection in the human genome from haplotype structure. Nature 419:832–837.

Sarkissian CD, Pichereau V, Dupont C, Ilsøe PC, Perrigault M, Butler P, Chauvaud L, Eiríksson J, Scourse J, Paillard C, et al. 2017. Ancient DNA analysis identifies marine mollusc shells as new metagenomic archives of the past. Molecular Ecology Resources 17:835–853.

Schiffels S, Durbin R. 2014. Inferring human population size and separation history from multiple genome sequences. Nat. Genet. 46:919–925.

Schraiber JG, Evans SN, Slatkin M. 2016. Bayesian Inference of Natural Selection from Allele Frequency Time Series. Genetics 203:493–511.

Schubert M, Ermini L, Sarkissian CD, Jónsson H, Ginolhac A, Schaefer R, Martin MD, Fernández R, Kircher M, McCue M, et al. 2014. Characterization of ancient and modern genomes by SNP detection and phylogenomic and metagenomic analysis using PALEOMIX. Nat. Protoc. 9:1056–1082.

Secher B, Fregel R, Larruga JM, Cabrera VM, Endicott P, Pestano JJ, González AM. 2014. The history of the North African mitochondrial DNA haplogroup U6 gene flow into the African, Eurasian and American continents. BMC Evol. Biol. 14:109.

Sheehan S, Harris K, Song YS. 2013. Estimating Variable Effective Population Sizes from Multiple Genomes: A Sequentially Markov Conditional Sampling Distribution Approach. Genetics 194:647–662.

Skoglund P, Ersmark E, Palkopoulou E, Dalén L. 2015. Ancient Wolf Genome Reveals an Early Divergence of Domestic Dog Ancestors and Admixture into High-Latitude Breeds. Curr. Biol. 25:1515–1519.

Skoglund P, Malmström H, Raghavan M, Storå J, Hall P, Willerslev E, Gilbert MTP, Götherström A, Jakobsson M. 2012. Origins and Genetic Legacy of Neolithic Farmers and Hunter-Gatherers in Europe. Science 336:466–469.

Skoglund P, Northoff BH, Shunkov MV, Derevianko AP, Pääbo S, Krause J, Jakobsson M. 2014. Separating endogenous ancient DNA from modern day contamination in a Siberian Neandertal. Proc. Natl. Acad. Sci. 111:2229–2234.

Skoglund P, Sjödin P, Skoglund T, Lascoux M, Jakobsson M. 2014. Investigating Population History Using Temporal Genetic Differentiation. Mol. Biol. Evol. 31:2516–2527.

Skoglund P, Storå J, Götherström A, Jakobsson M. 2013. Accurate sex identification of ancient human remains using DNA shotgun sequencing. J. Archaeol. Sci. 40:4477–4482.

Skoglund P, Thompson JC, Prendergast ME, Mittnik A, Sirak K, Hajdinjak M, Salie T, Rohland N, Mallick S, Peltzer A, et al. 2017. Reconstructing Prehistoric African Population Structure. Cell 171:59–71.e21.

Slatkin M. 2016. Statistical methods for analyzing ancient DNA from hominins. Curr. Opin. Genet. Dev. 41:72–76.

Smith CI, Chamberlain AT, Riley MS, Stringer C, Collins MJ. 2003. The thermal history of human fossils and the likelihood of successful DNA amplification. J. Hum. Evol. 45:203–217.

Steinrücken M, Bhaskar A, Song YS. 2014. A novel spectral method for inferring general diploid selection from time series genetic data. Ann. Appl. Stat. 8:2203–2222.

Sunnåker M, Busetto AG, Numminen E, Corander J, Foll M, Dessimoz C. 2013. Approximate Bayesian Computation. PLoS Comput Biol 9:e1002803.

Tajima F. 1989. Statistical method for testing the neutral mutation hypothesis by DNA polymorphism. Genetics 123(3):585–595.

Thalmann O, Shapiro B, Cui P, Schuenemann VJ, Sawyer SK, Greenfield DL, Germonpré MB, Sablin MV, López-Giráldez F, Domingo-Roura X, et al. 2013. Complete Mitochondrial Genomes of Ancient Canids Suggest a European Origin of Domestic Dogs. Science 342:871–874.

Thomas WK, Pääbo S, Villablanca FX, Wilson AC. 1990. Spatial and temporal continuity of kangaroo rat populations shown by sequencing mitochondrial DNA from museum specimens. J. Mol. Evol. 31:101–112.

Timmermann A, Friedrich T. 2016. Late Pleistocene climate drivers of early human migration. Nature 538:92–95.

Valdiosera CE, GarcíA N, Anderung C, DaléN L, CréGut-Bonnoure E, Kahlke R-D, Stiller M, BrandströM M, Thomas MG, Arsuaga JL, et al. 2007. Staying out in the cold: glacial refugia and mitochondrial DNA phylogeography in ancient European brown bears. Mol. Ecol. 16:5140–5148.

Vitti JJ, Grossman SR, Sabeti PC. 2013. Detecting Natural Selection in Genomic Data. Annu. Rev. Genet. 47:97–120.

Voight BF, Kudaravalli S, Wen X, Pritchard JK. 2006. A Map of Recent Positive Selection in the Human Genome. PLOS Biol. 4:e72.

Warmuth V, Eriksson A, Bower MA, Barker G, Barrett E, Hanks BK, Li S, Lomitashvili D, Ochir-Goryaeva M, Sizonov GV, et al. 2012. Reconstructing the origin and spread of horse domestication in the Eurasian steppe. Proc. Natl. Acad. Sci. 109:8202–8206.

Willerslev E, Cappellini E, Boomsma W, Nielsen R, Hebsgaard MB, Brand TB, Hofreiter M, Bunce M, Poinar HN, Dahl-Jensen D, et al. 2007. Ancient Biomolecules from Deep Ice Cores Reveal a Forested Southern Greenland. Science 317:111–114.

Wright S. 1931. Evolution in Mendelian Populations. Genetics 16:97–159.

Wright S. 1949. The Genetical Structure of Populations. Ann. Eugen. 15:323–354.

Yang MA, Fu Q. 2018. Insights into Modern Human Prehistory Using Ancient Genomes. Trends in Genetics 34:184–196.

Yi X, Liang Y, Huerta-Sanchez E, Jin X, Cuo ZXP, Pool JE, Xu X, Jiang H, Vinckenbosch N, Korneliussen TS, et al. 2010. Sequencing of Fifty Human Exomes Reveals Adaptation to High Altitude. Science 329(5987):75–78.